

WATER-ROCK INTERACTIONS IN THE DEEP RIVER BASIN, NORTH  
CAROLINA: A CANDIDATE BASIN FOR SHALE GAS DEVELOPMENT

by

Amanda Stone

A dissertation submitted to the faculty of  
The University of North Carolina at Charlotte  
in partial fulfillment of the requirements  
for the degree of Doctor of Philosophy in  
Infrastructure and Environmental Systems

Charlotte

2019

Approved by:

---

Dr. John Diemer

---

Dr. David Vinson

---

Dr. Valerie Reynolds

---

Dr. Andy Bobyarchick

---

Dr. Olya Keen

©2019  
Amanda Stone  
ALL RIGHTS RESERVED

## ABSTRACT

Stone, Amanda. 2019. Water-rock interactions of the Deep River basin, North Carolina: A candidate basin for shale gas development. Under the direction of Dr. John Diemer.

As a result of the rapid expansion of shale gas development in the United States, the public has become increasingly concerned about the proper management of hydraulic fracturing wastewater also referred to as produced water. Adverse environmental and human health implications may occur should there be a release of untreated or inadequately treated produced water into the environment. Consequently, there is a need to be able to identify environmental signatures of produced water to understand the fate of unrecovered fluids and to delineate the source and extent of accidental releases of produced water into the environment.

In a previously little-drilled basin, few geochemical data exist on natural formation waters. The objective of this study was to simulate potential geochemical signatures in formation water from a non-marine, Mesozoic rift basin in order to predict the environmental signature of produced water. A series of sequential leaching extractions were conducted to simulate the influence of mineralogy, grain size, lithofacies and lithofacies association on the potential water-rock interactions in the Mesozoic Deep River basin, North Carolina. A comprehensive mineralogical study was completed to characterize the mineralogy and grain size of the sedimentary deposits involved in the water-rock interactions. The sequential extractions examined (1) the possible sources of extractable elements such as exchangeable sites on clay minerals and/or carbonate minerals, and (2) the solubility and leaching potential of a suite of elements into the

environment. These data may provide insight into the naturally-sourced components of produced water should hydraulic fracturing occur in the Deep River basin.

The geochemical data from this study suggest that the mineralogy and degree of post-depositional alteration of a deposit such as the presence or absence of carbonate minerals and/or grain size influence the water-rock interactions in the Deep River basin. The average concentration of extractable boron released from all of the Deep River basin samples and from all steps of the sequential extractions was lower ( $0.3 \mu\text{g/g}$ ) than the average concentration of extractable strontium and barium,  $11.9 \mu\text{g/g}$  and  $19.3 \mu\text{g/g}$ , respectively. Boron was extracted primarily from carbonate minerals (average  $0.7 \mu\text{g/g}$ ). Strontium and barium were both preferentially leached from exchangeable sites, average  $25.2 \mu\text{g/g}$  and  $51.8 \mu\text{g/g}$ , respectively, with lesser amounts of strontium leached from carbonate minerals, average  $18.8 \mu\text{g/g}$ .

Although strontium and barium were preferentially leached from exchangeable sites on clay minerals, the geochemical data show that grain size may play a more influential role compared to clay mineral abundance in determining the solubility of extractable strontium and barium. While clay mineral abundance does not strongly influence the water-rock interactions, the clay mineral assemblage, does influence the water-rock interactions in the Deep River basin. For example, deposits with kaolinite as the predominant clay mineral leached lower concentrations of ammonium acetate extractable strontium and barium ( $9.2 \mu\text{g/g}$  and  $45.2 \mu\text{g/g}$ , respectively) compared to deposits with smectite as the predominant clay mineral,  $35.9 \mu\text{g/g}$  and  $64.9 \mu\text{g/g}$ , respectively. Lastly, the geochemical data indicate that carbonate mineral content is strongly positively correlated to the concentration of extractable strontium

The geochemical data from this study suggest that should hydraulic fracturing occur in the Deep River basin, the produced water generated by fine-grained deposits such as mudstones and shales that are characterized by the highest abundance of carbonate minerals are likely to generate elevated concentrations of extractable strontium and barium. The geochemical data also suggest that compared to the marine deposits of the Marcellus Shale, the non-marine, lacustrine deposits of the Deep River basin will likely generate significantly lower concentrations of total dissolved solids.

## Acknowledgments

I would like to express my very deepest gratitude to my advisor, Dr. John Diemer, for his patient guidance, valuable and constructive suggestions, advocacy, and encouragement throughout the many years of this research work. His willingness to give his time so generously has been very much appreciated. I would like to express my great appreciation to Dr. David Vinson for his generous assistance with the geochemical laboratory work, his valuable guidance in analyzing the leaching data, and for his experienced comments on the manuscript, all of which helped guide this research project. I would like to extend my deepest appreciation to Dr. Valerie Reynolds for letting me sit in on her optical mineralogy class, helping me with the mineral identification using XRD and petrography, reviewing the manuscript, and for being a positive role model for female students. I am extremely grateful to Dr. Andy Bobyarchick and Dr. Olya Keen for providing valuable suggestions and reviewing the manuscript.

I would like to express my appreciation to the North Carolina Geological Survey staff especially Dr. Kenneth Taylor and Dr. Kathleen Farrell for allowing me access to the cores used in this study and for many thoughtful discussions. I would like to express my deepest gratitude to Mr. Jon Watkins for his willingness to give his time so generously to provide analytical assistance in the many labs I worked in and for his valuable advice throughout this process. I would also like to express my heartfelt gratitude to Tyler Gilkerson, Austin Johnson, Cecilia Tierney, and Juan Tejada for their assistance processing the 187 samples used for this research work. I would like to extend my sincere thanks to Dr. Jy Wu for helping fund my doctorate degree by providing financial assistance from the Infrastructure and Environmental Systems PhD program. I

am also grateful to the American Federation of Mineralogical Societies for a scholarship grant which also helped fund my doctoral degree. Funding used for this research work was provided, in part, by a student research grant from the Geological Society of America and a Faculty Research Grant from the UNC Charlotte.

I cannot begin to thank my parents, Mike and Ellen Stone. The completion of my doctoral research and grad school would not have been possible without their love and support. Their dedication to my success is second to none. Their sacrifice and unyielding love have allowed me to focus on and reach my goals. I would like to extend my greatest appreciation to my friend, Joe Galante, whose profound belief in me and my abilities and whose unwavering support have helped me persevere through one of the most difficult challenges in my life. I would like to extend my deepest gratitude to my Grandma Betty whose financial assistance was instrumental in the completion of my doctoral degree. I would like to thank my friend, Steve Rachide, who provided invaluable insight and perspective during this long graduate school adventure. In memoriam of Lyn Morgan and Dik van Meerten whose love and support helped me believe that I was enough to get a doctorate degree. Finally, I would like to thank God who, throughout this very humbling and sometimes excruciating process, has continually reminded me that I can get through anything as long as I keep my eyes on Him.

## Table of Contents

List of Figures .....	xvi
List of Tables .....	xxiv
1: INTRODUCTION .....	1
1.1 Overview .....	1
1.2 Significance of the Study .....	3
1.3 Statement of Purpose .....	5
1.4 Research Questions and Hypotheses .....	6
2: BACKGROUND .....	8
2.1 Shale Gas Production in East Coast Mesozoic Basins in the United States .....	8
2.2 North Carolina’s Mesozoic Basins .....	9
2.3 Deep River Basin .....	10
2.3.1 Hydrocarbon generation .....	13
2.3.2 Organic geochemical data .....	14
2.3.3 Assessing potential shale gas reserves in the Sanford sub-basin .....	15
2.4 Hydraulic Fracturing and Disposal Options for Produced Water .....	16
2.4.1 Deep injection.....	18
2.4.2 Treatment options.....	18
2.4.3 Recycling and reuse of produced water .....	20
2.5 Hydrocarbon Resources in a Marine Basin: The Marcellus Shale .....	21
2.5.1 Location and extent of the Marcellus Shale .....	22

2.5.2 Depositional history of the Marcellus Shale .....	23
3. SEDIMENTARY PETROLOGY .....	33
3.1 Introduction.....	33
3.2 Depositional Environments.....	33
3.3 Fluvial Environments .....	34
3.3.1 Alluvial fan environments.....	35
3.3.2 Meandering stream environments .....	37
3.3.3 Braided stream environments.....	38
3.4 Lacustrine Environments.....	39
3.5 Lithofacies Descriptions .....	41
3.5.1 Clast- and matrix-supported conglomerates.....	41
3.5.2 Thin-bedded (flat-laminated) sandstones.....	42
3.5.3 Cross-bedded sandstones.....	43
3.5.4 Cross-laminated sandstones and siltstones.....	44
3.5.5 Laminated siltstones and mudstones .....	44
3.5.6 Massive siltstones and mudstones.....	44
3.5.7 Organic-rich mudstones and shales .....	45
3.5.8 Other features .....	46
3.6 Methods for Acquiring Compositional Data.....	47
3.7 Sedimentary Petrography.....	49

3.8 Petrographic Analyses: Mineral Identification and Grouping .....	51
3.8.1 Quartz mineral group.....	52
3.8.2 Feldspar mineral group.....	52
3.8.3 Mica mineral group .....	54
3.8.4 Chlorite mineral group .....	55
3.8.5 Carbonate mineral group.....	55
3.8.6 Matrix mineral group.....	56
3.8.7 Opaque mineral group.....	57
3.8.8 Other mineral group .....	58
3.8.9 Unknown mineral group.....	59
3.9 Results of the Petrographic Analyses: General Mineral Grouping .....	59
3.10 Sandstone Classification.....	61
3.10.1 Quartz and feldspar categories .....	62
3.10.2 Rock fragment category .....	62
3.10.3 Matrix category .....	63
3.11 The Results of the Petrographic Analyses .....	67
3.11.1 Introduction .....	67
3.11.2 Mineral groups based on the sequential extractions.....	69
3.11.3 Petrographic data: Deep River basin samples .....	71
3.11.4 Petrographic data: Wadesboro sub-basin samples .....	71

3.11.5 Petrographic data: Sanford sub-basin samples .....	72
3.11.6 Petrographic data: Durham sub-basin samples .....	73
3.11.7: Trends in basin-wide mineralogy based on petrographic analysis.....	73
3.11.8 Variation in Deep River basin mineralogy with respect to grain size.....	74
3.12 Lithofacies Associations and Depositional Environments in Rift Basins .....	77
3.13 Lithofacies Associations and Depositional Environments of the Deep River Basin .....	79
3.14 Alluvial Fan Environments and Lithofacies Associations .....	83
3.14.1 Petrographic mineralogy of alluvial fan environments .....	84
3.15 Meandering Stream Environments and Lithofacies Associations.....	84
3.15.1 Petrographic mineralogy of meandering stream environments.....	85
3.15.2 The results of the petrographic analyses of the sub-environments of a meandering stream .....	86
3.16 Lacustrine Environments and Lithofacies Associations .....	87
3.16.1 Petrographic mineralogy of lacustrine environments.....	87
3.17 Summary: The Results of the Petrographic Analysis .....	88
3.18 X-Ray Diffraction Methods .....	89
3.18.1 Introduction .....	89
3.19 Sample Selection and Preparation for XRD Analyses .....	91
3.20 Total organic carbon analyses and results .....	92
3.21 XRD Mineral Identification and Grouping .....	93

3.21.1 Quartz mineral group.....	94
3.21.2 Feldspar mineral group.....	95
3.21.3 Clay mineral groups .....	96
<i>Kaolinite group</i> .....	98
<i>Smectite group</i> .....	99
<i>Mica group</i> .....	101
<i>Chlorite group</i> .....	103
<i>Mixed-layer clay group</i> .....	103
3.21.4 Carbonate mineral group.....	104
3.21.5 ‘Other’ mineral group.....	105
3.22 The Results of the XRD Analyses: Deep River Basin .....	105
3.22.1 XRD analysis of Wadesboro sub-basin samples.....	107
3.22.2 XRD analysis of Sanford sub-basin samples .....	107
3.22.3 XRD analysis of Durham sub-basin samples .....	108
3.22.4 Trends in basin-wide mineralogy based on XRD analysis.....	108
3.22.5 Variation in Deep River basin mineralogy with respect to grain-size .....	109
3.23 Stratigraphic Logs Representing the Depositional Environments of the Deep River Basin.....	110
3.24 XRD Mineralogy of Alluvial Fan Environments .....	111
3.25 XRD Mineralogy of Meandering Stream Environments .....	112

3.26 XRD Mineralogy of Lacustrine Environments .....	112
3.27 Summary: The Results of the XRD Analysis .....	113
3.28 Discussion: Synthesis of the Petrographic and XRD Mineralogical Data Sets ..	114
3.28.1 An analysis of the consistency of the mineralogical data sets .....	114
3.28.2 Mineralogical characteristics and the post-depositional history of the Deep River basin.....	118
3.28.3 Mineralogical data of the sub-basins.....	123
3.28.4 Synthesis of mineralogical data by grain size .....	127
3.29 Synthesis of the Petrographic and XRD Mineralogical Datasets as They Relate to the Depositional Environments of the Deep River Basin.....	127
3.29.1 Mineralogical characteristics of alluvial fan sub-environments.....	130
3.29.2 Mineralogical characteristics of meandering stream sub-environments .....	131
<b>4. THE INORGANIC GEOCHEMISTRY OF EXTRACTABLE ELEMENTS FROM THE DEEP RIVER BASIN .....</b>	<b>239</b>
4.1 Introduction.....	239
4.2 An Overview of Leaching Experiments and Sequential Extractions.....	243
4.3 Sequential Extraction Procedure.....	245
4.4 The Sequential Extraction Results .....	247
4.5 The Relationship between Grain Size and the Concentration of Extractable Elements.....	248
4.6 The Leaching Behavior of Extractable Elements as it Relates to the Sub-basins and Depositional Environments of the Deep River Basin .....	249

4.6.1 The leaching behavior of extractable strontium and barium according to sub-basin.....	249
4.6.2 The leaching behavior of extractable strontium and barium based on the depositional environment .....	250
<i>The leaching behavior of extractable strontium and barium in alluvial fan environments .....</i>	<i>251</i>
<i>The leaching behavior of extractable strontium and barium in meandering stream environments .....</i>	<i>252</i>
<i>The leaching behavior of extractable strontium and barium in lacustrine environments .....</i>	<i>253</i>
4.7 The Relationship between Mineral Content, Grain Size, and the Leaching Behavior of Extractable Strontium and Barium in the Deep River Basin.....	253
4.7.1 The relationship between mineral content, grain size, and concentrations of extractable strontium .....	256
4.7.2 The relationship between mineral content, grain size, and the concentration of extractable barium .....	257
4.8. The Relationship between Mineral Content and the Concentration of Extractable Strontium and Barium in the Sub-basins.....	258
4.9 The Relationship between Mineral Content, Grain Size, and the Concentration of Extractable Elements in Depositional Environments.....	262
4.9.1 The relationship between clay mineral content, grain size, and the concentration of strontium from alluvial fan sub-environments.....	265
4.9.2 The relationship between clay mineral content, grain size, and the concentration of extractable strontium from meandering stream sub-environments.....	266

4.9.3 The relationship between grain size and the concentration of ammonium acetate extractable strontium in lacustrine environments.....	267
4.10 A Summary of the Sequential Extraction Results: The Relationship between Mineral Content, Grain Size, and the Concentration of Extractable Elements from the Deep River Basin .....	268
CHAPTER 5: DISCUSSION AND CONCLUSIONS .....	304
5.1 Discussion.....	304
5.2 The Inorganic Geochemistry of Extractable Strontium and Barium Compared to the Mineralogy of the Sub-basins .....	306
5.3 The Inorganic Geochemistry of Extractable Strontium and Barium Compared to the Mineralogy of the Depositional Environments.....	308
5.4 Conclusions.....	309
5.5 Recommendations for Future Geochemical Studies in Non-Marine Basins .....	311
6. REFERENCES .....	316
Appendix A: Petrographic Data.....	326
Appendix B: Occurrence of Intergrowths of Quartz and Feldspar .....	327
Appendix C: XRD Data .....	328
Appendix D: Relative Abundance of Mineral Groups .....	333
Appendix E: Geochemical data .....	340
Appendix F: Cation and anion data .....	346

## List of Figures

Figure 1: Generalized map of North Carolina showing the major geologic regions and the locations of the exposed Triassic basins and sub-basins .....	7
Figure 2: Map of the Eastern United States showing the locations of the five quantitatively assessed East Coast Mesozoic basins .....	26
Figure 3: Generalized cross-sections of the Sanford sub-basin of the Deep River basin .	27
Figure 4: Detailed map of part of Lee and Chatham counties, showing the city of Sanford and the locations of several shut-in and previously drilled wells .....	28
Figure 5: Generalized geologic map of North Carolina and adjacent states, showing major geologic regions and locations of drill holes in Mesozoic basins.....	29
Figure 6: Distribution of total organic carbon from wells in the Deep River Basin, Sanford sub-basin.....	30
Figure 7: Structure map of the Marcellus Formation.....	31
Figure 8: Schematic facies model for an alluvial fan .....	134
Figure 9: The sub-environments of a meandering stream together with a graphic log of the sedimentary unit produced through lateral migration of such a stream.....	135
Figure 10: A block diagram of flood plain aggradation with very sinuous rivers.....	136
Figure 11: Block diagram of a braided stream summarizing the major morphological elements, and their associated bedforms and stratification.....	137
Figure 12: Block diagram of sandy braided systems with low sinuosity channels. ....	138
Figure 13: Model for continental half-graben rift basin. ....	139
Figure 14: Clast-supported conglomerate with very coarse sandstone.....	140

Figure 15: A thin-bedded, matrix-supported conglomerate located at Bogan’s Cut in the Wadesboro sub-basin .....	141
Figure 16: Trough cross-bedded sandstones with areas of muddy very fine- to-fine sandstone.....	142
Figure 17: Cross-laminated sandstone .....	143
Figure 18: Interbedded fissile siltstone and thinly laminated sandstones.....	144
Figure 19: Laminated, organic-rich mudstones .....	145
Figure 20: A fine sandstone .....	146
Figure 21: A layer of muddy very fine- to-fine sandstone overlain above and below by trough cross-bedded sandstones.....	147
Figure 22: The locations of the exposed Triassic basins in North Carolina. Black circles represent the approximate locations of samples collected for this study .....	148
Figure 23: Flow diagram of the data collected from samples from the Deep River Basin.. .....	149
Figure 24: Example of a clast-supported fabric as illustrated by sample DB-49. ....	150
Figure 25: Example of a matrix-supported fabric as illustrated by sample WB-7 .....	151
Figure 26: Several polycrystalline and monocrystalline quartz grains and a plagioclase grain surrounded by fine-grained matrix in sample WB-7. ....	152
Figure 27: Calcite matrix in sample WB-11 in cross-polarized light .....	153
Figure 28: Calcite matrix in sample WB-11 in plane-polarized light (Same field of view as Figure 27). .....	154
Figure 29: An example of an orthoclase grain altered to sericite in sample WB-7.....	155

Figure 30: A granophyre, an intergrowth of quartz and feldspar, present in sample WB-7. .....	156
Figure 31: Examples of biotite, muscovite, chlorite, and epidote grains found in sample DB-49 viewed in plane-polarized light. ....	157
Figure 32: Examples of biotite, muscovite, chlorite, and epidote grains found in sample DB-49 viewed in cross-polarized light (same field of view as Figure 31). ....	158
Figure 33: Sample WB-13 shows an example of a detrital muscovite grain and an elongate, rounded sericite grain that may represent a detrital feldspar grain that has been completely replaced by sericite. ....	159
Figure 34: Sample WB-13 shows an example of a detrital muscovite grain and an elongate, rounded sericite grain that may represent a detrital feldspar grain that has been completely replaced by sericite. Both forms of mica are colorless in plane-polarized light. Same field of view as Figure 33. ....	160
Figure 35: Examples of opaque minerals and a chlorite grain in plane-polarized light in sample DB-41. ....	161
Figure 36: An example of a calcite grain in cross-polarized light from sample WB-6. .	162
Figure 37: An example of a calcite grain in plane-polarized light from sample WB-6. Same field of view as Figure 36. ....	163
Figure 38: Sample DB-49 is a poorly sorted, very fine to fine-grained sandstone.....	164
Figure 39: Sample DB-49 is a poorly sorted, very fine to fine-grained sandstone. Same field of view as Figure 38. ....	165
Figure 40: Sample SB-37 is a grain-supported, very fine- to fine-grained sandstone that shows an example of a zircon crystal and several opaque mineral grains.....	166
Figure 41: WB-7 XPL Chert nodule surrounded by fine-grained matrix. ....	167

Figure 42: Sample DB-34 contains a high percentage of opaque minerals such as hematite.....	168
Figure 43: Classification of sandstones .....	169
Figure 44: Ternary diagram with end members quartz, feldspar, and rock fragments ...	170
Figure 45: Flow diagram for the sequential extractions procedure used in this study ...	171
Figure 46: Schematic diagram of the lateral relationships of the major depositional environments and sub-environments .....	172
Figure 47: Graphic log of core W11 MP9. Image 1 of 3.....	173
Figure 48: Graphic log of core W11 MP9. Image 2 of 3.....	174
Figure 49: Graphic log of core W11 MP9. Image 3 of 3.....	175
Figure 50: Graphic log of core W10 MP5. Image 1 of 3.....	176
Figure 51: Graphic log of core W10 MP5. Image 2 of 3 .....	177
Figure 52: Graphic log of core W10 MP5. Image 3 of 3.....	178
Figure 53: Graphic log of core W32 MP14. Image 1 of 3 .....	179
Figure 54: Graphic log of core W32 MP14. Image 2 of 3.....	180
Figure 55: Graphic log of core W32 MP14. Image 3 of 3.....	181
Figure 56: Graphic log of core W31 DP3. Image 1 of 4.....	182
Figure 57: Graphic log of core W31 DP3. Image 2 of 4.....	183
Figure 58: Graphic log of core W31 DP3. Image 3 of 4.....	184
Figure 59: Graphic log of core W31 DP3. Image 4 of 4.....	185
Figure 60: A device used to prepare a powdered sample for XRD analysis .....	186

Figure 61: The x-ray diffractogram of sample SB-28 generated from the XRD analysis. .....	187
Figure 62: Integrated X-ray powder diffraction software program called PDXL2 .....	188
Figure 63: The auto search function used to identify the minerals in the samples. ....	189
Figure 64: The auto search identified the candidate phases .....	190
Figure 65: The auto search identified the candidate phases and the associated peaks of each mineral identified below the sample's diffractogram.....	191
Figure 66: An example of the varieties of plagioclase such as anorthite and labradorite that may fit the diffraction pattern. ....	192
Figure 67: The x-ray diffractogram of sample DB-45 generated from the XRD analysis.. .....	193
Figure 68: The x-ray diffractogram of sample SB-29 generated from the XRD analysis. .....	194
Figure 69: Diagram illustrating the structures of clay minerals .....	195
Figure 70: The x-ray diffractogram of sample SB-23 generated from the XRD analysis.. .....	196
Figure 71: The x-ray diffractogram of sample DB-47 generated from the XRD analysis. .....	197
Figure 72: The x-ray diffractogram of sample SB-2 generated from the XRD analysis. .....	198
Figure 73: The x-ray diffractogram of sample WB-19 generated from the XRD analysis. .....	199
Figure 74: Stratigraphic column of a clay pit in the Wadesboro sub-basin. Image 1 of 6 .....	200

Figure 75: Stratigraphic column of a clay pit in the Wadesboro sub-basin. Image 2 of 6 .....	201
Figure 76: Stratigraphic column of a clay pit in the Wadesboro sub-basin. Image 3 of 6 .....	202
Figure 77: Stratigraphic column of a clay pit in the Wadesboro sub-basin. Image 4 of 6 .....	203
Figure 78: Stratigraphic column of a clay pit in the Wadesboro sub-basin. Image 5 of 6 .....	204
Figure 79: Stratigraphic column of a clay pit in the Wadesboro sub-basin. Image 6 of 6 .....	205
Figure 80: Vertical profile of a roadcut in the Sanford sub-basin .....	206
Figure 81: Geologic map of the Deep River basin, North Carolina .....	207
Figure 82: The average concentration of B, Sr, and Ba extracted by each extraction step from all of the samples in this study. ....	270
Figure 83: The average concentration of B, Sr, and Ba extracted by each extraction step from all of the samples in this study organized by the grain size of the sample. ....	271
Figure 84: The average concentration of Sr and Ba extracted by each extraction step from all of the samples in this study organized by the sub-basin.....	272
Figure 85: The average concentration of Sr and Ba extracted by each extraction step from all of the samples from this study organized by depositional environment.....	273
Figure 86: The average concentration of Sr and Ba extracted by each extraction step from samples from an alluvial fan environment.....	274
Figure 87: The average concentration of Sr and Ba extracted by each extraction step from samples from a meandering stream environment .....	275

Figure 88: The average concentration of B, Sr, and Ba extracted by each extraction step from samples from a lacustrine environment..... 276

Figure 89: The concentration of ammonium acetate extracted strontium compared to the abundance of clay minerals based on petrographic analysis (top figure) and XRD (lower figure)..... 277

Figure 90: The concentration of acetic acid extracted strontium compared to the abundance of carbonate minerals based on petrographic analysis (top figure) and XRD (lower figure). .... 278

Figure 91: The range and median concentration of ammonium acetate extracted strontium based on grain size (top) and the range and mean concentration of acetic acid extracted strontium based on grain size (bottom)..... 279

Figure 92: The concentration of ammonium acetate extracted barium compared to the abundance of clay minerals based on petrographic analysis (top figure) and XRD (lower figure)..... 280

Figure 93: The concentration of hydrochloric acid extracted barium compared to the abundance of oxide minerals based on petrographic analysis. .... 281

Figure 94: The concentration of ammonium acetate extracted barium based on grain size (top) and the concentration of HCl-extracted barium based on grain size based on petrographic analyses (bottom)..... 282

Figure 95: The range and median concentration of ammonium acetate extracted strontium compared to the abundance of clay minerals in each of the sub-basins of the Deep River basin. .... 283

Figure 96: The range and median concentration of acetic acid extracted strontium compared to the relative abundance of carbonate minerals in each of the sub-basins of the Deep River basin..... 284

Figure 97: The range and median concentration of ammonium acetate extracted barium compared to the relative abundance of clay minerals in each of the sub-basins of the Deep River basin. .... 285

Figure 98: The range and median concentration of ammonium acetate extracted strontium compared to the relative abundance of clay minerals for the depositional environments of the Deep River basin. .... 286

Figure 99: The range and median concentration of acetic acid extracted strontium compared to the relative abundance of carbonate minerals for the depositional environments of the Deep River basin. .... 287

Figure 100: The range and median concentration of ammonium acetate extracted barium compared to the relative abundance of clay minerals for the depositional environments of the Deep River basin. .... 288

Figure 101: The range and median concentration of ammonium acetate extracted strontium compared to the relative abundance of clay minerals (top) and grain size (bottom) for alluvial fan sub-environments ..... 289

Figure 102: The range and median concentration of acetic acid extracted strontium compared to the relative abundance of carbonate minerals (top) and grain size (bottom) for meandering stream sub-environments..... 290

Figure 103: The range and median concentration of ammonium acetate extracted strontium compared to grain size in lacustrine environments.. .... 291

Figure 104: Cross section of the Sanford sub-basin of the Deep River basin. Representative core logs of each lithofacies association are included. .... 314

## List of Tables

Table 1: East Coast Mesozoic basin assessment results .....	32
Table 2: The results of the petrographic analysis. ....	208
Table 3: The average percentage of plagioclase compared to the average percentage of orthoclase .....	209
Table 4: The modified categories for sandstone classification. ....	210
Table 5: The petrographic data organized in the four categories used for sandstone classification. ....	211
Table 6: The essential constituents including quartz, feldspar, and rock fragments, recalculated to 100%.....	212
Table 7: Mineral groups applicable for the leaching analyses.....	213
Table 8: Petrographic data organized in the mineral groups applicable for the sequential extraction analyses. ....	214
Table 9: Petrographic data of the samples from the Wadesboro sub-basin.....	215
Table 10: Petrographic data of the samples from the Sanford sub-basin. ....	216
Table 11: Petrographic data of the samples from the Durham sub-basin. ....	217
Table 12: The average percent of identified minerals in each of the three sub-basins... ..	218
Table 13: The average percent of identified minerals organized by grain size. ....	219
Table 14: Petrographic data of samples from an alluvial fan environment. ....	220
Table 15: Petrographic data of samples from a meandering stream environment.....	221
Table 16: Average composition of sub-environments in a meandering stream environment. ....	222

Table 17: Petrographic data of samples from a lacustrine environment.....	223
Table 18: Average composition of samples from alluvial fan, meandering stream, and lacustrine environments. ....	224
Table 19: Percentage of total organic carbon (TOC) for tested samples.....	225
Table 20: Mineral groups identified by XRD analyses and applicable for the leaching analyses. ....	226
Table 21: Relative abundance of mineral groups identified by XRD in the Deep River Basin and its sub-basins.....	227
Table 22: Relative abundance of mineral groups identified by XRD and organized by grain size. ....	228
Table 23: Relative abundance of mineral groups identified by XRD in samples from alluvial fan environments.....	229
Table 24: Relative abundance of mineral groups identified by XRD in samples from meandering stream environments. ....	230
Table 25: Relative abundance of mineral groups identified by XRD in samples from lacustrine environments. ....	231
Table 26: Relative abundance of mineral groups identified by XRD in samples from alluvial fan, meandering stream, and lacustrine environments.....	232
Table 27: The two mineralogical data sets, the petrographic data and XRD data, organized by sub-basin. ....	233
Table 28: The two mineralogical data sets, the petrographic data and XRD data, organized by grain size.....	234
Table 29: The two mineralogical data sets, the petrographic data and XRD data, for alluvial fan environments in the DRB.....	235

Table 30: The two mineralogical data sets, the petrographic data and XRD data, for meandering stream environments in the DRB. ....	236
Table 31: The two mineralogical data sets, the petrographic data and XRD data, for lacustrine environments in the DRB. ....	237
Table 32: The two mineralogical data sets, the petrographic data and XRD data, from alluvial fan, meandering stream, and lacustrine environments in the DRB.....	238
Table 33: The average concentration of B, Sr, and Ba extracted from all steps of the sequential extractions from all of the samples organized by sub-basin.....	292
Table 34: The average concentration of B, Sr, and Ba extracted by each extraction step from all of the samples in this study organized by sub-basin .....	293
Table 35: The average concentration of B, Sr, and Ba extracted from all steps of the sequential extractions from all of the samples organized by grain size.....	294
Table 36: The average concentration of B, Sr, and Ba extracted by each extraction step from all of the samples in this study organized by the grain size of the sample .....	295
Table 37: The average concentration of B, Sr, and Ba extracted from all steps of the sequential extractions from all of the samples from this study organized by depositional environment. ....	296
Table 38: The average concentration of B, Sr, and Ba extracted by each extraction step from all of the samples from this study organized by depositional environment.....	297
Table 39: The average concentration of B, Sr, and Ba extracted from all steps of the sequential extractions from samples from an alluvial fan environment. ....	298
Table 40: The average concentration of B, Sr, and Ba extracted by each extraction step from samples from an alluvial fan environment. ....	299
Table 41: The average concentration of B, Sr, and Ba extracted from all steps of the sequential extractions from samples from a meandering stream environment.....	300

Table 42: The average concentration of B, Sr, and Ba extracted by each extraction step from samples from a meandering stream environment.....	301
Table 43: The average concentration of B, Sr, and Ba extracted by each extraction step from samples from a lacustrine environment.....	302
Table 44: The average concentration of B, Sr, and Ba extracted from all steps of the sequential extractions from samples from a lacustrine environment.....	303
Table 45: The average relative abundance of clay minerals phases present in the sub-basins of the Deep River basin.....	315

# 1: INTRODUCTION

## 1.1 Overview

There are four Mesozoic basins in North Carolina with surface exposures (Figure 1) (Olsen et al., 1991; Smith and Ozer, 2012). In order of descending areal extent, those basins are the Deep River Basin, Dan River Basin, Davie Basin, and Ellerbe Basin. These basins are located in the Piedmont geologic province and were formed during the early Mesozoic as a consequence of crustal thinning and extension during the rifting of the supercontinent Pangea (Clark et al., 2011).

The depositional environments in the basins included alluvial fans, typically confined to the faulted basin margins, and axial rivers and lakes in the basin centers (Olsen et al., 1991; USGS, 2012). The alluvial fans and axial fluvial systems deposited red conglomerates and sandstones, whereas the anoxic lacustrine systems accumulated fine-grained dark gray to black muds (Olsen et al., 1991). Because the rift basins were tectonically controlled, many of the lakes were likely long-lived and sufficiently deep that they became thermally stratified. As these basins were proximal to the equator at the time they formed, and received nutrients from the surrounding uplands, their surface waters could have been highly productive with abundant algae. It is possible, therefore, that the dark gray to black organic-rich lacustrine mudstones and shales now serve as hydrocarbon source and reservoir rocks in the Mesozoic Basins (Horton and Zullo, 1991; Schlische, 1993).

Unconventional sources for natural gas are now more economically accessible due to technological advances such as horizontal and directional drilling and hydraulic fracturing (fracking). These techniques have been used in other hydrocarbon fields

including the Barnett Shale in Texas, the Bakken field in North Dakota, and the Marcellus Shale and Utica Shale in Pennsylvania, Ohio and West Virginia (Arthur et al., 2008; Vengosh et al., 2013). The process of hydraulic fracturing involves the injection of fluids including water, and various chemicals and proppants under high pressure into the subsurface. The high-pressure fluid is used to fracture low permeability rocks such as shales or tight sandstones and the proppants keep the fractures open to allow oil and/or gas to flow from small pore spaces in the rock to the production well. A portion of this fluid known as flowback and produced water is returned to the surface as wastewater. Flowback and produced water are a mixture of injected fluids (water and chemicals introduced during hydraulic fracturing) and naturally-sourced fluids (formation water) from the shale and/or adjacent rock units. As a result, the flowback and produced water can have high total dissolved solids (TDS), high concentrations of metals and salts, soluble organic compounds (both volatile and semivolatile), and possibly some radioactivity associated with it (Gregory et al., 2011; Vengosh et al., 2014). The high concentrations of these constituents, and the sheer volume of wastewater generated, make proper disposal of flowback and produced water a challenge as seen in numerous shale plays such as the Marcellus Shale region of Pennsylvania and adjacent states, and the Woodford Shale region in Oklahoma.

The public has become more concerned about the proper management of oil and gas wastewater due to the potential for adverse human health and environmental impacts should there be a release of untreated or inadequately treated wastewater into the environment (Vidic et al., 2013). In addition, not all of the hydraulic fracturing fluid and

formation water generated during shale gas development is brought to the surface. The fate of these unrecovered fluids is currently unknown (Vidic et al., 2013).

## 1.2 Significance of the Study

The development of unconventional natural gas plays such as coalbed methane, tight sandstones, and shales has been increasing in the United States (EIA, 2017). It is possible that the shale gas in the Deep River basin, North Carolina may be developed in the future using hydraulic fracturing. The development of shale gas plays must be completed as safely as possible to protect surface and groundwater resources.

Some of the characteristic constituents of flowback and produced water are natural fluids (formation water) sourced from the shale and/or adjacent rock units, whereas other constituents are introduced during fracking (Gregory et al., 2011; Vengosh et al., 2014). The composition of the flowback and produced water changes as a function of the amount of time the fluids are in contact with the target formation (Gregory et al., 2011). Initially, these fluids tend to be composed predominantly of injected fracturing fluids, but over time the composition of the fluids is modified by minerals and organic constituents present in the formation and in formation water and/or reactions between injected fluids and the host formation in which both salts and radionuclides may be leached (Gregory et al., 2011; Jackson et al., 2013). Concentrations of total dissolved solids (TDS), suspended solids, and major cations and anions were found to increase over time in flowback water (Gregory et al., 2011). Additionally, studies in the Marcellus Shale region found a positive correlation between the concentrations of toxic elements such as barium, strontium, and radioactive radium and the salinity of produced and flowback waters (Warner et al., 2013; Vengosh et al., 2014). There is, therefore, a

potential benefit from increasing our understanding of the characteristics of the natural, in situ water-rock interactions prior to shale gas development in an area. Jackson and others (2013) suggested there is an urgent need for hydrogeological baseline reporting that includes the geochemical characterization of formation waters in order to address concerns regarding the potential for contamination of groundwater associated with unconventional gas development.

This study examines lithologic variables such as grain size, mineralogy, lithofacies, lithofacies assemblages and degree of post-depositional alteration to determine their influence on water-rock interactions in the Deep River basin, North Carolina. The data provide a baseline of the water-rock interactions that likely influence the formation water in the basin. Thus, the study will improve our understanding of the geologic evolution and geochemical and hydrogeologic nature of the basin. Sequential extractions conducted for the study provide data about the mobility of certain cations including strontium, barium, boron, calcium and magnesium, and anions such as chloride and sulfate. Understanding the mobility of these components may provide insight into the naturally-sourced components of flowback and produced water should the practice of hydraulic fracturing begin in the Deep River basin of North Carolina. Knowledge of these characteristics may aid in properly managing the wastewater in order to minimize adverse human health and environmental impacts such as impacts to surface and groundwater resources.

An improved understanding of the composition of formation water, and by extension, the possible characteristics of flowback and produced water allows industry and government agencies to have a more accurate picture of the challenges, costs, and

methods of properly managing the wastewater before beginning operations in an area. In North Carolina, where shale gas resources are much smaller compared to areas like the Marcellus Shale region, knowledge of the cost of managing the wastewater may impact a company's decision whether to develop the resource. Additionally, areas such as the United States, Brazil, China, South America, Africa, and southeast Asia have lacustrine sources and reservoirs of hydrocarbons that represent important exploration opportunities both currently and in the future (Bohacs et al., 2000; Sladen, 1994). Hydrocarbon production from lake deposits probably accounts for more than 20% of the current worldwide production (Bohacs et al., 2000). This study aims to understand the possible characteristics of flowback and produced water by examining the water-rock interactions in a rift basin containing nonmarine deposits. Thus, it may be possible to apply the methodology utilized in this study to similar rift basins worldwide.

### 1.3 Statement of Purpose

The purpose of this research is to 1) provide baseline data of water-rock interactions and the hydrogeologic nature of an undisturbed Mesozoic basin in advance of drilling and hydraulic fracturing, 2) to simulate the formation water that may be brought to the surface during shale gas development, and 3) to examine the geochemical fingerprint that could be used to identify this formation water in the environment. This study will provide information about the geologic evolution and geochemical and hydrogeologic nature of the Deep River Basin. This baseline geochemical information can provide opportunities for exploration of current and/or undiscovered resources and insight into the possible characteristics of hydraulic fracturing wastewater.

#### 1.4 Research Questions and Hypotheses

Several questions were developed to guide the study. First, does the mineralogy of samples influence the composition of leachate resulting from sequential extractions in a laboratory setting? Second, does the grain size of the samples influence the composition of leachate resulting from sequential extractions in a laboratory setting? Lastly, does the degree of post-depositional alteration of a sample, as indicated by the presence or absence of authigenic minerals such as carbonate, influence the composition of the resulting leachate in a laboratory setting?

The depositional history of a sample influences its mineralogy, grain size, lithofacies, lithofacies association, and degree of post-depositional alteration (Tucker, 2001). Thus, it is hypothesized that North Carolina Mesozoic basin formation water will exhibit different chemical characteristics than other basins because of different depositional histories. Specifically, the fluvial, alluvial fan, and lacustrine (non-marine) deposits of the Deep River basin likely generate lower salinities than the marine brines of the Appalachian Basin (e.g Marcellus Shale). Thus, it is hypothesized that mineralogy will influence the composition of leachate resulting from sequential extractions. Additionally, it is hypothesized that fine-grained lithologies such as shales and fine-grained sandstones will leach trace elements such as strontium and barium more readily than coarse-grained lithologies. Lastly, it is hypothesized that post-depositional alteration will result in authigenic minerals such as carbonates and oxides that will influence the composition of leachate resulting from sequential extractions. Thus, the overall hypothesis of this study suggests that the depositional history of a deposit will likely influence the composition of formation water.

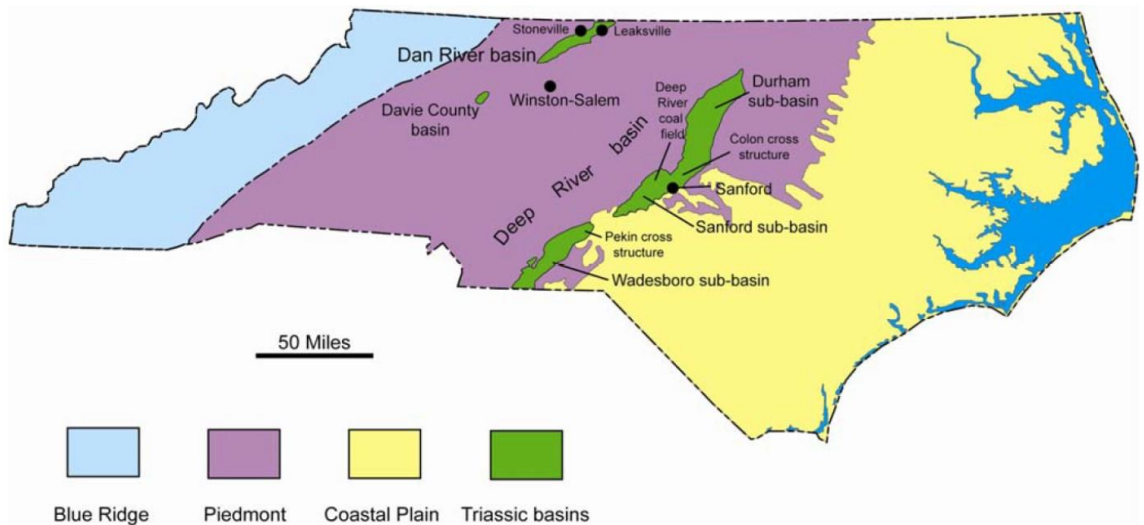


Figure 1: Generalized map of North Carolina showing the major geologic regions and the locations of the exposed Triassic basins and sub-basins (source: Reid and Milici, 2008.)

## 2: BACKGROUND

### 2.1 Shale Gas Production in East Coast Mesozoic Basins in the United States

Along the eastern margin of North America from Florida northward to New England, and into parts of adjacent Nova Scotia and New Brunswick, lie numerous rift basins of Mesozoic age (Figure 2) (USGS, 2012). These basins formed during the Late Triassic Period and early Jurassic Period as continental extension associated with the breakup of the supercontinent Pangea was occurring (Horton and Zullo, 1991; Schlische, 1993). The basins generally occur from the offshore Atlantic continental margin westward beneath the Atlantic Coastal Plain to the Appalachian Mountains and they locally overprint the Appalachian orogen (USGS, 2012; Schlische, 1993). Various deposits, collectively termed the Newark Supergroup, occur within the basins and comprise boulder beds, coarse- to fine-grained sandstones, mudstones, gray and black shales, and coal beds. These deposits likely formed in fluvial to deltaic and lacustrine environments that existed during rifting (USGS, 2012).

The Mesozoic rift basins are becoming areas of increased interest because many of the basins have strata that may be potential source rocks for hydrocarbons, most notably natural gas (Reid and Milici, 2008). In 2012, the United States Geological Survey (USGS) published an assessment of undiscovered oil and gas resources in the Mesozoic basins, both onshore and offshore, found along the eastern margin of the United States. The assessment of potential hydrocarbon reserves is based on the geologic and geochemical characteristics of the individual total petroleum systems (TPS) that were recognized within the basins. The geologic and geochemical data allowed the USGS to define a composite TPS for each of the fourteen major Mesozoic rift basins. Five of the

total petroleum systems display the most potential for generating and accumulating hydrocarbons. As a result, the USGS focused on quantitatively assessing the technically recoverable, undiscovered resources within these five basins (Table 1). According to the geology-based assessment method utilized by the USGS, an estimated mean of 3,860 billion cubic feet of undiscovered natural gas, as well as a mean of 135 million barrels of undiscovered natural gas liquids exist within the five assessed basins: the Deep River, Dan River-Danville, and Richmond basins in North Carolina and Virginia; the Taylorsville Basin in Virginia and Maryland; and the southern part of the Newark Basin located in New Jersey (USGS, 2012).

## 2.2 North Carolina's Mesozoic Basins

Four exposed Mesozoic rift basins, the Deep River, Dan River, Davie, and Ellerbe basins, are located in the Piedmont Province of North Carolina (Figure 1). These basins form two subparallel belts that strike northeasterly and are aligned subparallel to the Paleozoic Appalachian orogen (Figure 1). The Deep River basin and the Ellerbe basin make up the eastern belt while the western belt includes the Dan River basin and a small outlier which lies to the south, the Davie basin (Olsen et al., 1991; Smith and Ozer, 2012).

Of these four basins, the Deep River basin potentially contains the most hydrocarbons with estimates of its composite TPS at 1,600 billion cubic feet (Table 1). The Deep River basin is a half-graben with basin fill that is intruded by through-going north- and northwest-striking diabase dikes (Figure 3). The stratigraphy generally dips southeastward toward the major normal fault zone, the Jonesboro fault zone, that bounds the basin. In general, a tripartite stratigraphy is found in the basin consisting of a lower

sequence of fluvial deposits composed mainly of reddish-brown, arkosic, coarse-grained sandstones and conglomerates, a middle lacustrine sequence of predominantly gray to black fossiliferous siltstone, carbonaceous shale, and thin coal beds, and an upper sequence with both fluvial and lacustrine deposits consisting mainly of arkosic and pebbly sandstone, reddish-brown siltstone, mudstone, and conglomerate (Figure 3). Most of the Newark Supergroup basins of the eastern U.S. exhibit this stratigraphic pattern suggesting an extensional basin filling model with the assumption that the area of the basin increased over time (Olsen et al., 1991).

### 2.3 Deep River Basin

The Deep River basin is 240 km long and ranges from 9 to 25 km wide and is the southernmost of the large exposed rift basins in the Carolinas and in the Newark Supergroup (Figure 2). The Jonesboro fault system, a system of west-dipping normal faults, is located along the east and southeast margins of the basin (Figure 3). Along the northwestern margin of the basin lies a regional unconformity between basin fill material and adjacent pre-Triassic metamorphic rocks and granitic rocks (Reinemund, 1955; Olsen et al., 1991). The nearly 7,000 feet of sedimentary material deposited in the basin, collectively referred to as the Chatham Group, dips southeastward toward the Jonesboro fault system (Olsen et al., 1991; Smith and Ozer, 2012).

The Deep River basin which covers approximately 3137 square kilometers consists of three interconnected sub-basins: (from north to south) the Durham, Sanford, and Wadesboro sub-basins (Figure 1) (Smith and Ozer, 2012). A constriction and possible basement high point known as the Colon cross-structure separates the Durham and Sanford sub-basins. The Pekin cross-structure and Coastal Plain overlap separate the

Sanford and Wadesboro sub-basins. A similar stratigraphy is displayed in all three sub-basins, composed of three basic lithofacies along the basin axis: 1) lower pebbly sandstone; 2) middle clay shale and mudstone; and an 3) upper sandstone; with conglomerates found along the borders (Figure 3). However, only the Sanford sub-basin is formally divided into three stratigraphic subdivisions. The Sanford sub-basin is divided into an upper and lower unit of red terrigenous clastic rocks named the Sanford and Pekin Formations, respectively, with a middle unit of gray to black shale, coal, and sandstone called the Cumnock Formation (Figure 3) (Olsen et al., 1991).

The sub-basins collectively forming the Deep River basin formed at the same time and in the same general depositional environments, but the relative abundance of the lithologies of the individual sub-basins vary somewhat. Emmons (1852) was the first to recognize and map the lithology of the Sanford sub-basin. He identified a coarse-fine-coarse sequence consisting of an upper and lower unit of red sandstone and conglomerates with a middle unit of finer-grained gray sandstone, black shale and coal. In 1923, Campbell and Kimball modified Emmons work and formally named the three units he identified as the Pekin, Cumnock, and Sanford Formations, providing type localities for each formation. Campbell and Kimball applied the new formation names to the entire Deep River basin, but further research determined that the three-layer system of formations in the Sanford sub-basin was not present in the Durham or Wadesboro sub-basins. A “coarse-fine-coarse” sequence similar to that of the Sanford sub-basin was recognized by Randazzo and others in 1970 in the Wadesboro sub-basin, but no detailed geologic map was produced

In the current literature, the Wadesboro sub-basin is mapped as undifferentiated

Triassic deposits related to the Pekin Formation. However, Brazell (2013) conducted a detailed study of part of the Wadesboro sub-basin and suggested that general sedimentary differences throughout the sub-basin exist and warrant a distinction between two formations, the lower Pekin Formation and a newly proposed, overlying Wadesboro Formation. The Pekin Formation is composed of red and gray mudstone, shale, siltstone, sandstone, and conglomerates. In the Wadesboro sub-basin, the Pekin Formation is characterized by large channelized deposits that contain trough cross-bedded coarse sandstones interbedded with thick layers of finer-grained mudstones, siltstones, and shales. The proposed Wadesboro Formation is characterized by thin massive, sheet siltstones and sandstones interbedded with thin layers of mudstone and siltstone. The composition of the sandstones differs between the two formations. The sandstones of the Pekin Formation are more feldspathic and classified as lithic arkoses to feldspathic litharenites. The sandstones of the Wadesboro Formation are more quartz-rich and classified as feldspathic litharenites and litharenites (Brazell, 2013). In the Durham sub-basin, no formal formations are identified predominantly due to the absence of good marker beds or horizons (such as the Cumnock Formation) which can be used to assign strata to specific formations. The Durham sub-basin strata are therefore identified using the lithofacies system of nomenclature of Smoot and others (Clark, et al., 2001).

All three sub-basins contain a middle clay-shale and mudstone interval 50 to 400 m thick, but, as previously mentioned, the sequence is best developed as the coal-bearing Cumnock Formation within the Sanford sub-basin (Figure 3). The Cumnock Formation is interpreted as having been deposited in a lacustrine and paludal (marshy) environment. Therefore, the formation is a potential source rock for hydrocarbon generation and

accumulation. Two major coal seams ranging from a few centimeters to 3 m thick and several thinner coal beds are located approximately 60 to 80 m above the base of the Cumnock Formation in the Sanford sub-basin. Overlying the coal-bearing interval is 150 to 170 m of locally calcareous and organic carbon-rich gray and black shales with minor amounts of fine-to coarse-grained sediment which coarsen upward. The upper section of the Cumnock Formation consists of siltstone and sandstone which grade upward into the sandstones of the Sanford Formation (Olsen et al., 1991).

### 2.3.1 Hydrocarbon generation

The hydrocarbons that create coal, oil, and natural gas are typically formed in quiet-water environments such as lakes, swamps, lagoons, and seas. As clay is deposited on the bottoms of these features, organic matter, such as the remains of algae and plankton also settle to the bottom creating an organic-rich, muddy ooze. For the organic material in the ooze to remain preserved, it must be deposited in an oxygen-poor environment that does not promote aerobic respiration. Over time, the ooze may lithify into an organic-rich shale, commonly referred to as a source rock, that contains the raw materials for hydrocarbon generation (Marshak, 2012). In general, if the source rock is compressed under more and more sediment, the temperature and pressure experienced by the rock will increase. Additionally, in rift basins geothermal gradients are affected by crustal thinning, sediment loading, and magmatic heat flow. The heat and pressure cause chemical reactions to occur that break down the carbon bonds in the organic matter (Natural Gas Supply Association, 2010). At lower temperatures (~90-160°C) and shallower depths (3.5-6.5 km), oil will form. At higher temperatures (~160-225°C) and greater depths (~ 6.5-9 km), natural gas will form. Natural gas formed by compression

and heating is known as thermogenic natural gas or thermogenic methane (Marshak, 2012; Natural Gas Supply Association, 2010). Due to the low permeability of shale, some natural gas may remain trapped in the source rock creating what is termed 'shale gas'.

### 2.3.2 Organic geochemical data

Organic geochemical data from 8 wells show that potential hydrocarbon source rocks exist in the Cumnock Formation of the Sanford sub-basin in the Deep River basin (Reid and Milici, 2008) (Figure 5). The data suggest that the sediments are more likely gas prone than oil prone although both types of hydrocarbons were generated. Geologists use three indicators in shale to determine the potential for hydrocarbon reserves: total organic carbon (TOC), kerogen type, and thermal maturity (Smith and Ozer, 2012). Total organic carbon is the quantity of organic material available to form hydrocarbons (PA DCNR, 2009). A minimum amount of organic material ranging generally, from 0.4%-1.4% TOC is necessary to generate and expel oil from shale rocks. 66 samples from 8 wells were collected in the Cumnock Formation of the Sanford sub-basin revealing an average TOC value of 5.09 percent, 3.6 times the 1.4% TOC threshold (Figure 6) (Reid and Milici, 2008; Smith and Ozer, 2012).

Kerogen type provides an indication of the type of organic matter and shows the nature of the hydrocarbon (oil, gas, or both) most likely to be generated by a source rock. Type I kerogen indicates lacustrine deposits which generate primarily oil; Type II kerogen is indicative of marine environments and will typically generate both oil and gas; and Type III kerogen is plant derived and generates primarily gas prone source rocks (Reid and Milici, 2008; Smith and Ozer, 2012). Geochemical data show that the organic material in the Cumnock Formation was primarily derived from Type III woody (coaly)

material and secondarily from Type I lacustrine (algal) material indicating both oil and gas may be present (Reid and Milici, 2008).

Thermal maturity gives an indication of the maximum temperature a particular rock has experienced and is evaluated based on vitrinite reflectance values (%Ro), thermal alteration, and a parameter known as Tmax (Smith and Ozer, 2012). Vitrinite reflectance values for the Cumnock Formation are commonly variable and the data from some wells exhibit sharp vitrinite reflectance peaks indicating locally steep thermal gradients. These peaks probably are a result of contact metamorphism caused by intrusive diabase bodies (Reid and Milici, 2008). The Cumnock Formation in the Sanford sub-basin has a thermal maturity which is indicative of the dry gas window (Reid and Milici, 2008). The thermal alteration index (TAI) data, although limited to one drill hole within the Sanford sub-basin of the Deep River basin, show thermal maturation ranks that range from peak dry gas generation (TAI = 3) nearly to the limit of dry gas preservation (TAI = 3.7) (Reid and Milici, 2008). Tmax data ranging from 400-500° C compared to kerogen type for the Sanford sub-basin indicates both oil prone and gas prone source rocks exist (Reid and Milici, 2008; Smith and Ozer, 2012). In summary, the Sanford sub-basin of the Deep River basin, North Carolina may be a potential resource for shale gas.

### 2.3.3 Assessing potential shale gas reserves in the Sanford sub-basin

The North Carolina Department of Environment and Natural Resources (NC DENR) used limited data from two wells obtained by the N.C. Geological Survey to assess the resource potential for shale gas within the Sanford sub-basin (an area of approximately 59,000 acres) of the Deep River basin. Both currently shut-in wells, Simpson #1 and Butler #3, were drilled in 1998 by a company exploring potential hydrocarbon reserves in the state (Figure 4). Since the data set is very small and the data

from the individual wells vary significantly, it is unclear how representative these estimates will be for the gas resource in the entire Sanford sub-basin. Once more data become available, the estimates will very likely change. Also, because the data only come from the Sanford sub-basin, the estimates cannot be generalized to the entire Deep River basin.

Based on the data from these two wells, NC DENR has estimated that the mean ratio of cubic feet of gas per cubic feet of rock is 3.02 with a standard deviation of 2.62. These data can be used to estimate the volume of technically recoverable gas for the entire Sanford sub-basin. NC DENR estimated that in the 59,000-acre area of the sub-basin, 368 wells could potentially be drilled with a spacing of one well per 160 acres for an estimated volume of technically recoverable gas of 309 billion cubic feet of gas (Smith and Ozer, 2012). Again, this estimate was formulated using a very small data set and will likely change as more data are gathered.

From the limited data available for the Mesozoic basins in North Carolina, the Deep River basin, and specifically the Sanford sub-basin, is estimated to have 309 billion cubic feet of technically recoverable gas (Smith and Ozer, 2012). In contrast, recent estimates of the Marcellus Shale located in the northeastern U.S suggest technically recoverable gas reserves as high as 500 tcf (Kargo et al., 2010). A comparison of these data shows that significantly less natural gas is assumed to be available in North Carolina.

#### 2.4 Hydraulic Fracturing and Disposal Options for Produced Water

The first large-scale commercial production of natural gas from shale began in 2000, in the Barnett Shale located in north-central Texas. By 2005, the Barnett Shale was

producing close to half a trillion cubic feet per year (tcf/yr) (EIA, 2016). With the success seen in the Barnett Shale, other shale plays in the United States such as the Fayetteville Shale in Arkansas, the Haynesville Shale in Texas and Louisiana, and the Marcellus and Utica shales in northern Appalachia were developed (EIA, 2016). As a result of development in numerous shale plays, dry shale gas production increased from less than 5 billion cubic feet per day (bcf/day) in 2005 to nearly 45 bcf/day in 2016 (EIA, 2017a). In 2013, shale gas became the largest source of total natural gas production in the United States (EIA, 2014).

The produced water generated by hydraulic fracturing is often impounded on-site for subsequent treatment, reuse, or disposal. Deep-well injection is the primary method of disposal for produced water in the United States (Gregory et al., 2011; Vidic et al., 2013). However, in some areas where shale gas resources may be developed, such as North Carolina, deep-well injection is not currently available due to geologic and/or regulatory constraints (Gregory et al., 2011; Smith and Ozer, 2012).

Other possible disposal and management options include treatment of the wastewater and/or recycling and subsequent reuse. Treatment options include the discharge and dilution of produced water into publicly owned municipal wastewater treatment plants (POTWs), centralized waste treatment plants (CWTs), and municipal wastewater treatment plants (WWTPs). As a result of possible environmental impacts associated with deep injection and treatment options, produced water is increasingly being recycled and reused for future hydraulic fracturing operations (Gregory et al., 2011; Smith and Ozer, 2012; Vidic et al., 2013; Vengosh et al., 2014). Each of these management options has its own challenges and drawbacks which are discussed further in

subsequent sections.

#### 2.4.1 Deep injection

The use of deep well injection to manage produced water can present concerns such as induced seismicity. It has been documented that fluid injection into the subsurface can trigger earthquakes. In the 1960s, earthquakes occurred in Colorado at the Rocky Mountain Arsenal as a result of fluid injection into the subsurface. The largest associated earthquake was magnitude 5.2 (Healy et al., 1968). In the 1990s, fluid injection in Paradox Valley, Colorado triggered earthquakes with the largest magnitude quake registering a magnitude 4.3 (Ake et al., 2005).

In Oklahoma, deep injection of hydraulic fracturing wastewater is potentially associated with a dramatic increase in earthquake frequency and magnitude. From 2010 through 2012, more than 300 earthquakes with a magnitude 3 or less occurred compared to an average rate of 21 events/year from 1967 to 2000 (Ellsworth, 2013). In central Arkansas, Horton (2012) was able to identify a previously unknown fault, the Guy-Greenbriar fault, as a result of earthquakes that were triggered by deep well injection.

#### 2.4.2 Treatment options

POTWs, WWTPs, and CWTs are mostly designed for biological treatment and are not designed to deal with the increasing volume nor the challenging characteristics such as the total dissolved solids associated with produced water. Thus, inadequately or improperly treated wastewater may be released into the environment (Vengosh et al., 2014).

Concern has been raised over the concentration of bromide in rivers in Pennsylvania due to the potential health effects associated with disinfection by-products

(Vidic et al., 2013). Along the Allegheny River in Pennsylvania, bromide enrichment was observed downstream from wastewater treatment facilities whose effluent discharge from unconventional Marcellus Shale gas wells had high salinity (TDS up to 120,000 mg/L), various toxic elements (e.g., strontium, barium), radioactive elements, and organic components (Warner et al., 2013; Brantley et al., 2014; Vengosh et al., 2014). Despite dilution, chloride concentrations were elevated 6000-fold above stream background levels and bromide was found in concentrations 12,000-fold greater than background levels. Bromide concentrations were still elevated above background stream levels ~2 km downstream from the point of wastewater effluent discharge (Vengosh et al., 2014).

The high bromide concentrations present challenges when the water is taken in further downstream for municipal water treatment where there is a potential for the formation of carcinogenic trihalomethanes (THMs) in chlorinated drinking water (Brantley et al., 2014; Vengosh et al., 2014). Along the Monongahela River in Pennsylvania, bromide concentrations have increased downstream from wastewater effluent discharge and the concentration of THMs has also increased in municipal drinking water in Pittsburgh, PA. The sources of contamination were both directly linked to the ineffective removal of bromide and subsequent disposal of produced water from shale gas operations in the Marcellus Shale region (Vengosh et al., 2014).

The disposal of produced water also presents other challenges including, but not limited to, the accumulation of metals, salts, and organics in sediments and soil near disposal sites (Warner et al., 2013; Vengosh et al., 2014). The properties (e.g., solubility, reactivity) of the compounds in the produced water and the physicochemical conditions (e.g., pH, temperature) of surface waters will determine how the compounds interact with

particulate matter or river sediments. As a result of these properties, reactive contaminants may adsorb onto soil, stream, or pond sediment potentially posing long-term environmental and health hazards (Vengosh et al., 2014).

Some produced water, like that generated from the Marcellus Shale, may contain elevated levels of naturally occurring radioactive materials (NORM) in the form of radium isotopes. In western Pennsylvania, radium has accumulated on stream sediments downstream from a treatment facility that handles wastewater from both conventional and unconventional oil and gas operations (Warner et al., 2013). The isotopic ratio of  $^{228}\text{Ra}/^{226}\text{Ra}$  in the stream sediments matches those associated with produced water from the Marcellus Shale, thus linking the radium in the sediment to the disposal of unconventional shale gas wastewater (Warner et al., 2013).

#### 2.4.3 Recycling and reuse of produced water

Reusing produced water either directly, or after dilution or pretreatment, is a promising new method for managing produced water. Produced water generated in the Marcellus Shale region is increasingly being managed through reuse (Vidic et al., 2013). Reusing produced water is an attractive management option especially in areas where deep-injection is limited or unavailable (Gregory et al., 2011). Another benefit of reuse is it helps to reduce the volume of wastewater that requires treatment and disposal. This can greatly reduce the environmental risks associated with disposal while increasing the economic feasibility of shale gas development (Gregory et al., 2011; Vidic et al., 2013).

There are also challenges associated with the reuse of produced water. The chemical constituents of hydraulic fracturing wastewater interacting with the formation water may cause the precipitation of very low-solubility solids such as  $\text{BaSO}_4$  and, to a

lesser extent,  $\text{SrSO}_4$  and  $\text{CaCO}_3$  (Gregory et al., 2011; Vidic et al., 2013). The solids may form in the shale formation, or the wellbore, potentially reducing gas production from the well (Gregory et al., 2011). A low-concentration radioactive waste may also be generated during the treatment process if radioactive radium is present in the produced water. The radium may be incorporated in the solids formed during treatment. The radioactive waste generated would require proper handling and may represent a potential on-site human health risk (Vidic et al., 2013).

Finally, within any shale play, reuse programs represent a temporary solution to wastewater management practices. Reuse is a viable option only as long as there is a net water consumption in a given well field. Once production has peaked in a well field, the rate of hydraulic fracturing declines and the field becomes a net water producer. This occurs because more wastewater is generated at the well field than is needed for hydraulic fracturing activities (Vidic et al., 2013). The resulting wastewater will require subsequent treatment and/or disposal.

In summary, the proper disposal of produced water from unconventional shale gas development especially in the Marcellus Shale region is particularly challenging because of the volume of wastewater generated and the distinctive elevated salinity and radioactivity of the produced water.

## 2.5 Hydrocarbon Resources in a Marine Basin: The Marcellus Shale

Although the quantity of the shale gas resource is significantly smaller in North Carolina; the Marcellus Shale can serve as an analog to increase our understanding of the impacts of shale gas development so that we can apply that understanding to the Mesozoic basins in North Carolina. The chemical characteristics of produced water vary

depending on the geographic location of the basin and the geologic formation from which the waters were produced (Benko and Drews, 2008). Thus, it is hypothesized that the geochemical characteristics of formation water in North Carolina are likely different than those of the Marcellus Shale because of different depositional environments (section 1.4). The distinctive geochemical fingerprint of Marcellus Shale wastewater such as high TDS and elevated levels of radioactivity is primarily reflective of naturally occurring hypersaline formation brines associated with deposition that was occurring in a shallow sea (Soeder and Kappel, 2009; Warner et al., 2013 Brantley et al., 2014; Vengosh et al., 2014). As a result of the non-marine alluvial fan, fluvial, and lacustrine environments present in the Deep River basin, should hydraulic fracturing occur within basin the produced water will likely be characterized as containing lower concentrations of TDS.

#### 2.5.1 Location and extent of the Marcellus Shale

The Marcellus Shale is the most expansive shale gas play in the U.S. covering an area of 240,000 km<sup>2</sup> (95,000 mi<sup>2</sup>) (Kargo et al., 2010). The Marcellus Shale spans 6 states extending from its northern reaches in west central New York on a northeast to southwest trend down into Pennsylvania, Ohio, and West Virginia with lesser portions in Maryland and Virginia (Figure 7) (Arthur et al., 2008). The shale is estimated to vary in thickness from 50-200 ft. with an estimated production depth between 4,000 to 8,500 ft (NETL, 2013). Current gas-in-place estimates for the Marcellus Shale are around 1,500 tcf (Ground Water Protection Council, 2009). Gas-in-place estimates include both recoverable and non-recoverable gas. With current technology, recent estimates suggest technically recoverable reserves as high as 500 tcf (Kargo et al., 2010).

Due to its large resource potential, the Marcellus Shale is an important shale gas

play in the United States. The first economically productive well was drilled by Range Resources Corporation in 2005. Since that time, thousands of wells have been drilled across Pennsylvania, northern West Virginia, and eastern Ohio (NETL, 2013). As a result, there have been numerous scientific studies undertaken to improve the overall understanding of the Marcellus Shale and the Appalachian basin where it is located.

### 2.5.2 Depositional history of the Marcellus Shale

The Marcellus Shale is located within a thick wedge of Devonian age sedimentary rocks in the Appalachian basin (Soeder and Kappel, 2009). The Marcellus Shale, an organic-rich black shale, was deposited approximately 380 million years ago (Engelder and Lash, 2008; Moss, 2009). At the time of deposition, significant lithospheric plate movement was occurring as the present continents of North America and Africa, and an intervening micro-continent known as Avalonia, were moving toward each other along a convergent boundary. These continents were once part of larger lithospheric plates known as Laurentia and Gondwana, respectively. A shallow (less than 200 m) interior sea, possibly the result of unusually high sea levels, existed in the area that now makes up the eastern United States west of the Appalachian Mountains (Soeder and Kappel, 2009). It was in this shallow sea, an area presently referred to as the Appalachian Basin, that the clay and organic matter that would later form the Marcellus Shale were deposited.

As deposition was occurring in the shallow sea, Avalonia was continuing to move toward Laurentia which caused extensive thrust faulting and crustal thickening along the edge of the continent. The thickening at the edge of Laurentia and resulting Acadian highland created a substantial load along the continental margin which caused the floor of

the Appalachian basin epicontinental sea to sink below a pycnocline. A pycnocline is a sharp boundary in the ocean water column that separates warmer, oxygenated water above from cooler, oxygen-deficient water below (Knippenberg, 2011). As thrust loading continued, many fluvial systems were delivering nutrient-rich water as well as clastic sediments to the basin. As a result of the nutrient and sediment flux, the sediments that were accumulating at the bottom of the shallow sea, below the pycnocline, had a high concentration of total organic carbon (TOC), therefore, forming an organic-rich black shale. The lack of oxygen along the seafloor helped preserve the organic material thus assisting in the eventual formation of hydrocarbons.

Over time, the fluvial systems reorganized and sedimentation rates in the basin increased so gray shale covered the black shale (Engelder and Lash, 2008). As the regional depositional environment changed over time due to the proximity of an active plate boundary, coarser-grained rocks such as siltstone and sandstone prograded over the shales. As a result of a later relative sea level rise, carbonates such as limestone were also deposited. A cycle of thrust loading and subsequent deposition repeated at least eight times over the next 20 million years resulting in thick wedge-shaped deposits that are thicker in the east and thin to the west (Roen, 1984). These cycles resulted in basal carbonaceous shales overlain by clastic rocks which were mostly silty shales, coarsening up into siltstones and sandstones, which were in turn overlain by carbonates. The burial of the black shale layers caused temperatures and pressures to increase to the point where natural gas was able to form.

In summary, the Marcellus Shale can serve as an analog to increase our understanding of the impacts of shale gas development. Additionally, the hypotheses of

the study propose that the formation water in North Carolina will have different geochemical characteristics from the Marcellus Shale as a result of different depositional environments.

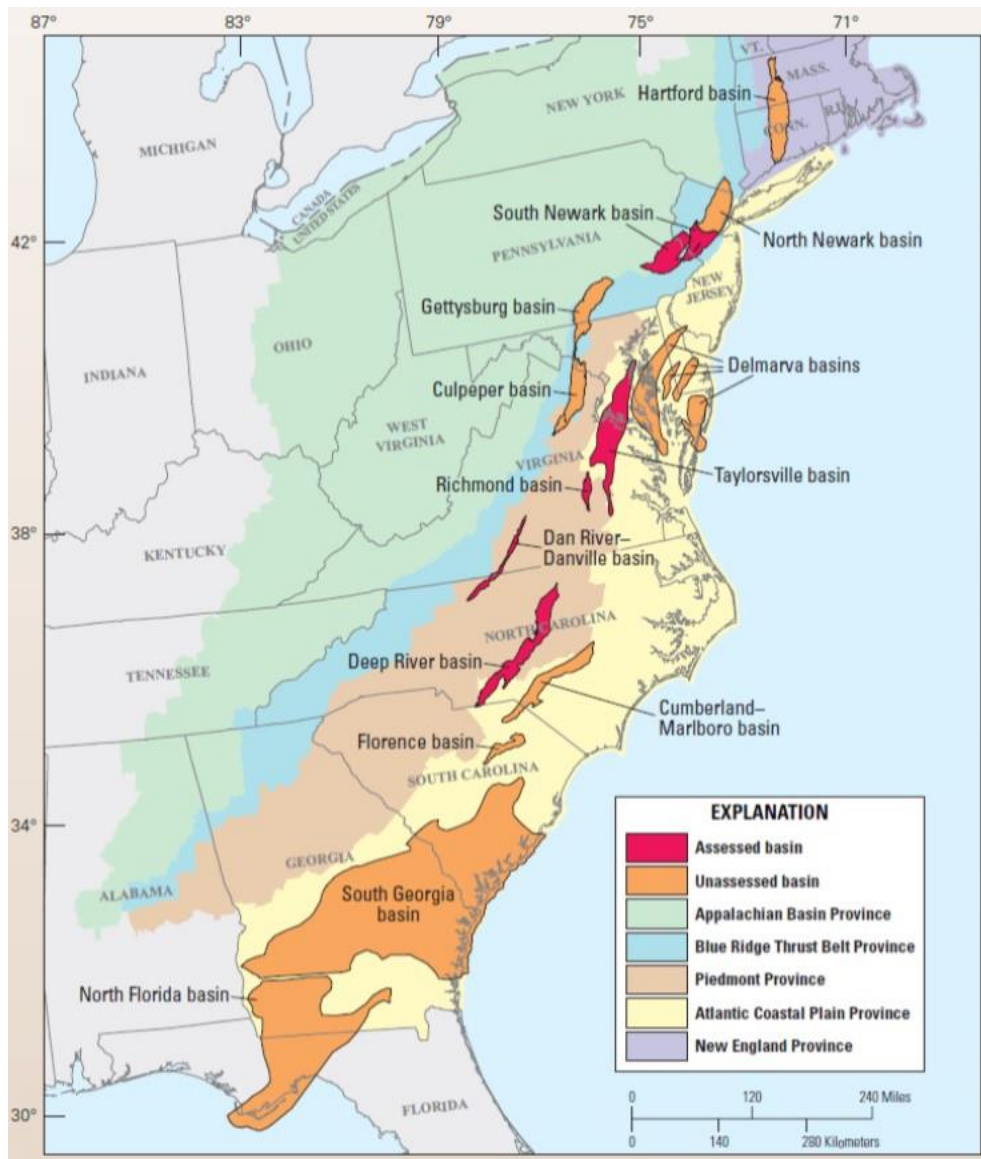


Figure 2: Map of the Eastern United States showing the locations of the five quantitatively assessed East Coast Mesozoic basins in red, the nine basins that were not volumetrically assessed in orange, and the U.S. Geological Survey province boundaries. Appalachian Basin Province (green), Blue Ridge Thrust Belt Province (blue), Piedmont Province (brown), Atlantic Coastal Plain Province (yellow), and New England Province (purple). (Source: U.S. Geological Survey, 2012)

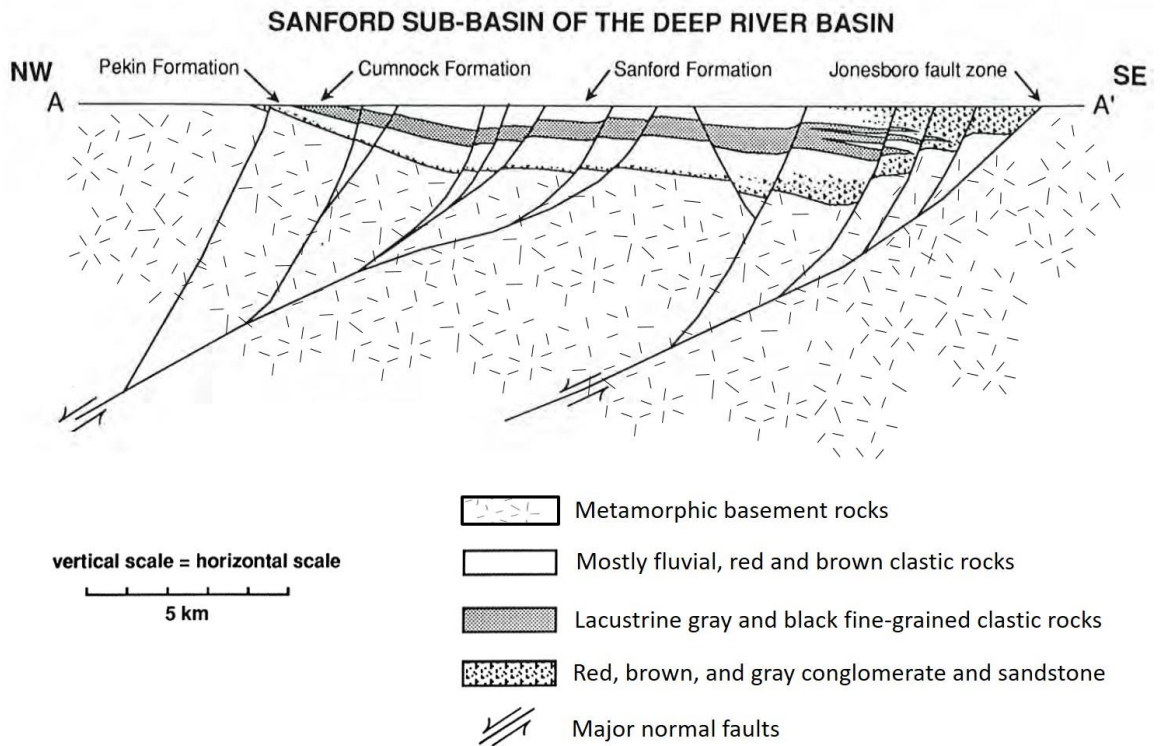


Figure 3: Generalized cross-sections of the Sanford sub-basin of the Deep River basin (Modified from: Olsen et al., 1991).

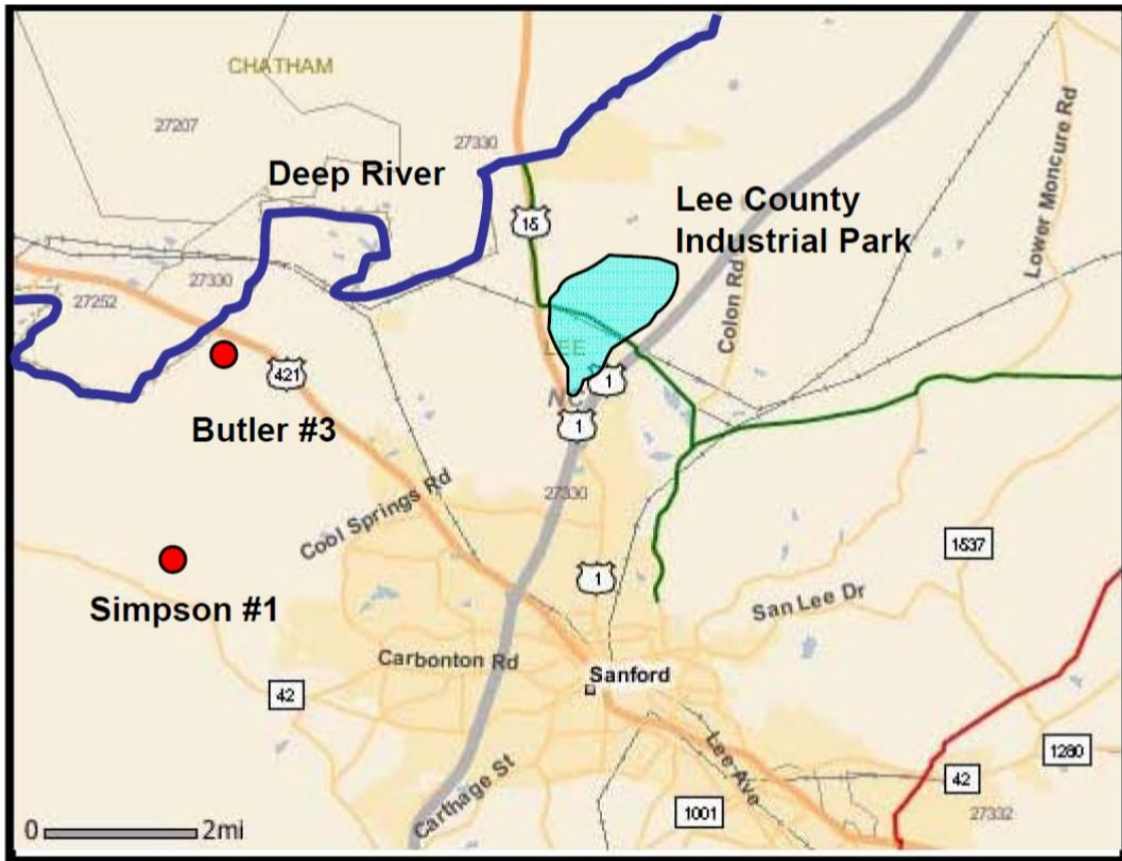


Figure 4: Detailed map of part of Lee and Chatham counties, showing the city of Sanford and the locations of several shut-in and previously drilled wells. Natural gas distribution line is shown as a green line and the regional transmission is shown in red. The Butler #3 well is located within 3.5 miles of a six-inch natural gas distribution line (green) with a four-inch feeder line and multiple large gas users. (Source: Reid and Taylor, 2009, NCGS).

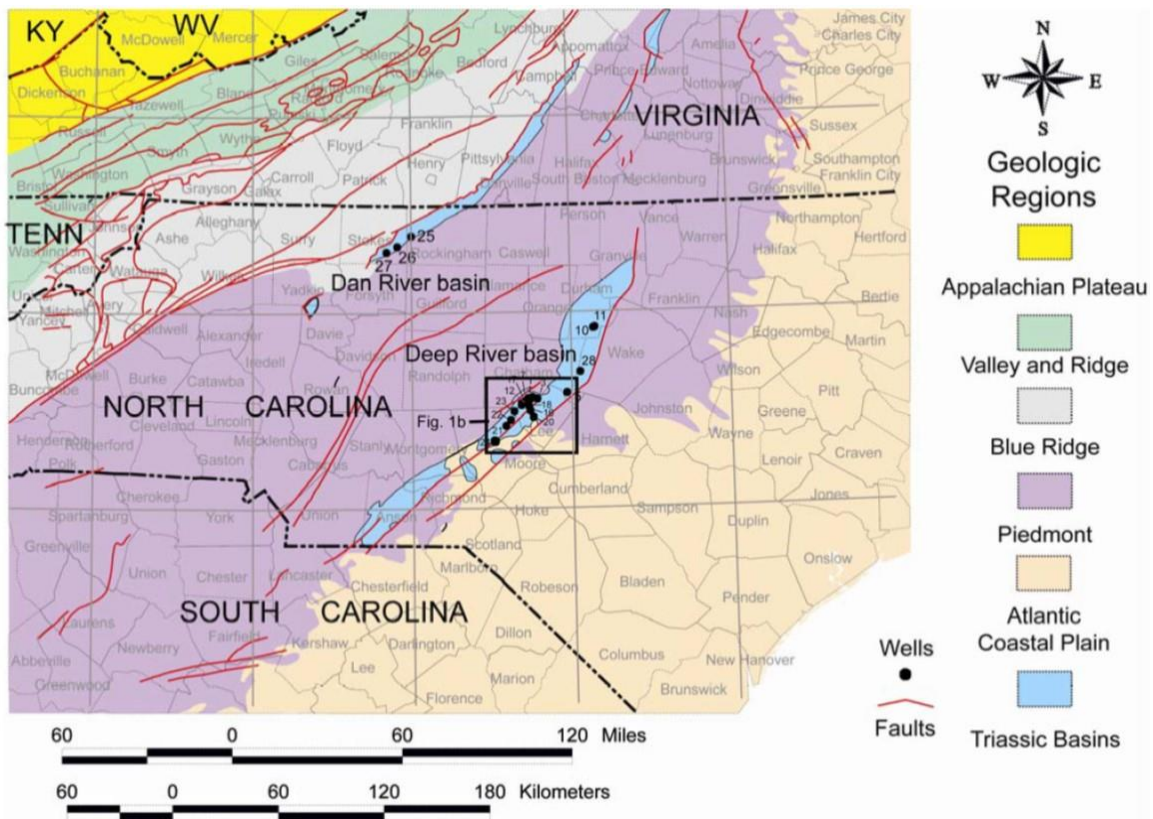


Figure 5: Generalized geologic map of North Carolina and adjacent states, showing major geologic regions and locations of drill holes in Mesozoic basins. The Sanford sub-basin is outlined with a black box (Source: Reid and Milici, 2008, USGS).



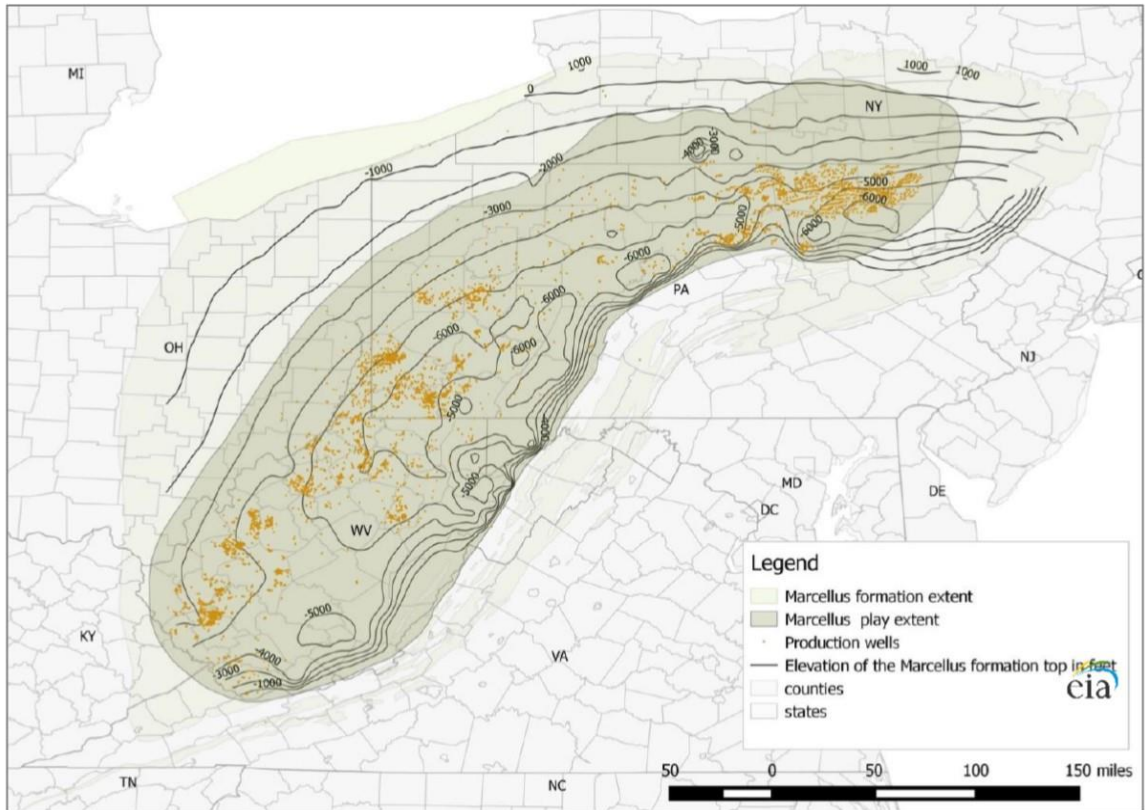


Figure 7: Structure map of the Marcellus Formation (Source: U.S. Energy Information Administration, 2017).

Table 1: East Coast Mesozoic basin assessment results. [BCFG, billion cubic feet of gas; MMBNGL, million barrels of natural gas liquids; TPS, total petroleum system; AU, assessment unit.] Results shown are fully risked estimates. For gas accumulations, all liquids are included as NGL (natural gas liquids). F95 represents a 95-percent chance of at least the amount tabulated; other fractiles are defined similarly. (Modified from USGS, 2012).

Total Petroleum System (TPS) and Assessment Unit (AU)	Field type	Total undiscovered resources							
		Gas (BCFG)				NGL (MMBNGL)			
		F95	F50	F5	Mean	F95	F50	F5	Mean
<b>Taylorsville Basin Composite TPS</b>									
Taylorsville Basin Continuous Gas AU	Gas	516	985	1,880	1,064	16	34	71	37
<b>Richmond Basin Composite TPS</b>									
Richmond Basin Continuous Gas AU	Gas	99	194	382	211	4	10	20	11
<b>Newark Basin Composite TPS</b>									
South Newark Basin Continuous Gas AU	Gas	363	785	1,698	876	1	4	10	4
<b>Deep River Basin Composite TPS</b>									
Deep River Basin Continuous Gas AU	Gas	779	1,527	2,990	1,660	35	75	158	83
<b>Dan River-Danville Basin Composite TPS</b>									
Dan River-Danville Basin Continuous Gas AU	Gas	17	42	106	49	0	0	1	0
<b>Total continuous resources</b>		<b>1,774</b>	<b>3,533</b>	<b>7,056</b>	<b>3,860</b>	<b>56</b>	<b>123</b>	<b>260</b>	<b>135</b>

### 3. SEDIMENTARY PETROLOGY

#### 3.1 Introduction

As discussed in Chapter 1, this study examines lithologic variables such as mineralogy, grain size, and degree of post-depositional alteration and their influence on the geochemical characteristics of formation water. As a result, the purpose of this chapter is to characterize the rock material in the Deep River basin involved in water-rock interactions. Since the mineralogy, grain size, and degree of post-depositional alteration of a deposit is influenced by the depositional environment, the generally accepted interpretations of the depositional environments present in the Deep River basin will first be presented (for example, Reinemund, 1955; Smoot, 1991; Chem-Nuclear Systems, 1993; Clark et al., 2011; Taylor and Reid, 2011; Brazell and Diemer, 2012; Brazell, 2013). The generally accepted interpretations of depositional environments will be supplemented by additional observations concerning the grain size distributions, mineralogy and degree of alteration of representative rock samples from the basin.

#### 3.2 Depositional Environments

The Deep River basin which comprises three sub-basins, from northeast to southwest, the Durham sub-basin, the Sanford sub-basin, and the Wadesboro sub-basin, is one of several rift basins of Mesozoic age along the east coast of the North America (Figures 1 and 2) (Horton and Zullo, 1991; Schlische, 1993; USGS, 2012). The depositional environments that existed in the basins included alluvial fans, axial rivers and associated floodplains, and lakes and swamps in the basin centers (Reinemund, 1955; Olsen et al., 1991; Smoot, 1991; Chem-Nuclear Systems, 1993; Clark et al., 2011; Taylor and Reid, 2011; Brazell and Diemer, 2012; USGS, 2012; Brazell, 2013). Examples of

depositional models used to interpret those environments include the: 1) alluvial fan model, 2) meandering stream model, 3) braided stream model, and 4) lacustrine model.

### 3.3 Fluvial Environments

Fluvial environments include alluvial fans, and axial meandering and braided stream networks all of which are complex systems of erosion, sediment transport, and deposition. Thus, fluvial environments possess a wide variety of landforms and sedimentary deposits (Tucker, 2001). Fluvial sediments range in grain size from conglomerates through sandstones to mudstones. In general, fluvial sandstones are texturally and compositionally immature to mature, where degree of maturity depends on the climate, sediment provenance and transport distance (Tucker, 2001). Fluvial sandstones are generally arkoses and litharenites that are usually sharp-based and cross-bedded. Some flat bedding and cross-lamination may also be present. Fluvial sandstones may be lenticular (filling channels) or laterally more extensive (from channel or point-bar migration) (Tucker, 2001). Fluvial conglomerates usually have a grain-supported fabric and many are polymictic. Fluvial conglomerates are often lenticular, commonly with a crude cross-bedding (Tucker, 2001).

Semi-arid climates usually generate fluvial sediments that are red in color from the diagenetic formation of hematite (Walker and Cant, 1984; Tucker, 2001).

Additionally, calcretes are evidence of soil formation in fluvial successions formed in semi-arid climates with low water tables. In contrast, humid conditions with high water tables produce vertisols with rootlets, siderite nodules, and possibly coal (Walker and Cant, 1984; Tucker, 2001). The fluvial environments present in the Deep River basin (including alluvial fans and meandering and braided streams) are discussed in greater detail below.

### 3.3.1 Alluvial fan environments

Alluvial fans are wedge-shaped aprons of sediment adjacent to upland areas such as those resulting from lithospheric uplift at continental margins and from intracontinental faulting (Figure 8) (Rust and Koster, 1984; Tucker, 2001). Alluvial fans are clastic bodies that occur in many fault-bounded basins, such as grabens, half-grabens, and pull-apart basins, and they build out onto a valley floor comprising playas, floodplains, and even lakes (Rust and Koster, 1984; Tucker, 2001). Alluvial fan deposits associated with extensional rifting can be relatively thin if the rifting process is short-lived resulting in wearing down of the adjacent fault scarps thereby diminishing relief (Rust and Koster, 1984). Alternatively, if tectonic rifting is a prolonged process, the associated alluvial fan deposits can be 100s to 1000s of meters thick since relief is maintained for extended periods. In either case, due to a short transport distance compared to other fluvial sediments, the sediments of alluvial fans tend to be coarser, consisting of gravel and coarse sand, and are poorly sorted and compositionally immature (Berendsen, et al., 1988; Tucker, 2001). Alluvial fans are characterized by debris flow deposits in the proximal portions of the fan, a rapid fining in the downslope direction, and replacement of debris flow deposits by traction load deposits (Figure 8) (Rust and Koster, 1984; Berendsen et al., 1988; Tucker, 2001). These rapid downslope facies changes, a principal feature of alluvial fans, creates a proximal-, mid-, and distal- fan facies (Rust and Koster, 1984; Chem-Nuclear, 1993; Tucker, 2001).

In alluvial fan systems, deposition is dominated by water-laden debris flows, channelized stream flows, and sheet floods (Figure 8) (Rust and Koster, 1984; Tucker, 2001). Sediments deposited by debris flows generally lack erosive bases, and are both lenticular in shape (filling channels) and tabular in shape (deposited on fan aprons outside

of the channels). Debris flow deposits consist of abundant fine sediment acting as a matrix, together with clasts up to boulder size creating muddy matrix-supported conglomerates. Stream floods occurring in a network of channels on the surface of the fan deposit lenticular, trough cross-bedded, clast-supported, possibly imbricated, pebbly sands and gravels. Stream channel deposits are mostly found in the proximal- to mid-fan region. Sheet flood deposits are thin, laterally continuous beds of sand and gravel with sharp bases. These deposits are commonly found on more distal parts of the fans, and may show graded bedding, and planar and cross-stratification (Berendsen et al., 1988; Tucker, 2001). Like the sediments associated with the floodplains of meandering streams, alluvial fan sediments may undergo extensive soil formation. For example, a red coloration and evaporitic paleosols suggest a semi-arid to arid climate (Rust and Koster, 1984; Berendsen et al., 1988; Tucker, 2001).

In alluvial fan successions, vertical changes in facies may indicate active fan progradation such as may occur when faulting causes elevation of the source area or basin subsidence. The change in relief rejuvenates the alluvial system and the fan progrades resulting in a broadly coarsening and thickening upward sequence (Rust and Koster, 1984; Tucker, 2001). As the effects of rejuvenation wear off, and relief on the border faults is reduced, the grain sizes transported in the fan system diminishes. This results in a broadly fining and thinning upward sequence that is deposited as the fan retrogrades (Rust and Koster, 1984; Tucker, 2001). Periodic faulting may cause a cyclic repetition of coarsening and thickening upward units (progradation) and fining and thinning units (retrogradation) (Rust and Koster, 1984; Berendsen et al., 1988).

### 3.3.2 Meandering stream environments

Meandering streams have two distinct sub-environments: 1) channel sub-environments and 2) overbank sub-environments (Figure 9) (Tucker, 2001). Sandy channel deposits are usually trough cross-bedded resulting from the migration of large dune structures on the channel floor and on the lower parts of the point bars. Flat-bedded sands associated with the upper flow regime may be deposited on the point bar, while in shallower parts of the flow, higher on the point bar, finer cross-laminated sands with mud drapes and lenses are common (Figure 9) (Walker and Cant, 1984; Tucker, 2001).

Overbank sub-environments associated with meandering streams include levees, floodplains and crevasse splays. Overbank flooding carries suspended sediment onto floodplains resulting in laminated mudstones (Tucker, 2001; Chem-Nuclear Systems, 1993). Desiccation cracks may form in the silt and mud after the retreat of flood waters (Walker and Cant, 1984). Coarser sediments are taken onto floodplains during overbank flood events and produce sharp-based, locally erosive crevasse splays which are generated as crevasse channels cut through the main channel bank and its levees (Walker and Cant, 1984; Tucker, 2001). The combination of overbank flooding and crevasse splays results in thin-bedded sandstones interbedded with floodplain silts (Figures 9). Floodplains are often sites of soil formation, swamps, lakes, and even salt precipitation, if the climate conditions are appropriate (Walker and Cant, 1984; Tucker, 2001).

Meandering stream deposits usually consist of in-channel deposits (lateral accretion) and overbank fines (vertical accretion) (Figures 9 and 10) (Walker and Cant, 1984). The lateral migration of a meandering stream through bank erosion and point-bar deposition generates a fining-upward unit, or storey (Walker and Cant, 1984; Tucker,

2001). If a channel system remains in one part of a floodplain for extended periods while net aggradation is taking place, then multiple point bar deposits can be stacked one on top of the other in a multi-storey sandstone deposit (Figures 9 and 10). When the channel abandons that position on the floodplain by avulsion, then the channel belt composed of the multi-storey sandstone can be buried beneath vertical accretion deposits. Sequences of meandering stream deposits can, therefore, consist of many multi-storied sandstones (Figures 9 and 10) (Walker and Cant, 1984; Tucker, 2001).

### 3.3.3 Braided stream environments

Braided streams, which consist of many broad, shallow channels that branch and rejoin, are the most common fluvial environment in nearly all rift basins (Figures 11 and 12) (Walker and Cant, 1984; Lorenz, 1988; Tucker, 2001). This is due to the availability of coarse sediment and the relatively steep gradients present in the basins (Chem-Nuclear, 1993; Tucker, 2001). Sandy braided streams are morphologically complex and include bed forms such as sinuous-crested dunes on the channel floor, small straight-crested to linguoid-shaped sand bars, large bar complexes known as sandflats, and vegetated islands and floodplains (Figure 11) (Cant and Walker, 1978; Walker and Cant, 1984; Tucker, 2001).

The deposits of sandy braided streams are dominated by channel and bar facies (Figure 12) (Tucker, 2001). The channels of braided streams do not conform to the simple pattern illustrated by meandering streams and often vary in depth and width (Walker and Cant, 1984). Channel lag deposits are common on channel floors and sand transported as bedload may be deposited above the lag. During high stage, the position of the channels may be altered as sand bars and dunes migrate downstream resulting in large

sets of planar, tabular cross-bedded sandstones and trough cross-bedded sandstones, respectively (Figure 11) (Walker and Cant, 1984; Tucker, 2001). During flood events, small dunes and sand waves may form in shallow channels and on bar tops when these areas are submerged.

Some channel deposits show a fining upwards of grain size and may be capped by fine-grained overbank deposits, but unlike meandering streams, braided stream deposits are characterized by more irregularities in grain size trends and overbank deposits that are less fine grained (Figure 11) (Tucker, 2001). Additionally, the vertical accretion deposits such as shales and cross-laminated siltstones interbedded with mudstones tend to be patchy, laterally discontinuous, and of no great thickness in most braided stream systems (Figure 12) (Walker and Cant, 1984; Miall, 1996; Tucker, 2001). If formed, the overbank deposits are only rarely preserved due to the relatively frequent lateral migration of channels. Frequent alteration of the position of channels is documented by an abundance of erosional scours with intraclasts and possible crude cross-bedding found in many braided stream sequences (Miall, 1977; Tucker, 2001). Thus, on a large scale, sandy braided streams are dominated by laterally extensive intercutting channel and bar deposits formed from coalescing bars and sand flats unconfined by fine-grained sediment (Figure 12) (Walker and Cant, 1984; Tucker, 2001). This contrasts with meandering stream depositional environments which, as previously discussed, tend to form elongate shoestring sand bodies surrounded by overbank deposits such as siltstones and mudstones (compare Figures 10 and 12) (Walker and Cant, 1984; Tucker, 2001).

### 3.4 Lacustrine Environments

Sladen (1994) distinguished two major categories of lakes: 1) relatively long-lived (e.g. for more than 1 Ma), tectonically-induced lakes occurring in flexural and

extensional basins, and 2) relatively short lived (e.g lasting only a few thousand to a few hundred thousand years), floodplain lakes occurring between river channels and distributaries. Lakes can be hydrologically open (ones with an outlet and relatively stable water levels) or hydrologically closed and sites of evaporite and limestone deposition (Tucker, 2001). The natural evolutionary sequence of rift-basin development could result in changes in whether lakes are hydrologically open or closed (Berendsen et al., 1988). The distribution of lake deposits in half-grabens is usually strongly asymmetrical suggesting that the depocenter of the lake was located near the faulted basin margin (Figure 13) (Sladen, 1994).

The relatively quiet water of a lake environment cannot move coarse sediment by fluid flow. Therefore, where a sediment-laden river enters a lake, a Gilbert-type delta composed of coarse (proximal) to fine (distal) sediment often forms (Tucker, 2001). These deltas typically have a steep slope (delta front) where sand and gravel cascade downward producing sloping foreset beds. Coarse topset beds and finer bottomset beds may also be well developed. Coarse sediments are also deposited along lake shorelines and muds on deep-lake basin floors (Figure 13). The sands and gravels of the lakeshore are generally less well sorted and rounded compared to their marine counterparts due to less wave activity and no tides. Finer-grained sediments along lakeshores and in nearshore environments may show evidence of wave-formed ripples, desiccation cracks, and syneresis cracks (Tucker, 2001). On the deep lake floors, graded beds with scoured bases are produced as sediment-laden river underflows cut sub-lacustrine channels (Figure 13). These sediment-laden underflows are denser than the ambient lake water, therefore they result in sediment gravity flows (turbidity currents) which result in the

graded beds (turbidites) on the lake floor. Fine-grained sediments such as silt and clay can reach the center of the lake as suspended sediments that gradually settle out of the water column. Settling of these fine-grained sediments out of suspension commonly produces finely-laminated sediments (rhythmites) which may occur with the deposits of low-density turbidity currents. (Tucker, 2001).

### 3.5 Lithofacies Descriptions

The depositional models provide a powerful method for understanding the occurrence and range of lithofacies that are present in the sub-basins of the Deep River basin (Figure 13). Examples of lithofacies found in the Deep River basin include:

- Clast- and matrix-supported conglomerates
- Thin-bedded (flat-laminated) sandstones
- Cross-bedded sandstones
- Cross-laminated sandstones and siltstones
- Laminated siltstones and mudstones
- Massive siltstones and mudstones
- Organic-rich mudstones and shales
- Other features – most of which are indicative of paleosols (roots, burrows, carbonate nodules, mottling, and waxy “slickensides”)

#### 3.5.1 Clast- and matrix-supported conglomerates

Clast-supported conglomerates have pebbles that are in contact and have little matrix (Figure 14) (Tucker, 2001). They are commonly deposited in braided and meandering stream and alluvial fan environments. In braided and meandering stream environments, clast-supported conglomerates are commonly deposited as channel lags at the base of, or within sandy, fining-upward sequences (Figures 9 and 11). Channel lag deposits are massive, relatively thin, sharp-based beds. The clast-supported

conglomerates of channel lags are typically coarser and more poorly sorted than the associated channel deposits (Chem-Nuclear, 1993; Tucker, 2001). Cross-stratified, clast-supported conglomerates in association with cross-stratified sandstones may have formed as large (1 to 3 foot) dunes migrated downstream in perennial, seasonal, or ephemeral streams (Chem-Nuclear, 1993). In alluvial fan environments, clast-supported conglomerates may be deposited as cross-bedded, stream flood deposits (Figure 8). Stream flood deposits, predominantly located in the proximal- and mid-fan regions, are usually confined to stream channels and may show imbrication (Tucker, 2001.)

Matrix-supported conglomerates have pebbles floating in a matrix (Figure 15) (Tucker, 2001). Similar to clast-supported conglomerates, they are commonly deposited in braided and meandering stream and alluvial fan environments where they form distinct beds with sharp basal and upper contacts (Chem-Nuclear, 1993; Tucker, 2001). Like clast-supported conglomerates, matrix-supported conglomerates may be deposited as channel lags (Figures 9 and 11) (Chem-Nuclear, 1993). In addition to forming in the channels of braided and meandering streams, these channel lags may also be deposited in the network of channels cutting across the surface of an alluvial fan (Figure 8) (Chem-Nuclear, 1993).

### 3.5.2 Thin-bedded (flat-laminated) sandstones

This lithofacies includes thin-bedded sandstones such as those generated by crevasse splay events and flat-laminated sandstones such as the topset beds of a delta building into a lake. Thin-bedded (flat-laminated) sandstones form in meandering stream, alluvial fan, and lake environments. In meandering stream environments, crevasse splay deposits are sharp-based, thin-beds of coarse sandstones interbedded with fine-grained

floodplain deposits (Figure 9) (Walker and Cant, 1984; Tucker, 2001). Flat-laminated sands associated with the upper flow regime may be deposited on the point bar of meandering streams (Tucker, 2001). Thin-bedded sandstones with possible graded bedding and horizontal stratification may occur in sheet flood deposits on the distal portions of alluvial fans (Figure 8). These thin, laterally continuous beds of sand and gravel formed during flood events as waters overtopped the banks of the channel and spread laterally across adjacent areas. (Chem-Nuclear, 1993; Tucker, 2001). In a lake environment, flat-laminated sandstones may be deposited as topset beds on a delta (Figure 13). Additionally, on the deep floors of lakes, thin-bedded, possibly flat-laminated, sandstones may be deposited as graded beds with scoured bases. Similar to marine basin turbidity currents, coarse materials spill out of sublacustrine channels as sediment-laden rivers enter into a lake and these materials are deposited as graded beds (Tucker, 2001).

### 3.5.3 Cross-bedded sandstones

Cross-bedded sandstones occur in meandering and braided stream, and alluvial fan environments (Chem-Nuclear, 1993; Tucker, 2001). In meandering and braided stream environments, sandy channel deposits are usually trough cross-bedded resulting from the migration of large dune structures on the channel floor and on the lower part of the point bars (Figure 16) (Walker and Cant, 1984; Tucker, 2001). In alluvial fan environments, clast-supported, cross-bedded, sandstones may be deposited as stream flood deposits. Stream flood deposits, predominantly located in the proximal- and mid-fan region, are usually confined to the stream channel and may show imbrication (Figure 8) (Tucker, 2001.)

#### 3.5.4 Cross-laminated sandstones and siltstones

Cross-laminated sandstones and siltstones form in meandering stream and lake environments (Figure 17) (Walker and Cant, 1984; Chem-Nuclear, 1993; Tucker, 2001). In a meandering stream environment, finer cross-laminated channel sands with mud drapes and lenses are common in shallower parts of the flow, higher on the point bar (Figure 9) (Walker and Cant, 1984; Tucker, 2001). In lake environments, deltas formed at the mouths of rivers have a steep slope (delta front) where sand cascades downward producing cross-laminated foreset beds. Cross-laminated sandstones and siltstones may also be deposited along lake shorelines and in nearshore environments showing evidence of wave-formed ripples (Tucker, 2001).

#### 3.5.5 Laminated siltstones and mudstones

Laminated siltstones and mudstones form in meandering stream, alluvial fan, and lake environments. In meandering stream environments, overbank flooding carries suspended sediment onto floodplains resulting in laminated mudstones (Figure 18) (Tucker, 2001; Chem-Nuclear Systems, 1993). Desiccation cracks may form in the silt and mud after the retreat of flood waters (Walker and Cant, 1984). In alluvial fan environments, laminated siltstones and mudstones may be deposited in inter-channel areas of distal fan fringes (Chem-Nuclear, 1993). In a lake environment, laminated siltstones and mudstones may be deposited as the finer bottomset beds of a delta building into a lake. Additionally, fine-grained sediments such as silt and clay from low-density turbidity currents and settling out of suspension may generate sediments (rhythmites) near the center of the lake (Figure 13) (Tucker, 2001).

#### 3.5.6 Massive siltstones and mudstones

Massive siltstones and mudstones form in meandering stream, alluvial fan, and lake environments. The term massive is used to describe beds that are homogenous in composition and that lack internal stratification or other sedimentary structures (Tucker, 2001). Massive bedding may have formed as a result of rapid deposition from a high-density, sediment gravity flow or as a result of the destruction of original internal structures due to bioturbation, recrystallization-replacement, or dewatering. (Tucker, 2001). In meandering stream environments, massive bedding may form in overbank deposits including floodplain and crevasse splay deposits. These deposits are often sites of soil formation, therefore, bioturbation may have destroyed any original internal structures (Walker and Cant, 1984; Tucker, 2001). In alluvial fan environments, massive bedding may occur in gravel beds in the proximal-fan region, or in fine sandy mud or mud in the distal-fan regions. The massive gravel beds result from debris flows whereas the massive fine sandy mud or mud may be a consequence of soil formation and bioturbation (Rust and Koster, 1984; Tucker, 2001). In lake environments, as with meandering stream environments, soil formation and bioturbation may have destroyed any original internal structures generating massive siltstones and mudstones (Tucker, 2001).

### 3.5.7 Organic-rich mudstones and shales

Deep-water lacustrine systems were sites where dark gray to black fine-grained, organic-rich mudstones and shales accumulated (Figure 19) (Olsen et al., 1991). Tectonically-induced lakes such as those occurring in extensional basins were likely long-lived and sufficiently deep that they became thermally stratified (Horton and Zullo, 1991; Schlische, 1993; Sladen, 1994). As clay was deposited on the bottoms of these

deep lakes, organic matter, such as the remains of algae and plankton also settled to the bottom creating an organic-rich, muddy ooze. If the organic-rich, muddy ooze was deposited in anoxic conditions, the organic material would likely be preserved. Over time, the ooze may lithify into a dark gray to black organic-rich mudstones or shale (Chem-Nuclear, 1993; Marshak, 2012). The dark coloration of these mudstones and shales is an indication of the presence of organic matter (Maley, 2005).

#### 3.5.8 Other features

For the purposes of this study, this lithofacies category includes features that are considered to be indicative of paleosols in sedimentary rocks. This includes features such as roots and root traces (Figure 20), burrows, carbonate nodules (Figure 19), distinctive colors, color mottling (Figure 21), blocky textures, and “waxy” slickensides (Chem-Nuclear, 1993; Tucker, 2001). Soils developed upon/within sediments are relatively common in the geological record (Tucker, 2001). Paleosols, or ancient soils, represent a stable surface of the past that supported vegetation and other lifeforms. Thus, roots, root traces, and the preserved burrows of lifeforms are reliable evidence of an ancient soil (Maley, 2005). Paleosols may be present in sediments deposited in meandering stream, alluvial fan, and lake environments.

Two common types of soils are calcrete soils and clay-rich soils such as vertisols (Tucker, 2001). Calcretes which may vary from scattered to densely packed carbonate nodules, are evidence of soil formation in semi-arid climates (Walker and Cant, 1984; Tucker, 2001). Additionally, semi-arid conditions may cause soils to have a red, yellow, brown, or black coloration from the diagenetic formation of hematite and possibly, manganese oxides (Walker and Cant, 1984; Tucker, 2001; Maley, 2005). Humid

conditions with high water tables produce vertisols that are generally massive with rootlets, siderite nodules, and possibly coal (Walker and Cant, 1984; Tucker, 2001). Seasonal shrink-swell processes causing the repeated desiccation of expandable clays may produce “waxy” or slickensided surfaces, vertical fractures, and a blocky texture known as peds (Chem-Nuclear, 1993; Tucker, 2001). Color mottling in poorly drained, water-saturated soils may result in a grayish or bluish coloration as iron and manganese are reduced. Mottles in a poorly drained soil where the water table fluctuates may be gray, reddish brown, or yellow (Maley, 2005).

### 3.6 Methods for Acquiring Compositional Data

One hundred eighty-seven samples were collected for analysis from the Deep River basin. Fifty-five samples were from the Wadesboro sub-basin, 40 samples were from the Sanford sub-basin, and 92 samples were from the Durham sub-basin (Figure 22). The samples collected from the southern-most basins, the Wadesboro and Sanford sub-basins, were surface samples collected in the field including from road and stream cuts and from quarry exposures. 41 of the 55 samples from the Wadesboro sub-basin were collected as part of a previous study conducted by Brazell (2013). The samples from the Durham sub-basin are 1-inch diameter core sub-samples that were taken from larger diameter cores drilled by the North Carolina Geological Survey and stored at the Coastal Plain Office Core Repository.

The steps involved in collecting the additional observations concerning the sedimentary petrology of the Deep River basin samples are portrayed in Figure 23. Those steps include the use of X-ray diffraction (XRD), petrographic microscope, and an

organic elemental analyzer. Grain size observations were made using a hand lens and grain size comparator.

Several methods of analysis used for this study including XRD, the analysis of TOC with an organic elemental analyzer, and the sequential extractions require a similar sample preparation. The first step in sample preparation for these analyses was the disaggregation of the rock sample (Figure 23). In this step, all samples, regardless of lithology, were treated the same. Rock samples collected in the field were fragmented into coarse pieces using a rock hammer. Samples, including field and core samples, that were difficult to hand crush were initially crushed using a jaw crusher. The jaw crusher was adjusted such that the rock was crushed to the size of granules or pebbles, but not powdered. A small amount (20-30 g) of each fragmented rock sample was crushed in order to increase the specific surface area of the grains so that subsequent preparation steps were more effective. To crush the sample, a large mortar and pestle were used instead of grinders, shatter-boxes, or ball mills. The use of crushing devices other than a mortar and pestle can cause changes of phase and can potentially lead to strains on the crystal structure which may lead to XRD line broadening (Moore and Reynolds, 1997).

Once the samples were ground to a fine powder using a mortar and pestle, each sample was passed through a 100-mesh (0.149 mm) sieve (Figure 23). After passing through the 100-mesh sieve, each sample was split using a sample splitter. One half of the sample was labeled 100-mesh and was archived for analysis using the sequential extractions, and select dark gray to black fine-grained samples were analyzed for total organic carbon. The other half of the sample split was passed through a 325-mesh (0.044 mm) sieve (Figure 23). Material that passed through the 325-mesh sieve was labeled 325-

mesh and was archived for analysis with XRD. The material that passed through the 100-mesh sieve but did not pass through the 325-mesh was labeled 'residue' and was archived.

### 3.7 Sedimentary Petrography

Petrography is a reliable, non-destructive method used to identify and quantify minerals present in rocks and soils, with relatively high spatial resolution (Lynn et al., 2008; Raith et al., 2011). The use of polarized-light microscopy allows the mineral grains to be studied within their textural framework. Observations about specific textural characteristics such as grain size, shape, sorting, roundness, and the grain fabric of a sample provide clues to the history of the formation of the material in addition to information about its chemical composition. Thus, in many respects, petrography has an advantage over bulk-analytical methods that require the use of powdered samples for mineral and chemical analysis with XRD or XRF, respectively (Raith et al., 2011). As with all methods of analysis, limitations exist with polarized-light microscopy such as challenges associated with the identification of opaque minerals such as hematite and magnetite, red or yellow coatings of iron oxides on grains obscuring the passage of light, and the identification of mineral grains that are too fine-grained (Lynn et al., 2008; Raith et al., 2011). For the latter issue, the use of XRD permits the identification of mineral phases in fine-grained materials.

Grain sizes ranging from fine sand (0.125-0.25mm) to coarse silt (0.02-0.05mm) are well-suited for petrographic analysis (Lynn et al., 2008). Fine-grained material such as fine silt and clay are too small to accurately observe optical properties and coarse material such as medium sands may be so large that statistically significant point

counting cannot be achieved due to a lack of grains to count (Harwood, 1988; Lynn et al., 2008). The identity and quantity of the minerals present, the modal composition, of a sample is normally reported as percentages of grains counted in a thin section (Lynn et al., 2008). At least 300 grains per thin section should be identified by systematically traversing the central portion of a slide and identifying any grain under the crosshairs. This method is referred to as the line-count method or as spot identification (Harwood, 1988; Lynn et al., 2008). A tally of 300 to 500 points using the line-count method will result in statistically accurate percentages of the components present (Ingersoll et al., 1984; Harwood, 1988; Lynn et al., 2008).

This study used a modified version of the Gazzi-Dickinson method of point counting (Ingersoll et al., 1984). The primary way the Gazzi-Dickinson method differs from traditional methods of pointing counting is that sand-sized grains occurring within larger lithic clasts are classified in the category of the mineral, rather than the category of the clast (Ingersoll et al., 1984; Harwood, 1988). The Gazzi-Dickinson method of point counting reduces compositional dependence on grain size by eliminating the variation in modal composition resulting from the breakage of large fragments into their constituent grains. Thus, the method produces more uniform results for any grain size, including unsorted samples (Dickinson, 1970; Ingersoll et al., 1984). Additionally, the Gazzi-Dickinson method reduces the effects of alteration on composition because all monocrystalline grains are classified similarly whether they occur as phenocrysts or discrete grains. Thus, the method yields point counts that are less ambiguous, especially for diagenetically altered sandstones such as graywackes. In summary, the Gazzi-Dickinson method of point counting reduces compositional dependence on grain size and

the effects of alteration on composition thereby allowing an accurate reconstruction of original detrital compositions (Ingersoll et al., 1984). Because sand-sized grains occurring within larger lithic clasts are classified in the category of the mineral, rather than the category of the clast, the Gazzi-Dickinson method is likely to be better for relating sandstone composition to tectonic setting (Tucker, 2001). Additional information about the minerals identified in this study and the mineral groupings based, in part, on the Gazzi-Dickinson method of point counting is located in a subsequent section.

A suite of 18 very fine (0.0625-0.125mm) to very coarse (0.50-2.00mm) sand-sized samples and one fine to medium pebble (4.0-32.0mm) were chosen for petrographic analysis (Table 2). Several samples were collected from each sub-basin comprising the Deep River basin to ensure a basin-wide analysis of coarse-grained lithologies. Grain sizes ranging from fine sand (0.125-0.25mm) to coarse silt (0.02-0.05mm) are well-suited for petrographic analysis (Lynn et al., 2008). Although some of the samples used in this study are outside these suggested grain size parameters, specifically some samples are too coarse, at least 300 grains were counted per thin section resulting in accurate percentages of each mineral present (Ingersoll et al., 1984; Harwood, 1988; Lynn et al., 2008). The thin sections necessary for analysis were manufactured at National Petrographic Services in Texas using the methodology outlined in Lynn et al., (2008) and Nesse (2004).

### 3.8 Petrographic Analyses: Mineral Identification and Grouping

The suite of 19 sedimentary samples analyzed using polarized-light microscopy have a relatively homogenous composition with little diversity among the mineral groups identified (Appendix B). Petrographic analyses revealed 9 mineral groups including 1) quartz, 2) feldspars, 3) mica, 4) chlorite, 5) carbonate, 6) matrix, 7) opaque minerals, 8)

other, and 9) unknown (Table 2). These mineral groups are based on the Gazzi-Dickinson method of point counting (Ingersoll et al., 1984), but have been modified to maximize the information relevant for this study. For example, the Gazzi-Dickinson method does not count matrix toward point counting totals whereas, for this study, the amount of matrix, assumed to be predominantly fine-grained clay minerals, is pertinent information for the sequential extractions that were carried out as part of this study (Tessier et al., 1979; Ingersoll et al., 1984; Stewart et al., 2015). The sequential extractions are discussed in greater detail in Chapter 4. The minerals identified using petrographic analysis and the basis for the mineral groups selected for this study are discussed below.

#### 3.8.1 Quartz mineral group

Similar to the Gazzi-Dickinson method, the quartz mineral group represents various types of quartz ranging from single crystals of monocrystalline quartz to two or more crystals composing polycrystalline quartz (Figures 24-26). Additionally, where present, microcrystalline quartz called chert is classified within the quartz mineral group (Lynn et al., 2008; Tucker, 2001). Quartz has low relief and is usually colorless in plane polarized light (PPL) and is first-order gray in cross-polarized light (XPL) (Lynn et al., 2008). Undulose extinction, if present, may be a reflection of strain in the crystal lattice possibly indicating a metamorphic or igneous source (Tucker, 2001).

#### 3.8.2 Feldspar mineral group

The feldspar mineral group represents the potassium feldspars, orthoclase and microcline, and plagioclase feldspar. Feldspars have a lower mechanical and chemical stability than quartz which often leads to the disintegration of feldspar crystals during transport, and also later, during diagenetic processes (Tucker, 2001). It may be difficult to

distinguish different types of feldspars, therefore, twinning under crossed polarizers was often used to distinguish between the potassium feldspars, orthoclase and microcline, and plagioclase (Figures 24 and 26) (Lynn et al., 2008). Orthoclase may exhibit Carlsbad twinning or it may be untwinned (Figures 27-29). Orthoclase crystals frequently break along twin planes so the Carlsbad twinning may not be present (Tucker, 2001). Orthoclase, with its first order birefringence and possible untwinned nature, often looks like quartz (Figures 27 and 28). As Figure 27 illustrates, the strong cleavage of feldspar minerals often aids in identification. Microcline in thin section commonly exhibits “tartan” twinning, or the grid-iron (cross-hatch) twinning making this feldspar easily identifiable (Figure 24).

The plagioclase portion of the feldspar mineral group represents plagioclase feldspar minerals such as albite. The calcium-sodium plagioclase end members are anorthite and albite, respectively. Anorthite is rare and occurs in a few contact metamorphic deposits while albite is common in soils especially in the Blue Ridge, Piedmont, and Coastal Plain of the United States (Lynn et al., 2008). Plagioclase grains commonly exhibit polysynthetic (albite) twinning (Figure 26). It should be noted that feldspar grains that have been altered through processes such as sericitization and saussuritization have been included in the feldspar mineral group (Figure 29). This follows the Gazzi-Dickinson method of point counting and attempts to reduce the effects of alteration on composition (Ingersoll et al., 1984).

Additionally, trace quantities of intergrowths of quartz and feldspars such as myrmekites and granophyres have been documented in several samples (Barker, 1970) (Appendix C and Figure 30). These intergrowths are not listed in Appendix B or Table 2

because they are present in trace amounts and, for ease of analysis, the percentages of myrmekites and granophyres were evenly divided between the quartz mineral group and the feldspar mineral group.

### 3.8.3 Mica mineral group

The mica mineral group includes the most common micas in soil, muscovite and biotite, and a common hydrothermal alteration product, sericite (Newman and Brown, 1987; Lynn et al., 2008). Based on their platy nature and parallel extinction, muscovite and biotite, are easily identifiable sheet silicates (Tucker, 2001). Muscovite is usually colorless in plane-polarized light, but displays bright second-order interference colors in cross-polarized light (compare Figures 31 and 32) (Tucker, 2001; Lynn et al., 2008). Biotite is usually a shade of brown which may mask interference colors and it may exhibit brown-green pleochroism (compare Figures 31 and 32) (Harwood, 1988). Where interwoven with chlorite, biotite may be greenish (Tucker, 2001; Lynn et al., 2008). Muscovite and biotite are common detrital minerals derived from igneous rocks and metamorphic schists and phyllites (Harwood, 1988; Tucker, 2001). Although biotite is often more abundant in these crystalline source rocks, biotite's chemical instability causes it to be easily removed, therefore, muscovite is more common (Tucker, 2001).

Sericite is a fine-grained, white mica often resulting from the hydrothermal alteration of orthoclase and plagioclase feldspar (Figure 29) (Newman and Brown, 1987; Lynn et al., 2008). Sericite grains are often platy with high-order interference colors (compare Figures 33 and 34). Although similar to mica, it is unclear if and how sericite, a clay mica, should be classified with regards to other phyllosilicates such as other micas, kaolinite, and smectite because sericite is often interstratified (Newman and Brown,

1987; Lynn et al., 2008). Clay micas such as sericite and illite, many of which are interstratified, are part of an important clay mineral group that has no definition in terms of end-member composition nor clear constraints on their structural composition (Newman and Brown, 1987). Thus, since sericite is a fine-grained clay mica, for this study, it was grouped with the other micas which include muscovite and biotite. Additionally, for the analyses conducted as a part of this study, it was not relevant to distinguish between different types of micas (e.g. muscovite or biotite), therefore, the percentage of mica reported for a sample represents the total amount of mica in the sample regardless of the specific variety (muscovite, biotite, or sericite) of the mica group present.

#### 3.8.4 Chlorite mineral group

For the petrographic analyses, the chlorite mineral group broadly represents the chlorite group. Chlorite may form from the replacement of labile volcanic grains or as a result of various degrees of metamorphism (Lynn et al., 2008). Petrographic analyses identified chlorite minerals that were commonly green, but a few were brown, or red (Figure 35) (Lynn et al., 2008). Chlorite is often pleochroic, has a moderate relief, and low to moderate birefringence. XRD analyses were used to identify the specific member of the chlorite group such as clinocllore. The results of the XRD analyses are discussed in detail later in Chapter 3.

#### 3.8.5 Carbonate mineral group

The carbonate mineral group, for this study, comprises the mineral calcite. Calcite displays very high, fourth-order interference colors and can also be identified by its high relief and rhombic cleavage (compare Figures 36 and 37). (Harwood, 1988; Lynn et al.,

2008). In soils and sedimentary rocks such as sandstones, calcite may be present as detrital grains, cements in aggregates, and in other fine-grained masses often mixed with clay and other minerals (Tucker, 2001; Lynn et al., 2008). From petrographic analyses of the samples from the Deep River basin, calcite is predominantly present as a cement (Figure 27). Calcite, a common cement in sandstones, may displace grains causing them to appear to “float” in the cement (Tucker, 2001). Grains such as micas, feldspars, and even quartz may be forced to split as calcite is precipitated in cracks (Figure 27) (Tucker, 2001). In contrast to the amount of calcite cement present, there were a fewer number of calcite grains present in the samples (Figure 36 and 37).

#### 3.8.6 Matrix mineral group

For this study, the term “matrix” refers to fine-grained minerals between and surrounding larger crystals or mineral grains and that are too fine-grained to accurately identify using petrographic analyses (for example, Figures 25, 26, 30). Phyllosilicates (sheet silicates) such as micas, chlorite, and clay minerals such as kaolinite and smectite are often important constituents in the matrix of sandstones and coarse clastics and are the main component of mudrocks (Newman and Brown, 1987; Tucker, 2001). It is assumed then the matrix of the sedimentary samples collected from the Deep River basin is also predominantly composed of similar fine-grained phyllosilicates especially clay minerals, therefore, the matrix mineral group, for this study, represents these groups of minerals.

Clay minerals in sandstones are both detrital and authigenic in origin, whereas the clay minerals in mudrocks are predominantly detrital in origin (Tucker, 2001). Detrital clay minerals cannot be identified by petrographic analysis, but it is possible to identify

some authigenic clays such as illite and kaolinite if they are present in sandstones and coarser clastics (Tucker, 2001). Besides the aforementioned mica and chlorite grains that were coarse enough to be identified optically and classified appropriately, no other specific member of a phyllosilicate group was identified using petrographic analysis in the fine-grained matrix. Thus, the identification of the clay minerals and other phyllosilicates comprising the fine-grained matrix was completed using X-ray diffraction (Tucker, 2001). Clay minerals and the use of X-ray diffraction for their identification are discussed in greater detail in subsequent sections.

### 3.8.7 Opaque mineral group

For this study, the opaque mineral group refers to minerals that do not transmit light, and therefore, cannot be accurately identified using transmitted light petrographic analysis and a few, identifiable hematite grains (for example, Figures 38-42). Hematite and magnetite are two common opaque minerals (Tucker, 2001; Lynn et al., 2008). Magnetite and hematite, both oxide minerals, may be detrital in origin and are derived from metamorphic and igneous rocks. Hematite may also be authigenic such as the formation of hematite coatings around grains and the impregnation of hematite into infiltrated and authigenic clay minerals and feldspars (compare Figures 38 and 39) (Tucker, 2001). Figures 38 and 39 show both the detrital nature of opaque minerals in the form of isolated, often rounded grains and the authigenic nature of the opaque minerals as they appear to fill a fracture and coat numerous grains.

Lastly, the opaque mineral group is composed of a trace amount of hematite grains (Appendix B and Table 2). These grains were relatively coarse-grained and transmitted sufficient light to be identified (Figure 41). Well-formed hematite crystals are

typically flat hexagonal plates with extreme relief. Hematite crystals may be deep red-brown and may exhibit brownish red to yellowish-red or brown pleochroism. Hematite's opacity, however, often masks its pleochroism (Nesse, 2004). As a result of their chemical similarities, it was decided that the hematite grains would most appropriately be grouped with the opaque minerals.

#### 3.8.8 Other mineral group

For this study, the 'other' mineral group refers to minerals that comprise small quantities (on average less than ~ 3%) of the samples examined from the Deep River basin (Appendix B). Based on the petrographic data, the 'other' mineral group includes the common, non-opaque heavy minerals, epidote and zircon and several large lithic grains.

Heavy minerals like epidote and zircon may provide useful information about the geology of the source area (Tucker, 2001). Epidote is common in many types of igneous and metamorphic rocks. Epidote grains are usually irregularly shaped or roughly platy, have high relief, and are often a pistachio-green pleochroic color (Figure 31). In cross-polarized light, epidote exhibits strong yellow and red interference colors (Figure 32) (Lynn et al., 2008). A common detrital mineral, zircon, is derived from igneous and metamorphic source rocks (Tucker, 2001; Nesse, 2004). Zircon grains are characterized by very high relief and high-order interference colors (Figure 40) (Nesse, 2004). The rounded nature of the zircon grain in Figure 40 may suggest a long transport distance (Nesse, 2004).

For this study, most sand-sized grains occurring within larger lithic clasts were classified according to the category of the mineral, rather than as a lithic clast. Despite

the primary classification scheme, some lithic grains were identified (Appendix B). Some lithic fragments contained many fine-grained crystals with similar optical properties. As previously mentioned, untwinned orthoclase, with its first order birefringence, often looks like quartz. Thus, in some cases, specific mineral identifications were not possible. Instead of classifying the point under the cross-hairs as an ‘unknown’ mineral, the operator chose to categorize the point as a lithic clast. This decision was made because the information that a lithic clast was present in the sample was more accurate and informative for the purposes of the study than no information as would be indicated by an ‘unknown’ mineral designation.

#### 3.8.9 Unknown mineral group

For this study, the ‘unknown’ mineral group refers to minerals that were unable to be identified by petrographic analyses. Often these minerals were oriented such that the observer was looking down the optic axis, therefore, the minerals were extinct as the stage was rotated. Additionally, compaction and diagenetic alteration may render some grains indistinguishable from a fine-grained matrix (Tucker, 2001). Lastly, the observer’s lack of experience may have led to several grains receiving a designation of ‘unknown’.

#### 3.9 Results of the Petrographic Analyses: General Mineral Grouping

Petrographic analyses revealed the most abundant framework mineral was feldspar, comprising on average 28.2% of the samples examined (Table 2). The feldspar mineral group, as previously mentioned, consists of the potassium feldspars, orthoclase and microcline, and plagioclase feldspar. Table 3 shows the average percentage of plagioclase (6.8%) compared to the average percentage of orthoclase (21.3%) identified in the samples examined using petrographic analysis. Petrographic analyses revealed

microcline was present in one sample, therefore, it was included in the orthoclase category for ease of analysis. The petrographic analyses indicate that, for this study, the feldspar mineral group most frequently refers to orthoclase because, on average, 21.3% of the feldspars identified for the study were orthoclase (Table 3). The matrix mineral group was the second most abundant mineral group comprising, on average, 26.3% of the samples examined (Table 2). Quartz, the third most abundant mineral, comprises, on average, 16.5% of the samples analyzed. The last major mineral group identified were the opaque minerals such as hematite which constitute, on average, 14.3% of the samples analyzed.

The remaining mineral groups identified comprise smaller quantities (less than 10%) of the examined samples compared to the other mineral groups identified (Table 2). For example, the 'other' mineral group which includes minerals such as epidote and zircon comprise, on average, 2.9% of the samples examined. As previously stated, these heavy minerals may provide useful information about the geology of the source area (Tucker, 2001). Phyllosilicates including micas such as muscovite and sericite comprise, on average, 1.9% of the samples and chlorite constitutes, on average, 2.2% of the samples. Additionally, carbonates, predominantly in the form of calcite cement, comprise, on average, 1.6% of the samples. The 'unknown' mineral group constitutes, on average, 6.2% of the samples examined. In summary, the feldspar mineral group (28.2%), the matrix mineral group (26.3%), the quartz mineral group (16.5%), and the opaque mineral group (14.3%) respectively, are the major mineral groups identified in the 19 sedimentary rock samples collected from the Deep River basin (Table 2). The samples

are also composed of lesser amounts of phyllosilicates such as micas and chlorites, carbonates, and heavy minerals such as epidote and zircon.

### 3.10 Sandstone Classification

The petrographic data were used to apply a descriptive name to each sample based on the sandstone classification proposed by Dott (1964, modified by Pettijohn et al., 1987). This widely used sandstone classification scheme is based on the mineralogy and modal composition of the sediment and the presence or absence of a matrix (Figure 43) (Tucker, 2001). First, the texture of the sample is examined to determine if it is composed of only grains, and therefore an arenite, or if it is composed of at least 15% matrix, and therefore a wacke. These two major groups, the arenites and the wackes, are further subdivided using ternary diagrams with the end members of percent quartz (Q), percent feldspar (F), and percent rock fragments (L) (Tucker, 2001). These end member categories will be discussed in more detail in subsequent sections. The grain-supported arenites include sandstones such as quartz arenites, arkoses, and litharenites (Tucker, 2001). The wackes such as feldspathic greywackes and lithic greywackes are sandstones that contain more than 15% matrix. The wackes represent a transitional group between arenites and mudrocks (Figure 43).

The minerals identified by petrographic analyses for this study were reorganized from the nine mineral groups discussed above into four categories which were used for sandstone classification (Table 4). The four categories used for the sandstone classification are 1) quartz, 2) feldspar, 3) rock fragments, and 4) matrix (Tucker, 2001).

### 3.10.1 Quartz and feldspar categories

The quartz mineral group represents various types of quartz ranging from single crystals of monocrystalline quartz to two or more crystals composing polycrystalline quartz (Table 4). Additionally, where present, microcrystalline quartz called chert is classified within the quartz mineral group. The quartz mineral group from above is synonymous with the quartz end member used for sandstone classification. The feldspar mineral group represents the potassium feldspars, orthoclase and microcline, and plagioclase feldspar. Thus, the feldspar mineral group from above is synonymous with the feldspar end member used for sandstone classification (Table 4).

### 3.10.2 Rock fragment category

In the sandstone classification system, the rock fragment category generally includes various types of detrital lithic fragments such as metamorphic lithics, igneous lithics, and sedimentary lithics (Ingersoll et al., 1984; Tucker, 2001). As previously mentioned, the Gazzi-Dickinson method of point counting was used for all petrographic analyses. An issue arises because the Gazzi-Dickinson method yields petrographic data that does not include the percent lithic fragments of a sample. As discussed above, sand-sized grains occurring within larger lithic clasts were classified in the category of the mineral, rather than the category of the clast (Appendix B) (Ingersoll et al., 1984; Harwood, 1988).

In order to use the sandstone classification system, the rock fragment category was slightly modified to fit the available petrographic data (Table 4). The lithic fragments that traditionally compose the rock fragment category are predominantly detrital in nature (Tucker, 2001), therefore, the detrital minerals, except for quartz and feldspars, identified

for this study were categorized as rock fragments (Table 4). For example, the mica mineral group and the chlorite mineral group were assigned to the rock fragment category because in the samples from the Deep River basin analyzed using petrography, these minerals are predominantly detrital in nature. Additionally, the epidote and zircon grains as well as the few lithic fragments previously categorized as the 'other mineral' group were reorganized and assigned to the rock fragment category for the purposes of sandstone classification. As with the mica and chlorite grains, the epidote, zircon, and lithic grains are likely detrital in nature, therefore, most appropriately designated as rock fragments. Lastly, the 'unknown' mineral group was assigned to the rock fragment category because these minerals, though unidentified, were coarse-grained enough to possibly be identified, therefore, a designation of fine-grained matrix was not appropriate. Also, observations of the samples indicate many of the minerals and grains in the 'unknown' mineral group were likely detrital.

### 3.10.3 Matrix category

For the sandstone classification, the matrix category refers to fine-grained interstitial material (matrix) located between grains and authigenic minerals and cements precipitated during diagenesis. Though not clearly understood, two possibilities exist for the origin of the matrix, 1) the fine-grained sediment composing the matrix may have been deposited along with the sand-sized fraction, or shortly after as a result of infiltrating into the pore spaces, or 2) the diagenetic alteration of labile grains may have formed a secondary matrix or pseudomatrix (Tucker, 2001). According to Tucker (2001), it is believed that most of the matrix in sediments is of diagenetic origin, though some parts are likely to be characterized by fine-grained detritus.

Due to the primarily diagenetic origin of the matrix, for this study, the matrix category used for sandstone classification is predominantly composed of minerals and grains, likely of diagenetic origin, identified by petrographic analysis (Table 4). The matrix mineral group which is described in greater detail above is the predominant group in the matrix category (Appendix B and Table 4). Since most of the calcite identified in the samples was in the form of a cement, the carbonate mineral group was also included in the matrix category (Table 4).

Lastly, for the sandstone classification, the opaque mineral group was assigned to the matrix category (Table 4). As previously mentioned, the opaque mineral group refers to minerals that do not transmit light, therefore, cannot be accurately identified using petrographic analyses and a few, identifiable hematite crystals. Many of the opaque minerals are assumed to be hematite because it is a common opaque mineral and many of the opaque minerals present in the samples have a reddish-brown color especially along the edges of the crystals or grains. Hematite, an oxide mineral, may be formed in situ or it may originate as detritus (Tucker, 2001; Lynn et al., 2008). Some opaque minerals present in the Deep River basin samples appear to be detrital in origin, but most of the opaque minerals present in the samples appear to be authigenic in nature (see Figure 38, 41, 42). The samples from the Deep River basin frequently exhibited hematite coatings around grains and an impregnation of hematite into infiltrated and authigenic clay minerals and feldspars (Tucker, 2001). An authigenic origin for these opaque minerals is further supported by the absence of the reddish-brown coating at grain-to-grain contacts and the opaque minerals appear to fill or line fractures (Figure 42).

Several hematite grains were identified in the samples (Figure 41 and Appendix B). These grains were relatively coarse-grained and transmitted sufficient light to be identified. It was decided that these hematite grains should be classified with the opaque minerals because they are chemically similar, therefore, most appropriately grouped together. Due to the predominantly authigenic nature of the opaque minerals present in the Deep River Basin samples, the opaque minerals and associated hematite grains were classified in the matrix category for sandstone classification (Table 4).

The relative proportions of quartz, feldspars, and rock fragments in a representative suite of sedimentary samples were determined and used to place each sample into a sandstone classification as described by Folk (1980). Initially, the percent matrix category is used to determine if a sample is an arenite or a wacke. Table 5 shows each of the samples from the Deep River Basin are comprised of more than 15% matrix, therefore, are classified as wackes. Of the Deep River basin samples, a very fine- to fine-grained sandstone sample (SB-21) had the lowest percent matrix with 28% and another very fine- to fine-grained sandstone (DB-64) had the highest percent matrix with 73.1% (Table 5).

Once a sample is described as an arenite or wacke, the percentage of matrix and chemically-precipitated cements is ignored (Equation 1) (Folk, 1980). The essential constituents including quartz, feldspar, and rock fragments, are recalculated to 100% and are allotted to one of three end member categories used for sandstone classification (Equations 1-3 and Table 6) (Folk, 1980). The equations used to subtract the matrix and to recalculate the percentage of the essential constituents are shown below. The petrographic data from sample WB-6 is provided as an example.

$$100\% - \text{matrix (\%)} = \text{visible grains (\%)} \quad \text{Eq. 1}$$

$$100\% - 28.5\% = 71.5\%$$

$$\text{Quartz (\%)} / \text{visible grains (\%)} * 100 = \text{Quartz (\%)} \text{ of visible fraction} \quad \text{Eq. 2}$$

$$(37.5\% / 71.5\%) * 100 = 52.5\%$$

$$\text{Feldspar (\%)} / \text{visible grains (\%)} * 100 = \text{Feldspar (\%)} \text{ of visible fraction} \quad \text{Eq. 3}$$

$$(27.8\% / 71.5\%) * 100 = 38.8\%$$

$$\text{Rock fragments (\%)} / \text{visible grains (\%)} * 100 = \text{rock fragment (\%)} \text{ of visible fraction} \quad \text{Eq. 4}$$

$$(6.2\% / 71.5\%) * 100 = 8.7\%$$

Compositions of several sandstones and a conglomerate were used to classify the rocks from the Deep River Basin to a greywacke classification (Figure 44). Greywackes are characterized by a fine-grained matrix consisting of intergrowths of chlorite and sericite and silt-sized grains of quartz and feldspars (Tucker, 2001). Feldspathic greywackes are rich in feldspars and lithic greywackes are rich in rock fragments. Eighteen of the samples lie in the feldspathic greywacke classification. One sample, DB-34, lies on the boundary between feldspathic greywacke and lithic greywacke. Table 6 shows that the percent feldspar and rock fragments is nearly equal in sample DB-34 at approximately 40% while approximately 20% of the sample is composed of quartz.

### 3.11 The Results of the Petrographic Analyses

#### 3.11.1 Introduction

In order to discuss the occurrence and distribution of minerals in the Deep River basin as relevant for this study, the nine mineral groups identified in section 3.8 were reorganized into new mineral groups to better fit the objectives of the study (Table 7). This section serves to justify why it was necessary to reorganize the petrographic data and why the categories used for the sandstone classification, though helpful in providing a descriptive rock name, are inadequate for the analyses conducted as a part of this study.

As stated in section 1.3, the purpose of this research is to 1) provide baseline data of water-rock interactions in an undisturbed Mesozoic basin in advance of drilling and hydraulic fracturing, 2) to simulate the formation water that may be brought to the surface during shale gas development, and 3) to examine the geochemical fingerprint that could be used to identify this formation water in the environment. In order to understand the water-rock interactions that occur in the Deep River basin, this study examines lithologic variables including mineralogy, grain size, lithofacies and lithofacies associations, and degree of post-depositional alteration and their potential influence on the characteristics of formation water in the basin (section 1.4). The petrographic data collected as part of this study reflect these objectives and are intended to address the hypotheses of the study (section 3.8 and Table 2).

To investigate the water-rock interactions that occur in the Deep River basin, a series of sequential extraction experiments were conducted on samples collected from each of the sub-basins (Figure 45). The sequential extractions are discussed in greater detail in Chapter 4, but a brief overview is necessary here to justify the reorganization of

the petrographic data. Sequential extractions were selected for this study because they target different geochemical reservoirs for certain extractable cations including strontium, barium, boron, calcium and magnesium, and anions such as chloride, nitrate and sulfate (Tessier et al., 1979; Stewart et al., 2015). Sequential extractions provide data about the mobility of these components and may provide insight into the characteristics of formation water present in the basin.

For this study, the sequential extraction procedures were adapted from Tessier et al. (1979) and Stewart et al. (2015) and used reagents such as ammonium acetate and acetic acid to selectively target four specific geochemical fractions: 1) water-soluble components, 2) exchangeable cations, 3) carbonates, and 4) strong-acid (hydrochloric acid) soluble phases (Figure 45). Thus, the mineral groups identified in section 3.8 were reorganized into 6 mineral groups that reflect the geochemical fractions targeted by the sequential extractions. The resulting mineral groups include: 1) quartz, 2) feldspar, 3) clay minerals, 4) carbonates, 5) oxides, and 6) other (Table 7).

The mineral groups identified as relevant for the sequential extractions provide evidence of the limitations of the categories used for the sandstone classification in providing insight into the results of the sequential extractions. As previously stated, the sequential extractions selectively target specific geochemical fractions such as exchangeable cations, carbonates, and strong-acid soluble phases such as oxides (Figure 45). Also as previously stated, the four categories used for sandstone classification include quartz, feldspar, rock fragments, and matrix (Table 4). These categories, while useful for providing a descriptive approach to sandstone classification, do not supply enough mineralogical detail to thoroughly understand and appreciate the results of the

sequential extractions. For example, the matrix category used for sandstone classification consists of both the matrix mineral group and the carbonate mineral group. As previously discussed, the sequential extractions target different geochemical reservoirs such as those found in carbonate minerals and clay minerals (Figure 45). Thus, the combination of carbonate minerals and clay minerals into one group such as occurs with the sandstone classification, limits the mineralogical information available to understand the results and trends established by the sequential extractions. The categories associated with the sandstone classification, therefore, do not provide the specific mineralogical data necessary for a basin-wide understanding of the water-rock interactions that are occurring based on the use of sequential extractions. As a result, the six mineral groups identified as relevant for the sequential extractions (Table 7) will be used for all further analyses and discussions.

### 3.11.2 Mineral groups based on the sequential extractions

The mineral groups identified by petrographic analyses in section 3.8 were reorganized into 6 mineral groups based on the sequential extractions that were conducted as part of this study. The resulting mineral groups include: 1) quartz, 2) feldspar, 3) clay minerals, 4) carbonates, 5) oxides, and 6) other (Table 7).

The quartz mineral group represents various types of quartz ranging from single crystals of monocrystalline quartz to two or more crystals comprising polycrystalline quartz (Table 7). Additionally, where present, microcrystalline quartz called chert is classified within the quartz mineral group. The feldspar mineral group represents the potassium feldspars, orthoclase and microcline, and plagioclase feldspar (Table 7).

For the sequential extraction analyses, the clay mineral group was used to target exchangeable cations (Figure 45). Clay minerals such as kaolinite and smectite and other phyllosilicates like mica and chlorite are often important constituents in the matrix of sandstones and coarse clastics and are the main component of mudrocks (Newman and Brown, 1987; Tucker, 2001). Thus, the clay mineral group includes the matrix mineral group and the coarse-grained phyllosilicates identified in the samples which include mica and chlorite (Table 7).

The primary reason to group the matrix, mica, and chlorite mineral groups together for the sequential extractions is their similar sheet-like, or layered structures, and their ion exchange capacities (Newman and Brown, 1987). Within the layers of clay minerals and other phyllosilicates, ion exchange occurs near the surface of a mineral resulting in many types of isomorphous substitution (Carroll, 1959; Newman and Brown, 1987). For example, clay minerals such as smectites may experience extensive substitution of aluminum <sup>(3+)</sup> by iron <sup>(2+, 3+)</sup>, magnesium <sup>(2+)</sup>, and zinc <sup>(2+)</sup> (Newman and Brown, 1987, Tucker, 2001). Additionally, smectites such as the most common, montmorillonite, may contain interlayer water and calcium and sodium ions (Tucker, 2001). Micas may contain small quantities of strontium and barium located in interlayer sites (Newman and Brown, 1987).

For the sequential extractions, the carbonate mineral group is composed of the mineral calcite and was used to target the carbonate minerals (Table 7). From petrographic analyses of the samples from the Deep River basin, calcite is predominantly present as a cement and to a lesser degree as calcite grains. The oxide mineral group was used to target strong-acid soluble phases and includes the few coarse-grained hematite

grains identified in the samples and the opaque minerals (Table 7). This decision was based on the fact that the hematite grains and the opaque minerals are chemically similar, therefore, most appropriately grouped together. The ‘other’ mineral group consists of trace minerals not specifically targeted by the sequential extractions (Table 7). These minerals include the heavy minerals, epidote and zircon, a few lithic grains, and the ‘unknown’ mineral group.

### 3.11.3 Petrographic data: Deep River basin samples

The mineral groups described above are central to understanding the sequential extractions. As a result, these mineral groups were used to discuss the occurrence and distribution of minerals in the Deep River basin. Table 8 shows the petrographic data of the 19 sedimentary rock samples from the Deep River basin organized by the mineral groups used for the sequential extractions. Based on the prevalence of fine-grained matrix and feldspars in the samples, as indicated by the feldspathic greywacke classification (section 3.10), it is not surprising that clay minerals and feldspars make up the majority, 30.4% and 28.2% of the samples, respectively. The quartz mineral group and the oxide minerals constitute similar percentages of the samples comprising 16.5% and 14.3% of the samples, respectively. The ‘other’ mineral group which consists primarily of ‘unknown’ minerals (Appendix B) with lesser amounts of epidote, zircon, and lithic grains, comprises 9.1% of the samples (Table 8). Lastly, carbonate minerals constitute 1.6% of the samples examined from the Deep River basin.

### 3.11.4 Petrographic data: Wadesboro sub-basin samples

Four samples from the Wadesboro sub-basin, the southernmost basin in the Deep River basin, were examined using petrography (Table 9). The samples from the

Wadesboro sub-basin are characterized by a high percentage of clay minerals (36.4%). Quartz and feldspar minerals comprise an equal amount (26.4%) of the samples examined. The 'other' mineral group composes 4.6% of the Wadesboro sub-basin samples. Appendix B shows the 'other' mineral group for the Wadesboro sub-basin is characterized by 'unknown' minerals only. Thus, no epidote, zircon, or lithic grains were identified in the samples from the Wadesboro sub-basin (Appendix B). The oxide minerals such as hematite comprise 3.4% of the samples and carbonates, predominantly in the form of calcite cement, comprise the remaining 2.9% of the samples examined from the Wadesboro sub-basin (Table 9).

#### 3.11.5 Petrographic data: Sanford sub-basin samples

Three samples from the Sanford sub-basin of the Deep River Basin were examined using petrography (Table 10). The samples from the Sanford sub-basin are characterized by a high percentage of feldspar minerals (33.5%). The quartz mineral group and the clay minerals, the next most abundant mineral groups, constitute similar percentages of the samples comprising 19.8% and 17.0% of the samples, respectively. The oxide minerals constitute 16.6% of the samples and the 'other' mineral group comprises the remaining 13.1% of the samples from the Sanford sub-basin. Appendix B shows the 'other' mineral group for the Sanford sub-basin is characterized by 'unknown' minerals only. Thus, no epidote, zircon, or lithic grains were identified in the samples from the Sanford sub-basin (Appendix B). According to the petrographic data, the Sanford sub-basin samples do not contain any carbonate minerals (Table 10).

### 3.11.6 Petrographic data: Durham sub-basin samples

Twelve samples from the Durham sub-basin, the northernmost sub-basin in the Deep River basin, were examined using petrography (Table 11). The samples from the Durham sub-basin are characterized by abundant clay (31.7%) and feldspar (27.4%) minerals (Table 11). Oxide minerals are the third most abundant mineral group comprising 17.4% of the samples. The Durham sub-basin samples are comprised of a relatively low percentage of quartz (12.3%). The ‘other’ mineral group constitutes 9.6% of the samples from the Durham sub-basin. Appendix B shows the ‘other’ mineral group for the Durham sub-basin is characterized by ‘unknown’ minerals, epidote, zircon, and lithic grains. Of particular interest to some researchers are the heavy minerals, epidote and zircon, which were identified in the some of the samples (Appendix B). Carbonate minerals mainly in the form of calcite cement comprise the remaining 1.6% of the samples examined from the Durham sub-basin (Table 11).

### 3.11.7: Trends in basin-wide mineralogy based on petrographic analysis

The mineralogical data from the Deep River basin and its three sub-basins were compared to each other in order to examine spatial trends, if any, present across the basin (Table 12). Although each sample analyzed using petrography was classified as a greywacke, the average composition of the sandstones varies among the sub-basins (Table 12). The Wadesboro sub-basin is the most quartz-rich (26.4%) followed by the Sanford sub-basin with an average 19.8% quartz and the Durham sub-basin with 12.3% quartz. The average percentages of feldspar minerals are similar among the three sub-basins. The Sanford sub-basin is the most feldspathic with 33.5% feldspar, the Durham

sub-basin consists of 27.4% feldspar, and lastly, the Wadesboro sub-basin is comprised of 26.4% feldspar (Table 12).

The Wadesboro sub-basin samples have the most abundant clay and carbonate minerals, 36.4% and 2.9%, respectively. The Durham sub-basin has a similarly high average percentage of clay minerals (31.7%) and an average 1.6% carbonate minerals. The Sanford sub-basin is marked by a relative deficiency of clay minerals (17.0%) and carbonate minerals (0%) (Table 12).

The distribution of the oxide minerals in the Deep River basin is quite different compared to the distribution of clay minerals and carbonates. Unlike with the clay minerals and carbonates, the northernmost sub-basin, the Durham sub-basin, has the highest percentage of oxide minerals (17.4%). The percentage of oxide minerals decreases southward in the Deep River basin from 16.6% to 3.4% in the Sanford and Wadesboro sub-basins, respectively (Table 12). Each of the sub-basins from the Deep River Basin was comprised of minerals classified in the 'other' mineral group (Table 12), but unlike in the Wadesboro and Sanford sub-basins, the samples from the Durham sub-basin had epidote and zircon grains present (Appendix B).

#### 3.11.8 Variation in Deep River basin mineralogy with respect to grain size

As previously stated in section 1.3, the purpose of this research is to provide baseline data of water-rock interactions occurring in the Deep River basin. Additionally, mineralogy and grain size were hypothesized to influence the chemical characteristics of formation water (section 1.4). The petrographic data were, therefore, used to examine the variation in composition with grain size of the samples collected from the Deep River Basin (Table 13).

Modal composition varies with grain size for two reasons: 1) the splitting of

fragments into constituent grains, and 2) actual mineralogical variation with grain size (Ingersoll et al., 1984). This study used a modified version of the Gazzi-Dickinson method of point counting. The primary way the Gazzi-Dickinson method differs from traditional methods of pointing counting is that sand-sized grains occurring within larger lithic clasts are classified in the category of the mineral, rather than the category of the clast (Ingersoll et al., 1984; Harwood, 1988). Thus, the Gazzi-Dickinson method eliminates compositional dependence on grain size by eliminating the variation in modal composition due to the breakage of fragments into their constituent grains (Dickinson, 1970; Ingersoll et al., 1984).

The samples from the Deep River basin examined using petrographic analysis include: 10 very fine- to fine-sand sized samples, 8 medium-coarse-very coarse sand-sized samples, and 1 gravel (Table 8). Based on the petrographic data, modal composition varies with grain size in the samples from the Deep River basin (Table 13). Table 13 shows the very fine- to fine- sand-sized samples are predominately composed of clay minerals (32.1%) and feldspars (27.7%). Oxide minerals and quartz comprise 19.1% and 10.9%, respectively, of the very fine- to fine- sand-sized samples. The 'other' mineral group including epidote and zircon comprises 10% of the very fine- to fine- sand-sized samples (Appendix B). Lastly, carbonates comprise a trace percent (0.1%) of the samples very fine- to fine- sand-sized samples (Table 13).

The medium-coarse-very coarse sand-sized samples appear to contain similar percentages of clay minerals (29%), feldspars (28.5%), and quartz (21.5%) (Table 13). Oxide minerals (9.3%), the 'other' mineral group including epidote and zircon (7.9%), and carbonates (3.8%) each comprise less than 10% of the medium-coarse-very coarse

sand-sized samples (Table 13 and Appendix B). The gravel sample is predominantly composed of quartz (31.3%) and feldspar (30.3%) (Table 13). Clay minerals comprise 23.4% of the gravel sample. Oxide minerals (6.2%) and the 'other' mineral group (8.8%) excluding epidote and zircon, each constitute less than 10% of the gravel sample (Table 13).

Since the Gazzi-Dickinson method of point counting eliminates the compositional dependency on grain size, it can be assumed that the variation in modal composition with grain size in the samples from the Deep River basin is based on actual mineralogical variation. As grain size increases from very fine-sand to gravel, the percentages of quartz and feldspar increase (Table 13). On the contrary, as grain size increases, the percentages of clay minerals and oxide minerals decreases (Table 13).

The petrographic data suggest the percentage of carbonate minerals may be less related to grain size compared to the aforementioned mineral groups (Table 13). Medium-coarse-very coarse-sand sized samples are comprised of the highest percentage of carbonates (3.8%) and the very fine- to fine-sand-sized samples are composed of only trace amounts (0.1%) of carbonate minerals. Carbonate minerals were not present in the gravel-sized sample.

Because the 'other' mineral group contains 'unknown' minerals in addition to epidote and zircon, the variation in composition of this mineral group by grain size may be misleading (Table 13). As previously mentioned though, the very fine- to fine-sand-sized and medium-coarse-very coarse-sand sized samples contain epidote and zircon grains, whereas, the gravel sample does not (Appendix B). While the heavy minerals, epidote and zircon, may be of interest to some, these minerals and the additional

components of the ‘other’ mineral group constitute small quantities of the samples from the Deep River Basin and they are not targeted during the sequential extractions (Appendix B, Table 7, Figure 45). As a result, the ‘other’ mineral group was not included in any future analyses and discussions.

### 3.12 Lithofacies Associations and Depositional Environments in Rift Basins

A lithofacies is a sedimentary body with features such as composition (lithology), grain size, texture, sedimentary structures, color, and fossil content that distinguish it from other lithofacies. These features are products of deposition and may be characteristic of a particular depositional environment or a particular depositional process (Tucker, 2001). For example, the recognition of the significance of primary sedimentary structures such as crossbeds and parting lineation is essential for reassembling the specific depositional environment or sub-environment represented by the lithofacies (Lorenz, 1988; Chem-Nuclear, 1993). Lithofacies associations are distinctive suites or assemblages of genetically-related lithofacies that were likely deposited together in specific depositional environments such as in meandering stream, alluvial fan, or lake environments (Figure 46) (Lorenz, 1988; Chem-Nuclear, 1993; Tucker, 2001). Thus, lithofacies associations are often designated by the name of the depositional environment they represent (Chem-Nuclear, 1993).

Lithofacies associations are extremely useful in describing the regional stratigraphic architecture of the Deep River basin and its sub-basins, especially the Durham and Wadesboro sub-basins (Figure 46). This is due to the absence of good marker beds or horizons (such as the Cumnock Formation) in these sub-basins which are needed to delineate and map stratigraphic units and formations (Chem-Nuclear, 1993;

Clark et al., 2001; Brazell, 2013). Previous studies conducted in the Deep River basin such as Chem-Nuclear (1993), Olsen (1997), and Brazell (2013) have used lithofacies associations for stratigraphic analyses and the development of models that would explain and predict the characteristics and distributions of lithofacies associations. As described below, the various lithofacies recognized in the Deep River basin and other rift-basins often occur in characteristic and recurrent assemblages and vertical successions primarily as a result of basin tectonics (Figure 46) (Lorenz, 1988; Chem-Nuclear, 1993).

In rift basins, the deposits of flanking transverse alluvial fans may interfinger distally with fluvial, paludal, playa, and lacustrine deposits that are located near the basin center (Figures 13 and 46) (Lorenz, 1988; Miall, 1996). The nature of the sedimentary interaction between alluvial fan deposits and other lithofacies can provide insight into the conditions of deposition. For example, in blocked or interior-drainage situations, alluvial fan deposits may grade out into shoreline sandstones and lacustrine shales (Figure 13) (Lorenz, 1988). Past climate conditions may have influenced the characteristics of the lakes that developed at the basin center. During periods of increased precipitation and more humid conditions, perennial lakes and paludal deposits may interfinger with alluvial fan deposits (Berendsen et al., 1988; Lorenz, 1988; Miall, 1996). Alluvial fan deposits that grade distally into playas and evaporite deposits may reflect more arid conditions (Berendsen et al., 1988; Lorenz, 1988). During episodes of through-drainage, alluvial fan deposits interfinger distally with fluvial and overbank deposits located near the basin center (Figure 13) (Berendsen et al., 1988; Lorenz, 1988).

Periodic faulting may modify the sedimentary sequences. For example, axial river systems may be laterally displaced as a result of the progradation of large alluvial fans

into the basin center (Figure 13). Additionally, differential subsidence within the basin may lead to tilt-induced avulsion and the lateral migration of river systems, generally toward the footwall of the basin (Berendsen et al., 1988; Lorenz, 1988; Miall, 1996). Axial river systems may also be overwhelmed by large alluvial fans or lava flows which dam the rivers forming lakes (Lorenz, 1988). Periodic faulting may also be recorded as vertical changes in alluvial fan successions. A cyclic repetition of coarsening and thickening upward units and fining and thinning units suggests repeated alluvial fan progradation and retrogradation, respectively (Rust and Koster, 1984; Berendsen et al., 1988). Thus, the irregular pattern of tectonic/ fault activity is often recorded in the sedimentary patterns within a rift-basin as characteristic and recurrent lithofacies associations and vertical successions (Figure 46) (Rust and Koster, 1984; Berendsen et al., 1988; Lorenz, 1988; Chem-Nuclear, 1993).

### 3.13 Lithofacies Associations and Depositional Environments of the Deep River Basin

As discussed in section 3.6, this study used samples collected in the field including from outcrops along road, railroad, and stream cuts and samples that were collected as part of previous studies conducted by Chem-Nuclear (1993) and Brazell (2013). 41 of the 55 samples from the Wadesboro sub-basin used for this study were originally collected by Brazell (2013). The remaining 14 samples from the Wadesboro sub-basin were collected from outcrops along road, railroad, and stream cuts identified by Brazell and Diemer (2012). The 40 samples from the Sanford sub-basin were collected in the field from outcrops along road, railroad, and stream cuts identified by Reid et al. (2011) and Clark et al. (2011). The samples from the Durham sub-basin are 1-inch diameter core sub-samples that were taken from larger diameter cores that were

previously drilled by the North Carolina Geological Survey and were stored at the Coastal Plain Office Core Repository (Figures 47-59). These cores were originally collected for the study conducted by Chem-Nuclear (1993).

Because these previous studies used lithofacies associations for stratigraphic analyses and the development of lithofacies association models, the lithofacies association of 133 of the 185 samples used for this study had previously been determined. For example, Figures 47-59 display the graphic core logs of the four cores sampled at the Coastal Plain Office Core Repository. The graphic core logs show the depth and lithofacies association of the 92 samples collected for this study from the Durham sub-basin. These figures will be discussed in greater detail in a subsequent section.

The lithofacies and lithofacies association of the 52 field samples collected from the Wadesboro and Sanford sub-basins were determined using sedimentary features such as grain size, color, texture, cross-bedding, and lamination. Additionally, secondary modifications to primary sedimentary deposits such as color mottling, roots, and the formation of calcareous paleosols are also an important part of facies models (Lorenz, 1988). As a result, these features were also used to distinguish the lithofacies and lithofacies associations of the Deep River basin samples used in this study.

As stated above, lithofacies associations are often designated by the name of the depositional environment they represent (Chem-Nuclear, 1993). According to Chem-Nuclear (1993) and Brazell (2013) and corroborated by the present study, closely related lithofacies in the Deep River basin form four major assemblages or lithofacies associations which trend roughly parallel to the borders and axis of the sub-basin (Figure 46) (Chem-Nuclear, 1993). These lithofacies associations include: 1) distal fan lithofacies

association, 2) fan fringe lithofacies association, 3) lacustrine lithofacies association, and 4) meandering stream lithofacies association. The distal fan lithofacies association and fan fringe lithofacies association occur in alluvial fan environments (Figure 46). The meandering stream lithofacies association includes channel facies and overbank deposits including floodplain deposits and crevasse splays. Thus, three depositional environments were identified based on the four lithofacies associations (Figure 46). The depositional environments present in the Deep River basin include: 1) alluvial fans, 2) meandering streams, and 3) lacustrine environments (Figure 46).

Braided streams are the most common fluvial environment in rift basins as a result of the availability of coarse sediment and the relatively steep gradients present in the basins, but several highly sinuous, meandering streams have also been described (Walker and Cant, 1984; Lorenz, 1988; Tucker, 2001). As previously discussed, sandy braided streams are dominated by channel and bar facies (Figure 12) (Tucker, 2001). If formed, overbank deposits are only rarely preserved due to the relatively rapid lateral migration of channels, therefore, the vertical accretion deposits such as shales and cross-laminated siltstones interbedded with mudstones tend to be patchy, laterally discontinuous, and of no great thickness in most braided stream systems (Figure 12) (Walker and Cant, 1984; Miall, 1996; Tucker, 2001). As a result of the objectives and hypotheses of this study (section 1.3 and 1.4) and the absence of fine-grained overbank deposits in most braided stream systems, this study focused on the meandering stream deposits present in the Deep River basin (Figures 9 and 46).

The graphic core logs representing the four cores sampled at the Coastal Plain Office Core Repository show the depth above the top of the cored interval and lithofacies

association of the 92 samples collected for this study from the Durham sub-basin (Figures 47-59). As previously stated, 19 sedimentary samples from across the Deep River Basin were analyzed using petrographic analysis (Appendix A). Of these samples, only the 12 samples from the Durham sub-basin correlate with available graphic core logs or vertical profiles (stratigraphic columns) (Table 11; Figures 47-59). While 41 of the Wadesboro sub-basin samples and 9 of the Sanford sub-basins samples correlate with available stratigraphic columns, none of these samples were selected for petrographic analysis. The mineralogy of these 50 samples was, therefore, determined using XRD. As a result, the stratigraphic columns that show the depth and lithofacies association of the samples from the Wadesboro and Sanford sub-basins will be displayed and discussed in a subsequent section. The following section briefly discusses graphic core logs and stratigraphic columns.

Graphic core logs and stratigraphic columns depict the vertical grain size and compositional trends of sedimentary successions (Figures 47-59) (Chem-Nuclear, 1993). Additionally, textural characteristics such as sorting, primary sedimentary structures such as cross-bedding and lamination, and evidence of pedogenesis such as carbonate nodules and roots are systematically noted. Graphic core logs and stratigraphic columns also provide information about the nature of contacts (erosional, sharp, or transitional) between adjacent lithofacies and vertical changes within lithofacies units (Chem-Nuclear, 1993). As a result of the abundance of information provided by these descriptions, it may be possible to identify specific depositional processes that influenced the lithofacies and vertical trends present in the core. This information may then be used to distinguish the various lithofacies associations present (Figures 47-59). Through the recognition of

lithofacies associations, interpretations may be made regarding the depositional environments represented by these various lithofacies associations (Chem-Nuclear, 1993). In order to address the objectives and hypotheses of the study, the petrographic data were organized according to depositional environment (Tables 14-18). The 'other' mineral group is displayed in each of the tables in order to display total percentages, but, as previously mentioned, the mineral group is not relevant for the present study, therefore, it is not discussed.

#### 3.14 Alluvial Fan Environments and Lithofacies Associations

The alluvial fan lithofacies association is divided into two lithofacies associations: the fan fringe lithofacies association and the distal fan lithofacies association (Figure 46). The fan fringe is described as a low-gradient area located immediately beyond the toe (distal portion) of an alluvial fan (Figure 46). A variety of similar depositional processes such as fine-grained debris flows and mudflows are active in both the fan fringe and distal fan portions of alluvial fans, but important differences exist between the deposits which support the recognition of two distinct lithofacies associations (Chem-Nuclear, 1993). Some important criteria to note in making distinctions between fan deposits are the relative grain size of the deposits, the relative thickness of the beds, and the presence of root-disrupted intervals and paleocaliche horizons (Lorenz, 1988; Chem-Nuclear, 1993). The distal fan lithofacies association is characterized by coarse-grained debris-flows, crudely-stratified, coarse-grained channel deposits, and laminated sandstones without well-developed paleosols (Chem-Nuclear, 1993). In contrast, the fan fringe lithofacies association is characterized by a finer mean grain size, significantly smaller maximum clast size, thinner beds, and the presence of root-disrupted intervals and

paleocaliche horizons (Figures 46; 47-59) (Chem-Nuclear, 1993). Core W11 MP9 shown in Figures 47-49 is representative of the interfingering relationship between these two lithofacies associations.

#### 3.14.1 Petrographic mineralogy of alluvial fan environments

Table 14 shows the petrographic data for samples from an alluvial fan environment. All of the alluvial fan samples analyzed using petrography are from the fan fringe lithofacies association. The distal fan lithofacies association is not represented by the petrographic samples due to the coarse-grained sediments such as gravel and coarse sand characteristic of the lithofacies association (Figure 46). These coarse-grained samples may not provide statistically accurate percentages of the components present due to a lack of points or grains to count (section 3.7) (Ingersoll et al., 1984; Harwood, 1988; Lynn et al., 2008).

According to the petrographic analyses, the fan fringe lithofacies association is characterized by compositionally immature sediments consisting of a high average percentage of feldspar (28.7%) compared to quartz (19.1%) (Table 14). The petrographic analyses also revealed the fan fringe lithofacies association is characterized by a relatively high average percentage of clay minerals (22.8%) and oxides (18.4%). Based on the petrographic data, the fan fringe lithofacies association does not contain any carbonate minerals.

#### 3.15 Meandering Stream Environments and Lithofacies Associations

The meandering stream depositional environment is composed of three lithofacies associations: the channel, floodplain, and the crevasse splay lithofacies associations. The channel lithofacies association is characterized by well-sorted, fining-upward sandstone

bodies which are commonly cross-bedded (Figure 46) (Tucker, 2001). The overbank sub-environment associated with meandering streams results in the floodplain and crevasse splay lithofacies associations. The floodplain lithofacies association is characterized by laminated siltstones and mudstones and evidence of pervasive paleosol formation such as desiccation cracks, roots, carbonate nodules and color mottling (Figure 46) (Walker and Cant, 1984; Tucker, 2001; Chem-Nuclear Systems, 1993). The crevasse splay lithofacies association is characterized by poorly sorted, sharp-based, thin-bedded sandstones (Walker and Cant, 1984, Tucker, 2001). The combination of overbank flooding and crevasse splays results in thin-bedded sandstones interbedded with floodplain silts and muds (Figure 46) (Walker and Cant, 1984; Tucker, 2001). Core W32 MP14 displayed in Figures 53-55 shows the stratigraphic positions of samples collected from the Durham sub-basin representing each of the three lithofacies associations related to the meandering stream depositional environment.

#### 3.15.1 Petrographic mineralogy of meandering stream environments

Tables 15 and 16 show the petrographic data for samples from meandering stream deposits. The samples collected from the Deep River basin are representative of both channel and overbank sub-environments of the meandering stream depositional environment (Figure 46). As a result, the samples were categorized as being from either the channel, floodplain or crevasse splay lithofacies association (Table 15 and 16). The data in Table 15 examines the mineralogical data of meandering stream environment as a system, whereas, Table 16 provides mineralogical data based on the sub-environments and lithofacies associations.

Based on the petrographic data, the meandering stream lithofacies association is characterized by compositionally immature sediments consisting of higher average percentage of feldspar (27.8%) compared to the average percentage of quartz (16.2%) (Table 15). Petrographic analyses also revealed that clay minerals (32.2%) are the most abundant mineral group in the meandering stream lithofacies associations. Oxides such as authigenic hematite constitute an average 13.4% of the samples. Lastly, carbonate minerals, predominately in the form of calcite cement, comprise an average 2.2% of the meandering stream samples.

### 3.15.2 The results of the petrographic analyses of the sub-environments of a meandering stream

Table 16 shows the average composition of samples from the sub-environments in meandering stream environments as recorded in the channel, floodplain, and crevasse splay lithofacies associations. Similar to the overall meandering stream environment, each of the individual lithofacies associations is characterized by compositionally immature sediments. The channel lithofacies association consists on average of 28.8% feldspar and 20.0% quartz (Table 16) and is slightly more compositionally mature compared to the overbank deposits. The crevasse splay lithofacies association comprises on average 31.1% feldspar and 10.9% quartz, whereas the floodplain lithofacies association comprises on average 21.1% feldspar and 14.6% quartz (Table 16).

All three lithofacies associations are characterized by a similar, high average percentage of clay minerals. The channel lithofacies association is characterized by the highest abundance of clay minerals (34.8%). The crevasse splay and floodplain lithofacies associations are characterized by similar, lower percentages of clay minerals, 29.9% and 29.3%, respectively (Table 16). Carbonate minerals are present in the crevasse

splay and channel lithofacies associations, 4.1%, and 2.1%, respectively, but are absent from the floodplain lithofacies association. Oxide minerals are present in all three sub-environments of meandering streams (Table 16). The floodplain lithofacies association is characterized by the highest abundance of oxide minerals (average 25.5%). The crevasse splay and channel lithofacies associations have fewer oxide minerals present with an average of 14.2% and 7.8%, respectively (Table 16).

### 3.16 Lacustrine Environments and Lithofacies Associations

The lacustrine depositional environment is characterized by a variety of different processes related, in part, to whether deposition occurred along the lake margins or in open-water. For example, as illustrated by core W10 MP5, marginal lacustrine lithofacies include deltaic deposits with inclined foreset beds representative of the Gilbert-type deltas often formed where a sediment-laden river enters a lake (Figures 46; 50-52) (Tucker, 2001). The lacustrine lithofacies association is also characterized by laminated and massive siltstones and mudstones and organic-rich mudstones and shales (Figure 52). These fine-grained sediments can reach the center of the lake as suspended sediments that gradually settle out of the water column producing finely-laminated sediments (rhythmites) which may occur with the deposits of low-density turbidity currents (Figure 46) (Tucker, 2001). Dark gray to black fine-grained, organic-rich mudstones and shales accumulate in deep-water lacustrine systems where anoxic conditions likely preserve organic material (Olsen et al., 1991).

#### 3.16.1 Petrographic mineralogy of lacustrine environments

According to the petrographic data, the lacustrine lithofacies association is characterized by compositionally immature sediments and an abundance of clay minerals

(Table 17). Clay minerals are the most abundant mineral group comprising 34.9% of the sample. Feldspar minerals constitute a similar percentage, comprising 30.9% of the lacustrine sample. Quartz and oxide minerals are the least abundant minerals, comprising 8.9% and 10.3%, respectively, of lacustrine deposits. According to the petrographic data, carbonate minerals were not present in the lacustrine lithofacies association.

### 3.17 Summary: The Results of the Petrographic Analysis

In summary, the petrographic data show the deposits of the Deep River basin are compositionally immature consisting of an abundance of clay minerals and feldspars, 30.4% and 28.2%, respectively (Table 12). Quartz and oxide minerals constitute similar percentages of the Deep River basin samples comprising 16.5% and 14.3% of the samples, respectively. Lastly, carbonate minerals constitute 1.6% of the samples examined from the Deep River basin (Table 12).

The petrographic data of nineteen sedimentary samples including several sandstones and a conglomerate were used to apply a descriptive name to each sample based on the sandstone classification proposed by Dott (1964, modified by Pettijohn et al., 1987). This widely used sandstone classification scheme is based on the mineralogy and modal composition of the sediment and the presence or absence of a matrix (Figure 43) (Tucker, 2001). Based on the petrographic data, the rocks from the Deep River basin are predominantly described as feldspathic greywackes (Figure 44). Feldspathic greywackes are rich in feldspars and characterized by a fine-grained matrix consisting of intergrowths of chlorite and sericite and silt-sized grains of quartz and feldspars (Tucker, 2001).

The petrographic data also indicates the modal composition of samples from the Deep River basin varies with grain size (Table 13). As grain size increases from very fine-sand to gravel, the percentages of quartz and feldspar increase (Table 13). In contrast, as grain size increases, the percentages of clay minerals and oxide minerals decreases (Table 13).

Finally, the petrographic data may indicate that the depositional environment of a samples may influence its modal composition (Table 18). The depositional environments of the Deep River basin are characterized by compositionally immature deposits consisting of an abundance of clay minerals and feldspars. Alluvial fan deposits are characterized by the highest average quartz and oxide minerals, 19.1% and 18.4%, respectively, whereas lacustrine deposits have the lowest average quartz and oxide minerals, 8.9% and 10.3%, respectively (Table 18). Although absent from the alluvial fan and lacustrine deposits, carbonate minerals were present in the meandering stream deposits (average 2.2%) (Table 18).

### 3.18 X-Ray Diffraction Methods

#### 3.18.1 Introduction

X-ray diffraction (XRD) is an analytical technique primarily used to study the characteristics of crystalline structures and to determine the mineralogy of fine-grained sediments such as clays. XRD is attractive because it is a powerful and rapid (< 20 minutes per sample) technique that provides an unambiguous mineral determination with minimal sample preparation, and relatively straight forward data interpretation (Poppe et al., 2001; Dutrow and Clark, 2015). X-ray diffraction is used to analyze and identify crystalline structures because the wavelength of X-rays and the spacing of atoms in a

crystalline structure are approximately the same. This is an essential feature of the diffraction of waves which was identified by von Laue in 1912 (Moore and Reynolds, 1997).

Diffraction, or constructive interference, occurs when the interaction of the incident beam with the sample satisfies Bragg's Law (Equation 5) (Poppe et al., 2001; Dutrow and Clark, 2015).

$$n\lambda = 2d\sin\theta \qquad \text{Eq. 5}$$

Bragg's law explains that some of the x-rays are scattered in a certain direction in which they are in phase with each other (Poppe et al., 2001). Under this condition, the x-rays mutually reinforce each other resulting in a peak in intensity also known as a diffraction peak. Bragg's law, where  $n$  is a positive integer,  $\lambda$  is the wavelength of the x-ray,  $d$  is the spacing of the crystal lattice, and  $\theta$  is the incident angle, describes the angle ( $2\theta$ ) where constructive interference will be the strongest based on the spacing of parallel planes of atoms ( $d$ ) (Equation 5) (Moore and Reynolds, 1997, Nave, 2017; Poppe, et al., 2001; Dutrow and Clark, 2015).

A Rigaku Miniflex XRD located at the University of North Carolina at Charlotte was used for all XRD analyses. The procedure used to operate the XRD is described in Speakman (2015). In this diffractometer, the sample and the detector both slowly rotate which helps to keep the x-ray beam properly aligned.

### 3.19 Sample Selection and Preparation for XRD Analyses

X-ray diffraction is the most common analytical method used to determine the mineralogy of fine-grained sediments, especially clays (Poppe et al., 2001). As a result of limited funding which constrained the number of coarse-grained samples analyzed by petrographic analyses, the bulk mineral composition including the qualitative identification and semi-quantitative analyses of the mineral phases of one hundred eighty-five samples were determined using XRD (Appendix C) (Moore and Reynolds, 1997; Poppe et al., 2001). The samples sieved using the 325-mesh (0.044 mm) sieve were used for all XRD analyses. A device was provided by the Rigaku Corporation to prepare a powdered sample for XRD analysis (Figure 60). The device includes a metal pedestal, a round glass disk, a hollow metal disk, and a plastic ring. This device was assembled and a finely-powdered ( $< 0.044$  mm) sample was brushed through a 230-mesh (0.063 mm) sieve to achieve even distribution and to minimize preferred orientation of the particles (Poppe et al., 2001). Once enough sample was brushed through the 230-mesh sieve, the sieve was removed and a tamper was used to pack the sample into the metal disk firmly enough so that it did not fall out, but not so firmly that preferred orientation resulted on the opposite side. The metal disk with the sample was then gently removed from the sample preparation device and carefully placed in the XRD. The analyses were conducted through a range of  $2\theta$  from  $3^\circ$  to  $90^\circ$ . The sample holder rotated  $1.5^\circ$  per minute. This speed was selected because it was a compromise between accuracy and the time required for analysis. A rotation of  $1^\circ$  per min would result in a slightly more accurate result, but it would have taken significantly longer per sample to process. A rotation of  $2^\circ$  per minute

would have reduced exposure time, but it would also reduce the accuracy of the results. Thus, a rotation of 1.5° per minute was chosen.

Two additional mudstone and shale samples, SB-24 and SB-27, were collected from the Sanford sub-basin, but due to a relatively high percentage of organic matter, these samples were not analyzed using XRD (Table 19 and Appendix C). The presence of organic matter can cause challenges when using XRD for mineralogical analyses because it can cause broad X-ray diffraction peaks, increase background interference, and hinder the dispersal of other minerals (Moore and Reynolds, 1997). For example, Figure 61 displays the diffractogram of sample SB-28 which consists of 0.95% TOC (Table 19). The relatively high organic content caused broadening of the X-ray diffraction peaks and an increase in background interference which made mineral identification difficult. The peaks of the candidate phases selected by the PDXL2 software did not match very well. The TOC analyses are discussed in the following section.

### 3.20 Total organic carbon analyses and results

To assess the percentage of total organic carbon (TOC) in organic-rich samples, the samples were analyzed using a Thermo Scientific Flash 2000 Organic Elemental Analyzer located at the University of North Carolina at Charlotte. Ten (100 mesh; 0.149 mm) samples, selected based on a gray or black color indicating organic matter, were analyzed for TOC (Table 19). 9 of the 10 samples were collected from the Sanford sub-basin and 7 of those samples had a measureable amount of TOC ranging from 0.04% to 29.35% TOC. A minimum amount of organic material ranging generally from 0.4%-1.4% TOC is necessary to generate and expel oil from shale rocks. Thus, these 7 samples with a median of 1.42% TOC suggest the Sanford sub-basin may have contained

sufficient organic carbon to generate hydrocarbons. These data help to further characterize the organic content of the Sanford sub-basin.

### 3.21 XRD Mineral Identification and Grouping

An X-ray diffractogram was generated for each sample that was analyzed using XRD (e.g. Figure 61). Each diffractogram was loaded into an integrated X-ray powder diffraction software program called PDXL2 (Figure 62). PDXL2 is a comprehensive software package designed by the Rigaku Corporation to help users that are not specialists in the field of X-ray diffraction to easily perform many types of analysis (Rigaku, 2010). To determine the bulk mineral composition, information from the sample's X-ray diffractogram including peak position, intensity, and width were used (Figures 62-66). An automatic search for substances that were mineral-related was used to identify the peaks on a diffractogram, therefore, reducing the possibility of human error (Figure 63). The next step was phase identification which began by searching for a mineral that could account for the most intense peak or peaks present on a diffractogram (Figure 64). Once a mineral was identified, its presence was confirmed by matching the positions of lower intensity peaks on the diffractogram with the mineral's X-ray diffraction pattern (Moore and Reynolds, 1997). Once a set of peaks was confirmed as belonging to a mineral phase such as quartz, these peaks were eliminated from further consideration (Figure 65) (Rigaku, 2010). The process was repeated for each mineral identified by the PDXL2 software in the sample (Figure 66). The software was able to identify the mineral phases present in the sample by searching a reference database such as the International Center for Diffraction Data's (ICDD) PDF-2 (Rigaku, 2010). Although the PDXL2 software was useful for identifying mineral phases, several

minerals or varieties of minerals often were identified by the software that could fit a set of lower intensity peaks (Figure 66). Under these circumstances, time was given to identify the best fitting mineral by individually selecting the mineral and attempting to align its peaks to the peaks identified in a sample's diffractogram.

As previously stated, one hundred eighty-five samples were analyzed using XRD. Appendix C shows the results of the X-ray diffraction analyses in which 27 minerals were identified in the samples from the Deep River basin. The color scheme and abbreviations used for the semi-quantitative data are as follows: green, XX = highest intensity; yellow, X = high intensity; red, xx = medium intensity; orange, x = lowest intensity. These intensities were determined using the PDXL2 software. As the software identified candidate phases of minerals, they were presented in order of decreasing occurrence (for example see Figure 65).

In order to investigate the water-rock interactions that occur in the Deep River basin, a series of sequential extraction experiments were conducted on samples collected from each of the sub-basins. Thus, similar to the petrographic data, the XRD data were organized into mineral groups that reflect the geochemical fractions targeted by the sequential extractions. For the XRD data, five mineral groups were identified including: 1) the quartz mineral group, 2) the feldspar mineral group, 3) the clay mineral group, 4) the carbonate mineral group, and 5) the 'other' mineral group (Table 20 and Appendix C). The sequential extractions are discussed in greater detail in Chapter 4.

#### 3.21.1 Quartz mineral group

For the XRD data, the quartz mineral group represents quartz minerals identified using the PDXL2 software (Table 20). Low, or  $\alpha$  - quartz is thermodynamically stable

under sedimentary conditions and is, therefore, the most common of the silica minerals in sedimentary rocks (Pettijohn et al., 1987; Moore and Reynolds, 1997). Quartz is often present in the clay-size fraction of sedimentary rocks and its diffraction pattern can be used as an internal standard against which the accuracy and precision of peak positions of other phases present can be estimated (Moore and Reynolds, 1997). The strongest peak associated with quartz occurs at  $26.67^\circ 2\theta$  for  $\text{CuK}\alpha$  and the second-most-intense peak for quartz occurs at the  $20.8^\circ 2\theta$  position (Figure 67). Weaker peaks associated with quartz were also present and eliminated once confirmed.

### 3.21.2 Feldspar mineral group

The XRD data show the two principal feldspar families, the potassium feldspars, orthoclase and sanidine, and the plagioclase feldspars, albite and anorthite, were present in the samples from the Deep River basin (Table 20 and Appendix C). As a result of low symmetry and variable compositions, feldspars have complex diffraction patterns which complicate the identification and quantification of the varieties of feldspars present in a sample (Moore and Reynolds, 1997). The diffraction pattern of the plagioclase feldspars, anorthite and albite, are illustrated in Figures 61 and 67, respectively. Several diffraction peaks at  $22.05^\circ$ ,  $23.50^\circ$ ,  $24.90^\circ$ , and, the most intense peak, at  $\sim 28^\circ 2\theta$  are useful in identifying plagioclase minerals (Figure 67) (Moore and Reynolds, 1997). These characteristic peaks are less apparent in the diffractogram of sample SB-28 which consists of anorthite (Figure 61). As previously discussed, the relatively high organic content of sample SB-28 caused broadening of the X-ray diffraction peaks and an increase in background interference which made mineral identification difficult.

The diffraction pattern for orthoclase is shown in Figure 68. The diffraction peak at  $\sim 27.5^\circ 2\theta$  indicates some variety of potassium feldspar, k-feldspar, is present (Moore and Reynolds, 1997). Several diffraction peaks at  $21.05^\circ$ ,  $25.66^\circ$ ,  $26.75^\circ$ , and  $\sim 27.53^\circ 2\theta$  are useful in identifying orthoclase (Figure 68) (Moore and Reynolds, 1997). The K-feldspar, sanidine, has a similar diffraction pattern to orthoclase. As a result, the diffraction pattern shown in Figure 80 is representative of both varieties of K-feldspar (Moore and Reynolds, 1997).

### 3.21.3 Clay mineral groups

Clay minerals such as kaolinite and smectite and other phyllosilicates like mica and chlorite are often essential constituents in the matrix of sandstones and coarse clastics and are the main component of mudrocks (Pettijohn et al., 1984; Newman and Brown, 1987; Tucker, 2001). These phyllosilicate minerals are closely related in chemical composition (hydrous aluminosilicates) and crystal structure (a sheet-like, or layered structure). Additionally, phyllosilicates share a capability for ion-exchange (Carroll, 1959; Newman and Brown, 1987). For the purposes of this study, clay and clay minerals refer to hydrous aluminosilicates with a specific sheet-like structure (phyllosilicates). Clay minerals are typically less than 2 microns ( $\mu\text{m}$ ), but grains may reach 10  $\mu\text{m}$  or more (Tucker, 2001).

Clay minerals consist of sheets of silica tetrahedra (t sheets) mutually sharing certain oxygen ( $\text{O}^{2-}$ ) and hydroxyl ( $\text{OH}^-$ ) anions with octahedral sheets (o sheets) (Figure 69) (Newman and Brown, 1987; Pettijohn et al., 1987; Tucker, 2001). The t sheets consist of silicon-oxygen tetrahedra with three oxygen atoms internally linked together with the corner oxygen atoms of adjacent tetrahedra (Figure 69). The o sheets consist of

exchangeable cations such as aluminum, calcium, magnesium, and iron in octahedral coordination with OH<sup>-</sup> anions arranged around the cations (Figure 69) (Newman and Brown, 1987; Pettijohn et al., 1987; Tucker, 2001; Prothero and Schwab, 2014). Layers made of aluminum hydroxide, Al-O/OH, are referred to as gibbsite layers because the mineral gibbsite is composed entirely of these layers (Tucker, 2001; Prothero and Schwab, 2014).

Most clay minerals are classified as dioctahedral or trioctahedral minerals depending on the nature of the octahedrally coordinated cations. In dioctahedral minerals, about two-thirds of the available cation sites are occupied by trivalent cations such as aluminum (Al<sup>+3</sup>) and iron (Fe<sup>+3</sup>). In trioctahedral minerals, all or most of the available cation sites are occupied by divalent cations such as magnesium (Mg<sup>+2</sup>) and iron (Fe<sup>+2</sup>) (Newman and Brown, 1987). Most clay minerals are composed of packets of tetrahedral and octahedral sheets, which repeat over and over again (Figure 69). The stacking arrangement of these sheets and substitutions by exchangeable interlayer cations and, to a lesser extent octahedral cations, results in considerable chemical variability within the clay minerals (Pettijohn et al., 1987; Tucker, 2001; Prothero and Schwab, 2014).

As discussed in section 3.8, the clay mineral group was used to target exchangeable cations during the sequential extraction analyses (Figure 45). Thus, for the XRD analyses, the clay mineral group includes all of the major groups of clay minerals: the kaolinite group, the smectite group, the mica group, the chlorite group, and the mixed-layer group (Table 20 and Appendix C) (Tucker, 2001). These clay minerals will be discussed in greater detail in the following sections.

### *Kaolinite group*

The classification of clay mineral groups is primarily based on structure rather than composition. Thus, two basic groups of clay minerals are distinguished according to structural type, the kandite group and the smectite group (Figure 69) (Pettijohn et al, 1987, Tucker, 2001). The kandite group will be discussed here while the smectite group is discussed in the next section.

Kaolinite is the most common kandite mineral, therefore, its name is often used to refer to the kandite group (Grim, 1953; Prothero and Schwab, 2014). Thus, for this study, the kandite group is referred to as the kaolinite group. The kaolinite group is characterized by the simplest arrangement, one silica tetrahedral sheet (t sheet) linked to an aluminum octahedral sheet (o sheet) (Figure 69) (Prothero and Schwab, 2014). In this arrangement, referred to as a 1:1 group, the layers are tightly bonded together. Thus, unlike in most other clays, there is no room for water, hydroxyl anions, or larger cations between the layers. As a result, the kaolinite group is chemically and mineralogically simple compared to other clay minerals (Pettijohn et al, 1987; Prothero and Schwab, 2014).

Two varieties of clay minerals from the kaolinite group, dickite and halloysite, were identified by XRD (Appendix C) The clay mineral, dickite, is a stacking polymorph of kaolinite (Grim, 1953; Pettijohn et. al, 1987; Tucker, 2001). The clay mineral, halloysite, is closely related to, but distinctly different from kaolinite (Grim, 1953; Newman and Brown, 1987). Halloysite differs from kaolinite because the hydrated form of halloysite has water molecules located between the aluminosilicate layers. The interlayer water molecules are readily volatilized at room temperature and consequently,

the basal spacing decreases. Thus, two forms of halloysite can be distinguished: 1) halloysite (10 Å) is the more hydrous form with a basal spacing of 10 Å, and 2) halloysite (7 Å) is the less hydrated form which also has the same chemical composition as kaolinite (Grim, 1953; Newman and Brown, 1987). There is little agreement among clay mineralogists regarding the proper nomenclature for halloysite minerals. As a result, for this study, halloysite is used for all forms of the mineral regardless of level of hydration (Grim, 1953).

In addition to the dioctahedral kaolinite group, two species from the trioctahedral serpentine group, lizardite and guidottiite, were also identified by XRD (Appendix C) (Newman and Brown, 1987; Hudson Institute of Mineralogy, 1993-2018). Similar to the kaolinite group, the serpentine group is characterized by uncharged 1:1 layers. In serpentine minerals, all or most of the available cation sites are occupied by divalent cations such as  $Mg^{+2}$ ,  $Fe^{+2}$ , manganese ( $Mn^{+2}$ ), or nickel ( $Ni^{+2}$ ) (Newman and Brown, 1987). For example, lizardite is a Mg-rich serpentine mineral with a planar structure and guidottiite, a more fibrous serpentine mineral, contains abundant  $Mn^{+2}$  and/or  $Fe^{+3}$  (Newman and Brown, 1987; Hudson Institute of Mineralogy, 1993-2018; Mineralogical Society of America, 2004-2018). It was decided that because kaolinite and serpentine minerals are both characterized by uncharged 1:1 layers and few samples from the Deep River Basin were identified as containing serpentine minerals, these minerals would be grouped together as the kaolinite group (Appendix C).

#### *Smectite group*

The smectite group is characterized by a three-layered structure consisting of two silica tetrahedral sheets (t sheets) sandwiched around an aluminum octahedral sheet (o sheet), referred to as a 2:1 group (Figure 69) (Tucker, 2001; Prothero and Schwab, 2014).

A small amount of  $Mg^{+2}$ ,  $Fe^{+2}$ , and/or  $Zn^{+2}$  substitutes for  $Al^{+3}$  within the 2:1 layers causing the layers to carry a small net negative charge. This charge is balanced by easily exchangeable cations such as sodium ( $Na^+$ ), potassium ( $K^+$ ) and calcium ( $Ca^{+2}$ ) which are contained in interlayer positions (Newman and Brown, 1987; Pettijohn et al., 1987; Tucker, 2001; Prothero and Schwab, 2014). Water molecules are often absorbed with cations between the 2:1 layers. Consequently, the structure of the smectite group is very expandable and the distance between the layers is dependent on the degree of hydration (Newman and Brown, 1987; Prothero and Schwab, 2014). The typical basal spacing in smectites is 14 Å, but it may vary from 9.6 Å, at dehydration, up to 21.4 Å (Tucker, 2001). Substitutions within and between the 2:1 layers of the smectite group result in variations in the composition of the group, but the expanding-lattice structure of these minerals is generally considered to be an essential characteristic of the smectite group (Grim, 1953; Newman and Brown, 1987). Thus, this characteristic feature can be used to identify smectite minerals using XRD (Tucker, 2001).

Three varieties of minerals from the smectite group, montmorillonite, nontronite, and yakhontovite, were identified by XRD (Appendix C). The composition of these dioctahedral smectites ranges from the predominantly aluminum-rich end members, montmorillonite and beidellite, to the iron-rich end member, nontronite (Newman and Brown, 1987; Pettijohn et al., 1987). The aluminum-rich end member varieties are distinguished based on the site of the negative charge on the layers. In montmorillonite, the most common smectite, divalent cations, usually  $Mg^{+2}$ , in octahedral coordination give rise to the charge on the layers. The diffraction pattern of montmorillonite is displayed in Figure 67. In beidellite,  $Al^{+3}$  cations in tetrahedral sites are the source of the

charge. The iron-rich end member, nontronite, is comparable to a beidellite, but with all octahedral Al replaced by  $\text{Fe}^{+3}$  (Newman and Brown, 1987, Tucker, 2001). Occasionally, uncommon elements such as chromium, nickel, and copper substitute into the structures of smectites (Newman and Brown, 1987). For example, yakhontovite is a smectite mineral that is characterized by the substitution copper cations (Mineralogical Society of America, 2004-2018).

Similar to smectite, vermiculite is characterized by a 2:1 group with all octahedral positions occupied by  $\text{Mg}^{+2}$  and  $\text{Fe}^{+2}$  and the substitution of  $\text{Al}^{+3}$  cations in tetrahedral sites (Grim, 1953; Tucker, 2001). Additionally, the structure of vermiculite is expandable, although it is less so than smectite, and the distance between the 2:1 layers is dependent on the degree of hydration (Newman and Brown, 1987; Tucker, 2001; Prothero and Schwab, 2014). Because these two mineral groups are chemically and structurally similar and few samples from the Deep River Basin were identified as containing vermiculite minerals, it was decided that these minerals would be grouped together as the smectite group (Appendix C). The diffraction pattern of vermiculite is displayed in Figure 71.

#### *Mica group*

The mica group is characterized by a 2:1 group with unhydrated cations in interlayer positions (Figure 69). In micas such as muscovite and biotite, the substitution of  $\text{Al}^{+3}$  for  $\text{Si}^{+4}$  in tetrahedral layers results in a charge deficiency that is balanced by interlayer cations which are predominantly potassium (K) and sodium (Na) (Newman and Brown, 1987; Pettijohn et al., 1987; Tucker, 2001). Strong ionic bonding caused by the presence of the interlayer cations prevents the 2:1 structure from easily expanding (Prothero and Schwab, 2014). This results in a basal spacing of about 10 Å (Newman and

Brown, 1987; Tucker, 2001). Additionally, the strong ionic bonding limits the percolation of ions through the structure, therefore, most of the  $\text{OH}^-$ ,  $\text{Fe}^{+2}$ , and  $\text{Mg}^{+2}$  ions, if present, are found on the edges of the sheets unless weathering has degraded the structure (Tucker, 2001; Prothero and Schwab, 2014.)

For this study, the mica mineral group includes: muscovite, annite, and a common clay mica, illite (Appendix C). Muscovite is the simplest 2:1 clay with only potassium cations in interlayer positions (Prothero and Schwab, 2014). Figure 71 shows the diffraction pattern of muscovite. Annite, a variety of biotite mica, is characterized by  $\text{Fe}^{+2}$  in octahedral sites (Newman and Brown, 1987; Mineralogical Society of America, 2004-2018). The diffraction pattern for annite is shown in Figure 61.

Although similar to mica, it is unclear if and how illite, the most abundant clay mineral, should be classified with regards to other phyllosilicates such as smectites and other micas because it is often interstratified (Newman and Brown, 1987; Lynn et al., 2008). Illite is often described as a K-deficient muscovite because it has approximately 70-80% as much interlayer potassium as muscovite (Prothero and Schwab, 2014; Hudson Institute of Mineralogy, 1993-2018). As previously stated, clay micas such as sericite and illite, many of which are interstratified, are part of an important clay mineral group that has no definition in terms of end-member composition nor clear constraints on their structural composition (Newman and Brown, 1987). Thus, since illite is a fine-grained, clay mica, it was grouped with the other micas which include muscovite and annite (Table 22 and Appendix C). The diffraction pattern of illite is displayed in Figure 72.

### *Chlorite group*

The chlorite group, like smectites and micas, is characterized by a 2:1 structure (Tucker, 2001). In chlorite minerals, however, the net negative charge on the 2:1 layers is balanced by positively charged interlayer hydroxide sheets (Newman and Brown, 1987; Tucker, 2001; Prothero and Schwab, 2014). Thus, the chlorite structural unit consists of two octahedral sheets, one within the 2:1 layers and another one located between the layers (Newman and Brown, 1987).

In chlorite minerals, the octahedral sheets consist of exchangeable cations such as magnesium and iron in octahedral coordination with OH<sup>-</sup> anions arranged around the cations (Newman and Brown, 1987; Pettijohn et al., 1987; Tucker, 2001; Prothero and Schwab, 2014). The substitution of Fe<sup>+2</sup> is responsible for the familiar green color of the chlorite group. Octahedral layers made of magnesium hydroxide (Mg-OH) are referred to as brucite layers because the mineral brucite is composed entirely of these layers (Newman and Brown, 1987; Pettijohn et al., 1987, Tucker, 2001). For this study, the chlorite mineral group is represented by the mineral clinochlore (Appendix C). Clinochlore is described as the Mg-rich end member of the trioctahedral chlorites (Newman and Brown, 1987). The diffraction pattern of clinochlore is shown in Figure 68.

### *Mixed-layer clay group*

The 1:1 and 2:1 groups of clay minerals are very similar. Both are composed of tetrahedral and octahedral sheets strongly bonded internally, but relatively weakly bonded to each other (Newman and Brown, 1987; Prothero and Schwab, 2014). Additionally, the 1:1 and 2:1 groups have a similar surface geometry as the interlayer hydroxide sheets found in chlorites (Newman and Brown, 1987). As a result of these similarities, many clay minerals are mixed-layered, with either regular or random

mixtures of layers of different clay minerals (Grim, 1953; Newman and Brown, 1987; Prothero and Schwab, 2014).

Two varieties of mixed-layer clays were identified by XRD. Chlorite, discussed above and identified as an individual group for XRD, is an example of a regular mixed-layer mineral in which biotite mica layers are interstratified with brucite layers (Grim, 1953; Newman and Brown, 1987). Likewise, tosudite is a regular mixed-layer clay mineral consisting of layers of chlorite and smectite (Mineralogical Society of America, 2004-2018).

In summary, the clay mineral group includes: dickite, halloysite, lizardite, and guidottiite from the kaolinite group; montmorillonite, nontronite, yakhontovite, and vermiculite from the smectite group; muscovite, annite, and illite from the mica group; clinochlore from the chlorite group, and tosudite from the mixed-layer group (Table 20 and Appendix C).

#### 3.21.4 Carbonate mineral group

The carbonate mineral group, for this study, is comprised of the minerals calcite and dolomite (Table 20 and Appendix C). Calcite and dolomite are abundant in sandstones and may be found as even-to-patchy pore filling cements and replacements or as local segregations and concretions (Pettijohn et al., 1987; Tucker, 2001). Additionally, calcite may be present as detrital grains, cements in aggregates, and in other fine-grained masses often mixed with clay and other minerals (Tucker, 2001; Lynn et al., 2008). Petrographic analyses of the samples from the Deep River basin, showed calcite is predominantly present as a cement. The diffraction pattern of calcite is displayed in Figure 73.

The XRD data show dolomite was present in one sample, SB-23, from the Sanford sub-basin (Appendix C). Figure 19 shows this sample was collected from a large displacive nodule. The nodule likely formed in the sediments while they were still soft and not compacted. This can be recognized from the folded laminae in the black mudrock around the nodule. This suggests compaction took place after the growth of the nodule (Tucker, 2001). The diffraction pattern for the dolomite nodule is displayed in Figure 70.

#### 3.21.5 'Other' mineral group

For this study, the 'other' mineral group refers to minerals that were not specifically targeted by the sequential extraction analyses and/or were present in less than 3% of the samples (Table 20 and Appendix C). For example, franklinite, a spinel mineral was identified in two samples from the Deep River Basin (Figure 72 and Appendix C). Although present, spinel minerals are not of particular interest to this study, therefore, franklinite was grouped in the other mineral group. Hematite is an oxide mineral that was used to target strong-acid soluble phases in the sequential extractions, but XRD analyses identified hematite in only 2 of the 185 samples. Thus, for the XRD analyses, it was decided to categorize hematite with the 'other' mineral group.

#### 3.22 The Results of the XRD Analyses: Deep River Basin

One hundred eighty-five samples from the Deep River basin were analyzed using XRD. Appendix D shows the relative abundance of the mineral groups present in the Deep River basin samples and identified by XRD. The color scheme and abbreviations used for the semi-quantitative data are as follows: green, XX = highest intensity; yellow, X = high intensity; red, xx = medium intensity; orange, x = lowest intensity. In order to convert the semi-quantitative data into more quantifiable data, the symbols such as XX

were changed to a numerical value which ranged from a maximum value of 4 to a minimum value of 0. The conversion went as follows: green, XX, 4 = highest intensity; yellow, X, 3 = high intensity; red, xx, 2 = medium intensity; orange, x, 1 = lowest intensity. A cell left blank was counted as a zero indicating the mineral group was not present in the sample (Appendix D). Thus, a higher numerical value indicates a greater relative abundance of the mineral in a sample (Appendix D and Table 21).

Using the numerical values representative of relative abundance, the relative abundance of each mineral group identified in the Deep River basin was determined (Table 21). Table 21 summarizes the mineralogical data obtained through XRD which are also located in Appendices C and D. The values in Table 21 were obtained by converting the symbols such as XX to a numerical value as discussed above. These values were averaged to determine the relative abundance of the mineral groups in the Deep River basin as a whole as well as the individual sub-basins. Based on the XRD data, the Deep River basin is characterized by an abundance of quartz, feldspar, and clay minerals (Appendix D and Table 21). Carbonate minerals and the ‘other’ mineral group are also present, but in relatively small quantities.

Of the three most abundant mineral groups, quartz is the most common mineral group in the Deep River basin with a relative abundance of 3.8 (Table 21). Feldspar minerals such as albite, orthoclase, and sanidine are the second most abundant mineral group with a relative abundance of 2.1 (Appendix C and Table 21). In general, albite was the most common feldspar identified by XRD in the Deep River basin samples (Appendix C). Clay minerals such as muscovite, chlorite, and smectite comprise a relative abundance of 2.0 of the samples (Appendix C and Table 21). In samples from the

Deep River basin, the mica group appears to be the most common clay mineral group (Appendix C). Muscovite is the most common mica and illite, the clay mica, is also fairly common (Appendix C). The chlorite group represented by the mineral clinocllore is the second most common clay mineral group identified by XRD. Lastly, smectite minerals such as montmorillonite, nontronite and yakhontovite appear to be more common than kaolinite minerals and mixed-layer clays (Appendix C).

As previously stated, the XRD data show carbonate minerals such as calcite and dolomite and the ‘other’ mineral group constitute relatively small quantities of the samples collected from the Deep River basin (Table 21 and Appendix D). Carbonate minerals have a relative abundance of 0.5 (Table 21). The XRD data show calcite is more abundant than dolomite in the Deep River basin samples (Appendix C). The ‘other’ mineral group has a relative abundance of 0.1 (Table 21). As the ‘other’ mineral group is not pertinent for the sequential extractions, this group is not discussed further.

#### 3.22.1 XRD analysis of Wadesboro sub-basin samples

Fifty-five samples from Wadesboro sub-basin were analyzed using XRD (Appendices C and D). The samples from the Wadesboro sub-basin are characterized by a high relative abundance (3.8) of quartz minerals (Table 21). Feldspar minerals have a relative abundance of 1.9 and are the second most abundant mineral group. Clay minerals and carbonate minerals constitute similar relative abundances, 1.6 and 1.5, respectively (Table 21). In the Wadesboro sub-basin, calcite was found in 27 samples (Appendix C).

#### 3.22.2 XRD analysis of Sanford sub-basin samples

Thirty-eight samples from the Sanford sub-basin were analyzed using XRD (Appendices C and D). The samples from the Sanford sub-basin are characterized by a

high relative abundance (3.5) of quartz minerals (Table 21). Clay minerals are the second most abundant mineral group with a relative abundance of 2.4. Feldspar minerals are the third most abundant mineral group with a relative abundance of 2.0. In the Sanford sub-basin, carbonate minerals have a relative abundance of 0.1 (Table 21). As previously discussed in section 3.21, the XRD data show dolomite was present in one sample, SB-23, from the Sanford sub-basin (Appendix C). Figure 19 shows this sample was collected from a large displacive nodule that likely formed in the sediments while they were still soft and not compacted.

### 3.22.3 XRD analysis of Durham sub-basin samples

Ninety-two samples from the Durham sub-basin were analyzed using XRD (Appendices C and D). The samples from the Durham sub-basin are characterized by a high relative abundance (3.9) of quartz minerals (Table 21). Feldspar minerals are the second most abundant mineral group with a relative abundance of 2.3. Clay minerals are the third most abundant mineral group with a relative abundance of 2.0. In the Durham sub-basin, carbonate minerals have a low relative abundance of 0.2 (Table 21). 5 samples from the Durham sub-basin had calcite minerals present (Appendix C).

### 3.22.4 Trends in basin-wide mineralogy based on XRD analysis

The XRD data obtained from the three sub-basins were compared to each other in order to examine spatial trends, if any, present across the basin (Table 21). The Deep River basin and its sub-basins are characterized by compositionally immature sediments (Table 21). Quartz and feldspar minerals are the most abundant mineral groups in the sub-basins of the Deep River Basin (Table 21).

The sub-basins are also characterized by a high relative abundance of clay minerals. Basin-wide, clay minerals represent a similar relative abundance as feldspar minerals, 2.1 and 2.0, respectively (Table 21). The Sanford sub-basin is characterized by the highest relative abundance of clay minerals, 2.4 (Table 21). The Durham and Wadesboro sub-basins are characterized by a lower relative abundance of clay minerals, 2.0 and 1.6, respectively (Table 21).

The XRD data show the Deep River basin is characterized by a low relative abundance of carbonate minerals (0.5) (Table 21). However, the deposits of the Wadesboro sub-basin have different mineralogical characteristics compared to the Deep River basin as a whole and to the other sub-basins. The Wadesboro sub-basin is characterized by a high relative abundance of carbonate minerals (1.5) compared to the Deep River basin (0.5) and the Sanford and Durham sub-basins, 0.1 and 0.2, respectively (Table 21). Additionally, compared to the Deep River Basin and the other sub-basins, the Wadesboro sub-basin has lower relative abundances of both feldspar and clay minerals, 1.9 and 1.6, respectively (Table 21).

#### 3.22.5 Variation in Deep River basin mineralogy with respect to grain-size

As previously stated in section 1.3, the purpose of this research is to provide baseline data of water-rock interactions occurring in the Deep River basin. Additionally, mineralogy and grain size were hypothesized to influence the chemical characteristics of formation water (section 1.4). The XRD data were, therefore, used to examine the variation in mineralogy of the samples collected from the Deep River basin with respect to grain size (Table 22).

Based on the XRD data, the relative abundance of mineral groups varies with grain size in the samples from the Deep River basin. In general, the relative abundance of quartz and feldspar in samples from the Deep River basin increases with increasing grain size from mudstone and shale to gravel (Table 22). Gravel-sized samples appear to have an anomalous low relative abundance of feldspar minerals (1.5) compared to other coarse-grained samples such as medium-coarse-very coarse-sand sized samples (2.7) (Table 22).

The XRD data suggest the relative abundance of clay minerals and carbonate minerals appears to decrease with increasing grain size. Fine-grained deposits such as mudstones and shales have a high relative abundance of clay minerals (2.5) and carbonate minerals (1.2) while coarse-grained deposits such as medium-coarse-very coarse sandstones have a lower relative abundance of clay minerals (1.6) and carbonate minerals (0.2) (Table 22).

### 3.23 Stratigraphic Logs Representing the Depositional Environments of the Deep River Basin

As discussed in section 3.13, stratigraphic logs are available for 142 samples collected from the Deep River basin (Figures 47-59; 74-80). As a result of the abundance of information provided by these descriptions, it may be possible to distinguish among the various lithofacies associations present in the Deep River basin and make interpretations regarding the depositional environments (Figures 47-59; 74-80) (Lorenz, 1988; Chem-Nuclear, 1993). Figures 74-79 show the stratigraphic column of a clay pit in the Wadesboro sub-basin recording the depth and depositional environments of the samples collected for this study. The depositional environments listed were, in general, based on observations by Brazell (2013). Figure 80 is a stratigraphic log of a roadcut in

the Sanford sub-basin showing the general location and depositional environment of the samples collected for this study. The depositional environments listed were, in general, based on observations by Reid et al., 2011.

To address the objectives and hypotheses of the study, the XRD data were organized according to depositional environment and related lithofacies associations (Tables 23-26). The 'other' mineral group is displayed in each of the tables but, as previously mentioned, this mineral group is not important for the present study, therefore, it is not discussed.

### 3.24 XRD Mineralogy of Alluvial Fan Environments

Descriptions of alluvial fan environments and the lithofacies associations present in the Deep River basin are located in section 3.14. Based on the XRD data, alluvial fan environments in the Deep River basin are characterized by compositionally immature sediments consisting of a high relative abundance of quartz (4.0) and feldspar (2.7) minerals (Table 23). The XRD data also indicate that alluvial fans have a high relative abundance of clay minerals (1.9), but carbonate minerals were not present in the deposits (Table 23).

The fan fringe and distal fan lithofacies associations are both characterized by compositionally immature sediments (Table 23). The distal fan lithofacies association has a high relative abundance of quartz and feldspar minerals, 4.0 and 3.0, respectively. The fan fringe lithofacies association has a similarly high relative abundance of quartz and feldspar minerals, 4.0 and 2.7, respectively. The distal fan and fan fringe lithofacies associations are also characterized by abundant clay minerals, 2.0 and 1.8, respectively. Lastly, carbonate minerals were not present in the alluvial fan deposits.

### 3.25 XRD Mineralogy of Meandering Stream Environments

Descriptions of meandering stream environments and the lithofacies associations present in the Deep River Basin are located in Section 3.15. Based on the XRD data, meandering stream environments in the Deep River basin are characterized by compositionally immature sediments consisting of a high relative abundance of quartz (3.9), feldspar (2.0) and clay minerals (2.0) (Table 24). The XRD data also revealed that the meandering stream lithofacies association is characterized by a low relative abundance of carbonate minerals (0.7) (Table 24).

Table 24 shows the relative abundance of mineral groups in samples collected from the three sub-environments of a meandering stream: the channel, floodplain, and crevasse splay lithofacies association. Similar to the overall meandering stream environment, each of the individual lithofacies associations is characterized by compositionally immature sediments (Table 24). The channel and crevasse splay lithofacies associations have a high relative abundance of quartz (4.0) and feldspar minerals, 2.4 and 2.6, respectively. Furthermore, the channel and crevasse splay lithofacies associations are characterized by a high relative abundance of clay minerals, 1.9 and 1.5, respectively (Table 24). The floodplain lithofacies association is characterized by a high relative abundance of quartz (3.8) and clay minerals (2.1) (Table 24). Feldspar minerals also represent a high relative abundance (1.8) in the floodplain lithofacies association. Carbonate minerals are present in each of the lithofacies associations with the highest relative abundance (0.8) occurring in the floodplain followed by the crevasse splay (0.6) and channel (0.3) lithofacies associations (Table 24).

### 3.26 XRD Mineralogy of Lacustrine Environments

The descriptions of lacustrine environments and the lithofacies associations present in the Deep River basin are located in sections 3.16. Based on the XRD data, lacustrine environments in the Deep River basin are characterized by compositionally immature sediments consisting of a high relative abundance of quartz, (3.6), clay (2.5), and feldspar minerals (1.8) (Table 25). The XRD data also revealed the lacustrine lithofacies association is characterized by a low relative abundance of carbonate minerals (0.3).

### 3.27 Summary: The Results of the XRD Analysis

In summary, the bulk mineral composition including the qualitative identification and semi-quantitative analyses of the mineral phases of one hundred eighty-five samples were determined using XRD (Appendix C and D) (Moore and Reynolds, 1997; Poppe et al., 2001). According to the XRD data, the Deep River basin is characterized by compositionally immature sediments consisting of a high relative abundance of quartz, feldspars, and clay minerals, 3.8, 2.1, and 2.0, respectively (Table 21). In the Deep River basin, carbonate minerals are present in relatively small quantities (0.5) (Table 21).

The XRD data also indicate the composition of samples from the Deep River basin varies with grain size (Table 22). In general, as grain size increases from mudstone and shale to gravel, the relative abundance of quartz and feldspar increase (Table 22). On the contrary, as grain size increases, the percentages of clay and carbonate minerals decreases.

Finally, the XRD data may indicate that the depositional environment of a sample may influence its composition (Table 26). The depositional environments of the Deep River basin are characterized by compositionally immature deposits consisting of a high

relative abundance quartz, feldspar, and clay minerals. Alluvial fan deposits are characterized by the highest relative abundance of quartz and feldspar minerals, 4.0 and 2.7, respectively, whereas lacustrine deposits have the lowest relative abundance of quartz and feldspar minerals, 3.6 and 1.8, respectively (Table 26). Although absent from the alluvial fan deposits, carbonate minerals were present in the meandering stream and lacustrine deposits, 0.7 and 0.3, respectively (Table 26).

### 3.28 Discussion: Synthesis of the Petrographic and XRD Mineralogical Data Sets

This section examines the two mineralogical data sets, the petrographic data and XRD data, generated for this study. First, the consistency between the data sets is analyzed and possible explanations for any discrepancies among them are explored. The subsequent sections combine the petrographic and XRD data into a large-scale discussion about the mineralogical characteristics, depositional environments, and possible post-depositional history of the Deep River basin and its sub-basins.

#### 3.28.1 An analysis of the consistency of the mineralogical data sets

While the data sets agree that the deposits of the Deep River basin are compositionally immature with small quantities of carbonate minerals, some discrepancies exist between the data sets (Table 27). For example, the abundance of quartz and clay minerals in the Deep River basin does not appear to agree between the petrographic data and XRD data (Table 27). The petrographic data shows quartz (16.5%) is the third most abundant mineral group after clay minerals (30.4%) and feldspar minerals (28.2%). On the contrary, the XRD data, characterizes quartz and feldspar minerals as the most abundant mineral groups in the Deep River basin with a high relative abundance of 3.8 and 2.1, respectively, while clay minerals are third most

abundant (2.0) (Table 27). Additionally, petrographic analyses revealed an abundance of oxide minerals such as magnetite and hematite while XRD analyses identified only two samples with hematite (Appendices A and C and Table 27).

Several reasons may contribute to the differences observed between the mineralogical datasets. First, there are basic differences in the total number and grain-sizes of the samples in each dataset. The petrographic dataset consists of a suite of 18 very fine to very coarse sand-sized samples and one fine to medium pebble (Table 2). Several samples were collected from each sub-basin comprising the Deep River basin to ensure a basin-wide analysis of coarse-grained lithologies using petrography. The XRD dataset consists of all 185 samples used for this study (Appendix C and D). As a result, the XRD dataset is a robust dataset containing the mineralogical data of numerous samples from each sub-basin which represent a wide range of grain sizes from mudstones and shales to conglomerates. Thus, the limited number of samples analyzed with petrography may contribute to some of the differences observed between the petrographic and XRD datasets.

For example, the petrographic samples were predominantly classified as feldspathic greywackes with one lithic greywacke (section 3.10). On the other hand, the XRD dataset contains not only the feldspathic greywackes and the lithic greywacke analyzed using petrography, but the lithic arkoses, feldspathic litharenites, and litharenites that also characterize the Deep River basin (Chem-Nuclear, 1993; Brazell, 2013). The matrix of many sandstones, including the greywackes of the Deep River basin, is primarily authigenic in origin and consists of clay and silt and very fine-grained silica, micas, chlorites, and carbonates (Pettijohn et al. 1987; Chem-Nuclear, 1993;

Tucker, 2001). The samples from the Deep River basin frequently exhibited hematite coatings around grains and an impregnation of hematite into infiltrated and authigenic clay minerals and feldspars. Both the fine-grained nature of the matrix and the hematite staining may have caused much fine-grained quartz to be identified as clay minerals or oxide minerals in the petrographic data. XRD analyses are primarily used to determine the mineralogy of fine-grained sediments such as those found in the matrix of many of the sandstones (Poppe, et al., 2001; Dutrow and Clark, 2015). Consequently, the minerals comprising the fine-grained matrix, instead of being categorized as clay minerals or oxide minerals, were identifiable by their specific mineral phase using XRD (section 3.21). The more accurate identification of the fine-grained matrix including the clay minerals using XRD could possibly account for the lower relative abundance of clay minerals and the higher relative abundance of quartz compared to the petrographic data (Table 27).

The petrographic data may also underestimate the amount of quartz in the Deep River basin because the dataset was limited to greywackes. On the other hand, the XRD dataset contains not only the feldspathic greywackes and the lithic greywacke analyzed using petrography, but the lithic arkoses, feldspathic litharenites, and litharenites that also characterize the Deep River basin (Chem-Nuclear, 1993; Brazell, 2013). The two major groups of sandstones, the arenites and the wackes, are distinguished based on the presence or absence of a matrix (Section 3.10) (Tucker, 2001). Arenites such as arkoses and litharenites are grain-supported and possess little primary matrix (Tucker, 2001). Wackes such as feldspathic greywackes and lithic greywackes are characterized by more than 15% matrix and represent a transitional group between arenites and mudrocks (Figure 43) (Tucker, 2001). Though many minerals have been observed, carbonate

minerals such as calcite and silica comprise the bulk of the cement of many arenites (Pettijohn et al., 1987; Tucker, 2001). In many litharenites, the dominant cementing material is a combination of calcite and quartz cement and authigenic clays (Pettijohn et al., 1987; Tucker, 2001). The petrographic dataset is limited to graywackes and does not examine any arenites. Thus, it is possible that quartz is underestimated in the petrographic data since quartz, in the form of a cement or fine-grained matrix, is not accounted for in the petrographic data.

The two mineralogical data sets, the petrographic data and XRD data, appear to be in agreement that feldspar minerals are the second most abundant mineral group in the Deep River basin, but differ in which variety is most abundant (Table 27). Petrographic analyses revealed the feldspar mineral group consists of the potassium feldspars, orthoclase and microcline, and the plagioclase feldspar mineral, albite (section 3.8). Orthoclase was identified as the most abundant feldspar mineral comprising on average 21.3% of the samples (Table 3). The XRD data show the potassium feldspars, orthoclase and sanidine, and the plagioclase feldspars, albite and anorthite, were present in the samples from the Deep River basin (Table 20 and Appendix C). Albite was the most common feldspar mineral identified by XRD in the Deep River basin samples (Appendix C) (section 3.8).

One possible explanation for the discrepancy between the dominant variety of feldspar may be the observer's lack of experience. During petrographic analyses, some quartz grains may have been misidentified as orthoclase grains. Orthoclase, with its first order birefringence and possible untwinned nature, often looks like quartz (Lynn et al., 2008; Tucker, 2001). This would explain the apparent abundance of orthoclase in the

petrographic data and the lower abundance of quartz (Table 27). As a result of the possible misidentification of quartz as orthoclase and the presence of albite in both the petrographic and XRD datasets, it is surmised that albite is the most abundant feldspar mineral in the Deep River basin (Appendix C, Table 3).

The absence of oxide minerals such as hematite in the XRD dataset may be because hematite and magnetite exist in concentrations of less than 1% in sandstones and conglomerates (Tucker, 2001). It is possible that the abundance of quartz, feldspar, and clay minerals may have overshadowed the peaks associated with oxides. Only a small quantity of hematite is necessary to cause a red color and staining, therefore, the quantity of oxide minerals may have been overestimated in the petrographic analyses (Table 27) (Tucker, 2001). For example, the petrographic analyses revealed sample DB-34 contains a high percentage of oxide minerals such as hematite (Table 8). The XRD analyses, however, indicated no oxide minerals were present (Appendix D). As Figure 42 displays the oxide minerals appear to be predominantly authigenic in origin as the reddish-brown minerals surround and coat many grains. For the reasons discussed in this section, the XRD data were used to examine the relative abundance of quartz, feldspar, and clay minerals in the Deep River basin (Table 27). The petrographic data were used to analyze the abundance of oxide minerals in the basin and both mineralogical datasets were used to examine the abundance of carbonate minerals (Table 27).

### 3.28.2 Mineralogical characteristics and the post-depositional history of the Deep River basin

The mineralogical data collected for this study helps improve our understanding of the geologic history and evolution of the Deep River basin. This section combines the petrographic and XRD data generated for this study into a large-scale discussion about

the mineralogical characteristics, depositional environments, and possible post-depositional history of the basin. In rift basins like the Deep River basin, the nature of the fluvial and lacustrine deposits is controlled by a combination of tectonics, climate, and source area (Lorenz, 1988). The mineralogical characteristics of the sedimentary deposits of the Deep River basin provide evidence supporting this complex relationship (Table 27). High relief source terranes created by tectonic activity created a rugged topography into which vigorous streams cut deep valleys through intensely weathered material to fresh bedrock (Folk, 1980; Pettijohn et al., 1987; Brazell, 2013). It is possible that the irregular pattern of tectonic activity in the Deep River basin maintained the high relief and therefore, provided abundant sediment to the interior of the sub-basins (Folk, 1980; Pettijohn et al., 1987; Brazell, 2013). The short transport distance from the source area resulted in compositionally immature sediments consisting of an abundance of quartz and feldspar minerals throughout the Deep River basin (Table 27).

Quartz, the most stable mineral under sedimentary conditions, is the most abundant mineral group in the Deep River basin (Table 27) (Tucker, 2001). As a result of its abundance in granites and gneisses, orthoclase is the dominant feldspar mineral in many sandstones and clastic deposits. In terms of plagioclase feldspar, albite is often more abundant than anorthite (Folk, 1980; Pettijohn et al., 1987). In the Deep River basin, however, albite is the most abundant feldspar mineral far outweighing both orthoclase and anorthite (Appendix C). Albite was also found by Chem-Nuclear (1993) in the Durham sub-basin and by Brazell (2013) in the Wadesboro sub-basin. The abundance of plagioclase in a formation is unusual and may indicate a nearby volcanic source area (Folk, 1980). Thus, the high abundance of albite compared to orthoclase alludes to the

importance of source area to the mineralogical characteristics of the deposits in the Deep River basin. The source area of the Deep River basin will be explored in greater detail in a subsequent section.

The mineralogical data show clay, carbonate, and oxide minerals are an important components of the Deep River basin (Table 27). Although often present in trace quantities, these mineral groups may provide essential information related to the source area, the depositional environment and later (groundwater) environments, and post-depositional history of the deposits (Pettijohn et al., 1987; Tucker, 2001; Prothero and Schwab, 2014). The presence of these minerals may suggest periods of tectonic stability which allowed pedogenesis and diagenesis to occur. Moreover, the presence of carbonate and oxide minerals may provide clues about the past climate conditions of the Deep River basin. For example, the presence of oxide minerals such as hematite and carbonate minerals in fluvial successions are evidence of diagenetic processes occurring in semi-arid climates (Walker and Cant, 1984; Pettijohn et al., 1987; Tucker, 2001; Chem-Nuclear, 1993; Tucker, 2001; Prothero and Schwab, 2014). Thus, it is possible the Deep River basin was characterized by a semi-arid climate at some time in the past.

Clay minerals such as kaolinite, smectite, mica, and chlorite are abundant in the Deep River basin (Table 27 and Appendix C). In sandstones and coarser clastics, clay minerals are both detrital and authigenic in origin, whereas in mudrocks they are predominantly detrital in origin (Tucker, 2001). Detrital clay minerals also known as inherited clays formed in another area and were later eroded, transported, and deposited in a new location. Thus, inherited clays may provide insight into the provenance of a deposit and possibly the past climate condition of the area (Tucker, 2001). Authigenic

clay minerals in sediments and sedimentary rocks may originate from in situ processes, also called neof ormation, and by the process of transformation (Tucker, 2001).

Neof ormed clays which are precipitated from solution will reflect the pore-fluid chemistry, degree of weathering, and temperature that existed within the sample at some time (Tucker, 2001). Transformed clays are formed by the transformation of inherited clays by ion exchange or cation rearrangement. Many transformed clays still possess some inherited characteristics from the source area, but they also contain information about the chemical environment to which the sample was later subjected (Tucker, 2001).

Sample WB-13, a very-fine-to fine-grained, immature channel sandstone from the Wadesboro sub-basin, illustrates both the detrital and authigenic nature of clay minerals in the Deep River basin (Figure 33). The petrographic analysis of sample WB-13 shows a detrital muscovite grain and an elongate, rounded sericite grain (Figure 33). The sericite grain may indicate the weathering of feldspar grains in the source area which were later transported into the Deep River basin and rounded by fluvial processes. In addition, petrographic analysis of sample WB-13 shows a fine-grained matrix located between and surrounding larger mineral grains (Figure 33). As previously discussed, the matrix is predominantly authigenic in origin and the XRD analyses suggest much of the matrix present in sample WB-13 is most likely fine-grained quartz, feldspar, and chlorite (Appendix C).

In soils and sedimentary rocks such as sandstones, carbonate minerals may be present as detrital grains, cements in aggregates, and in other fine-grained masses often mixed with clay and other minerals (Tucker, 2001; Lynn et al., 2008). Detrital carbonate is abundant in calcareous sands, but is usually only present in minor amounts in

sandstones (Pettijohn et al., 1987). The mineralogical data show calcite is the most abundant carbonate mineral in the Deep River basin (Appendix C). Calcite cement may displace grains causing them to appear to “float” in the cement (Pettijohn et al., 1987; Tucker, 2001). Grains such as micas, feldspars, and even quartz may be forced to split as calcite is precipitated in cracks (Figure 28) (Tucker, 2001). In addition, calcite may replace labile grains such as feldspars (Pettijohn et al., 1987; Tucker, 2001). Carbonate nodules are diagenetic structures that result from the precipitation of some minor mineral such as calcite or dolomite in a host rock. These nodules often form along bedding planes as slowly moving groundwater encounters less permeable layers which restricts its flow. For example, sample SB-23 is a dolomite nodule located in laminated, organic-rich mudstones found along a tributary of the Deep River in the Sanford sub-basin (Figure 19). It is likely the nodule formed in the sediments prior to compaction as recognized by the folded laminae in the black mudrock around the nodule. (Tucker, 2001). Additionally, pedogenesis may result in the formation of carbonate nodules in soil horizons (Pettijohn et al., 1987; Chem-Nuclear, 1993; Brazell, 2013; Prothero and Schwab, 2014). For example, sample WB-26 is a gray to dark reddish-brown siltstone with ripples, desiccation cracks, and calcareous nodules (Figure 74) (Brazell, 2013). Brazell (2013) described the depositional environment of sample WB-26 as transitional, to a subaerial environment as a shallow, possibly short-lived floodplain lake dried up. The calcareous nodules and desiccation cracks are evidence of soil formation and diagenesis (Chem-Nuclear, 1993, Tucker, 2001; Brazell, 2013; Prothero and Schwab, 2014).

Hematite and magnetite are two common opaque, oxide minerals (Tucker, 2001; Lynn et al., 2008). For the purposes of this study, opaque minerals and oxide minerals are

synonymous. Both oxide minerals may be detrital in origin and are derived from metamorphic and igneous rocks. Hematite may also be authigenic such as the formation of hematite coatings around grains and the impregnation of hematite into infiltrated and authigenic clay minerals and feldspars (Tucker, 2001). Sample DB-49 is a poorly sorted, very fine to fine-grained sandstone collected from a crevasse splay deposit in the Durham sub-basin (Figures 38 and 53). This overbank deposit shows both the detrital nature of oxide minerals in the form of isolated, often rounded grains and the authigenic nature of the oxide minerals as they appear to fill a fracture and coat numerous grains (Figure 38).

### 3.28.3 Mineralogical data of the sub-basins

The mineralogical data from the three sub-basins were compared to each other in order to examine spatial trends, if any, present across the basin (Table 27).

The Durham and Wadesboro sub-basins are characterized by a high relative abundance of quartz, 3.9 and 3.8, respectively (Table 27). The Sanford sub-basin, however, has a slightly lower relative abundance of quartz (3.5). All three sub-basins are characterized by a high relative abundance of feldspar minerals (average 2.1), specifically albite, possibly suggesting a nearby volcanic or metamorphic source terrane (Table 27 and Appendix C). Reinemund (1955) suggested the deposits of the Deep River basin were mainly debris eroded from nearby pre-Triassic metamorphic and granitic rocks.

This study shows differences in composition between the sub-basins may suggest slight differences not only in the nature of the depositional environments present, but also a longitudinal variation, from north to south, in source terrane (Table 27). This source terrane interpretation is consistent with previous studies (Reinemund, 1955; Hu and Textoris, 1994). The results of this study show the Sanford sub-basin (2.4) has the highest

relative abundance of clay minerals followed by the Durham sub-basin (2.0) then the Wadesboro sub-basin (1.6) (Table 27). This is consistent with the presence of long-lived lakes in the Sanford sub-basin as discussed in sections 2.4 and 3.4. As previously stated, the lithofacies system of nomenclature of Smoot and others' is used to describe the deposits in the Durham and Wadesboro sub-basin because, unlike the Sanford sub-basin, these sub-basins lack good marker beds or horizons which can be used to assign strata to specific formations (Clark, et al., 2001). All three sub-basins contain a middle clay-shale and mudstone interval 50 to 400 m thick, but the sequence is best developed as the Cumnock Formation within the Sanford sub-basin. The Cumnock Formation is interpreted as having been deposited in a lacustrine and paludal (marshy) environment (Chem-Nuclear, 1993; Brazell, 2013). Thus, the absence of this formation in the Durham and Wadesboro sub-basins may suggest alluvial and fluvial depositional environments were more prevalent than lacustrine environments in those sub-basins.

Additionally, it is possible that differential subsidence caused the Sanford sub-basin to be positioned slightly lower in elevation relative to the Durham and Wadesboro sub-basins. This may have caused the axial fluvial systems present in the Durham and Wadesboro sub-basins to flow into the centrally located Sanford sub-basin (Figure 1). Paleocurrent data from the Durham and Wadesboro sub-basins support this interpretation. The Durham sub-basin was characterized by an overall drainage to the southwest toward the Sanford sub-basin (Textoris, 1994). Changes in depositional environments over time in the Wadesboro sub-basin are indicated by a change in paleoflow directions from south to southwestward in older deposits to a northeastward flow in younger deposits. Thus, it is possible the Wadesboro and Durham sub-basins were hydrologically linked with the

Sanford sub-basin feeding the long-lived deep lakes known to have been present (Brazell, 2013; Textoris, 1994). In this internal-drainage situation, fine-grained sediments were deposited in moist, poorly-drained swamps and relatively long-lived lakes in the Sanford sub-basin (Reinemund, 1955; Miall, 1996). The lower relative abundance of quartz minerals (3.5) and the higher relative abundance of clay minerals (2.4) in the Sanford sub-basin is consistent with this interpretation.

Although present in each sub-basin, the distribution of carbonate and oxide minerals among the sub-basins varies (Table 27). The composition of the Wadesboro sub-basin is quite distinctive among the sub-basins of the Deep River basin (Table 27). The mineralogical data indicate the Wadesboro sub-basin contains the highest abundance of carbonate minerals, but the lowest abundance of oxide minerals. The Sanford sub-basin contains trace quantities of carbonate minerals, but consists of a high average percentage of oxide minerals (Table 27). The Durham sub-basin consists of the median quantity of carbonate minerals, but the highest average percentage of oxide minerals (Table 27). Thus, the percentage of oxide minerals increases northward in the Deep River basin from 3.4% in the southern Wadesboro sub-basin to 17.4 % in the northern Durham sub-basin.

While there are only trace quantities of carbonate minerals in the Sanford sub-basin, oxide minerals account for an average 16.6% of the samples. The presence of the oxide minerals suggests a semi-arid climate for post-depositional processes, but the presence of black, organic-rich shales such as those associated with the Cumnock Formation were likely deposited in long-lived lakes and marshes. Thus, it may be possible that tectonic activity played an important role in the formation and longevity of

the lake environments in the Sanford sub-basin more so than climate as indicated by the presence of oxide minerals. These interpretations are supported by numerous studies such as Hu and Textoris (1994) and Reinemund (1955).

The longitudinal variation of carbonate and oxide minerals in the Deep River basin may provide evidence about differences in the source terrane bordering the basin (Figure 81). Based on the mineralogical analyses of Deep River basin samples conducted for this study, it is possible that the source terranes for the Durham and Sanford sub-basins were more mafic in composition compared to the source terranes for the Wadesboro sub-basin which likely included the Lilesville pluton (Table 27, Figure 81). Additionally, it is possible that tectonics caused the Durham sub-basin to provide more clastic material rich in iron to the Sanford sub-basin compared to the Wadesboro sub-basin. A more efficient hydraulic connectivity between the Durham and Sanford sub-basin may account for the abundance of oxide minerals in the Sanford sub-basin.

Previous studies provide evidence supporting these interpretations (Reinemund, 1955; Hu and Textoris, 1994; Coffey and Textoris, 2003). The Deep River basin is enclosed by pre-Triassic metamorphic rocks and silicic intrusives of the Raleigh metamorphic belt and the metamorphic rocks of the Carolina slate belt (Figure 81) (Reinemund, 1955; Hu and Textoris, 1994; Coffey and Textoris, 2003; Brazell, 2013). The Deep River basin is located along the eastern margin of the Carolina Slate belt in such a way that causes a longitudinal variation in the source terrane bordering the basin (Figure 81). In the Durham sub-basin, the most northern sub-basin, the Carolina slate belt lies in nonconformable contact with the western margin of the sub-basin and the Raleigh metamorphic belt lies in contact with the Jonesboro fault located along the eastern margin

of the sub-basin (Figure 81) (Gilmer et al., 2003). On the contrary, the Wadesboro sub-basin, the southernmost member of the Deep River basin, overlies the Carolina Slate Belt and, along the eastern margin of the sub-basin, portions of the Lilesville pluton (Figure 81) (Brazell, 2013). The Raleigh metamorphic belt does not extend as far south as the Wadesboro sub-basin. The rocks of the Raleigh Belt consist of medium to high-grade quartzofelspathic gneisses and lower-grade mica schists which may have contributed iron, magnesium, and other mafic components to the Durham sub-basin and, possibly, the Sanford sub-basin (Figure 81) (Gilmer et al., 2003).

#### 3.28.4 Synthesis of mineralogical data by grain size

In general, the abundance of quartz and feldspar in samples from the Deep River basin increases with increasing grain size from mudstone and shale to gravel (Table 28). On the contrary, as grain size increases, the abundance of clay, carbonate and oxide minerals decreases (Table 28).

#### 3.29 Synthesis of the Petrographic and XRD Mineralogical Datasets as They Relate to the Depositional Environments of the Deep River Basin

In rift basins such as the Deep River basin, high relief source terranes created by tectonic activity provide abundant sediment to the interior of the basins. As sediments are transported into rift basins from near-source alluvial fans to axial fluvial systems and/or lake systems, textural and compositional changes and changes in the thickness of the deposits can occur (Figure 13) (Reinemund, 1955; Lorenz, 1988). The mineralogical data collected for this study provide evidence of this inherent, transverse relationship among the depositional environments of rift basins such as the Deep River basin. Furthermore, the mineralogical characteristics of the depositional environments appears to be related to post-depositional alteration.

The mineralogical data show the relative abundance of quartz and feldspar decreases with increasing distance from the basin margin and the source area, whereas the abundance of clay minerals increases (Table 29-32). The alluvial fan lithofacies association is characterized by the highest relative abundance of quartz and feldspar minerals, 4.0 and 2.7, respectively (Table 32). The meandering stream lithofacies association is composed of slightly less quartz and feldspar minerals compared to the alluvial fan lithofacies with the relative abundance of 3.9 and 2.0, respectively. The meandering stream and alluvial fan lithofacies associations are characterized by a similar relative abundance of clay minerals, 2.0 and 1.9, respectively. The lacustrine lithofacies association is composed of the lowest amount of quartz and feldspar minerals 3.6 and 1.8, respectively, but the highest relative abundance of clay minerals (2.5) (Table 32).

Although absent from the alluvial fan lithofacies association, carbonate minerals were present in the meandering stream lithofacies association and lacustrine lithofacies associations, 0.7 and 0.3, respectively (Table 32). In contrast, the alluvial fan lithofacies association is characterized by the highest quantity of oxide minerals among the depositional environments. The meandering stream lithofacies association has the second most oxide minerals followed by the lacustrine lithofacies association.

Variations in mineralogy especially clay, carbonate, and oxide minerals among the depositional environments appears to be related to the inherent characteristics of the depositional environments and the degree of post-depositional alteration. For example, the mineralogy of the lacustrine lithofacies association is consistent with a low-energy environment (Tucker, 2001). As illustrated in core W10 MP5, laminated siltstones and mudstones may be deposited as the finer bottomset beds of a delta building into a lake

(Figure 50-52) (Chem-Nuclear, 1993; Tucker, 2001). Additionally, fine-grained sediments such as silt and clay from low-density turbidity currents generate graded beds and settling out of suspension may produce finely-laminated sediments (rhythmites) near the center of the lake (Tucker, 2001).

The meandering stream lithofacies association is characterized by carbonate and oxide minerals. Oxide minerals, however, represent a slightly lower relative abundance in the meandering stream lithofacies association. This may suggest that the iron, manganese, and/or magnesium ions needed to create oxide minerals were less abundant further away from the source area. This interpretation is also supported by the lower abundance of oxide minerals in the lacustrine lithofacies association.

The degree of post-depositional alteration to which the sample was subjected may be, in part, controlled by tectonic activity. For example, samples DB-3 and DB-57 are both poorly-sorted, matrix-supported debris or mud flow deposits, characterized by a similar abundance of quartz and feldspar, but with different amounts of authigenic minerals such as clay and oxide minerals (Table 14) (Figure 47 and 54). The debris or mud flow deposits both appear to be erosive in nature and cut across the underlying fine-grained sediments (Figure 47 and 54). Thus, these deposits may record a change in tectonic activity resulting in a pulse of relatively coarse-grained material into the basin. The relative tectonic stability of the basin after deposition influenced the degree of post-depositional alteration and, therefore, the mineralogy of the samples.

For example, the graphic core log describes the deposit represented by sample DB-3 as carbonaceous with poorly-developed root traces (Figure 47). This may suggest that after a period of renewed tectonic activity which resulted in the deposition of the

debris flow, the landscape was relatively stable for a sufficient period of time to support vegetation and possibly form soils. In contrast, the graphic core log shows the deposit represented by sample DB-57 appears to be one of several coarse-grained debris or mud flow deposits with erosive bases which may truncate the underlying fine-grained sediments (Figure 54). This may suggest that the landscape was relatively unstable for a period of time as fluctuations in tectonic activity resulted in several episodes of fan fringe progradation and retrogradation as a large-scale alluvial fan system gradually prograded into the floodplain of an axial river system (Figure 54). Additionally, evidence of landscape stability and soil formation such as roots, carbonate nodules, and carbonaceous material are absent from the fan fringe lithofacies in this section of the core (Figure 54).

Thus, the presence of carbonate and oxide minerals provides evidence that the landscape was likely relatively stable for a sufficient period of time to support vegetation and possibly to form soils. On the contrary, the absence of these mineral groups may suggest that the landscape was relatively unstable for a period of time due to changes in tectonic activity and/or slightly more humid conditions.

### 3.29.1 Mineralogical characteristics of alluvial fan sub-environments

Both the fan fringe and distal fan lithofacies associations are characterized by compositionally immature sediments, but the distal fan lithofacies association has a higher relative abundance of feldspar and clay minerals, comparatively speaking. This may be due to slight differences in the distance to the source area. The fan fringe is described as a low-gradient area located immediately beyond the toe (distal portion) of an alluvial fan (Figure 46). Thus, the distal fan lithofacies association is closer to the source area and may be subjected to a greater influence by coarse-grained debris-flows and the

input of fresh detritus compared to the fan fringe lithofacies association. The fan fringe lithofacies association is located farther from the source area and the presence of oxide minerals may suggest the landscape was relatively stable for a sufficient period of time to support vegetation and possibly form soils (Chem-Nuclear, 1993).

As a result of the downslope trends in alluvial fan deposits, the grain size and mineralogy of a sample may provide clues about its relative location on the alluvial fan and its distance from the source area. In an alluvial fan succession, it is likely that these relatively quartz-rich, coarse-grained conglomerates such as sample SB-39 may represent debris flow deposits that were relatively close to the source area compared to the other fan fringe samples. Additionally, because alluvial fan systems are sensitive to tectonic activity, vertical changes in grain size may indicate fan progradation and retrogradation while variations in the quantity of authigenic minerals between various deposits may provide clues to landscape stability and post-depositional alteration.

### 3.29.2 Mineralogical characteristics of meandering stream sub-environments

Similar to the overall meandering stream environment, each of the individual lithofacies associations is characterized by compositionally immature sediments (Table 30). The distribution of minerals among the sub-environments of meandering streams show that the proximity to the active stream channel may influence the mineralogy of a deposit (Table 30). The channel and crevasse splay lithofacies associations have a higher relative abundance of quartz and feldspar minerals compared to the floodplain lithofacies association. This is likely due to the nature of the depositional processes occurring in the sub-environments. The channel and crevasse splay lithofacies associations are more likely to receive inputs of quartz and feldspar from the source area. The lower-energy

floodplain is located away from the channel and is the site of overbank flooding which carries suspended sediment onto floodplains resulting in laminated mudstones.

Additionally, the floodplain lithofacies association is considered fairly stable and likely had pervasive soil formation and possibly vegetation such as trees (Chem-Nuclear, 1993; Tucker, 2001; Brazell, 2013). For example, core W10 MP5 illustrates the fine-grained, laminated-nature of the floodplain lithofacies and evidence of soil formation in the form of rubble zones, caliche nodules, and root traces (Figures 50-52) (Chem-Nuclear, 1993).

While clay minerals settling from suspension and pedogenesis are common in the floodplain lithofacies association (relative abundance of 2.1), it is likely that post-depositional alteration is the primary source of the high clay mineral content in the channel and crevasse splay lithofacies associations, 1.9 and 1.5, respectively (Table 30). For example, Table 15 and Figure 50 show sample DB-27 is a coarse-grained, very arkosic, cross-bedded channel deposit. The petrographic data show feldspar comprises 32.7% and quartz 23.9% of the channel deposit (Table 15). The close proximity to the source area contributes to the immature nature of this channel deposit. The petrographic data also show that the channel deposit represented by sample DB-27 is characterized by 32.0% clay minerals, 3.2% carbonate minerals, and 1.9% oxide minerals (Table 15). In the Deep River basin, these mineral groups are predominantly authigenic in origin, therefore, the high total percentage (37.1%) of these minerals in sample DB-27 indicates the channel deposit was likely subjected to an extended period of post-depositional alteration. Another source of clay minerals are mud drapes and lenses that may be deposited with finer-grained, cross-laminated sands on the upper portions of point bar

deposits (Walker and Cant, 1984; Tucker, 2001). The crevasse splay lithofacies association may also be characterized by clay drapes.

The distribution of oxide minerals among the meandering stream sub-environments shows the degree of alteration may be influenced by the proximity to the stream channel (Table 30). For example, the floodplain lithofacies association has the highest abundance of oxide minerals and likely experienced extended periods of sub-aerial exposure and post-depositional alteration, whereas the channel lithofacies association is characterized by the lowest quantity of oxide minerals indicating a more energetic depositional environment less conducive to post-depositional alteration (Table 30).

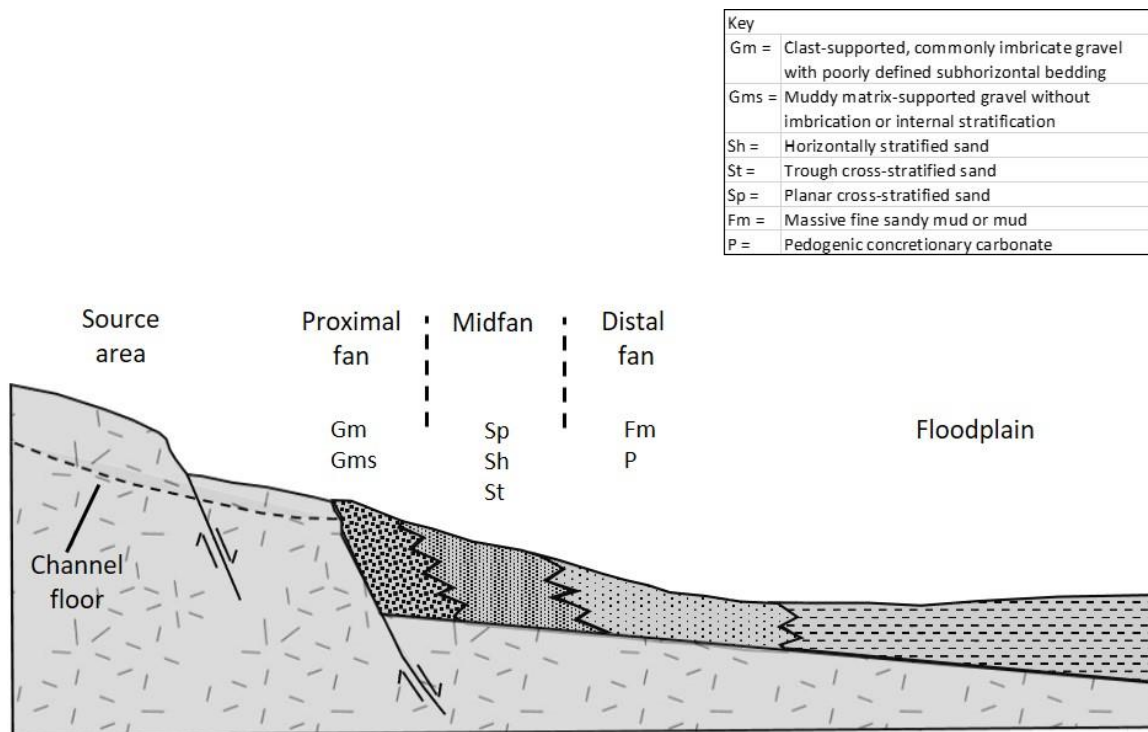


Figure 8: Schematic facies model for an alluvial fan: coarse gravels and sands of stream flood and debris-flow origin in the proximal fan pass down to pebbly sands and finer sediments of the mid-to distal fan, deposited by stream and sheet floods, which in turn grade into floodplain muds and/or lake (Modified from: Rust and Koster, 1984; Tucker, 2001).

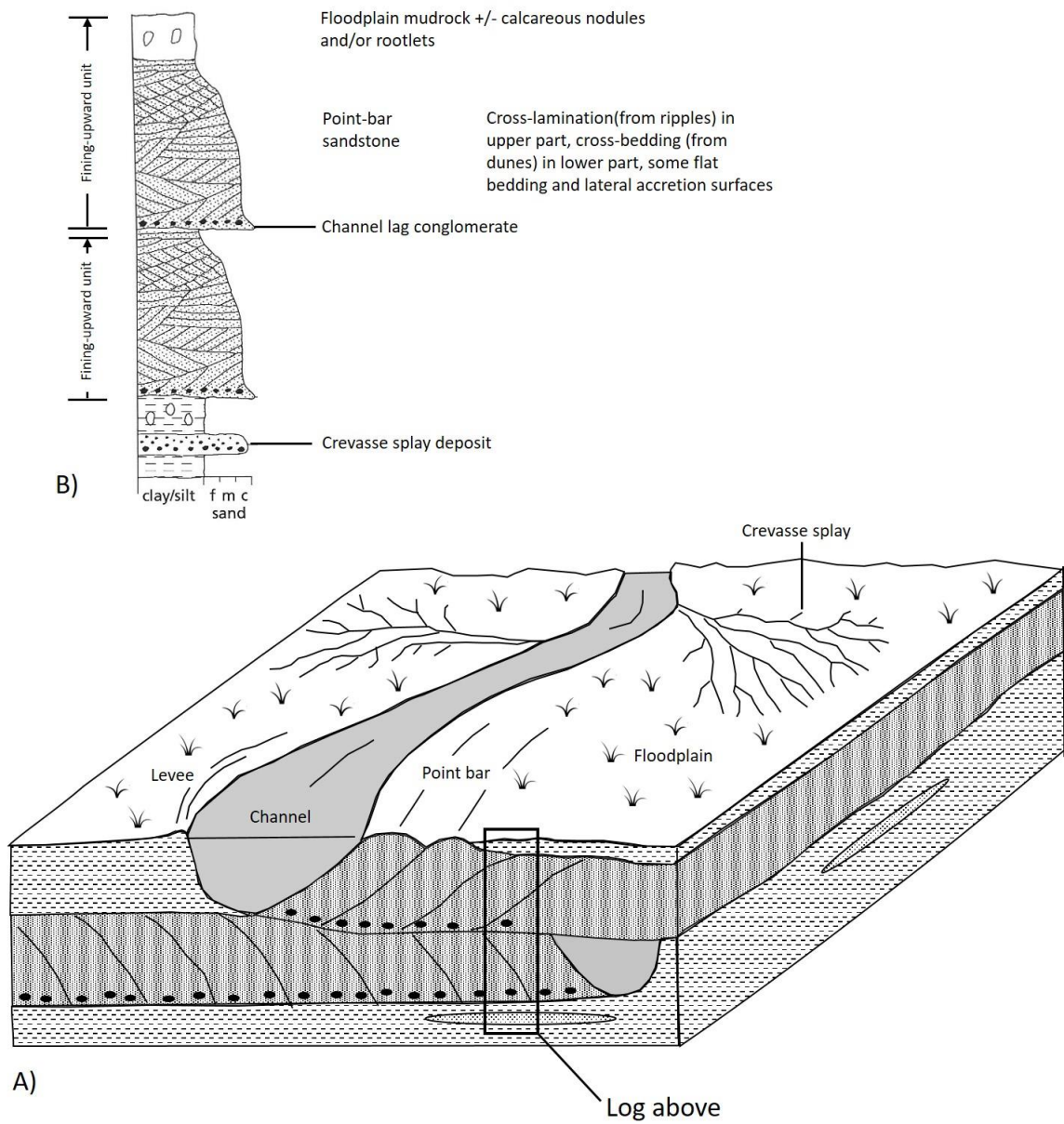


Figure 9: A) The sub-environments of a meandering stream together with B) a graphic log of the sedimentary unit produced through lateral migration of such a stream. Fluvial fining-upward units are usually between about 2 and 20 m thick (Modified from: Tucker, 2001).

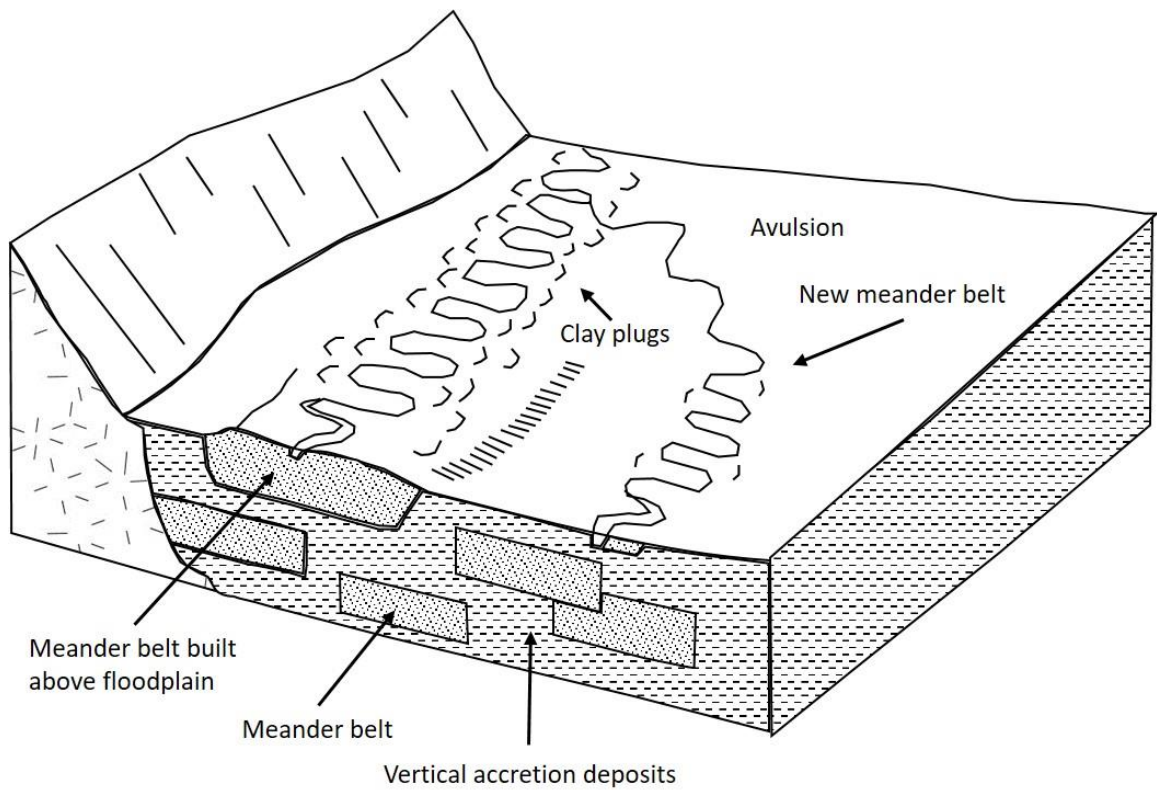


Figure 10: A block diagram of flood plain aggradation with very sinuous rivers. Shoestring sands composed of multistorey sandstone bodies are preserved, and are surrounded by vertical accretion siltstones and mudstones. If the river is confined by clay plugs and overbank fines, a meander belt can build above floodplain elevation. Avulsions can shift the meander belt to low areas of the floodplain. Clay plugs help confine the river to the meander belt until avulsions occur (Modified from: Walker and Cant, 1984).

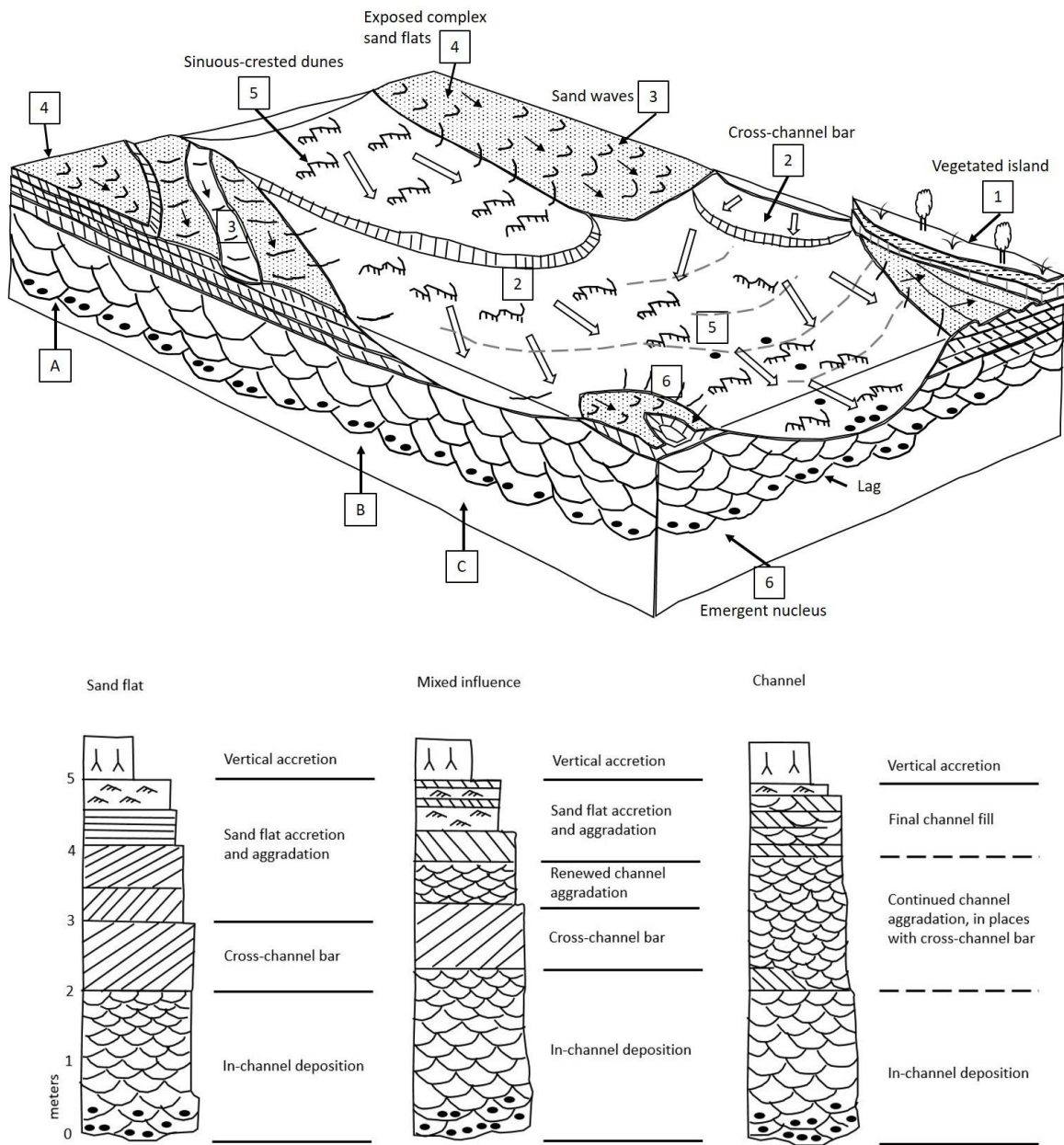


Figure 11: Block diagram of a braided stream summarizing the major morphological elements, and their associated bedforms and stratification. A locates stratigraphic sequence dominated by sand flat development, B has mixed sand flat and channel influence, and C is dominated by channel aggradation (Modified from: Cant and Walker, 1978).

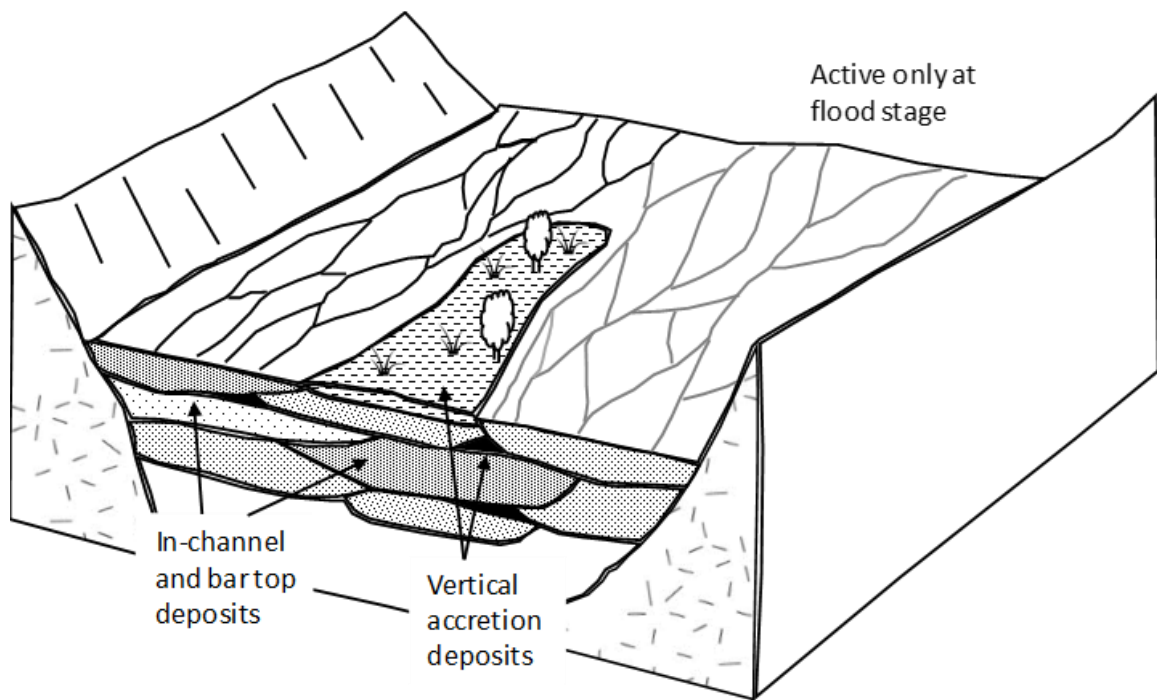


Figure 12: Block diagram of sandy braided systems with low sinuosity channels. Vertical accretion can occur during flood stage, but deposits are rarely preserved. (Modified from: Walker and Cant, 1984).

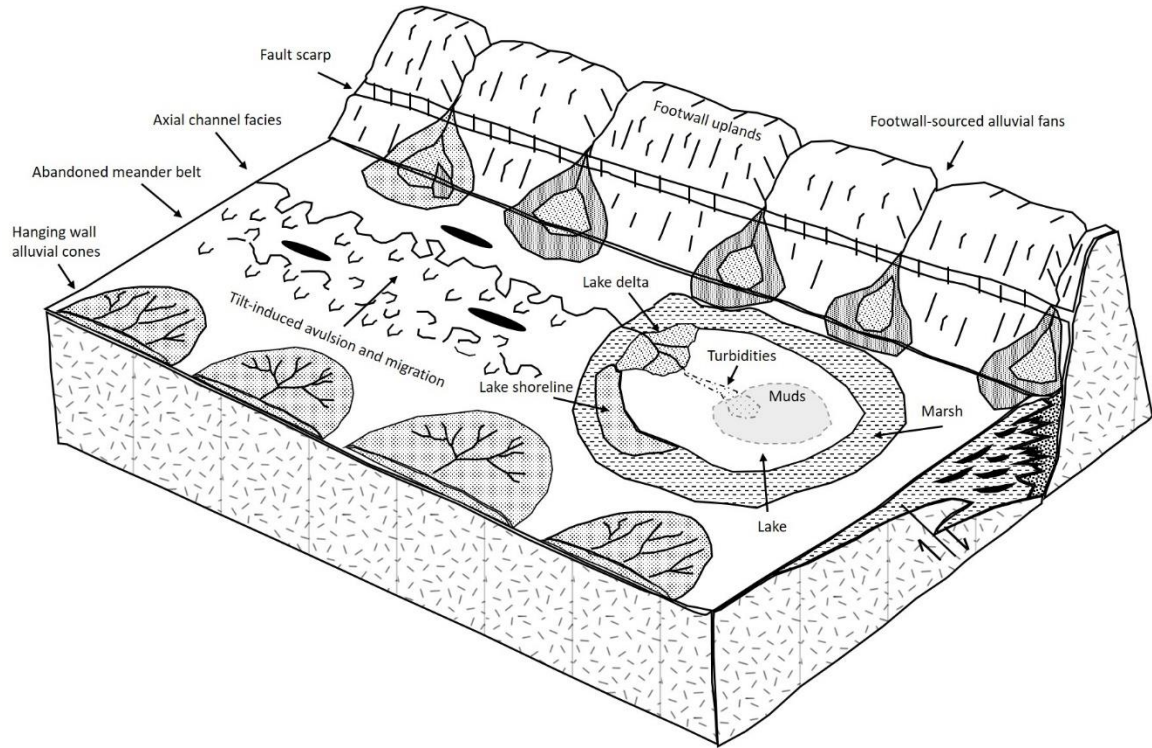


Figure 13: Model for continental half-graben rift basin. Alluvial fans located along the basin margins provide clastic material to axial fluvial systems and freshwater lakes. The natural evolutionary sequence of rift-basin development could result in changes in whether the basins are hydrologically open and characterized by axial fluvial systems or hydrologically closed with lakes and marsh environments. The lake depocenter would likely be positioned close to the major fault where subsidence is most likely to outpace sedimentation and be conducive for lake development (Modified from: Miall, 1996)



Figure 14: Clast-supported conglomerate with very coarse sandstone. Rounded cobbles and pebbles measure from 1 cm to 35 cm in length and angular to subangular pebbles measure 1 cm to 10 cm in length (Source: Malaza et al., 2013).



Figure 15: A thin-bedded, matrix-supported conglomerate located at Bogan's Cut in the Wadesboro sub-basin. The thin nature of the bed and the sharp basal and upper contact suggest this may be a granular channel lag (Brazell and Diemer, 2012).



Figure 16: Trough cross-bedded sandstones with areas of muddy very fine- to-fine sandstone. The sandstones are interpreted as channel deposits and the muddy sandstone layer is interpreted as an overbank deposit. This outcrop is located along Bogan's cut in the Wadesboro sub-basin. Person for scale.



Figure 17: Cross-laminated sandstone at Bogan's cut in the Wadeboro sub-basin. The diameter of the sub-vertical drill hole is approximately 5 cm.



Figure 18: Interbedded fissile siltstone and thinly laminated sandstones on the south side of US 742 in the Wadesboro sub-basin. The layers of sandstone and siltstone are 5-10 cm thick, and sandstone dominates the outcrop. The fluvial stratigraphy is interpreted as crevasse splay deposits in a floodplain setting (Source: Brazell and Diemer, 2012).



Figure 19: Laminated, organic-rich mudstones located along a tributary of the Deep River in the Sanford sub-basin. Camera lens cap for scale on a large displace nodule. Two samples of the dark gray to black Cumnock Formation (SB-22 and SB-24) and a sample of the displace nodule (SB-23) were collected. The nodule likely formed in the sediments while they were still soft and not compacted. This can be recognized from the folded laminae in the black mudrock around the nodule. This suggests compaction took place after the growth of the nodule (Tucker, 2001).



Figure 20: A fine sandstone along a railroad cut off Cotten Road in the Sanford sub-basin. The sandstone is interpreted as being a possible crevasse splay deposit. Mottling and a possible root structure are potential evidence of paleosol formation. The root structure may have been a site of carbonate cement precipitation. The nodular carbonate has since been weathered out.



Figure 21: A layer of muddy very fine- to-fine sandstone overlain above and below by trough cross-bedded sandstones. The sandstones are interpreted as channel deposits and the muddy layer sandstone is interpreted as an overbank deposit. The muddy sandstone appears to be mottled suggesting soil formation. This outcrop is located along Bogan's cut in the Wadesboro sub-basin. People for scale. (Brazell and Diemer, 2012).

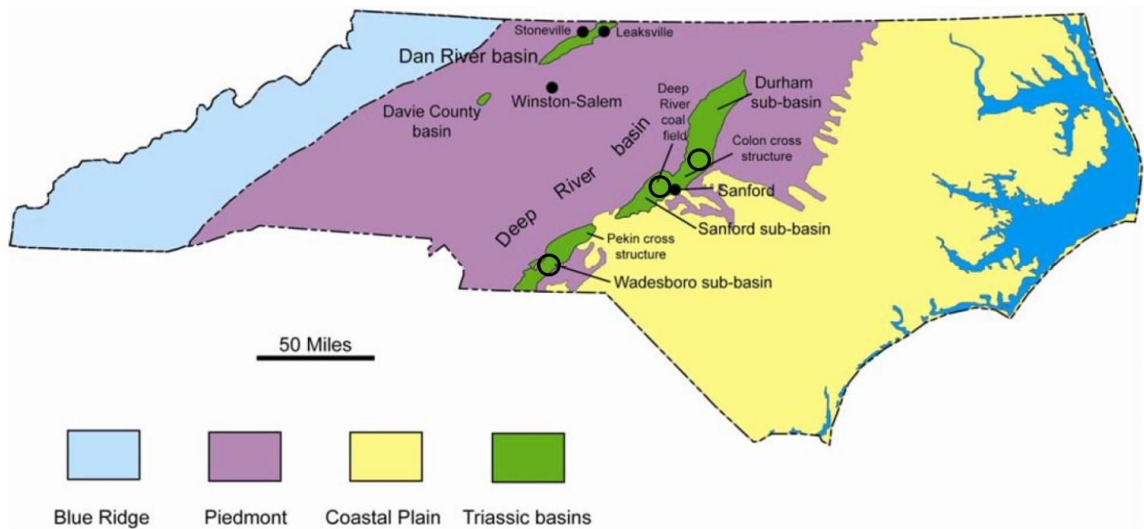


Figure 22: The locations of the exposed Triassic basins in North Carolina. Black circles represent the approximate locations of samples collected for this study (Modified from: Reid and Milici, 2008).

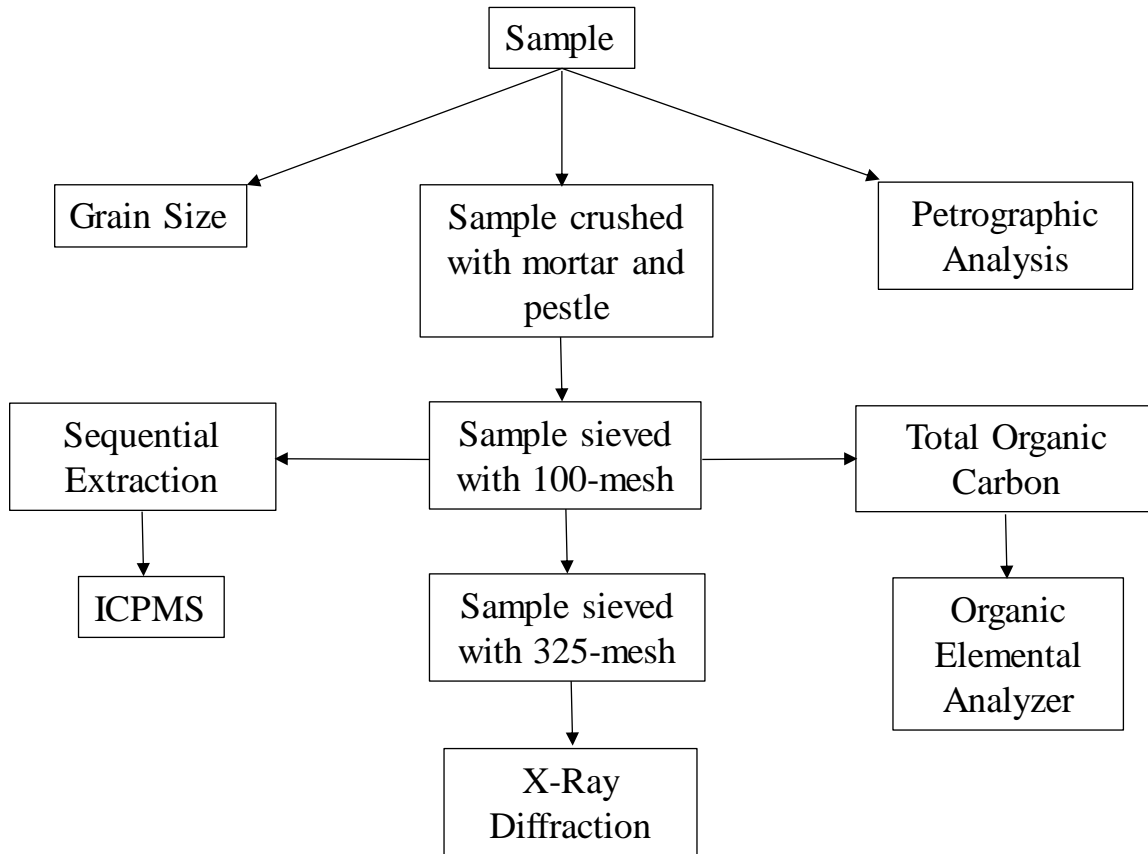


Figure 23: Flow diagram of the data collected from samples from the Deep River Basin. ICPMS = Inductively coupled plasma mass spectrometry. Select samples were chosen for petrographic analysis, X-ray diffraction, and/or total organic carbon.

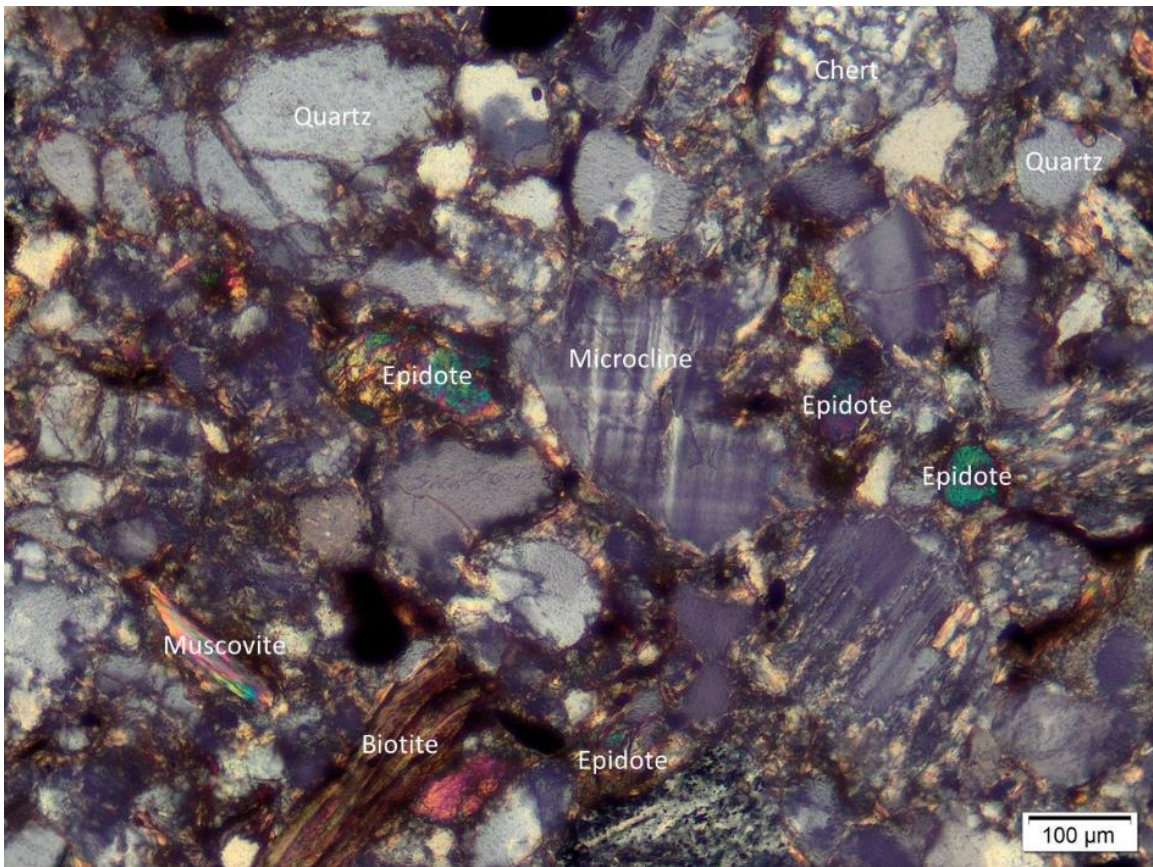


Figure 24: Example of a clast-supported fabric as illustrated by sample DB-49. Examples of single crystal quartz and chert are labeled. Both would be labeled as quartz for point counting.

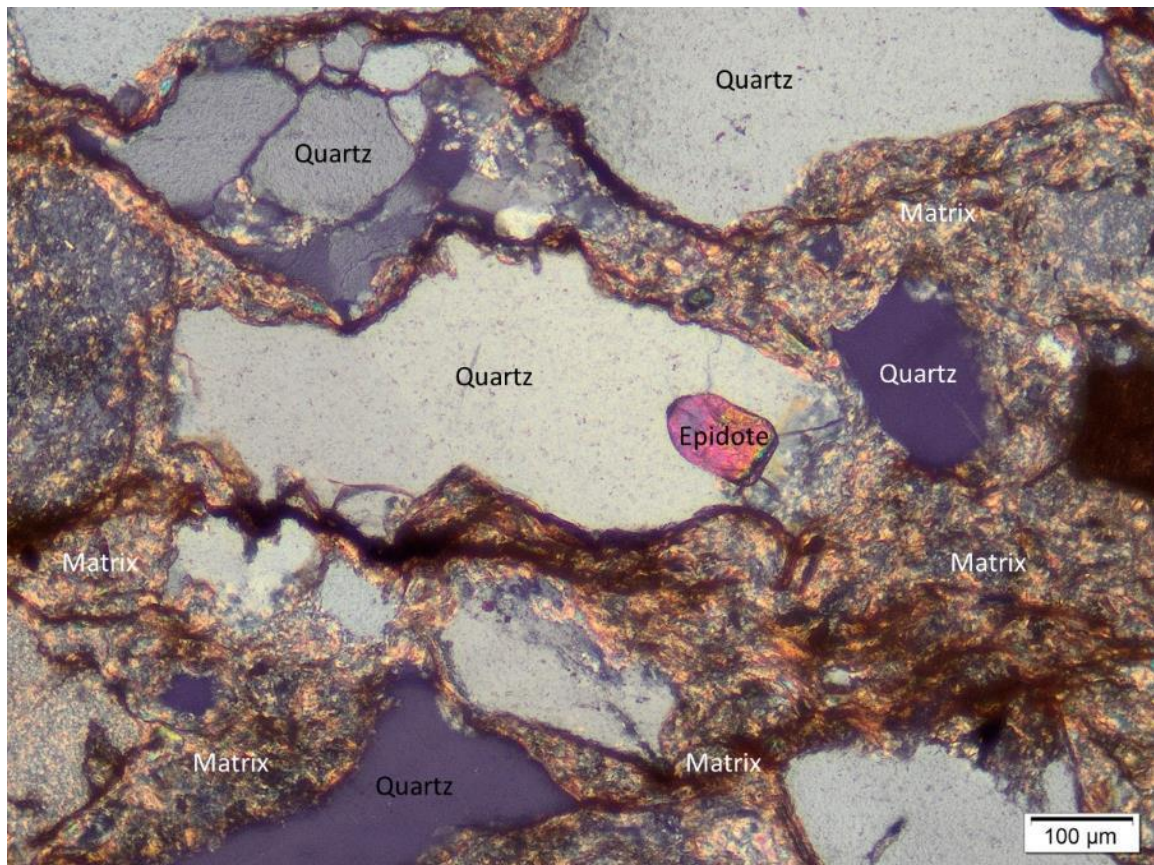


Figure 25: Example of a matrix-supported fabric as illustrated by sample WB-7. According to the Gazzi-Dickinson method of point counting, if the cross-hairs were located above a quartz grain within the lithic grain at the top left, the point would be classified as quartz. The single crystals of quartz would also be classified as quartz for point counting. Opaque minerals assumed to be hematite, appear to be impregnated with the fine-grained matrix. Opaque minerals also appear to fill a fracture below the large quartz crystal in the center.

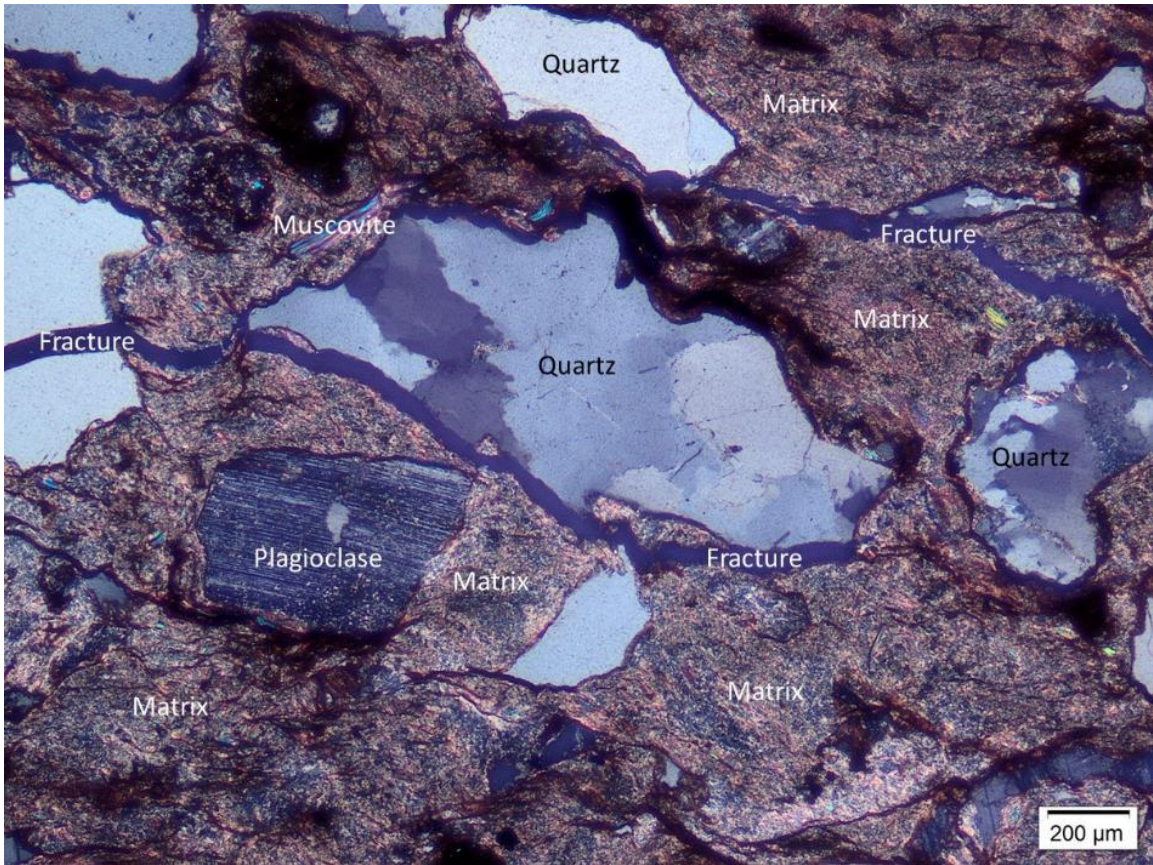


Figure 26: Several polycrystalline and monocrystalline quartz grains and a plagioclase grain surrounded by fine-grained matrix in sample WB-7. In cross-polarized light, the plagioclase grain shows the characteristic albite (polysynthetic) twinning. The matrix appears to consist of clay minerals such as muscovite.

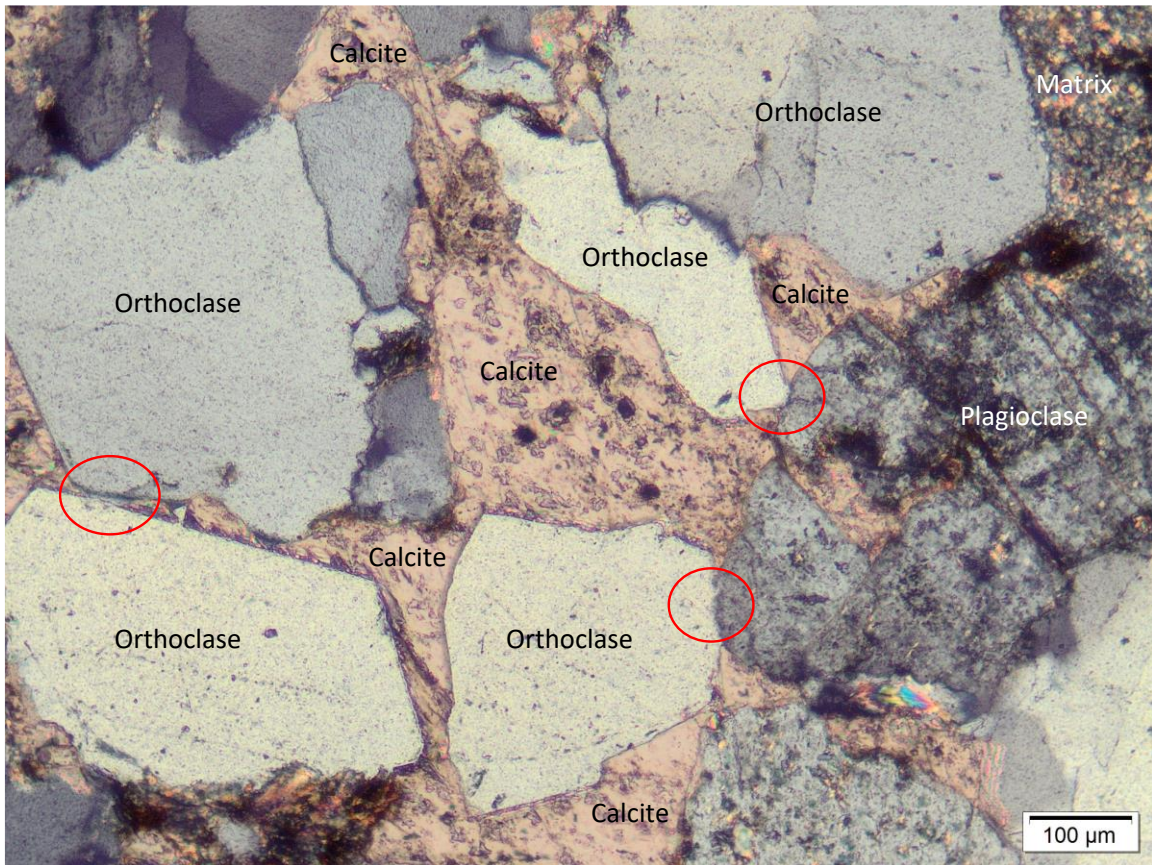


Figure 27: Calcite matrix in sample WB-11 in cross-polarized light. Large calcite crystals enclosing several orthoclase grains and a plagioclase grain. Red circles highlight point contacts and the absence of the calcite cement/matrix. The rest of the grains are surrounded by calcite suggesting post-depositional formation. At the center right, a plagioclase grain showing splitting by calcite cement.

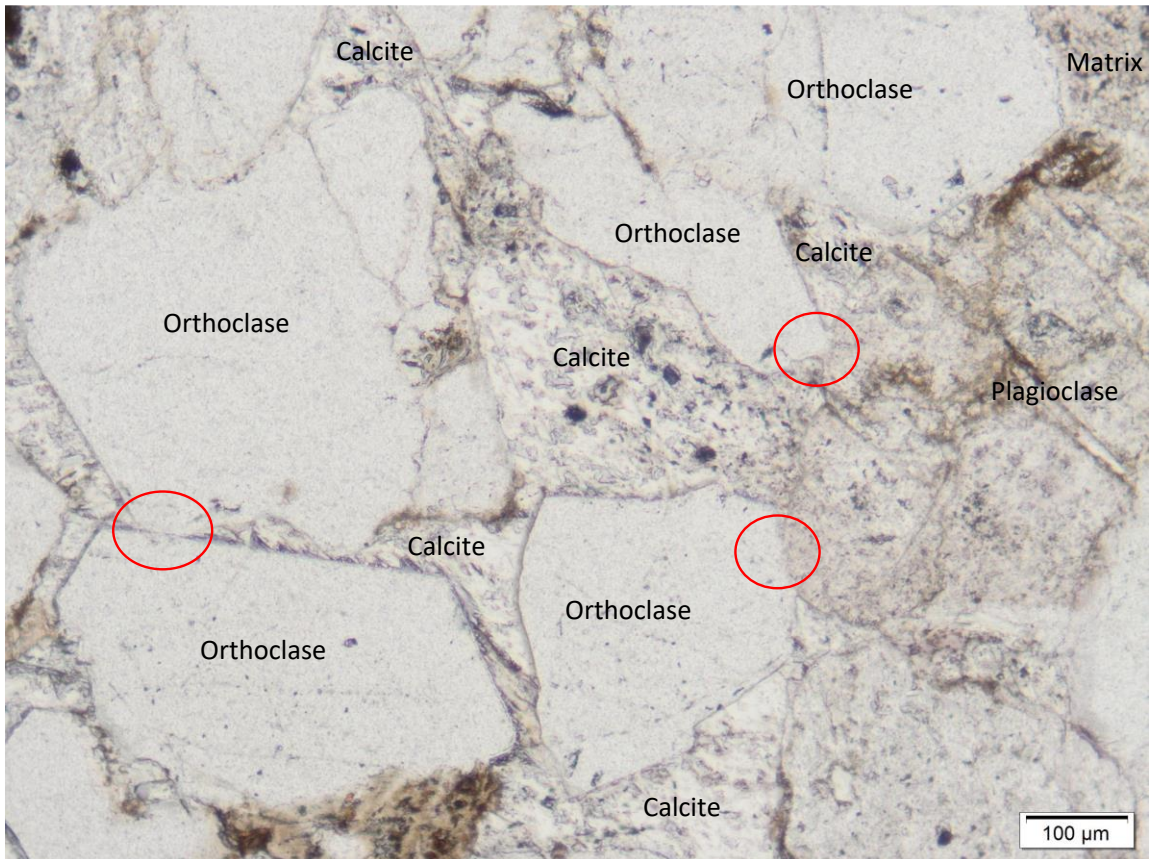


Figure 28: Calcite matrix in sample WB-11 in plane-polarized light. (Same field of view as Figure 27). Large calcite crystals enclosing several orthoclase grains and a plagioclase grain. Red circles highlight point contacts and the absence of the calcite cement/matrix. The rest of the grains are surrounded by calcite suggesting post-depositional formation. At the center right, a plagioclase grain showing splitting by calcite cement.

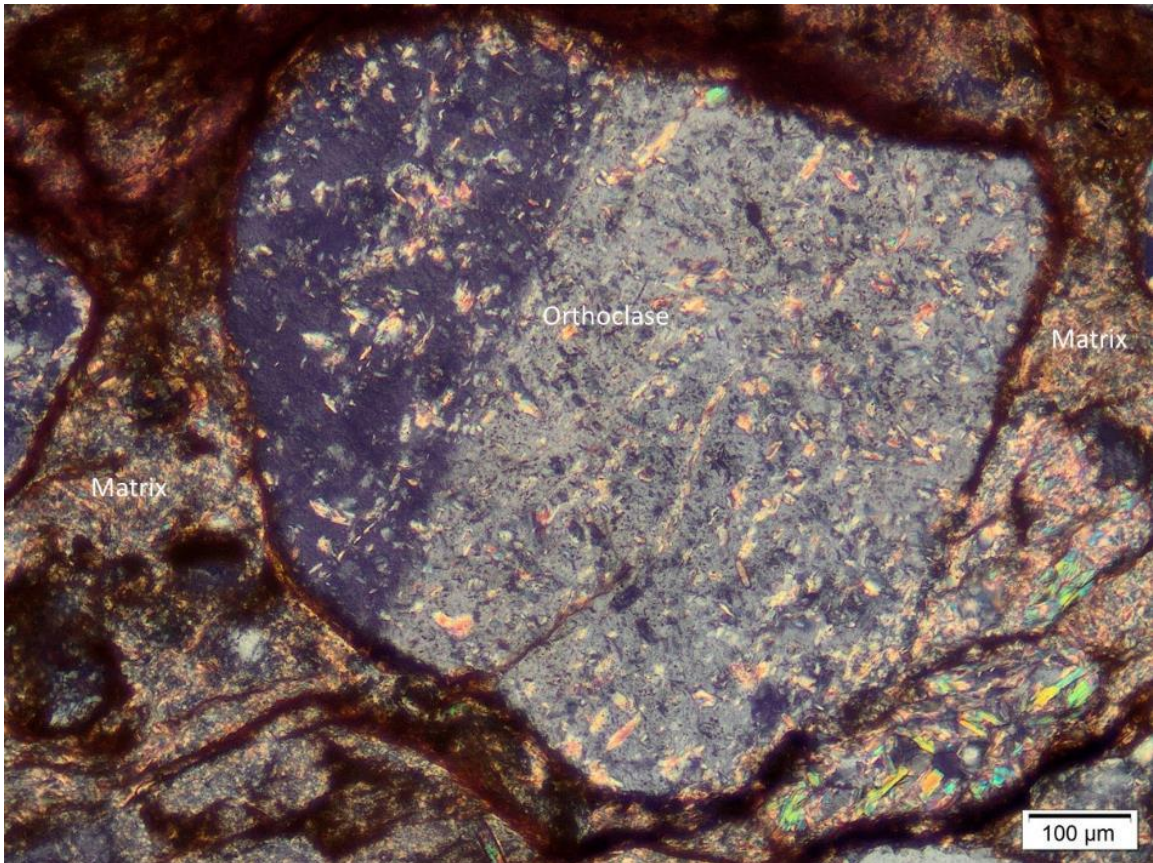


Figure 29: An example of an orthoclase grain altered to sericite in sample WB-7. The orthoclase is surrounded by a fine-grained matrix consisting predominantly of clay minerals and reddish-brown minerals possibly hematite. A reddish-brown coating is present around most of the orthoclase grain and adjacent matrix suggesting an authigenic origin for the coating. At the lower right, an elongate grain composed of fine-grained minerals with high-order interference colors may represent a feldspar grain that has been completely replaced by sericite.

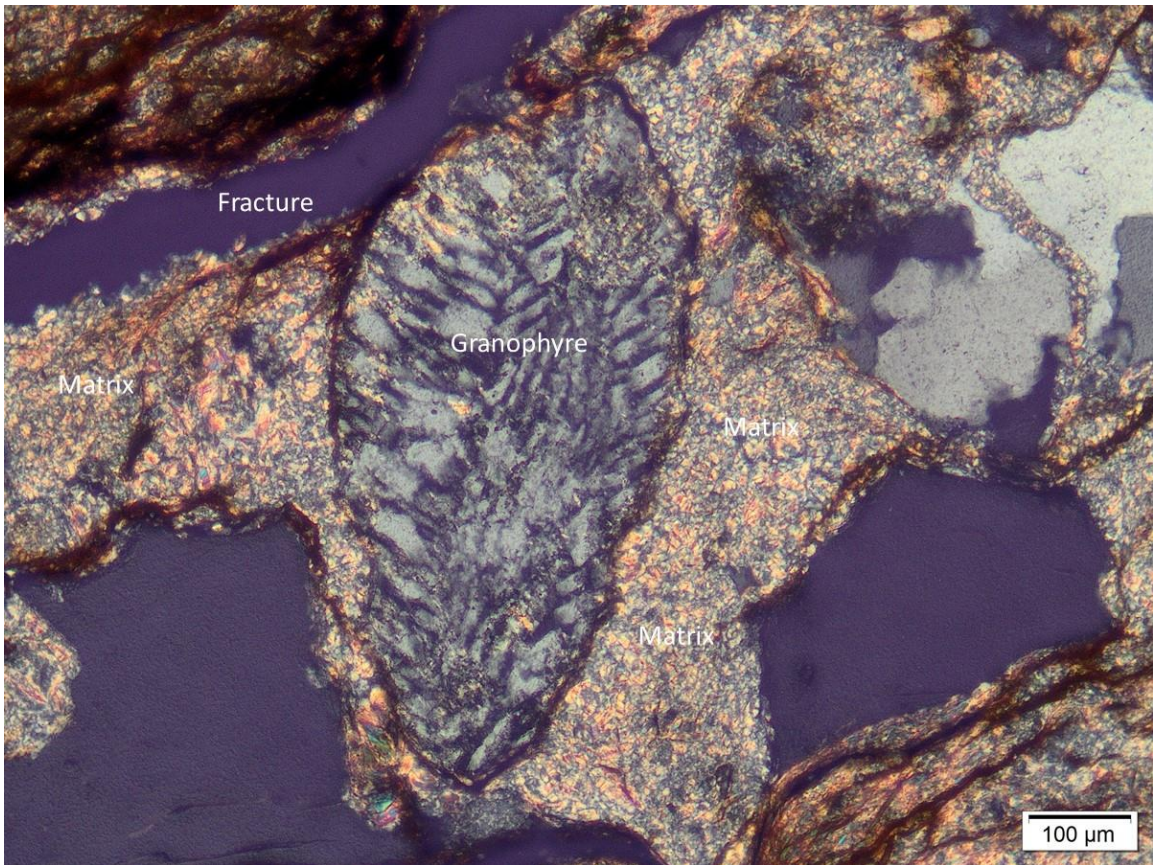


Figure 30: A granophyre, an intergrowth of quartz and feldspar, present in sample WB-7. This granophyre appears to be detrital in nature as indicated by the iron oxide coating around the grain.

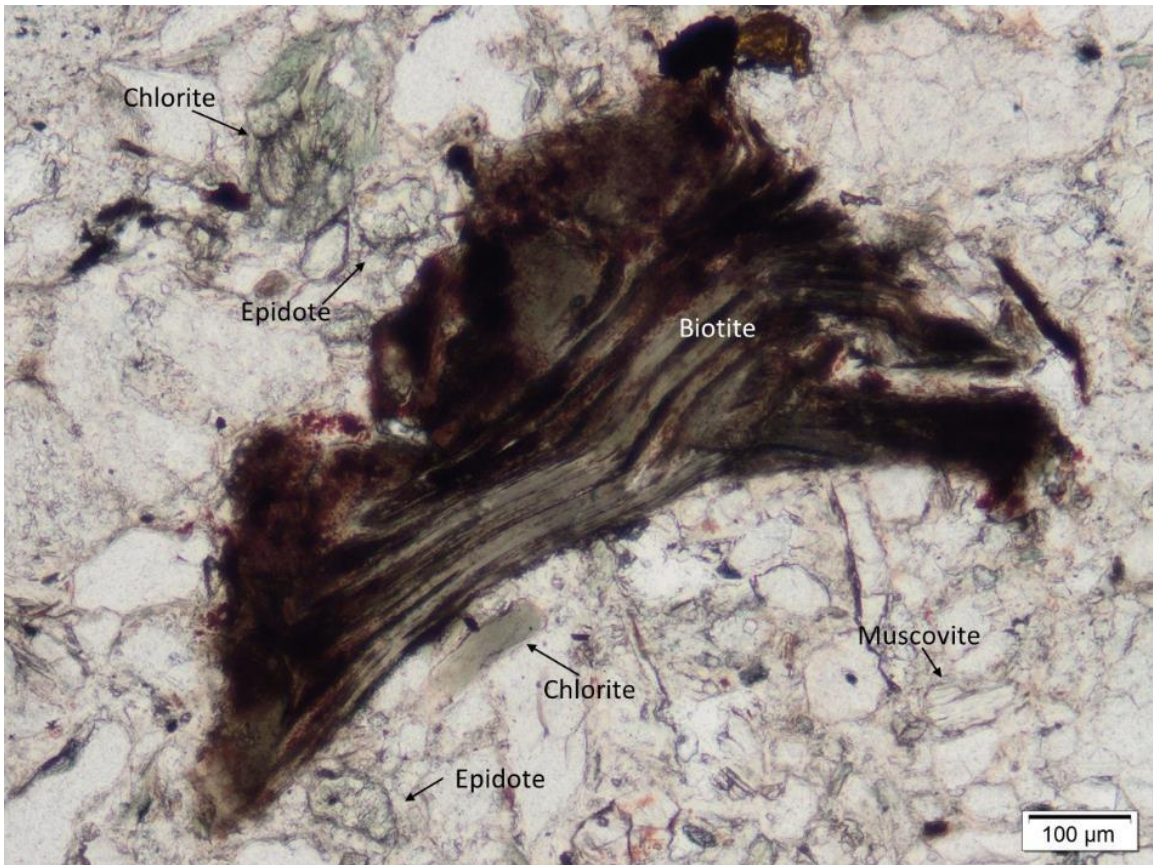


Figure 31: Examples of biotite, muscovite, chlorite, and epidote grains found in sample DB-49 viewed in plane-polarized light. Muscovite is usually colorless in plane-polarized light. Biotite is usually a shade of brown which may mask interference colors and it may exhibit brown-green pleochroism. Where interwoven with chlorite as seen here, biotite may be greenish.

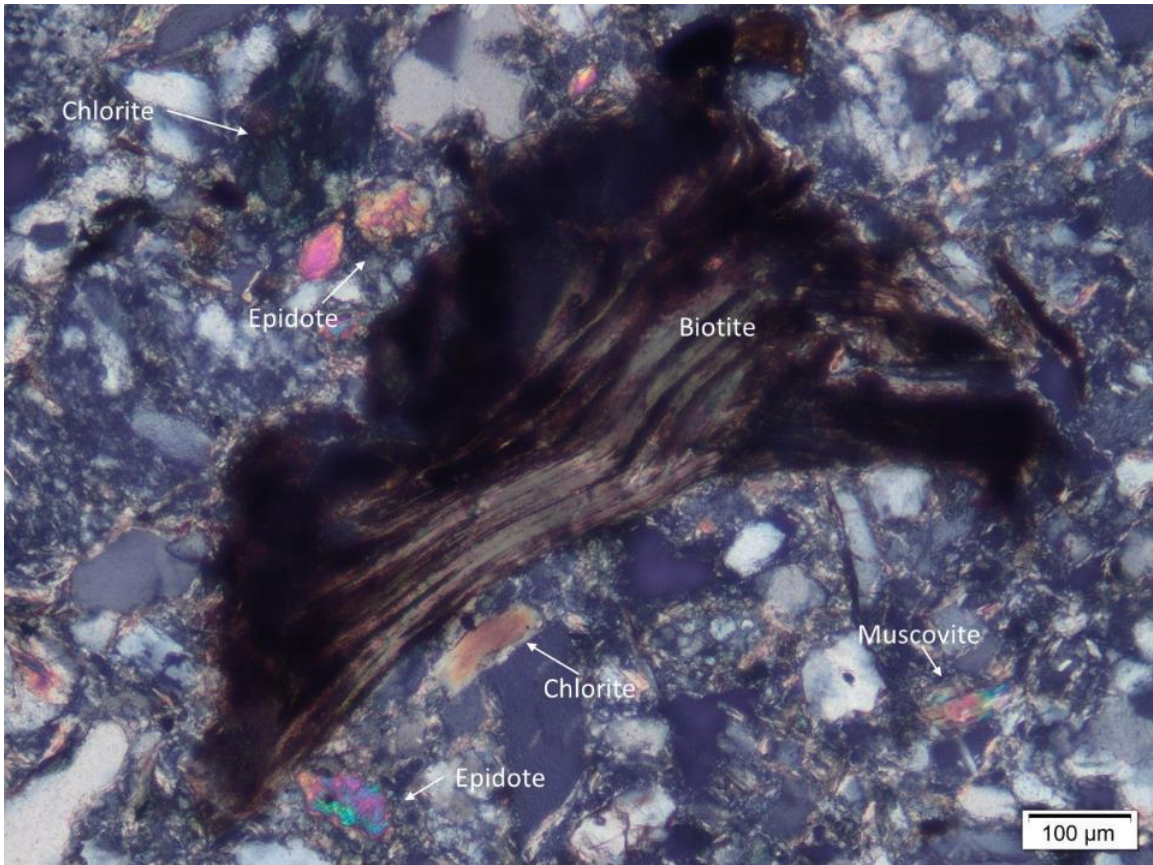


Figure 32: Examples of biotite, muscovite, chlorite, and epidote grains found in sample DB-49 viewed in cross-polarized light (same field of view as Figure 31). Muscovite displays bright second-order interference colors in cross-polarized light. Biotite is usually a shade of brown which may mask interference colors and it may exhibit brown-green pleochroism. Where interwoven with chlorite as seen here, biotite may be greenish.

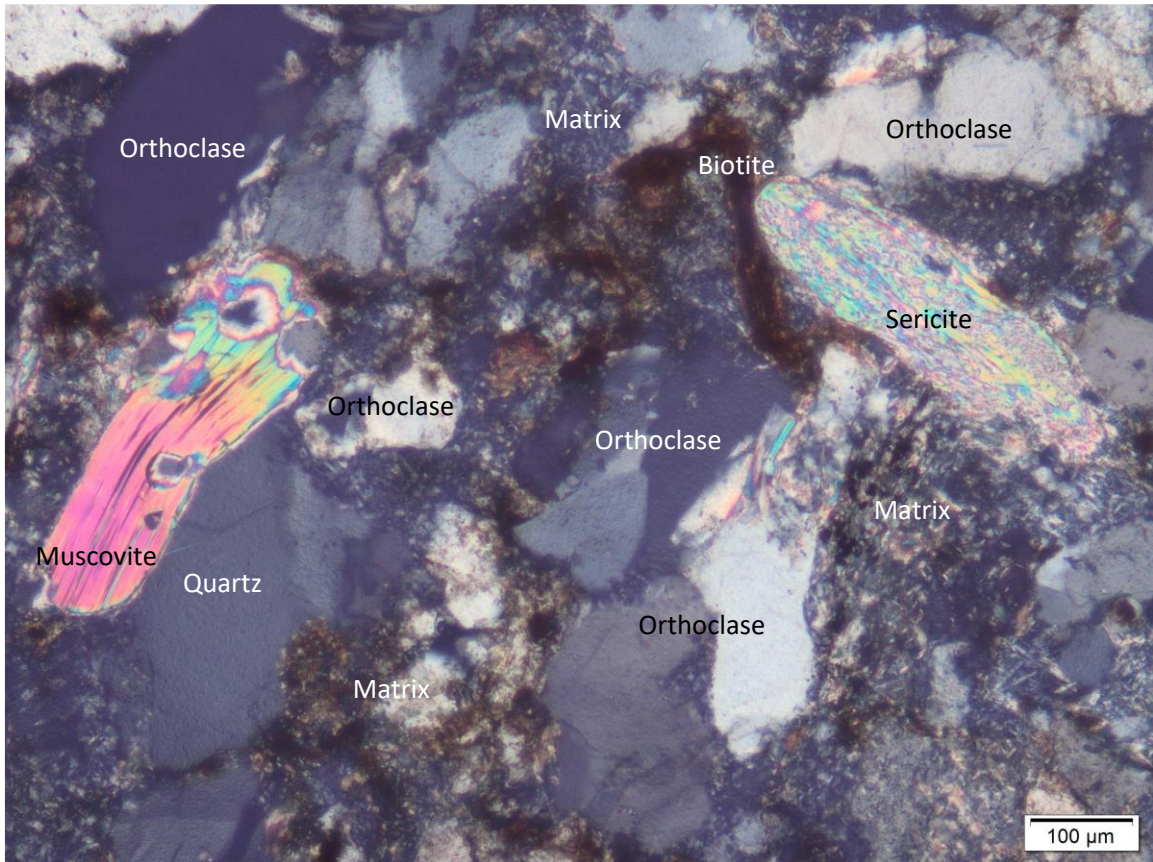


Figure 33: Sample WB-13 shows an example of a detrital muscovite grain and an elongate, rounded sericite grain that may represent a detrital feldspar grain that has been completely replaced by sericite. Both forms of mica display the characteristic bright second-order interference colors in cross-polarized light.

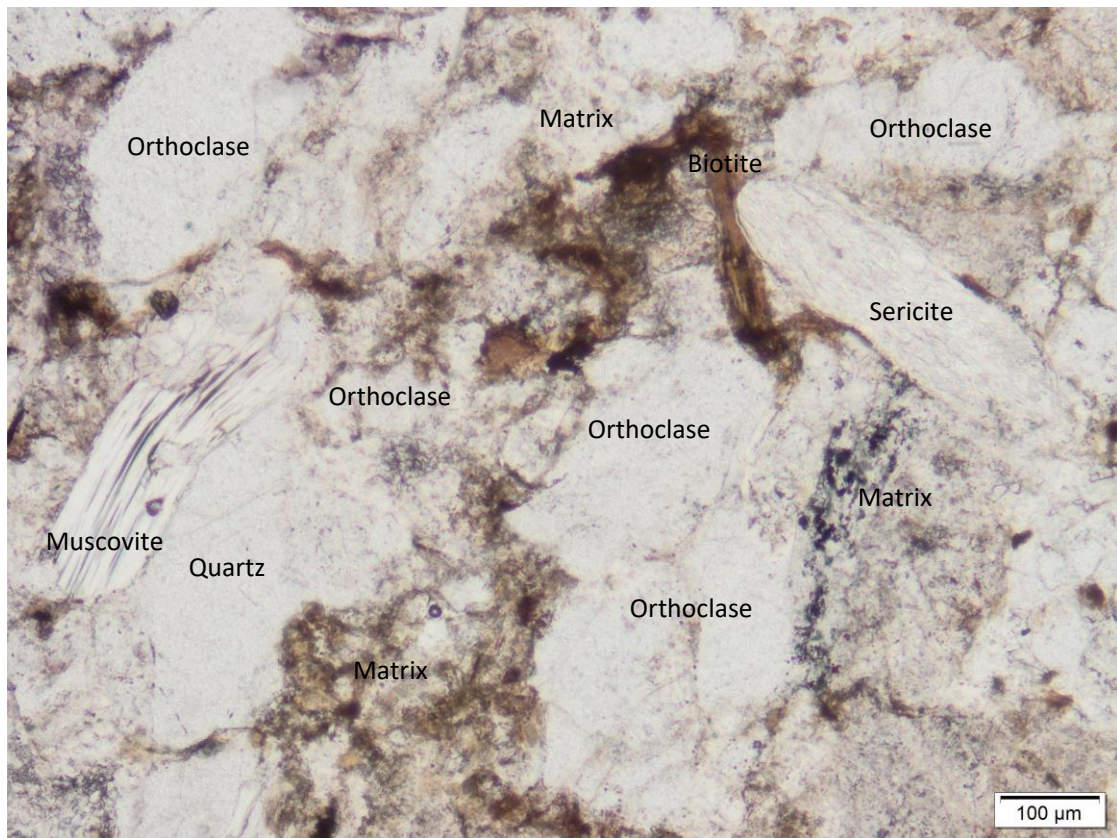


Figure 34: Sample WB-13 shows an example of a detrital muscovite grain and an elongate, rounded sericite grain that may represent a detrital feldspar grain that has been completely replaced by sericite. Both forms of mica are colorless in plane-polarized light. Same field of view as Figure 33.

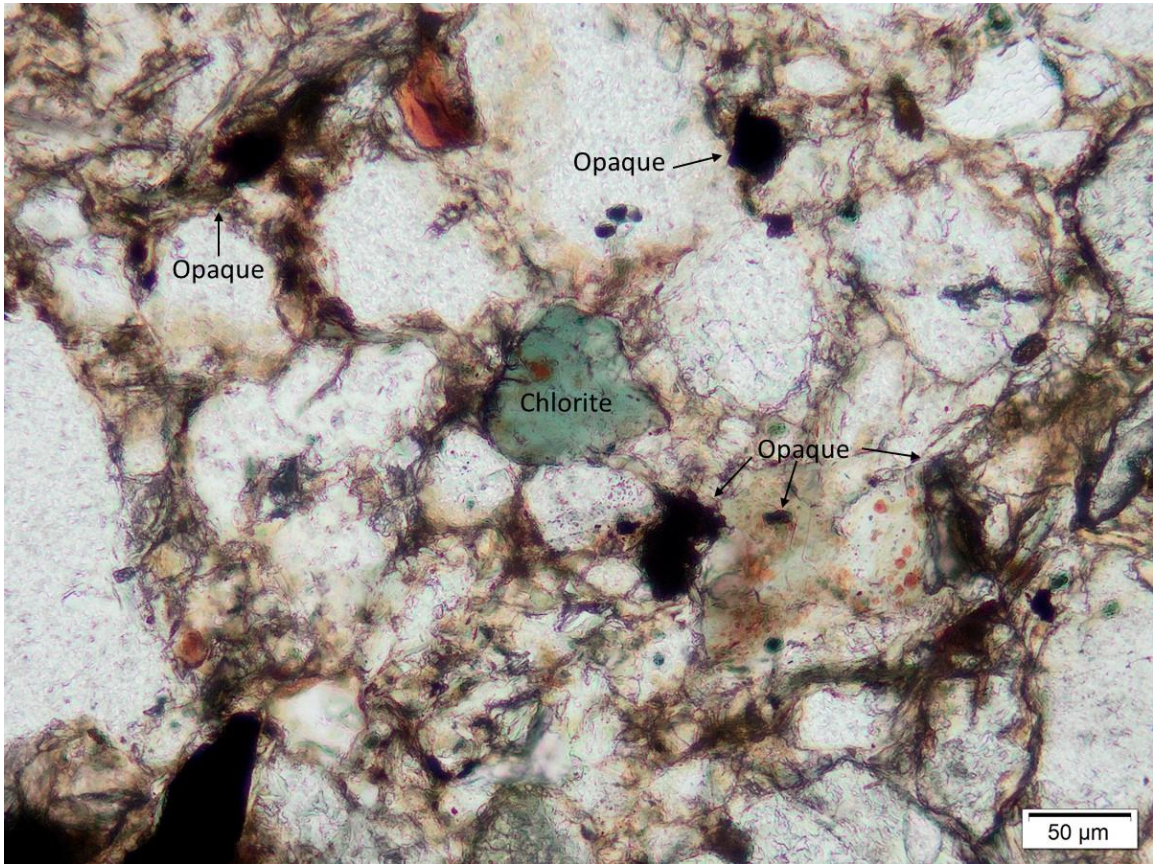


Figure 35: Examples of opaque minerals and a chlorite grain in plane-polarized light in sample DB-41.

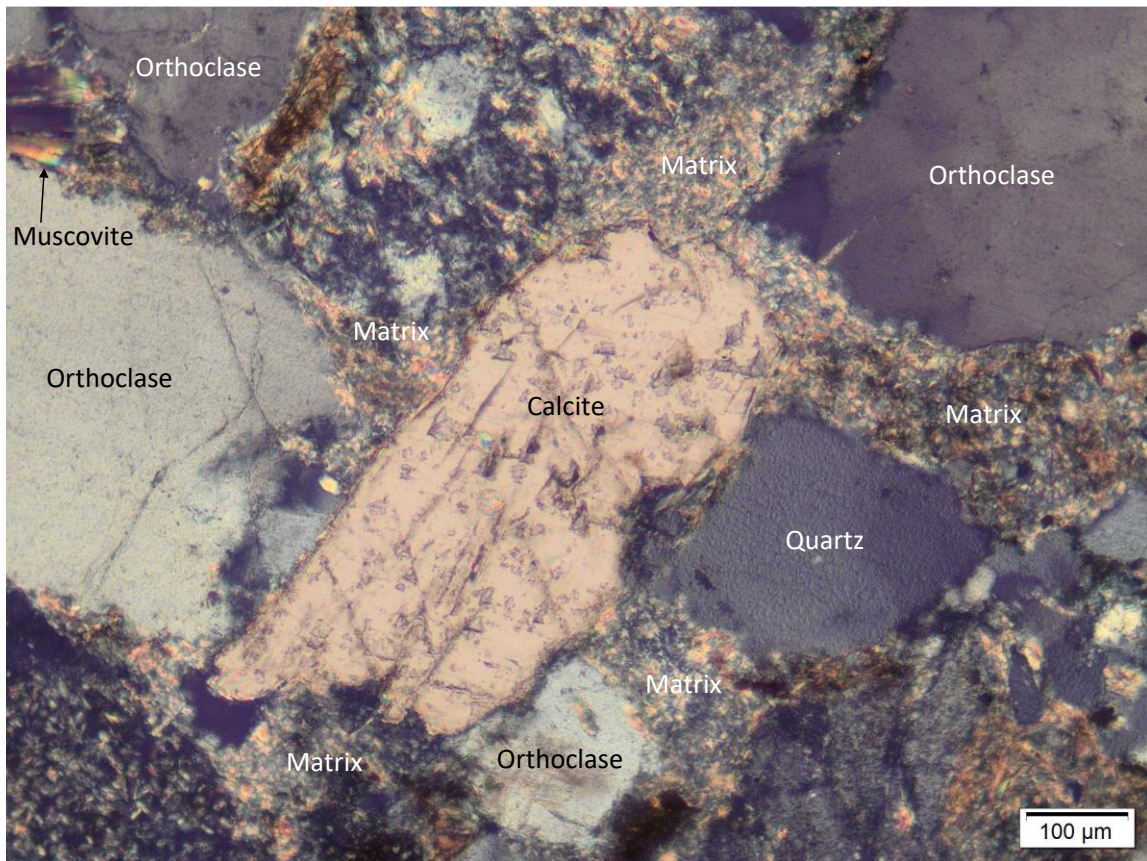


Figure 36: An example of a calcite grain in cross-polarized light from sample WB-6. Though most of the calcite present in the samples is in the form of a cement, few calcite grains were also noted.

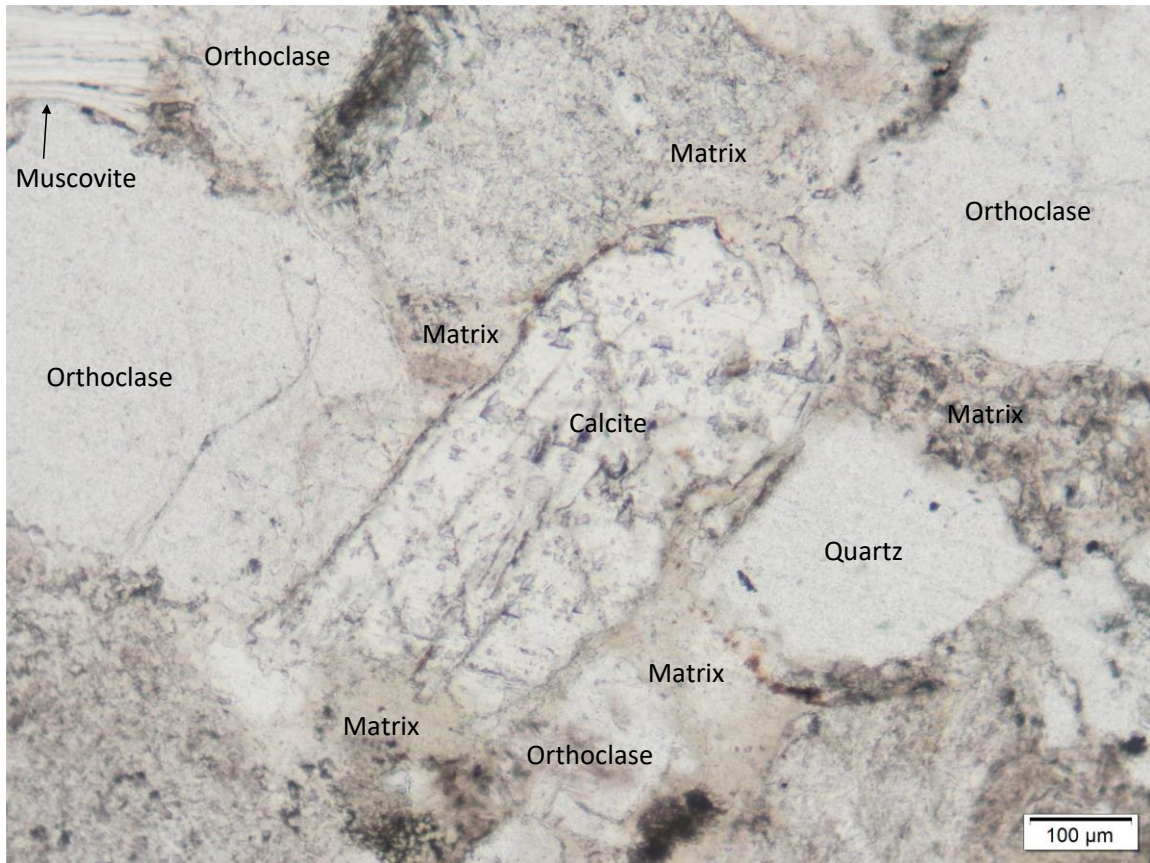


Figure 37: An example of a calcite grain in plane-polarized light from sample WB-6. Though most of the calcite present in the samples is in the form of a cement, few calcite grains were also noted. Same field of view as Figure 36.

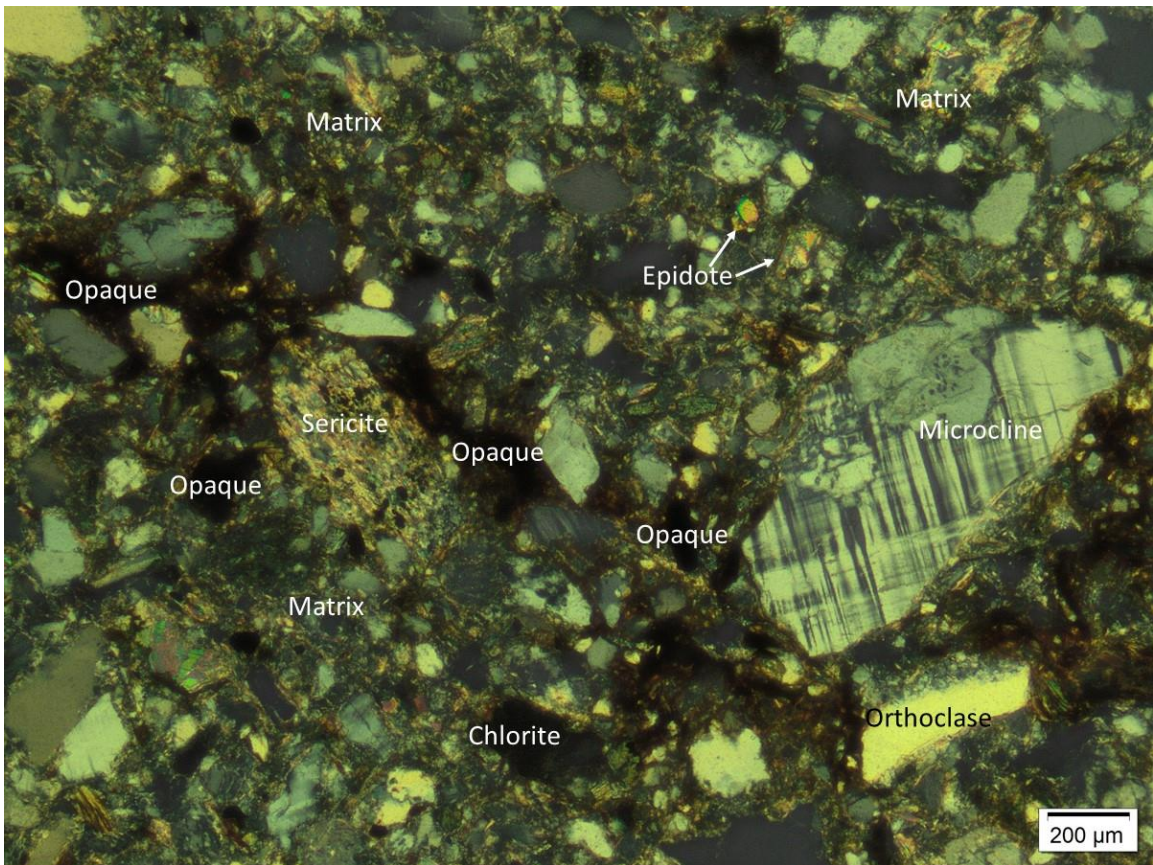


Figure 38: Sample DB-49 is a poorly sorted, very fine to fine-grained sandstone that is characterized by some well-rounded grains as well some very angular grains. This deposit is characterized as a crevasse splay. This sample shows both the detrital nature of opaque minerals in the form of isolated, often rounded grains and the authigenic nature of the opaque minerals as they appear to fill a fracture and coat numerous grains.

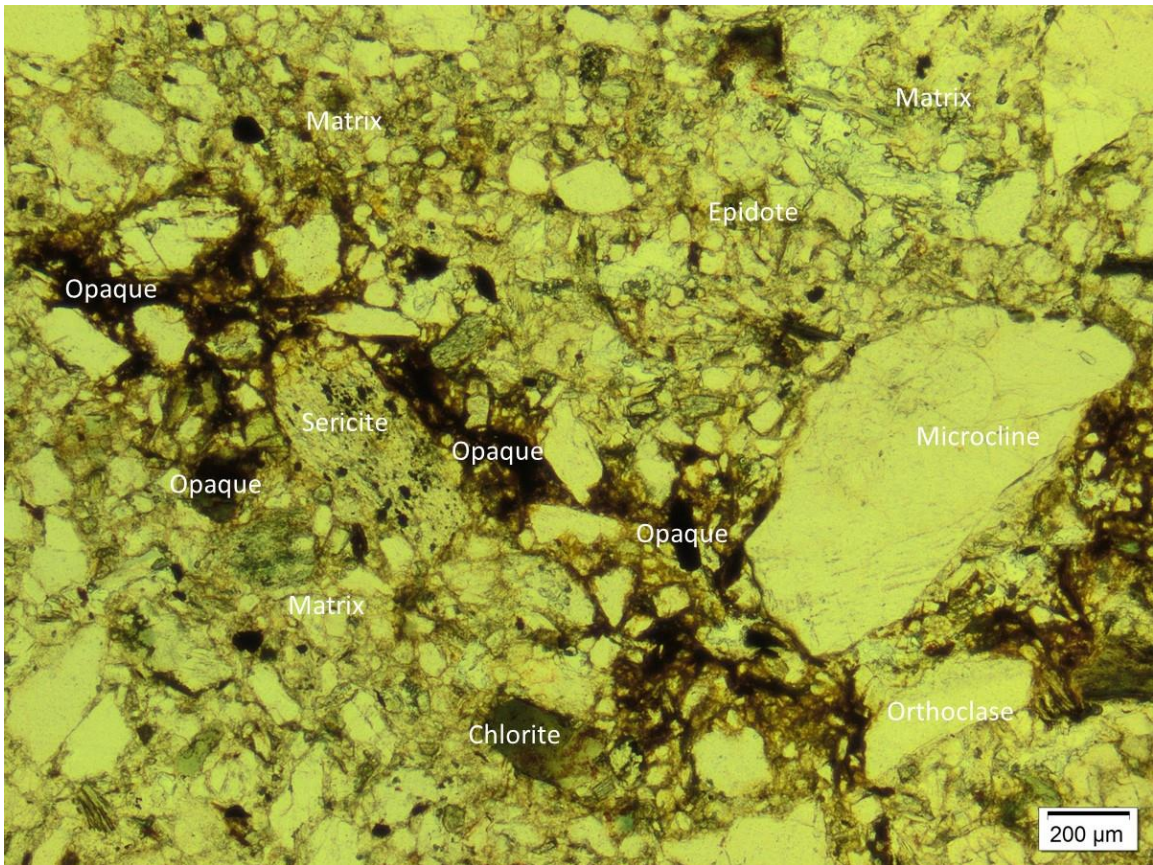


Figure 39: Sample DB-49 is a poorly sorted, very fine to fine-grained sandstone that is characterized by some well-rounded grains as well some very angular grains. This deposit is characterized as a crevasse splay. This sample shows both the detrital nature of opaque minerals in the form of isolated, often rounded grains and the authigenic nature of the opaque minerals as they appear to fill a fracture and coat numerous grains. Same field of view as Figure 38.

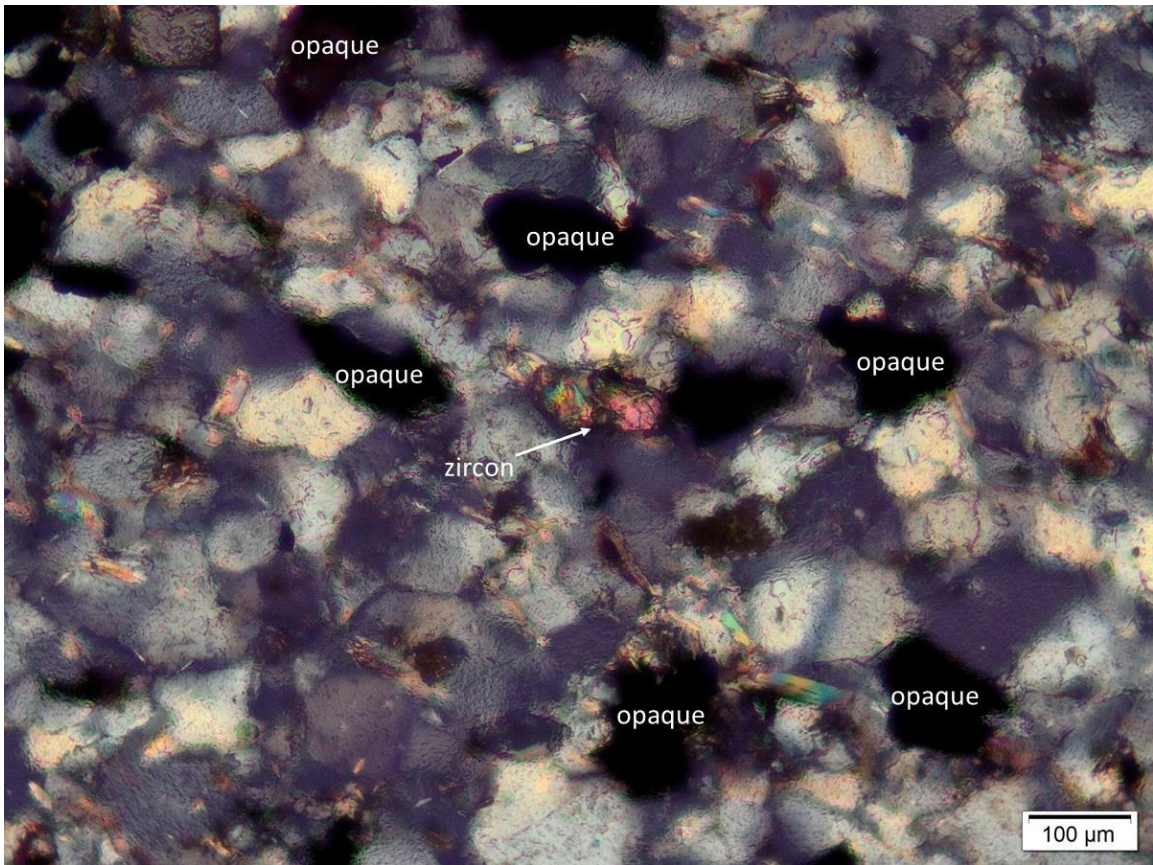


Figure 40: Sample SB-37 is a grain-supported, very fine- to fine-grained sandstone that shows an example of a zircon crystal and several opaque mineral grains. The zircon crystal is rounded due to a long transport distance (Nesse, 2004). This sample was not point counted as a result of its fine-grain size which prohibited mineral identification petrographically.

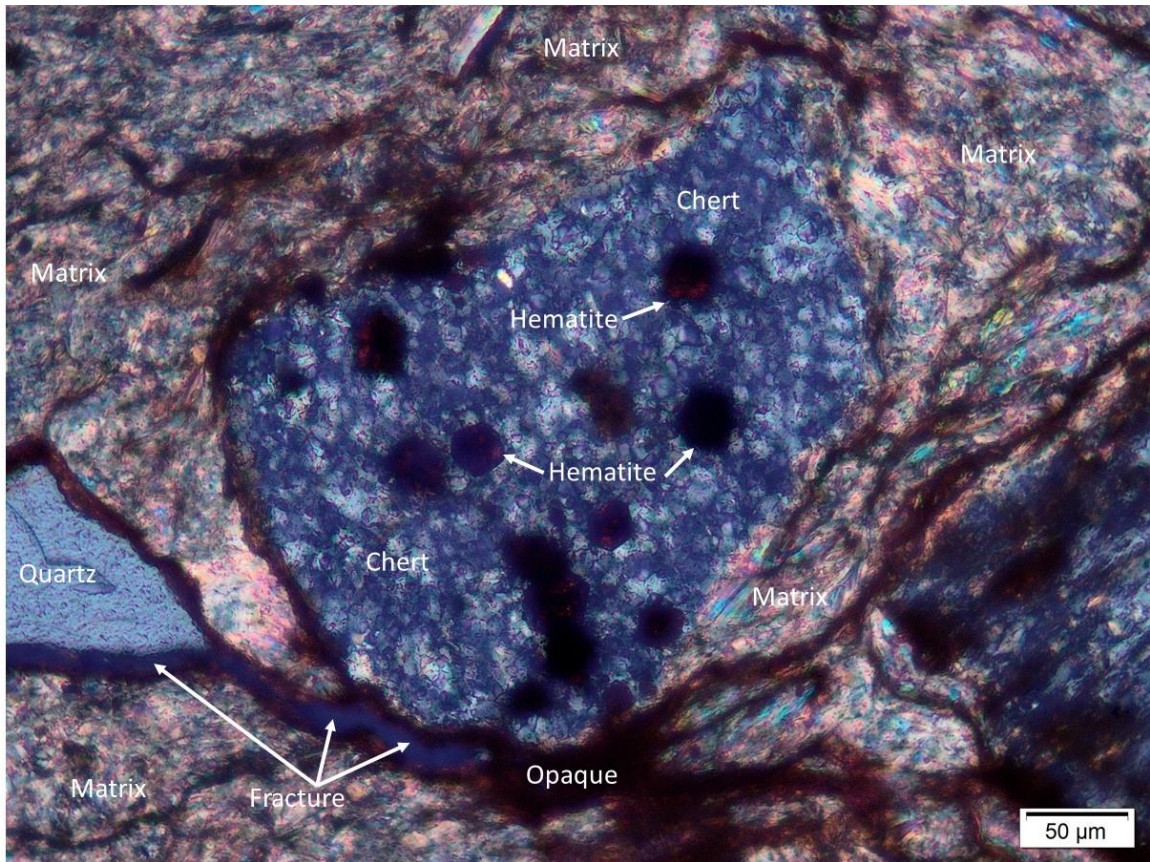


Figure 41: WB-7 XPL Chert nodule surrounded by fine-grained matrix. Hematite crystals are present on top of the chert nodule. Iron oxide staining and impregnation is present in the matrix and surrounds some edges of mineral grains and is also present lining a fracture in the matrix.

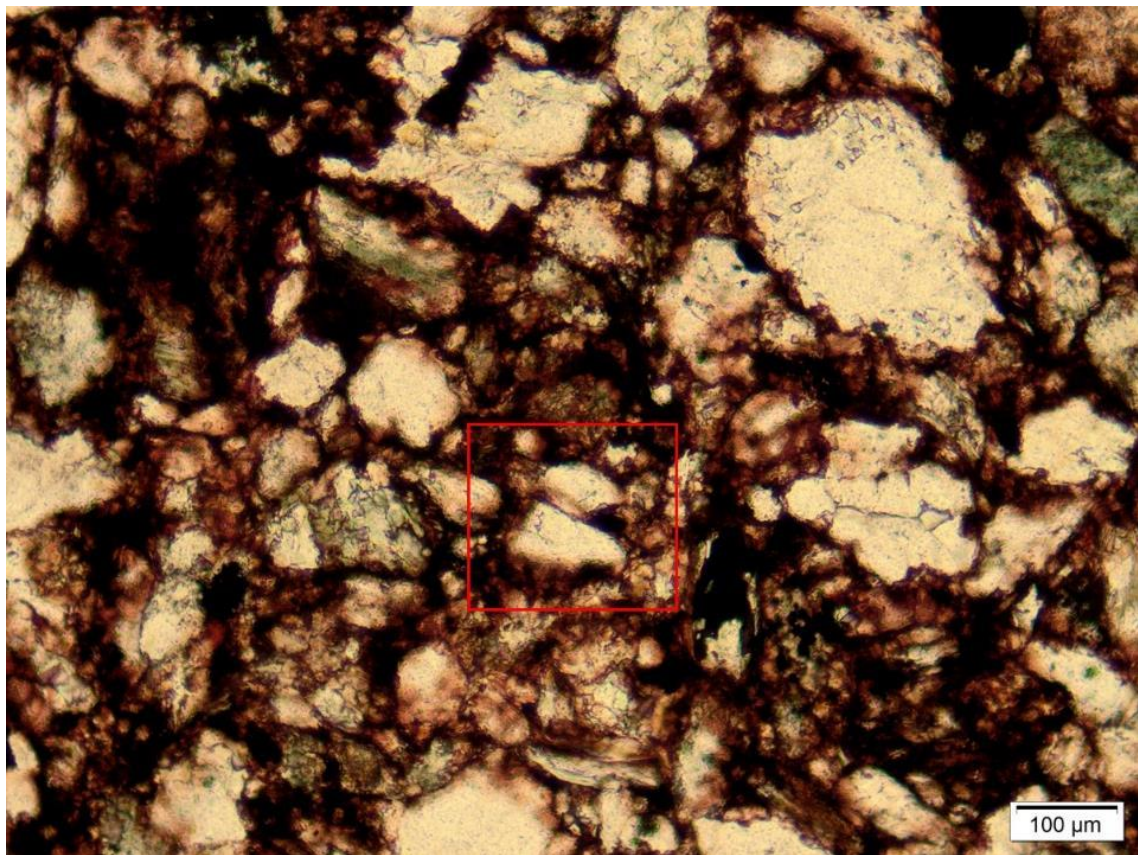


Figure 42: Sample DB-34 contains a high percentage of opaque minerals such as hematite. The opaque minerals appear to be predominantly authigenic as the reddish-brown minerals surround many grains. An important note is the point contact in the red box shows an absence of the opaque mineral coating, but the rest of the grain is surrounded by the opaque minerals.

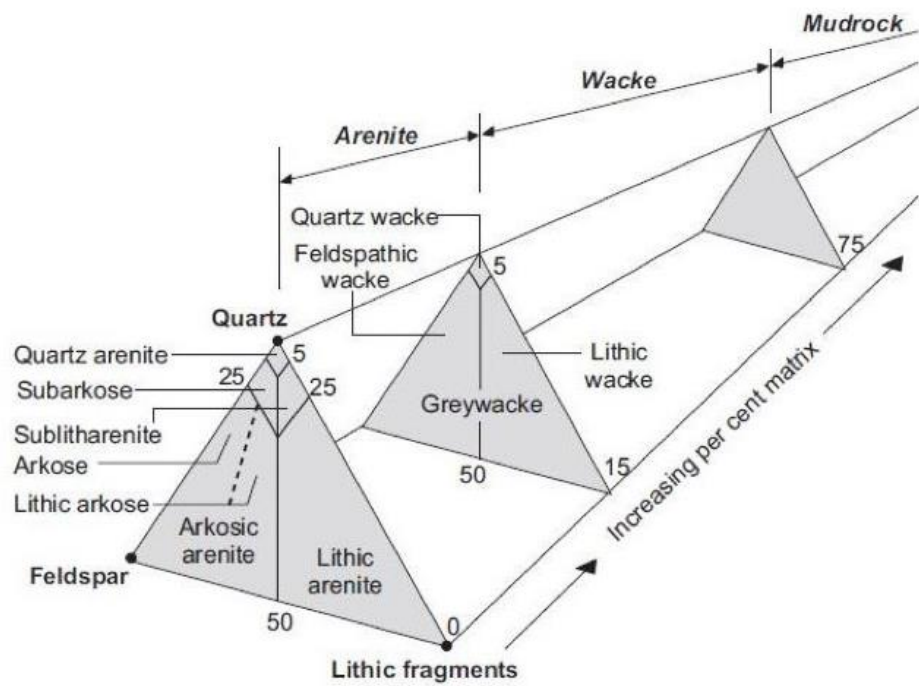


Figure 43: Classification of sandstones (Source: American Association of Petroleum Geologists AAPG Wiki, 2019).

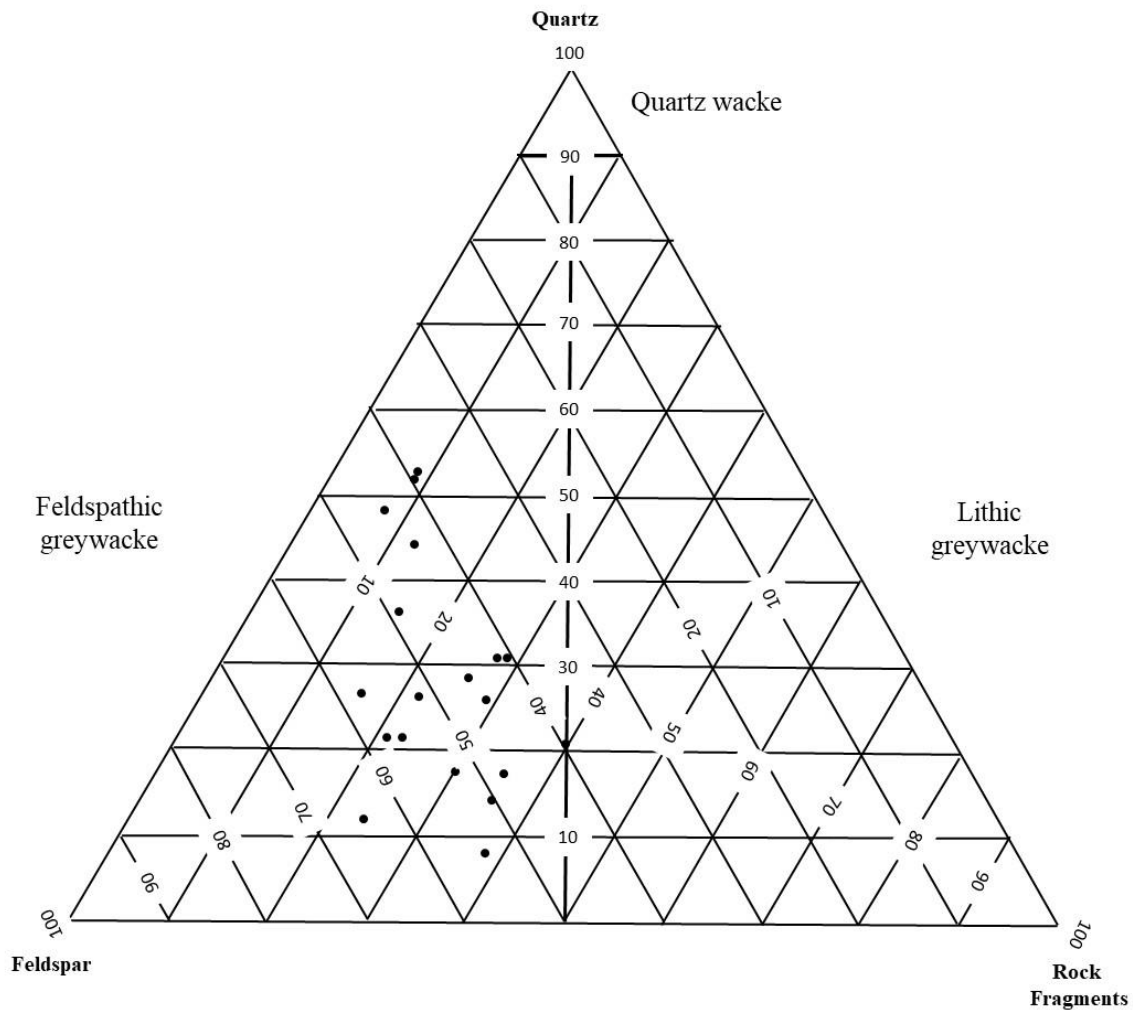


Figure 44: Ternary diagram with end members quartz, feldspar, and rock fragments. Eighteen of the sedimentary samples examined are classified as feldspathic greywackes. One sample, DB-34, is on the boundary between feldspathic greywackes and lithic greywackes.

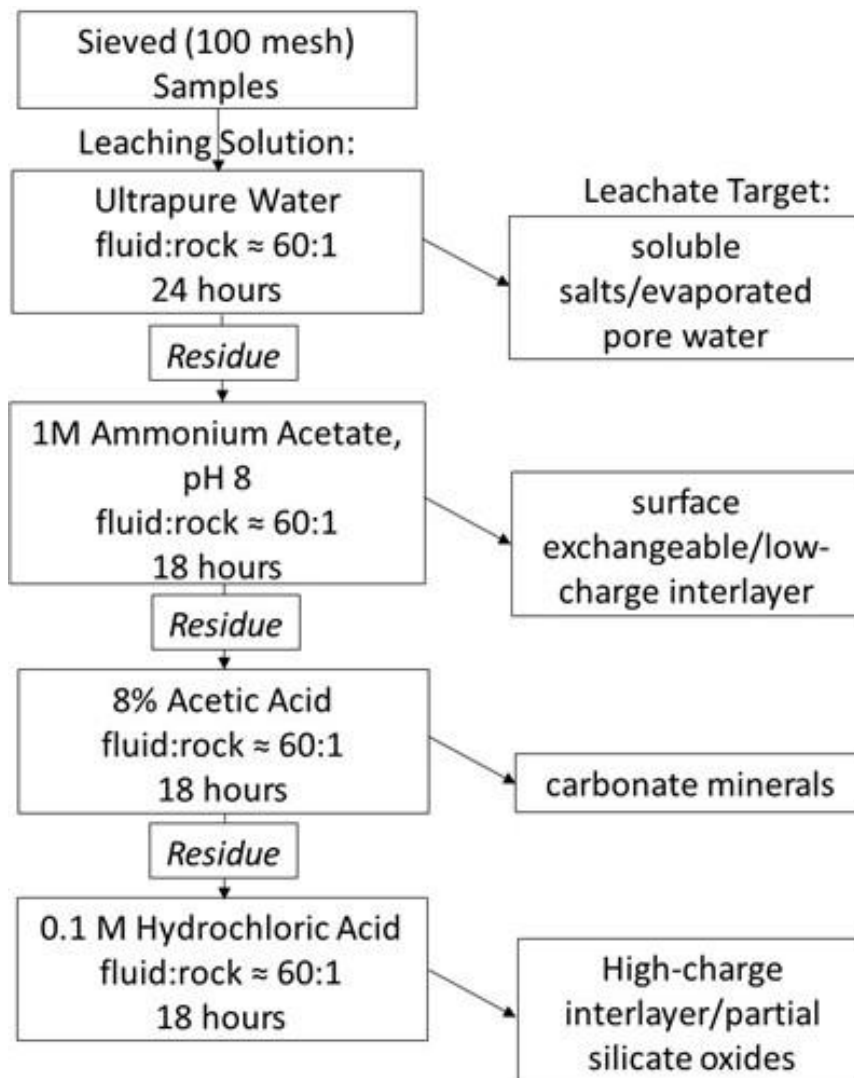


Figure 45: Flow diagram for the sequential extractions procedure used in this study (modified from Stewart et al., 2015).

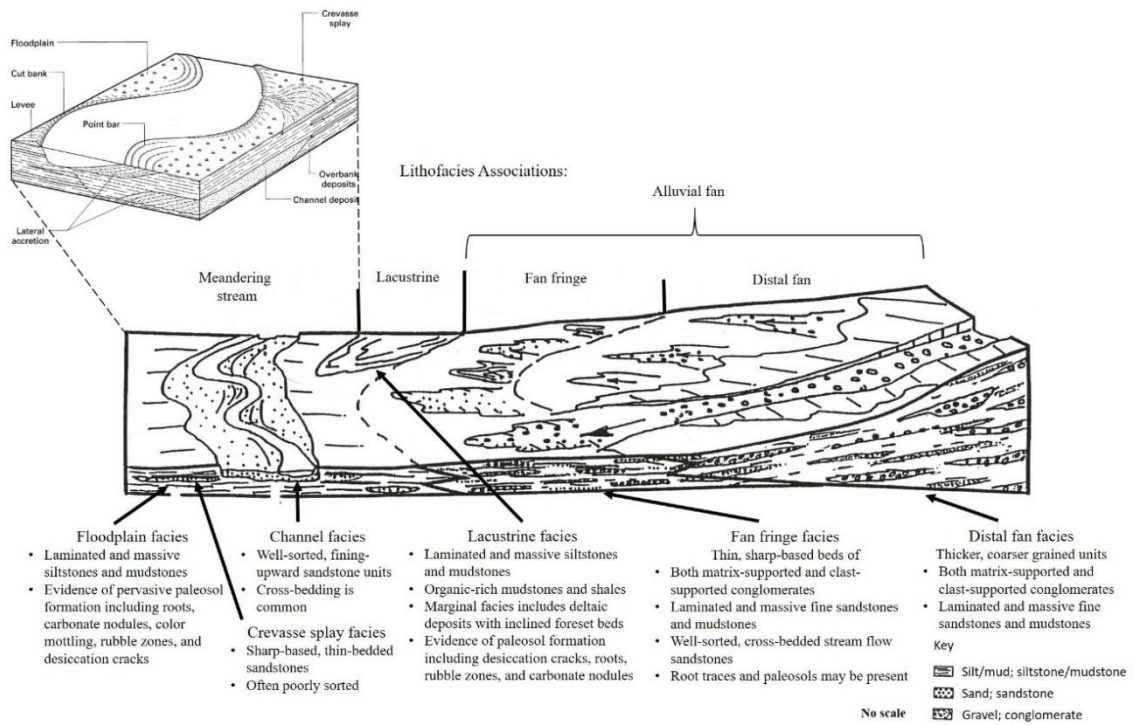


Figure 46: Schematic diagram of the lateral relationships of the major depositional environments and sub-environments associated the lithofacies associations identified for this study. (Modified from: Chem-nuclear, 1993).

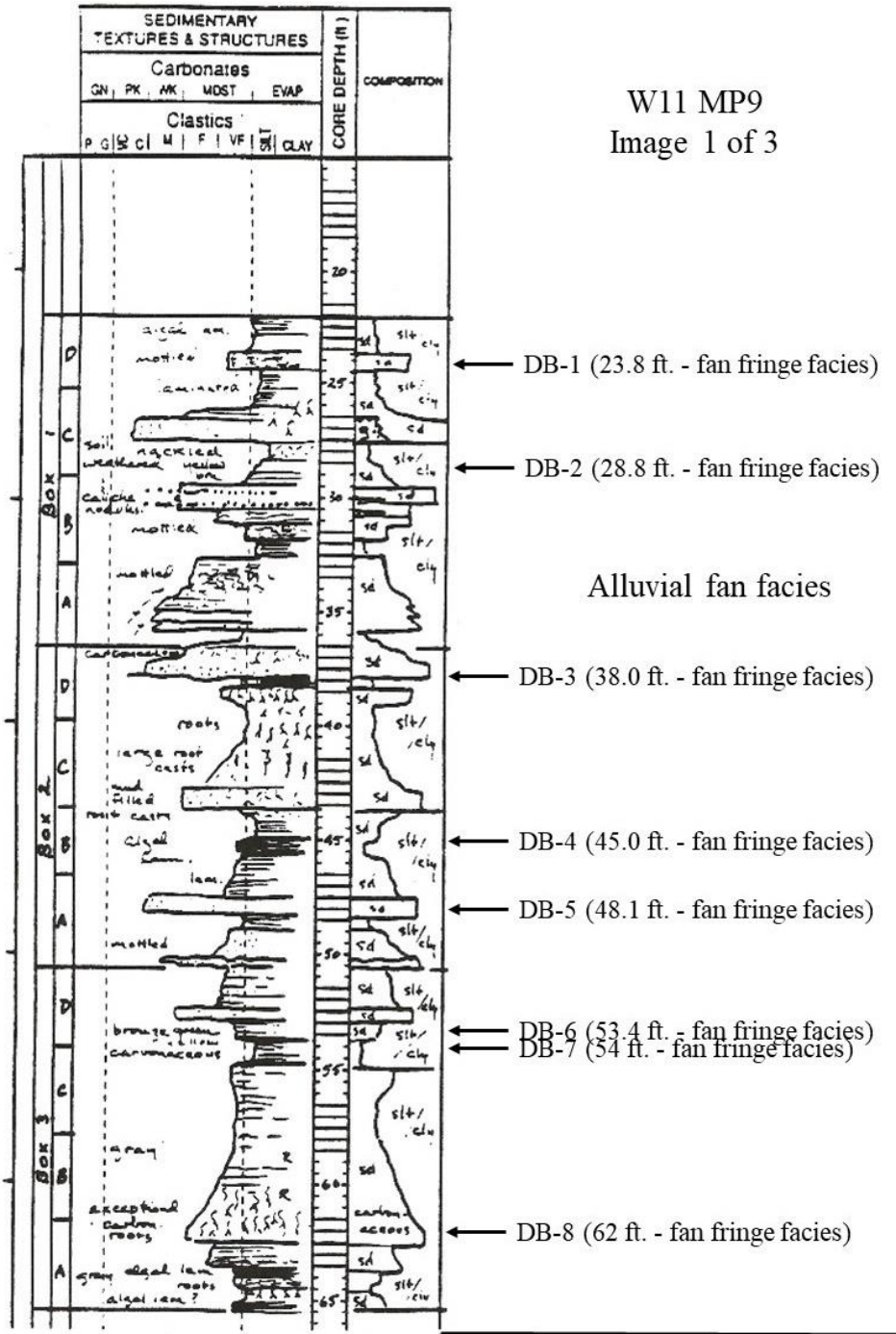


Figure 47: Graphic log of core W11 MP9 showing the depth (below the top of the cored interval) and depositional environment of the samples collected for this study. The depositional environments listed were, in general, based on observations by Chem-Nuclear, 1993. The core was approximately 150 ft. in length and is displayed in three consecutive images.

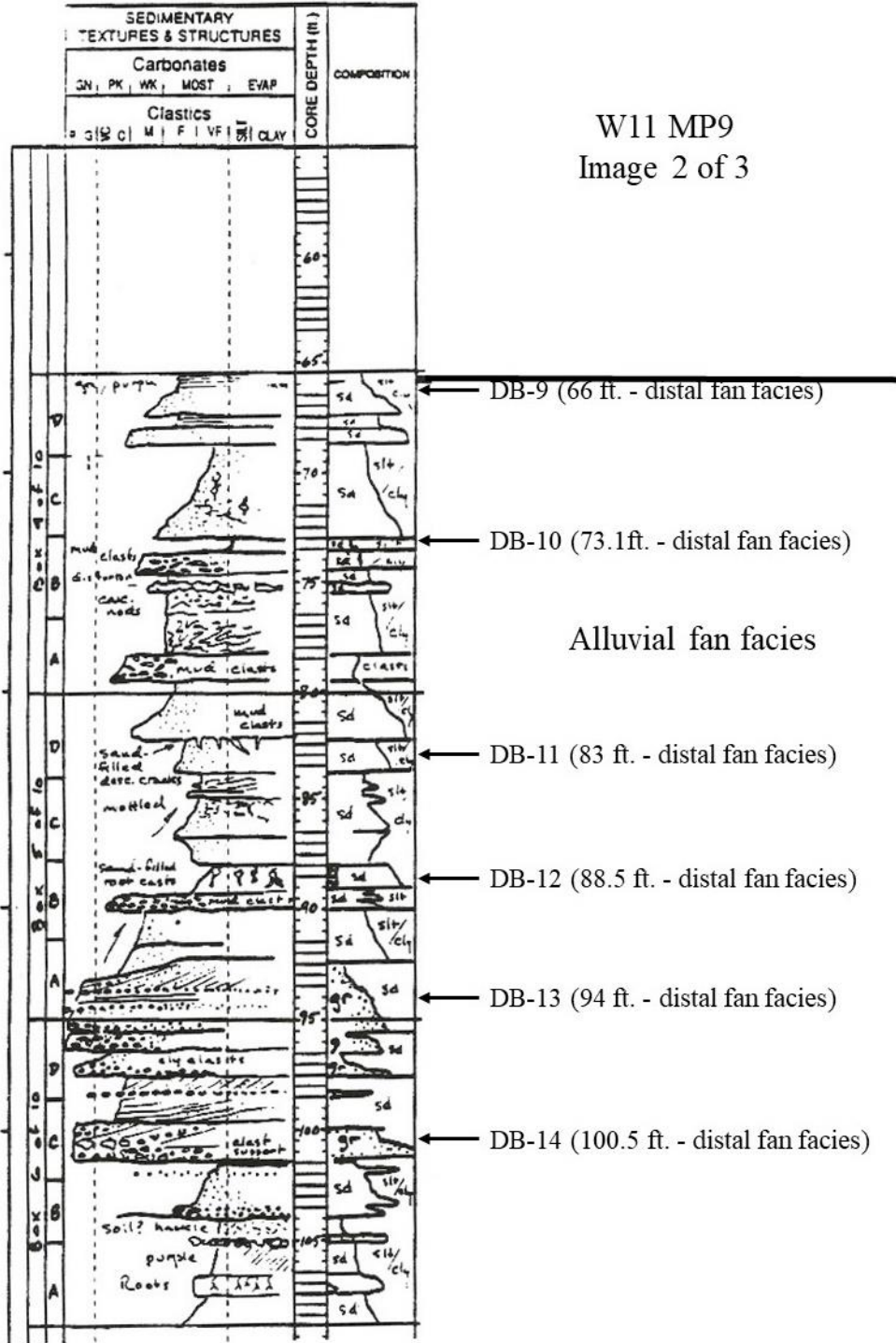


Figure 48: Graphic log of core W11 MP9 showing the depth (below the top of the cored interval) and depositional environment of the samples collected for this study. The depositional environments listed were, in general, based on observations by Chem-Nuclear, 1993. The core was approximately 150 ft. in length and is displayed in three consecutive images.

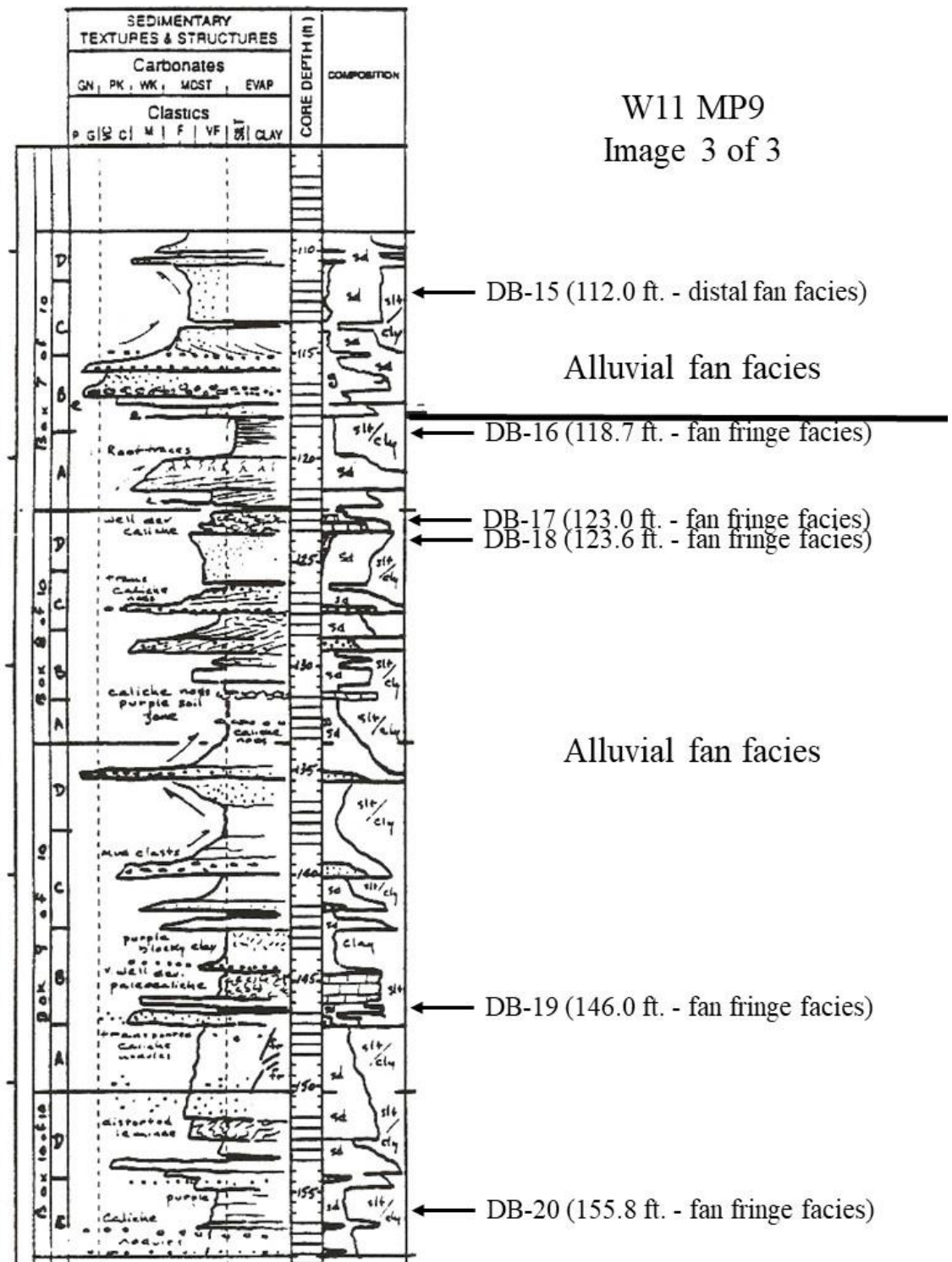


Figure 49: Graphic log of core W11 MP9 showing the depth (below the top of the cored interval) and depositional environment of the samples collected for this study. The depositional environments listed were, in general, based on observations by Chem-Nuclear, 1993. The core was approximately 150 ft. in length and is displayed in three consecutive images.

W10 MP5  
Image 1 of 3

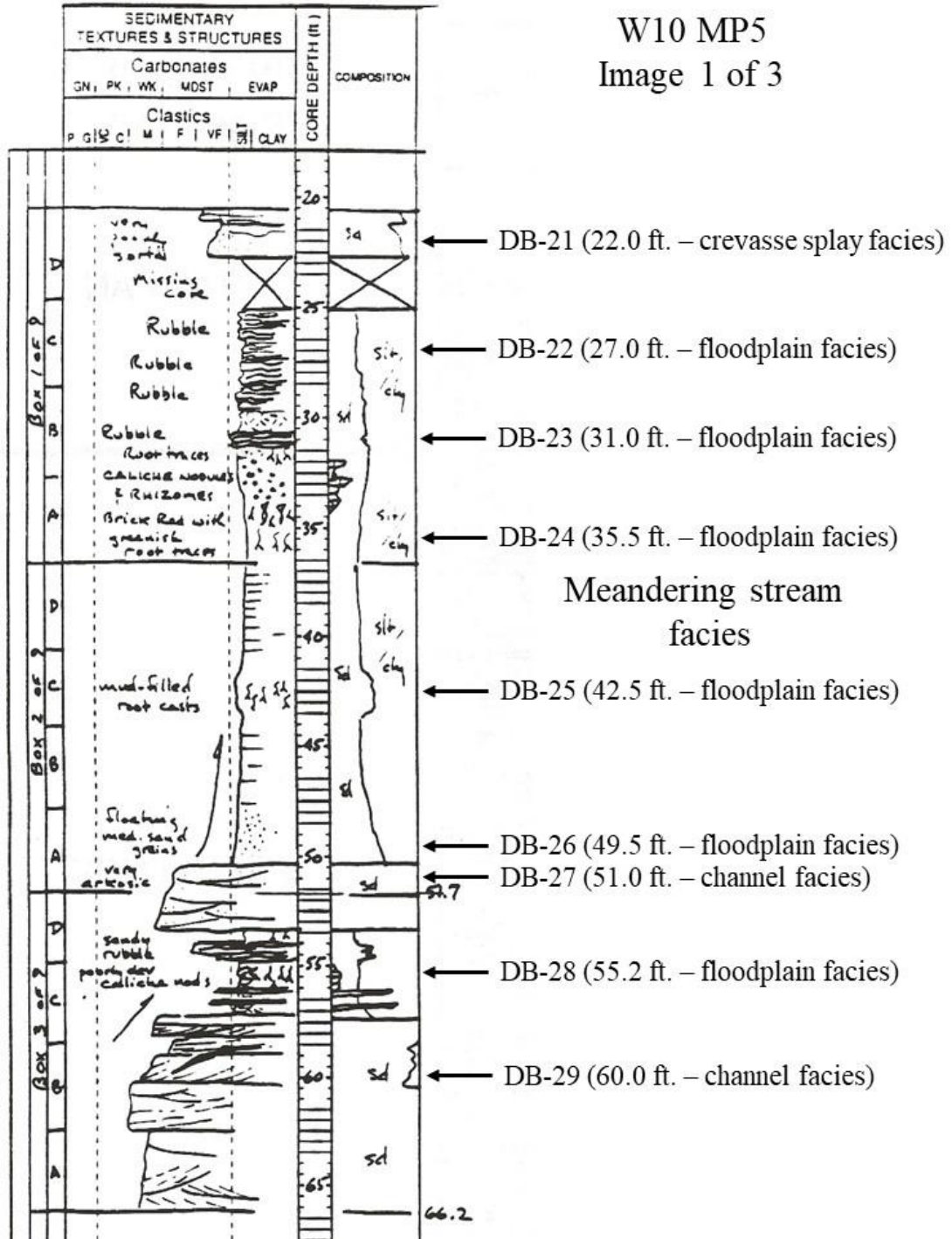


Figure 50: Graphic log of core W10 MP5 showing the depth (below the top of the cored interval) and depositional environment of the samples collected for this study. The depositional environments listed were, in general, based on observations by Chem-Nuclear, 1993. The core was approximately 150 ft. in length and is displayed in three consecutive images.

W10 MP5  
Image 2 of 3

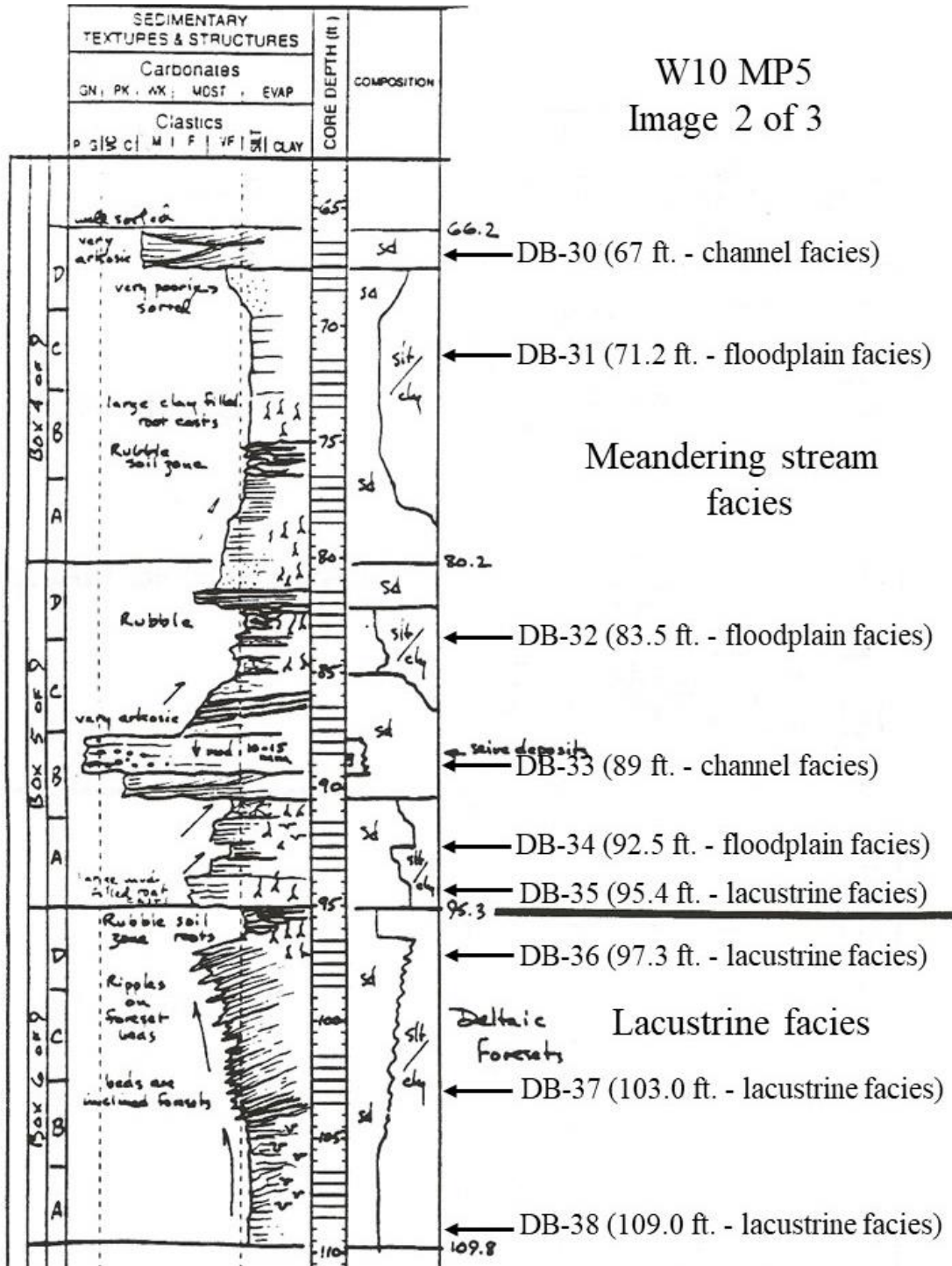


Figure 51: Graphic log of core W10 MP5 showing the depth (below the top of the cored interval) and depositional environment of the samples collected for this study. The depositional environments listed were, in general, based on observations by Chem-Nuclear, 1993. The core was approximately 150 ft. in length and is displayed in three consecutive images.

W10 MP5  
Image 3 of 3

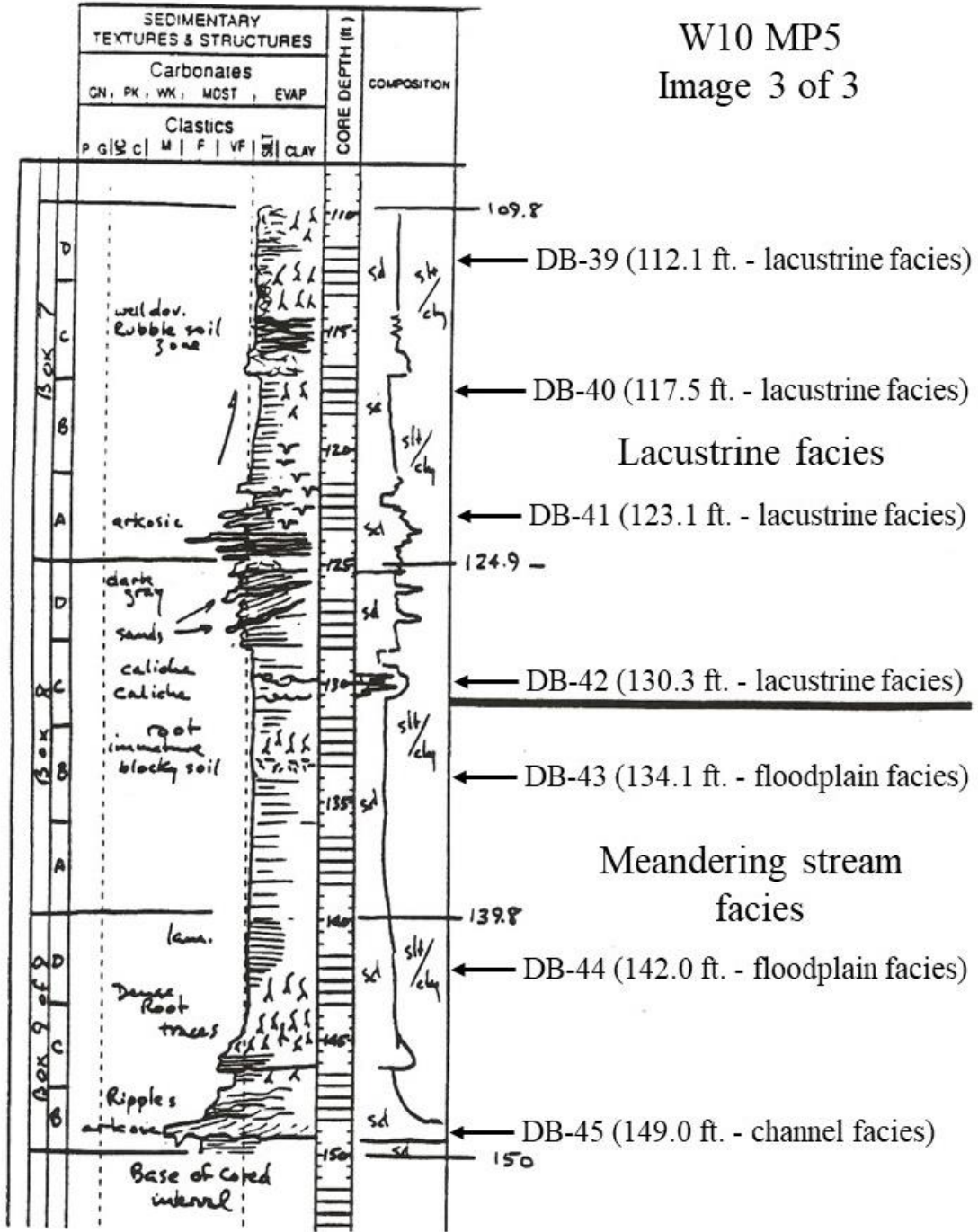


Figure 52: Graphic log of core W10 MP5 showing the depth (below the top of the cored interval) and depositional environment of the samples collected for this study. The depositional environments listed were, in general, based on observations by Chem-Nuclear, 1993. The core was approximately 150 ft. in length and is displayed in three consecutive images.



W32 MP14  
Image 2 of 3

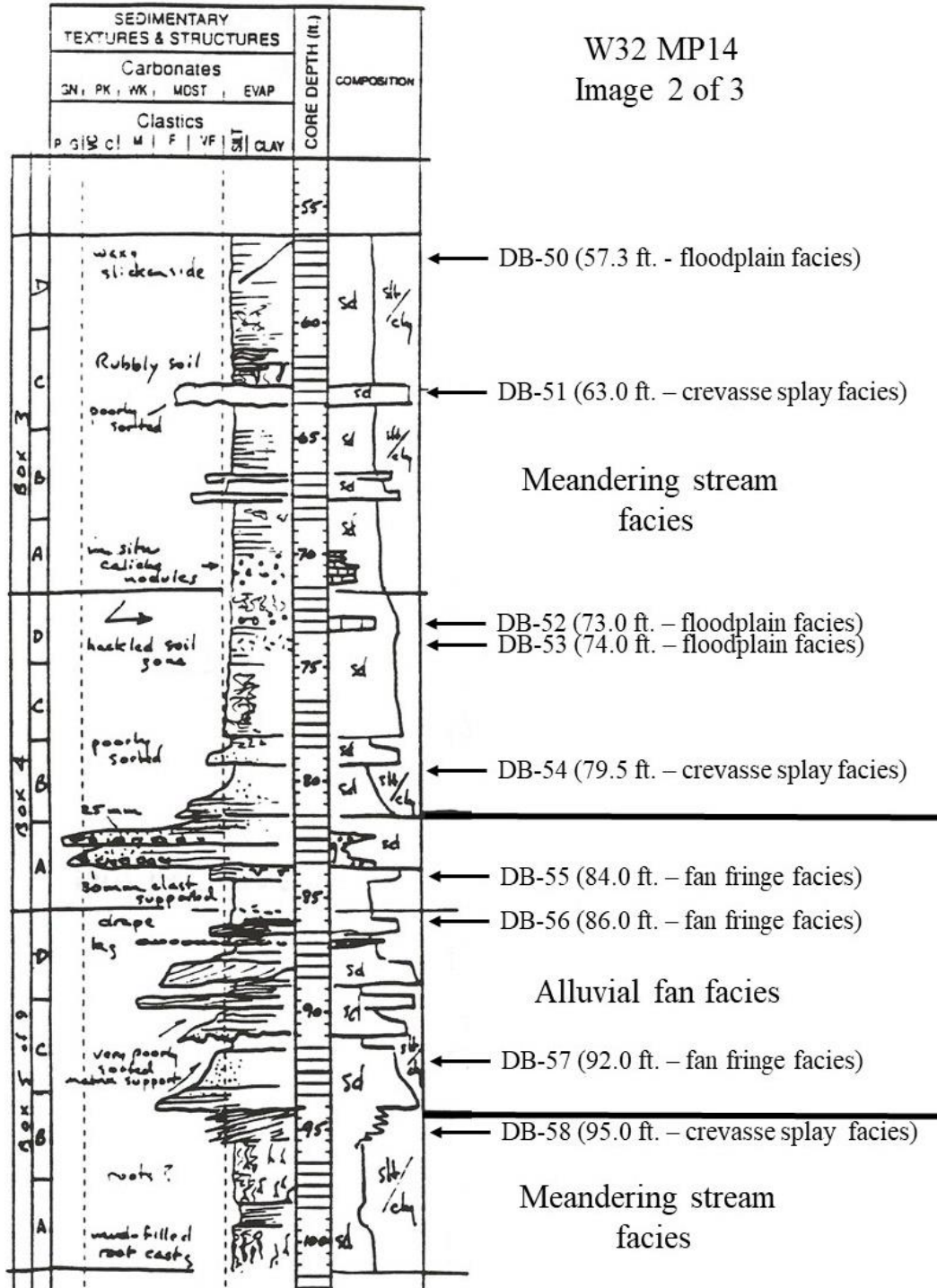


Figure 54: Graphic log of core W32 MP14 showing the depth (below the top of the cored interval) and depositional environment of the samples collected for this study. The depositional environments listed were, in general, based on observations by Chem-Nuclear, 1993. The core was approximately 150 ft. in length and is displayed in three consecutive images.

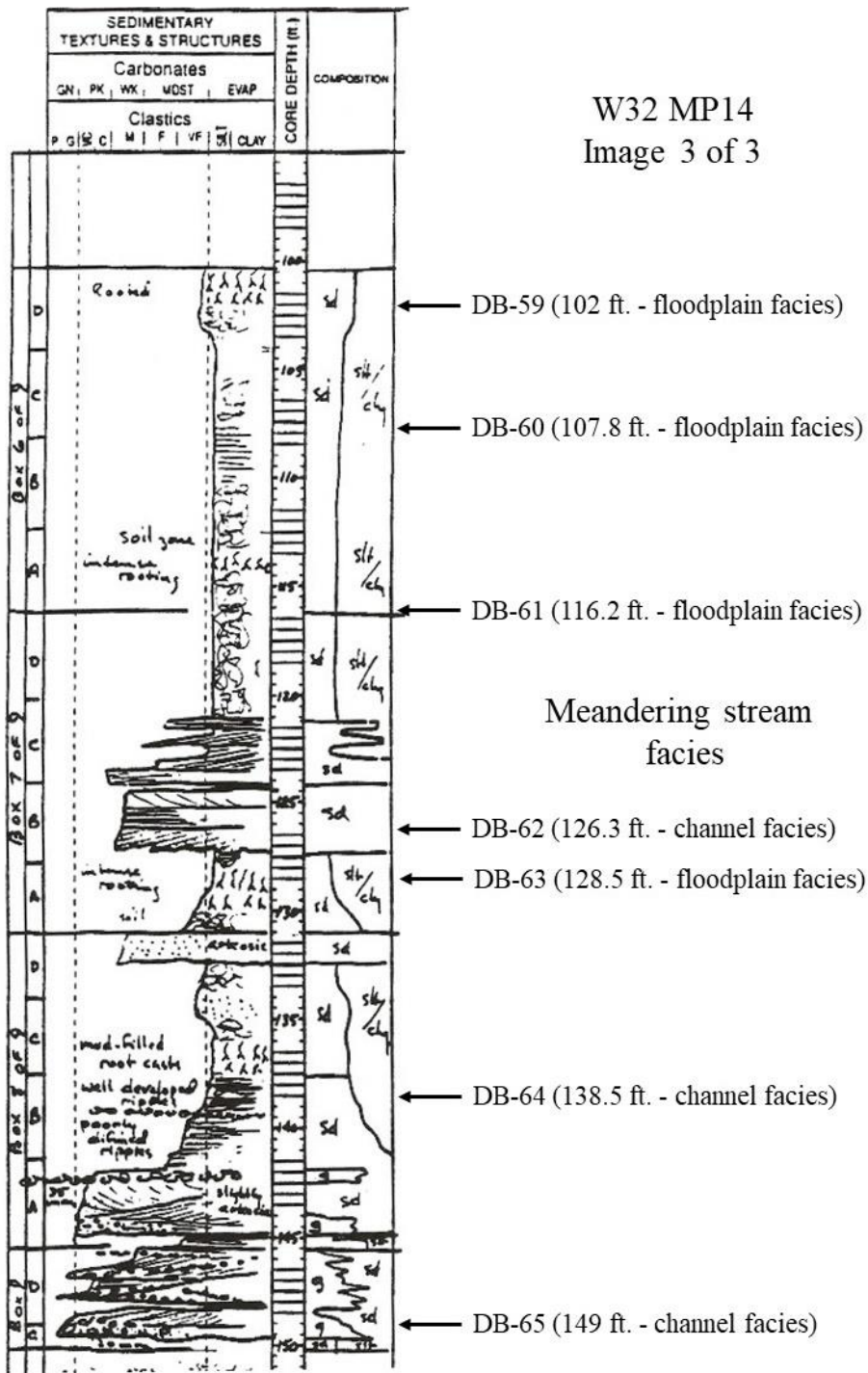


Figure 55: Graphic log of core W32 MP14 showing the depth (below the top of the cored interval) and depositional environment of the samples collected for this study. The depositional environments listed were, in general, based on observations by Chem-Nuclear, 1993. The core was approximately 150 ft. in length and is displayed in three consecutive images.

W31 DP3  
Image 1 of 4

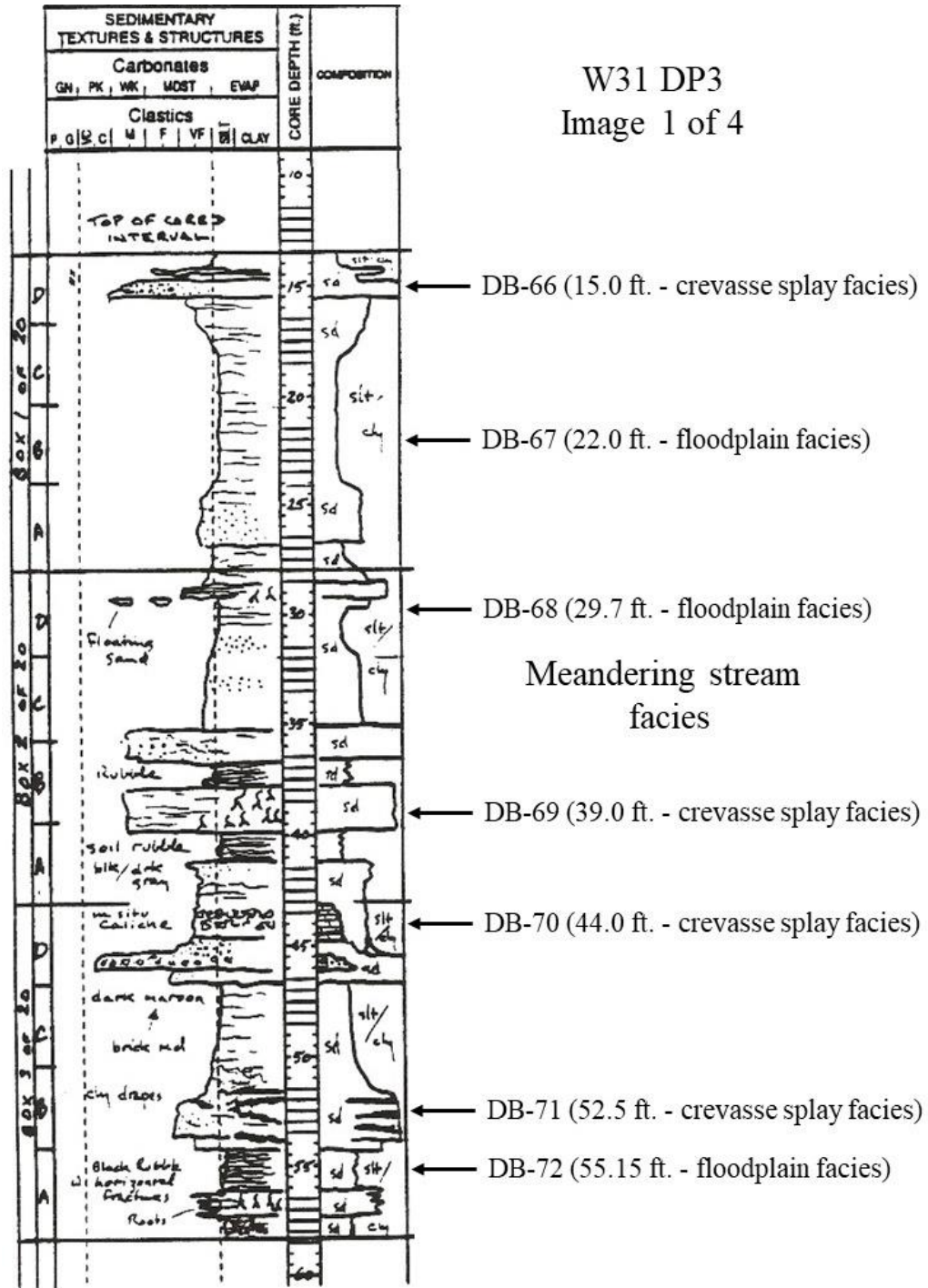


Figure 56: Graphic log of core W31 DP3 showing the depth (below the top of the cored interval) and depositional environment of the samples collected for this study. The depositional environments listed were, in general, based on observations by Chem-Nuclear, 1993. The core was approximately 300 ft. in length and is displayed in four consecutive images.

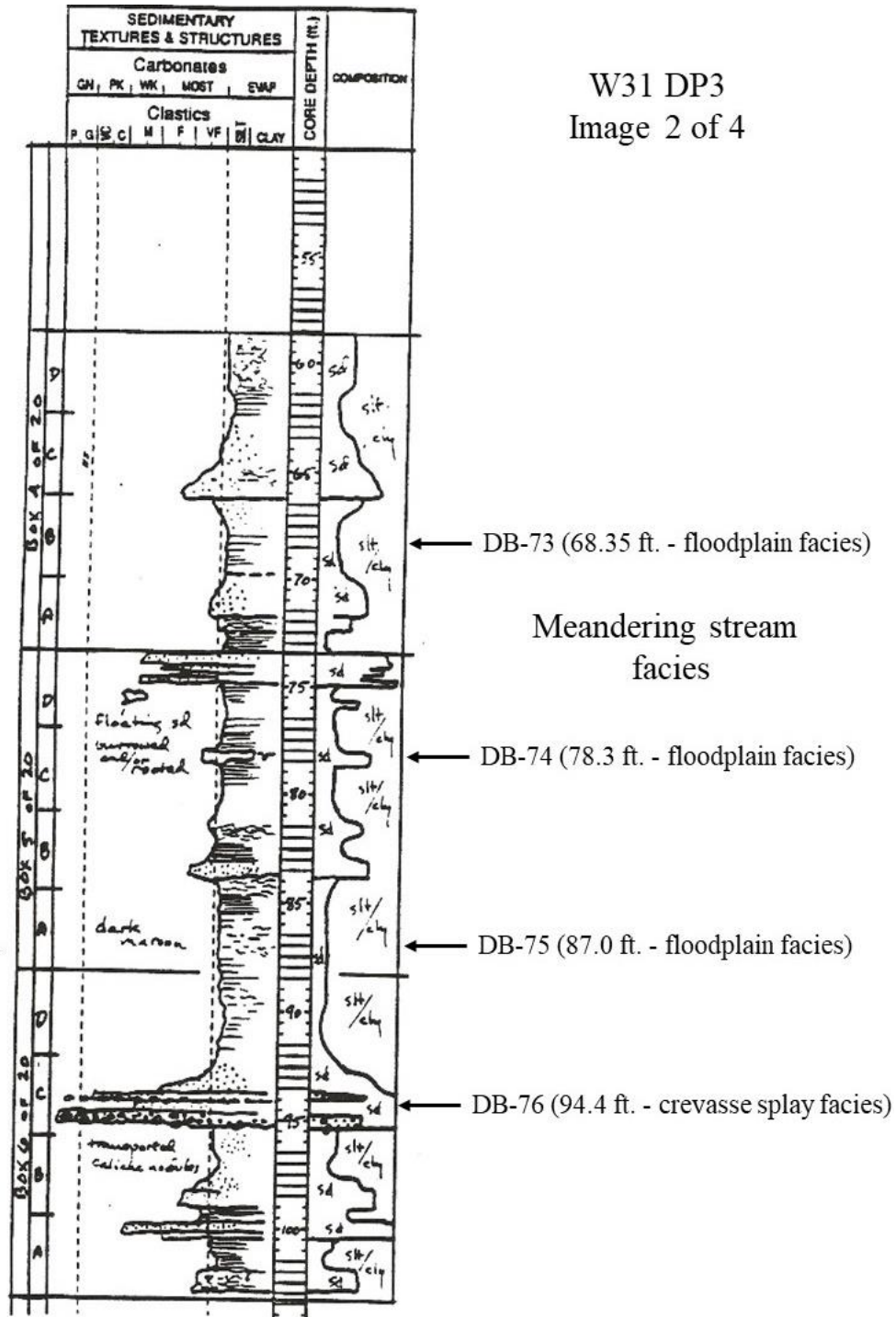


Figure 57: Graphic log of core W31 DP3 showing the depth (below the top of the cored interval) and depositional environment of the samples collected for this study. The depositional environments listed were, in general, based on observations by Chem-Nuclear, 1993. The core was approximately 300 ft. in length and is displayed in four consecutive images.



W31 DP3  
Image 4 of 4

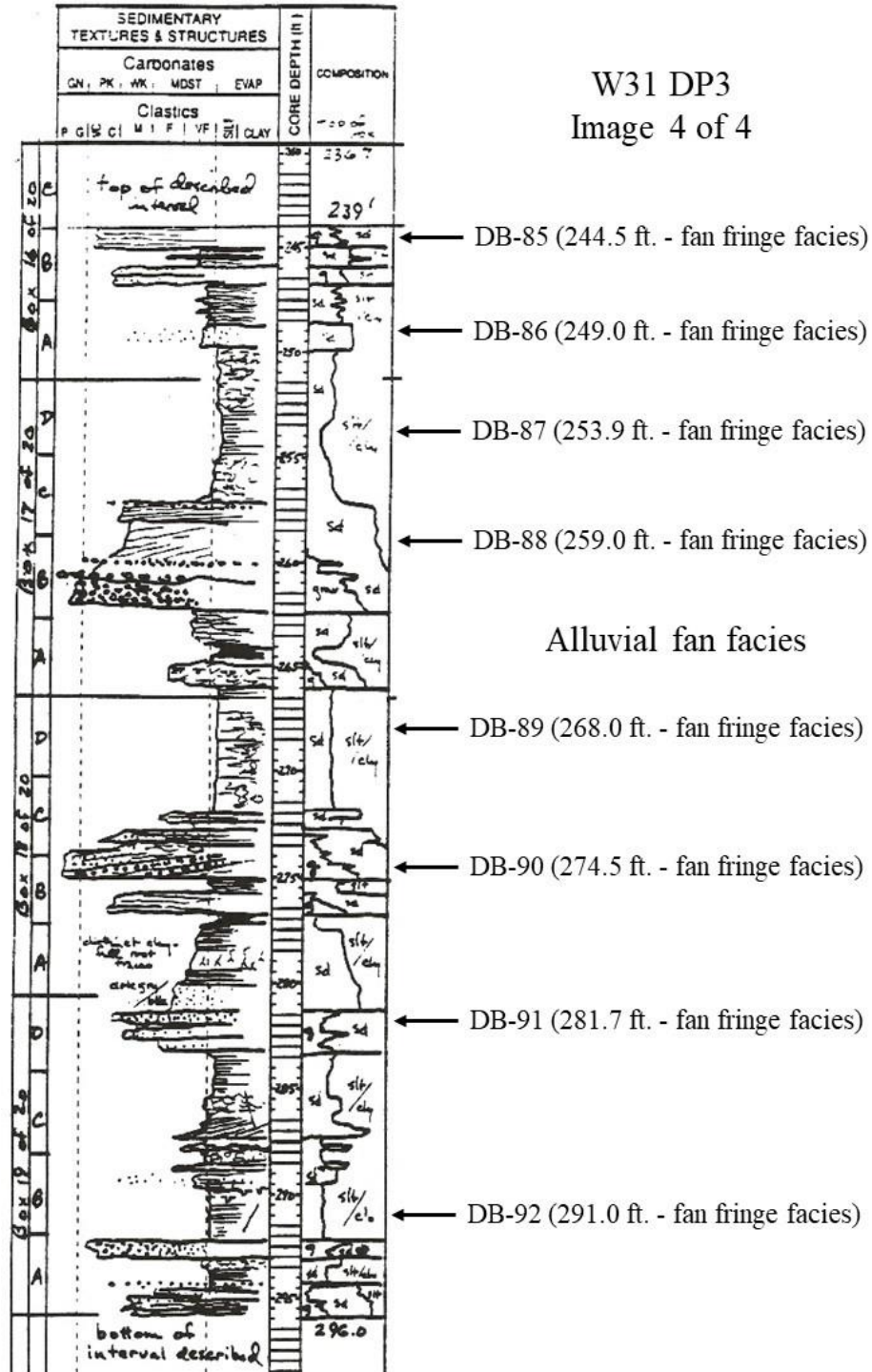


Figure 59: Graphic log of core W31 DP3 showing the depth (below the top of the cored interval) and depositional environment of the samples collected for this study. The depositional environments listed were, in general, based on observations by Chem-Nuclear, 1993. The core was approximately 300 ft. in length and is displayed in four consecutive images.



Figure 60: This device was provided by the Rigaku Corporation and was used to prepare a powdered sample for XRD analysis. This device was assembled and a finely-powdered (0.044 mm) sample was brushed through a 230-mesh (0.063 mm) sieve to achieve even distribution and to minimize preferred orientation of the particles. Once enough material was brushed through the sieve, the top of the sieve was removed and a tamper was used to pack the sample into the metal disk firmly enough so that it did not fall out, but not so firmly that preferred orientation resulted on the opposite side. The metal disk with the sample was then gently removed from the sample preparation device and delicately placed in the XRD machine.

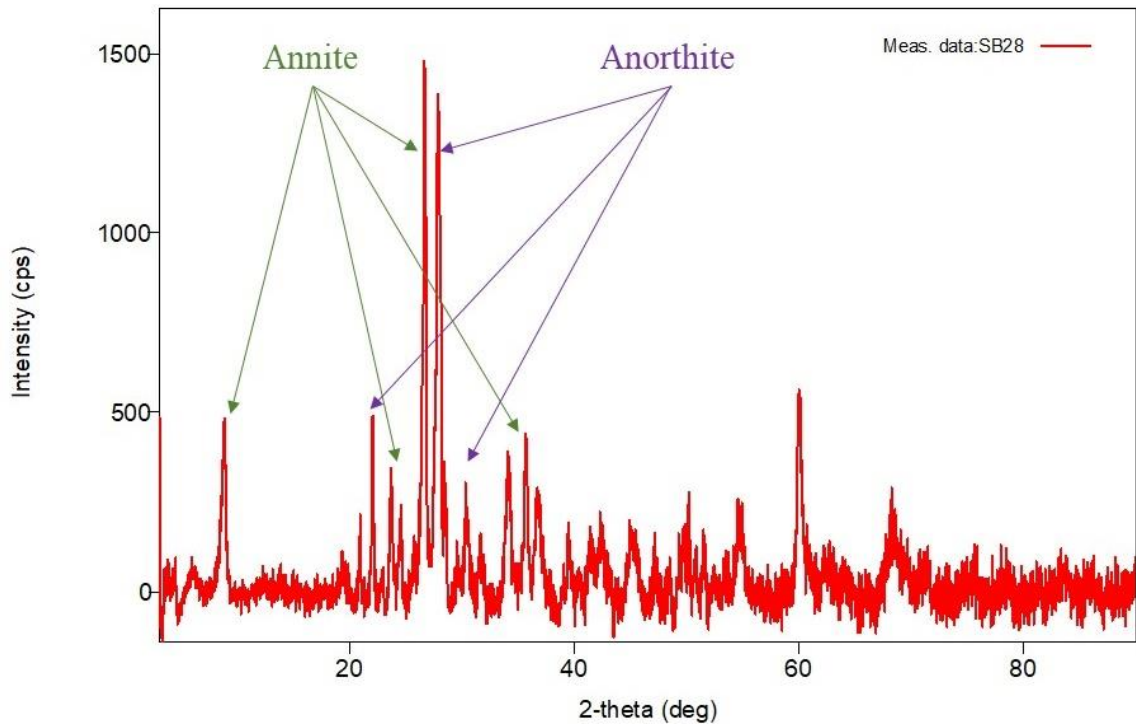


Figure 61: The x-ray diffractogram of sample SB-28 generated from the XRD analysis. This sample is composed of 0.95% TOC. The relatively high organic content of the sample caused broadening of the X-ray diffraction peaks and an increased amount of background interference. The minerals identified in the sample and their relative abundance are labeled. Several important peaks used to identify each mineral have been noted. Additionally, the color scheme shows relative abundance; green is the most abundant mineral while purple is the second most abundant mineral.

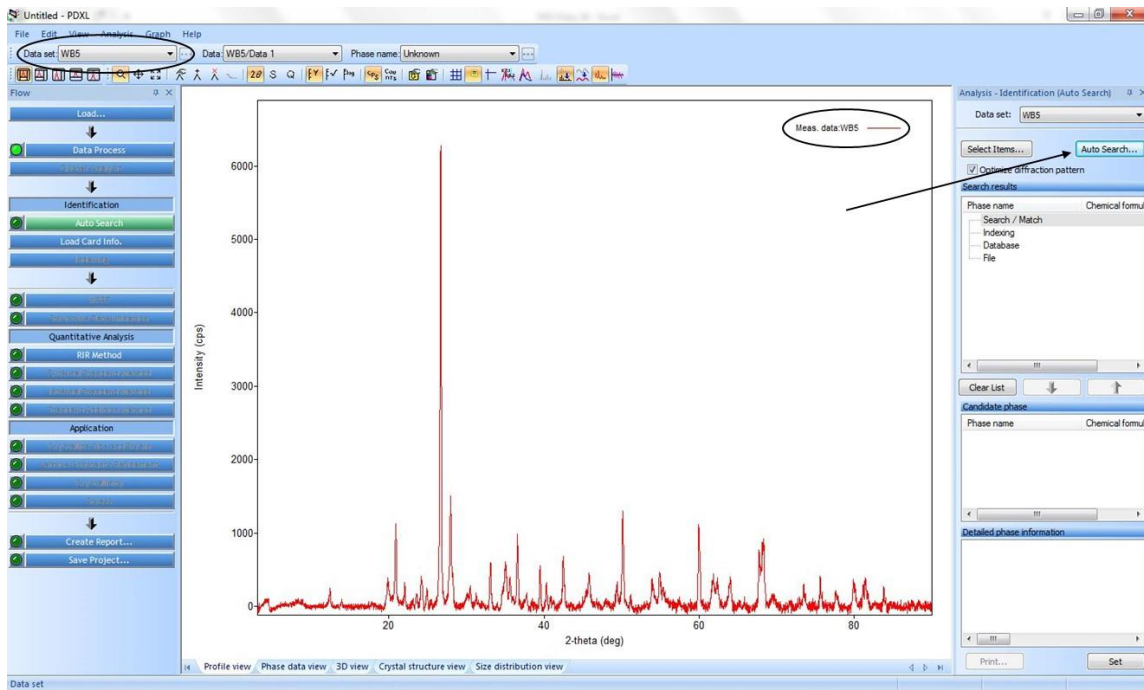


Figure 62: To determine the bulk mineral composition of the samples from the DRB, each diffractogram was loaded into an integrated X-ray powder diffraction software program called PDXL2 (shown in photo). PDXL2 is a comprehensive software package designed by the Rigaku Corporation to help users that are not specialists in the field of X-ray diffraction to easily perform many types of analysis (Rigaku, 2010). The black circles indicate the sample name and the black arrow points to the auto search function that was used to identify the minerals in the samples.

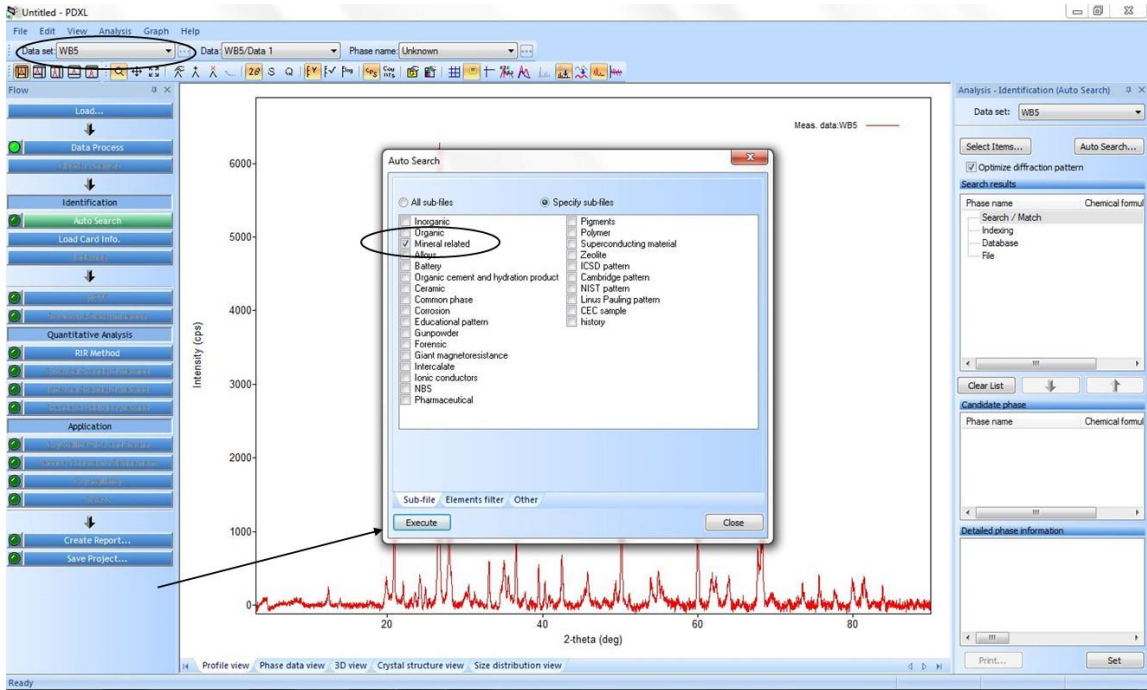


Figure 63: To determine the bulk mineral composition of the samples from the DRB, each diffractogram was loaded into an integrated X-ray powder diffraction software program called PDXL2 (shown in photo). The black circles indicate the sample name and the black arrow points to the auto search function that was used to identify the minerals in the samples.

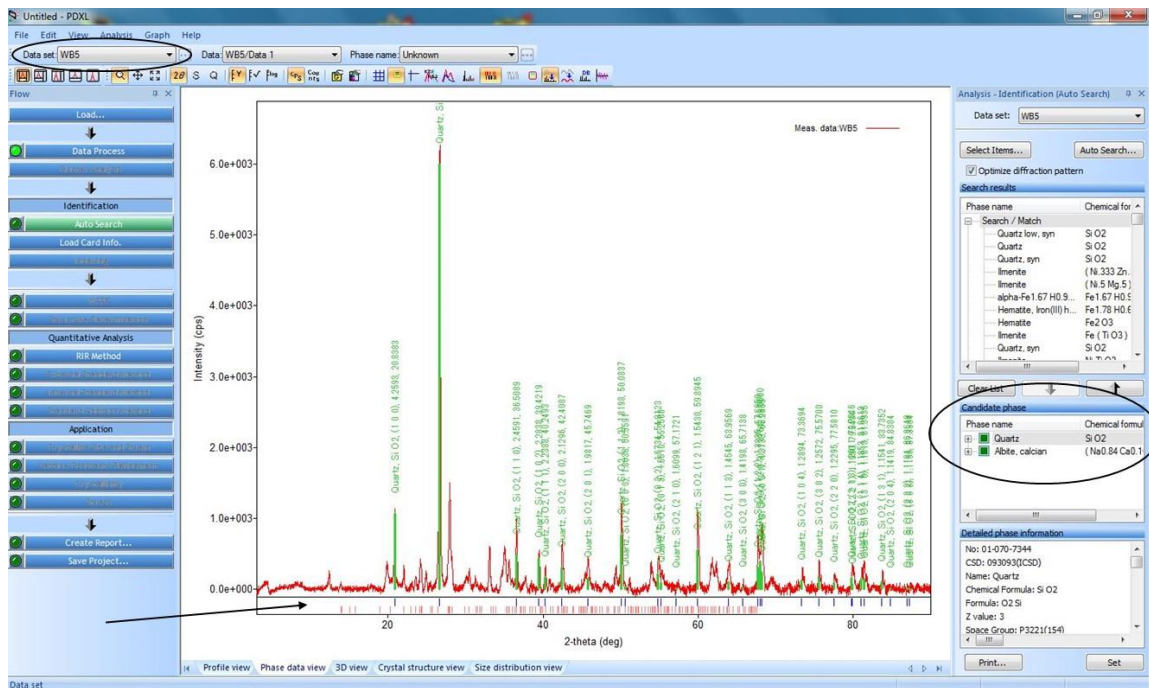


Figure 64: The auto search identified the candidate phases (black circle) present in a sample and displayed the associated peaks of each mineral identified below the sample's diffractogram (highlighted by the black arrow). Quartz was identified by its characteristics peaks (displayed in figure) and as the most abundant mineral based on its order of occurrence in the candidate phase list (black circle).

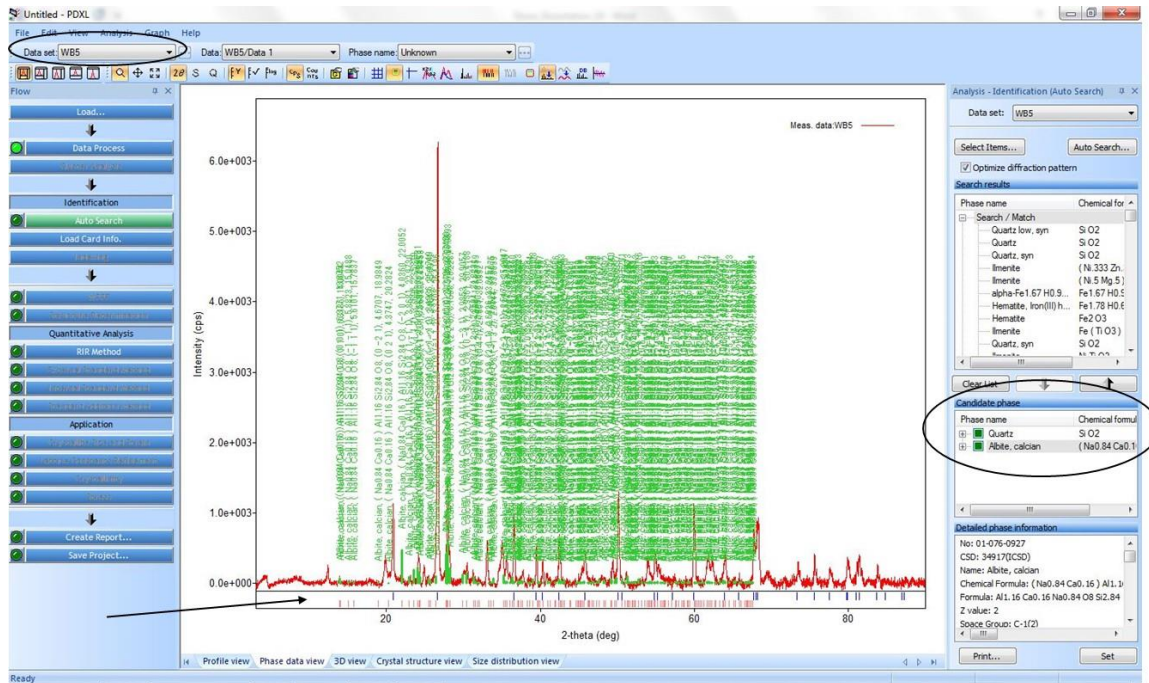


Figure 65: The auto search identified the candidate phases (black circle) present in a sample and displayed the associated peaks of each mineral identified below the sample's diffractogram (highlighted by the black arrow). Albite was identified by its characteristics peaks (displayed in figure) and as the second most abundant mineral based on its order of occurrence in the candidate phase list (black circle).

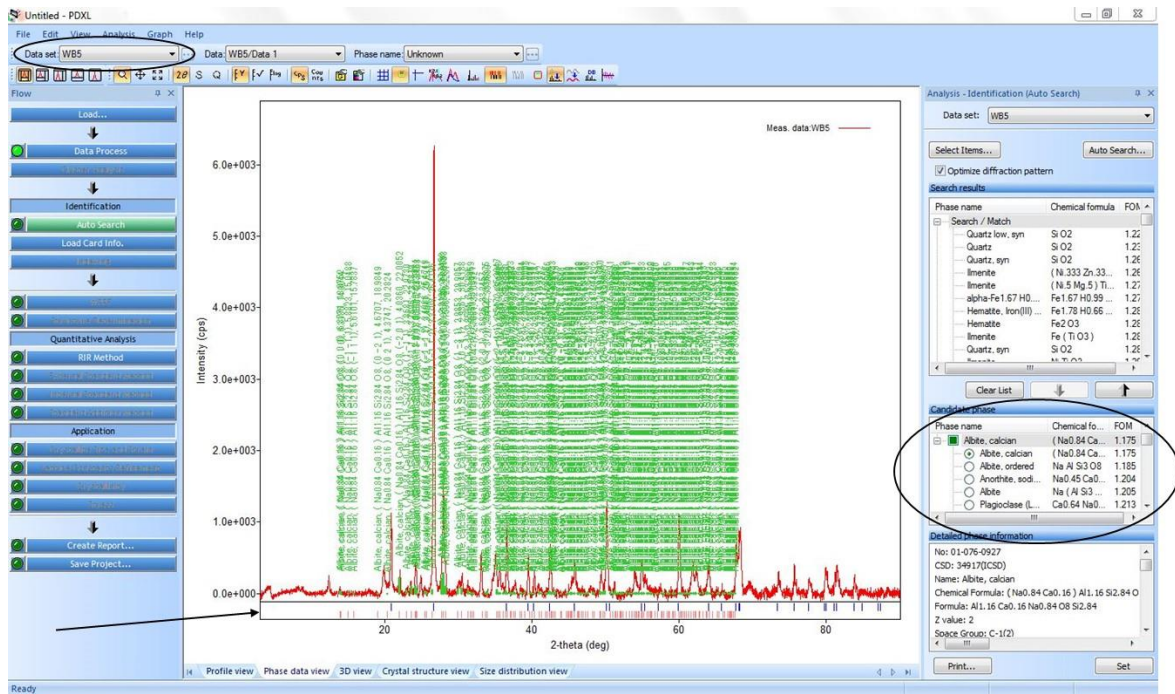


Figure 66: The auto search identified the candidate phases (black circle) present in a sample and displayed the associated peaks of each mineral identified below the sample's diffractogram (highlighted by the black arrow). Although albite was identified, the software suggested other varieties of plagioclase such as anorthite and labradorite that may fit the diffraction pattern.

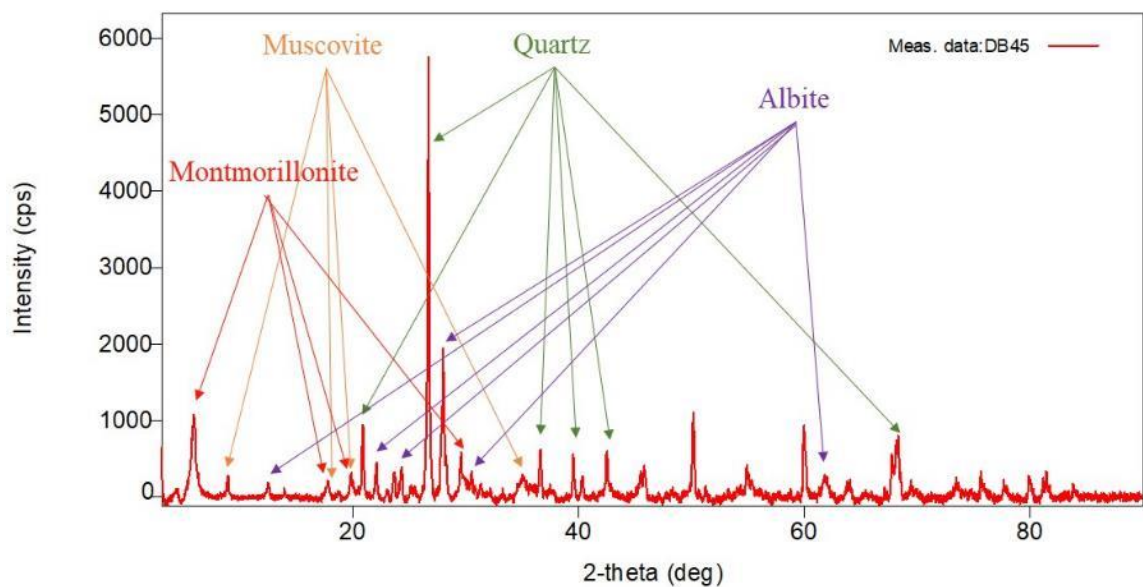


Figure 67: The x-ray diffractogram of sample DB-45 generated from the XRD analysis. The minerals identified in the sample and their relative abundances are labeled. Several important peaks used to identify each mineral have been noted. Additionally, the color scheme shows relative abundance. Green is most abundant, purple is second most abundant, and red is third most abundant. Where applicable, orange is the least abundant mineral.

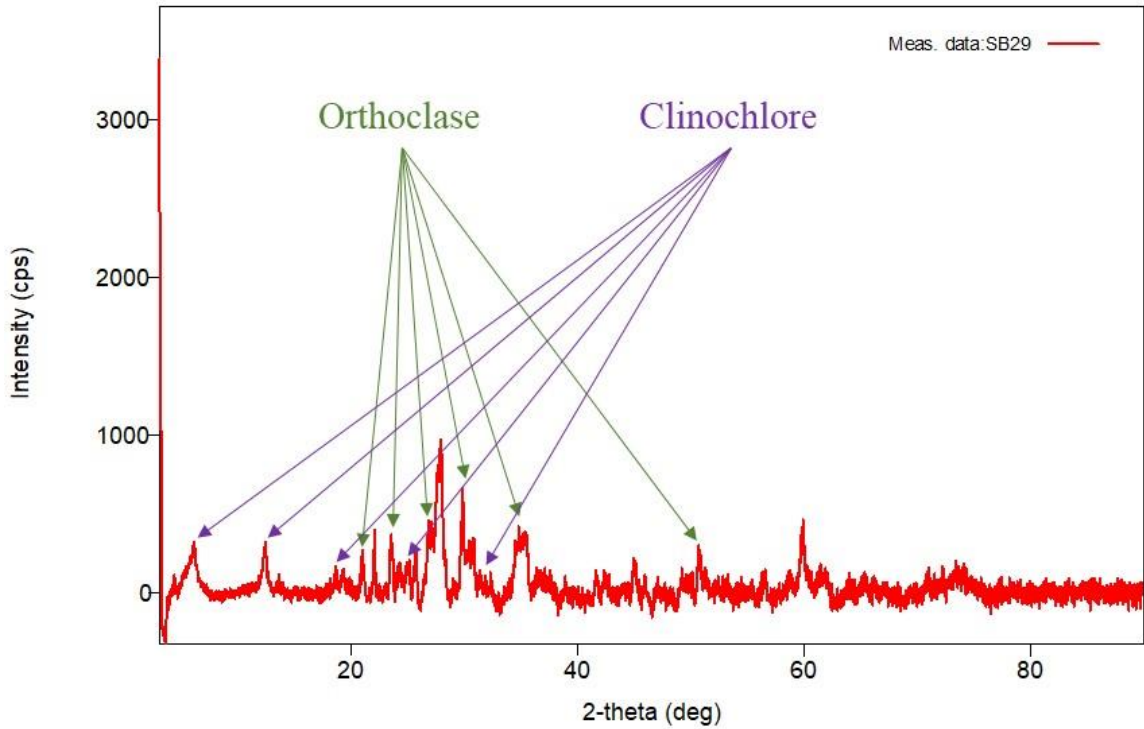


Figure 68: The x-ray diffractogram of sample SB-29 generated from the XRD analysis. The minerals identified in the sample and their relative abundances are labeled. Several important peaks used to identify each mineral have been noted. Additionally, the color scheme shows relative abundance. Green is most abundant and purple is second most abundant.

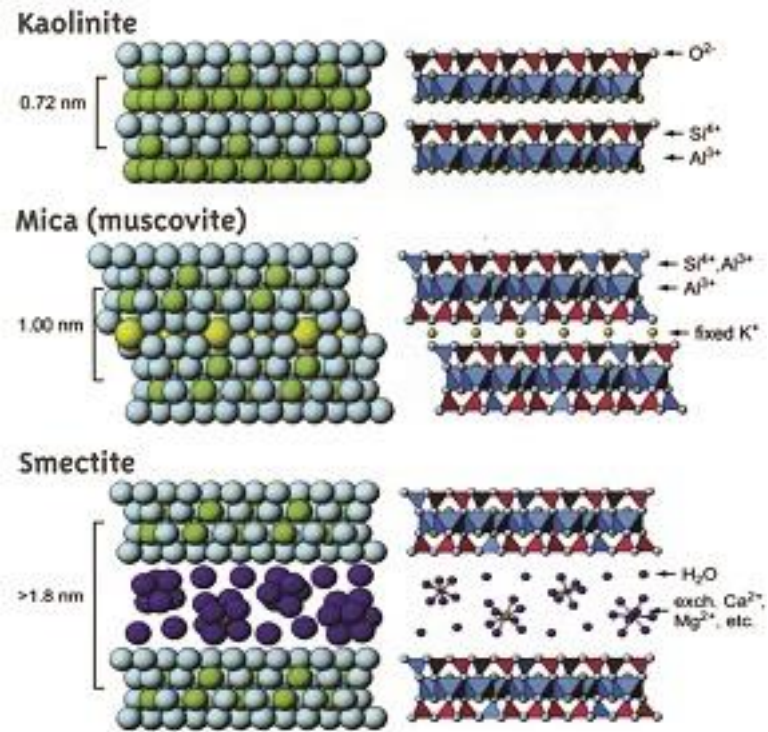


Figure 69: Diagram illustrating the structures of clay minerals (Source: Soil Science Society of America (SSSA), 2019).

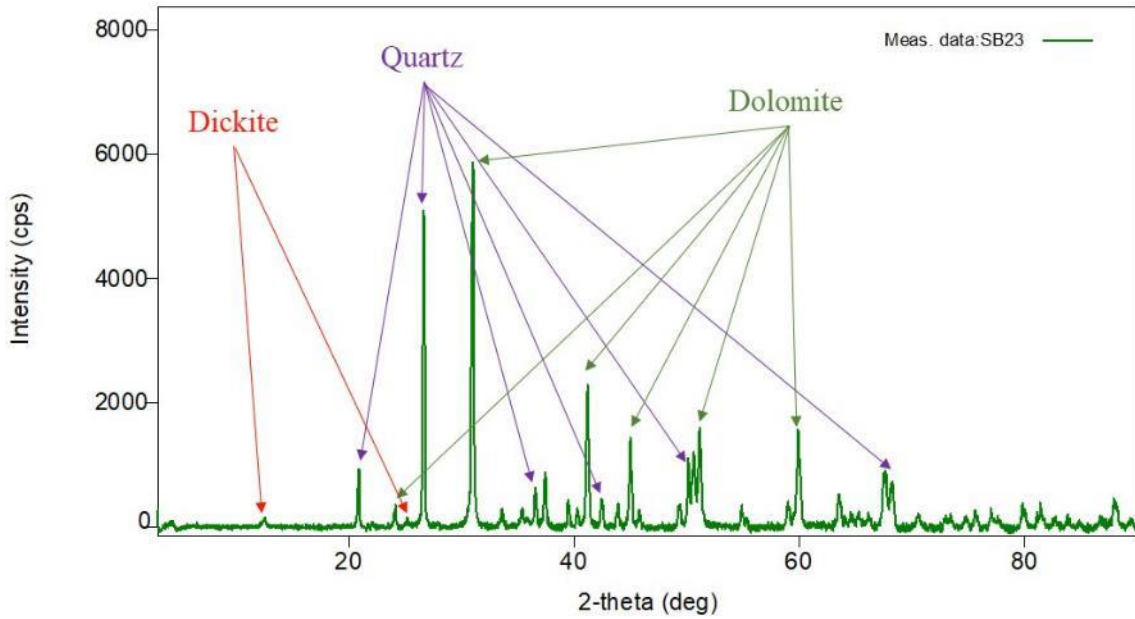


Figure 70: The x-ray diffractogram of sample SB-23 generated from the XRD analysis. The minerals identified in the sample and their relative abundance are labeled. Several important peaks used to identify each mineral have been noted. Additionally, the color scheme shows relative abundance. Green is most abundant, purple is second most abundant, and red is third most abundant.

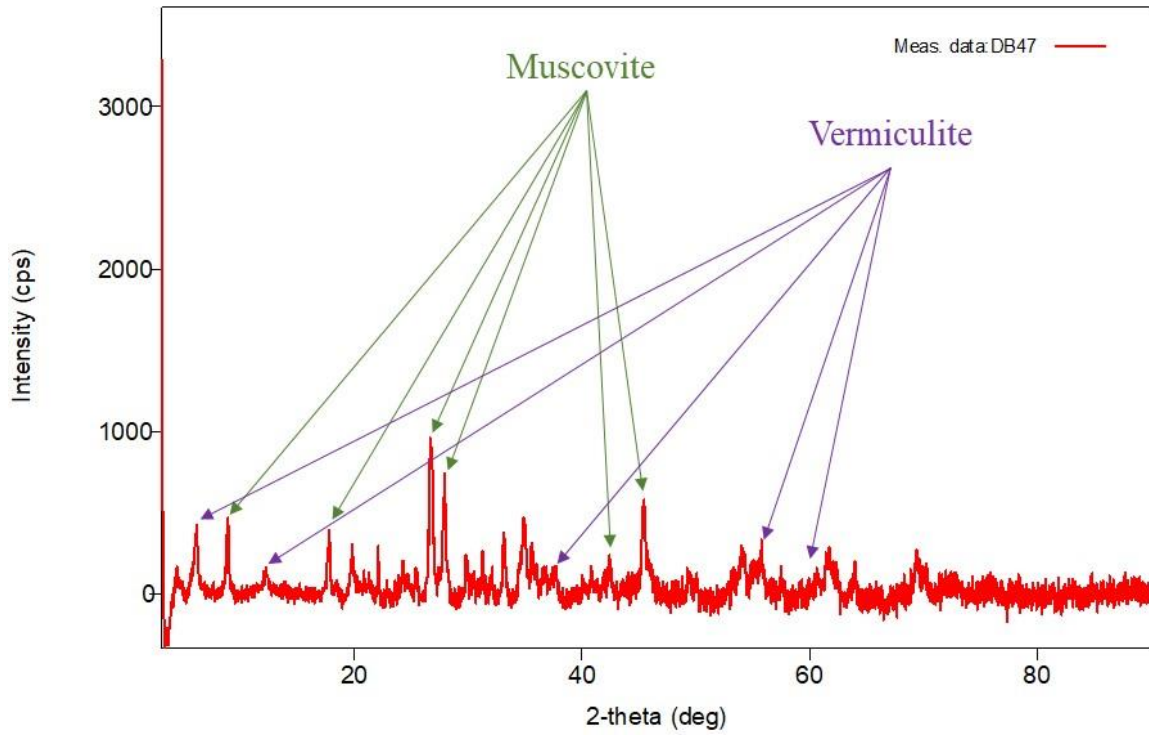


Figure 71: The x-ray diffractogram of sample DB-47 generated from the XRD analysis. The minerals identified in the sample and their relative abundance are labeled. Several important peaks used to identify each mineral have been noted. Additionally, the color scheme shows relative abundance. Green is most abundant, purple is second most abundant, and red is third most abundant.

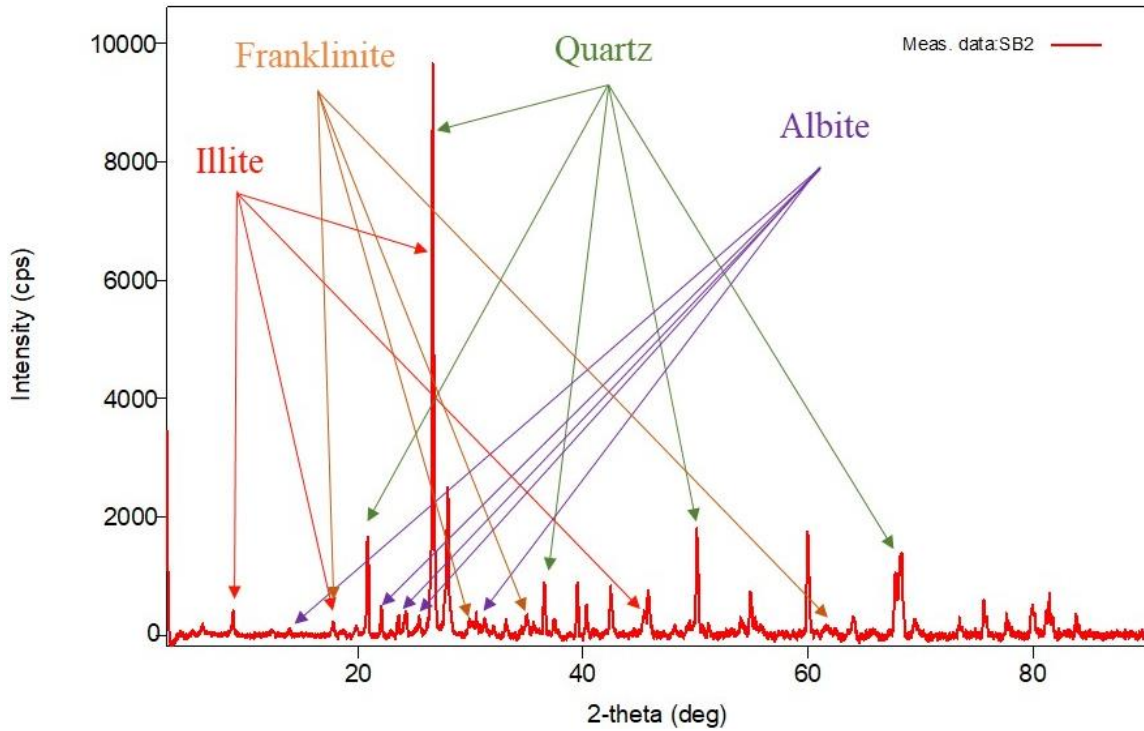


Figure 72: The x-ray diffractogram of sample SB-2 generated from the XRD analysis. The minerals identified in the sample and their relative abundance are labeled. Several important peaks used to identify each mineral have been noted. Additionally, the color scheme shows relative abundance. Green is most abundant, purple is second most abundant, and red is third most abundant. Where applicable, orange is the least abundant mineral.

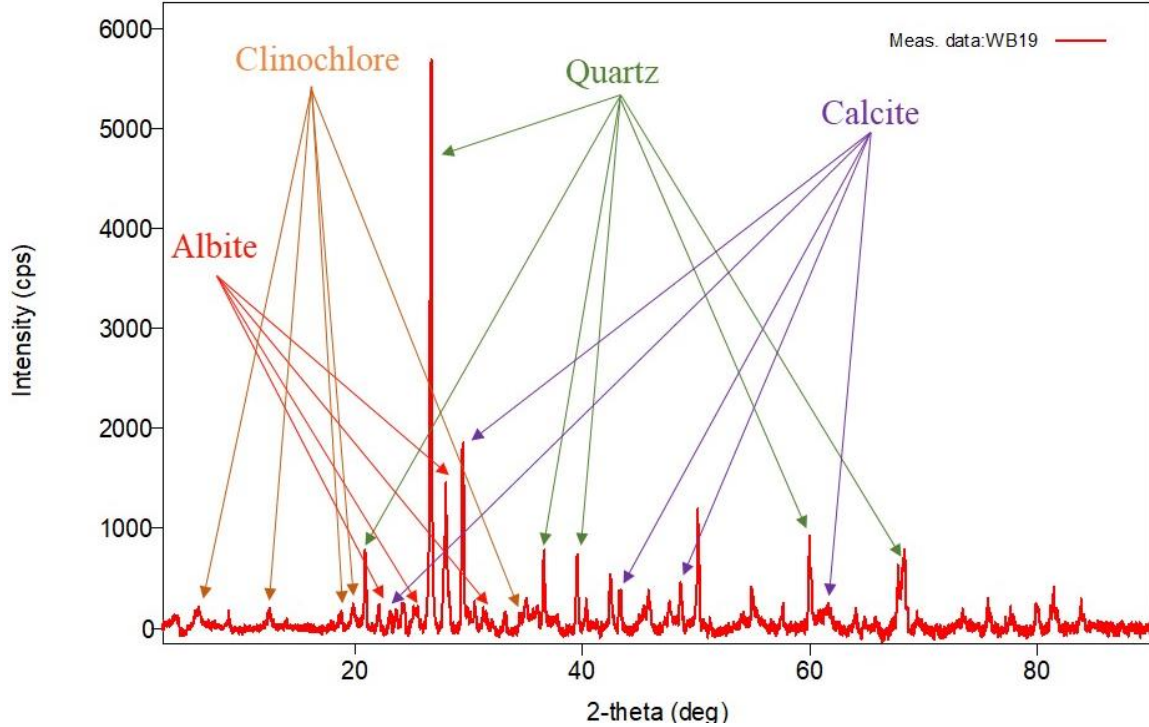


Figure 73: The x-ray diffractogram of sample WB-19 generated from the XRD analysis. The minerals identified in the sample and their relative abundance are labeled. Several important peaks used to identify each mineral have been noted. Additionally, the color scheme shows relative abundance. Green is most abundant, purple is second most abundant, and red is third most abundant. Where applicable, orange is the least abundant mineral.

Image 1 of 6

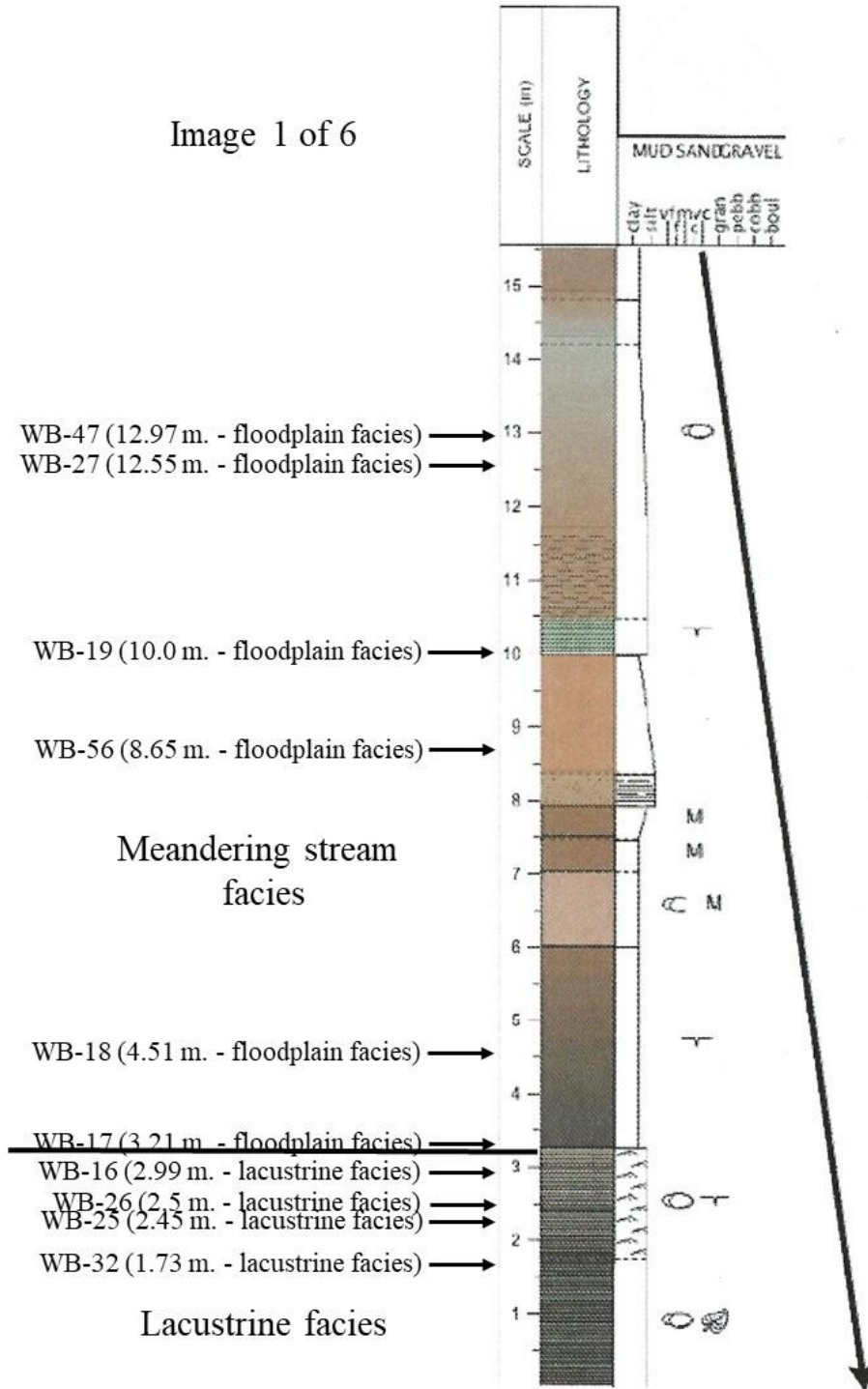


Figure 74: Stratigraphic column of a clay pit in the Wadesboro sub-basin showing the depth and depositional environment of the samples collected for this study. The depositional environments listed were, in general, based on observations by Brazell, 2013. The vertical profile is approximately 87.5 meters in length and is displayed in six consecutive images. (Modified from Brazell, 2013)

Image 2 of 6

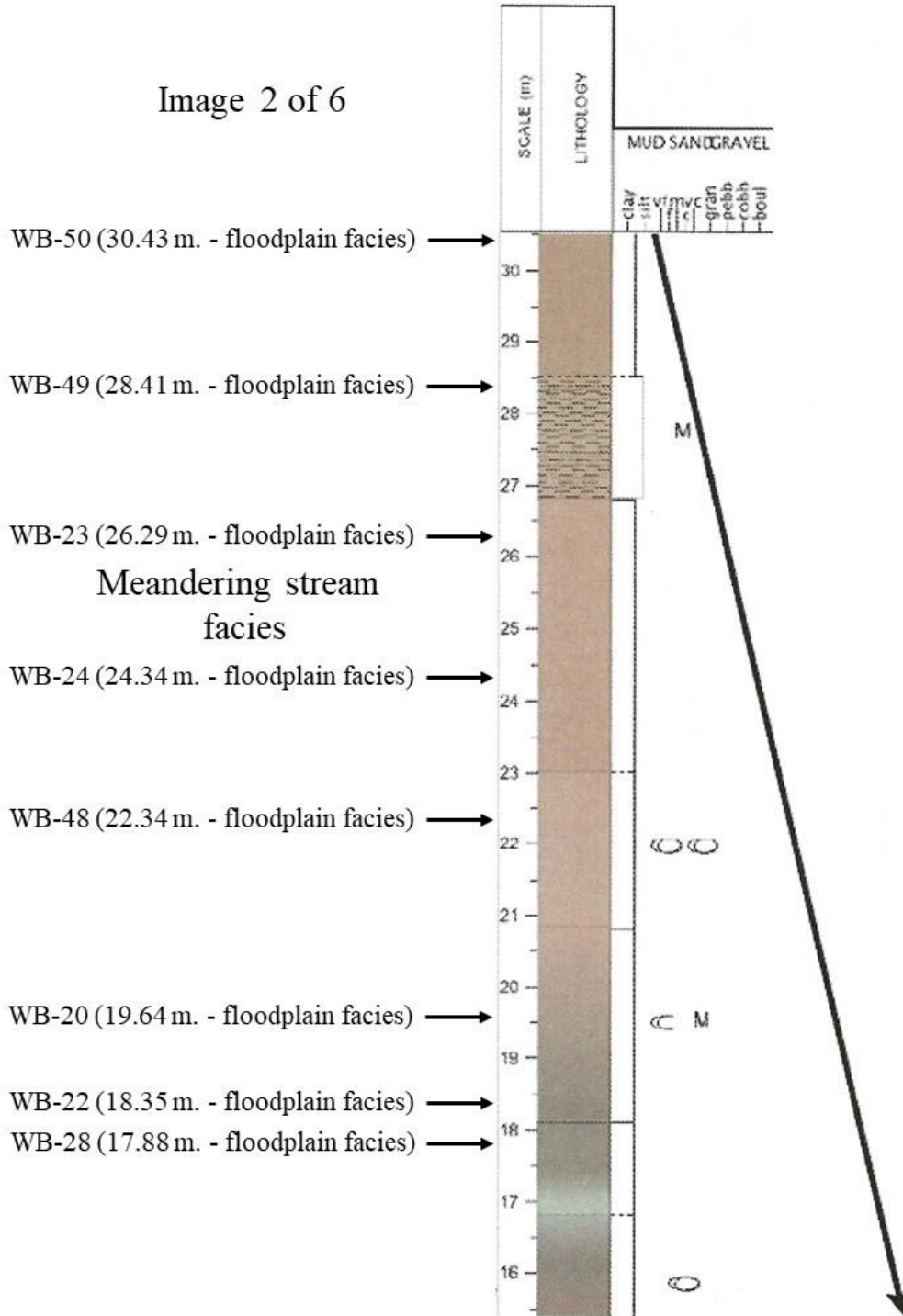


Figure 75: Stratigraphic column of a clay pit in the Wadesboro sub-basin showing the depth and depositional environment of the samples collected for this study. The depositional environments listed were, in general, based on observations by Brazell, 2013. The vertical profile is approximately 87.5 meters in length and is displayed in six consecutive images. (Modified from Brazell, 2013)

Image 3 of 6

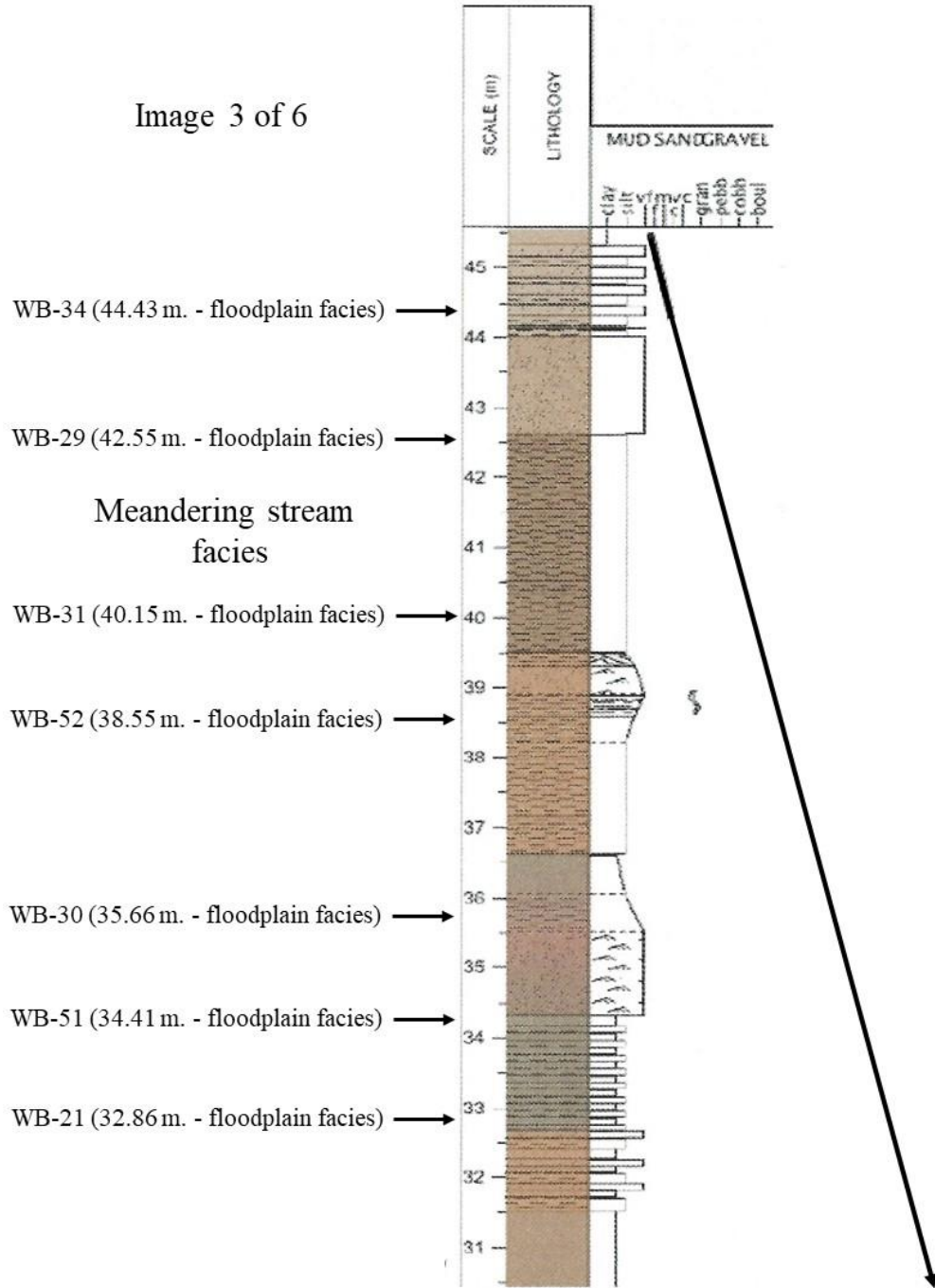


Figure 76: Stratigraphic column of a clay pit in the Wadesboro sub-basin showing the depth and depositional environment of the samples collected for this study. The depositional environments listed were, in general, based on observations by Brazell, 2013. The vertical profile is approximately 87.5 meters in length and is displayed in six consecutive images. (Modified from Brazell, 2013)

Image 4 of 6

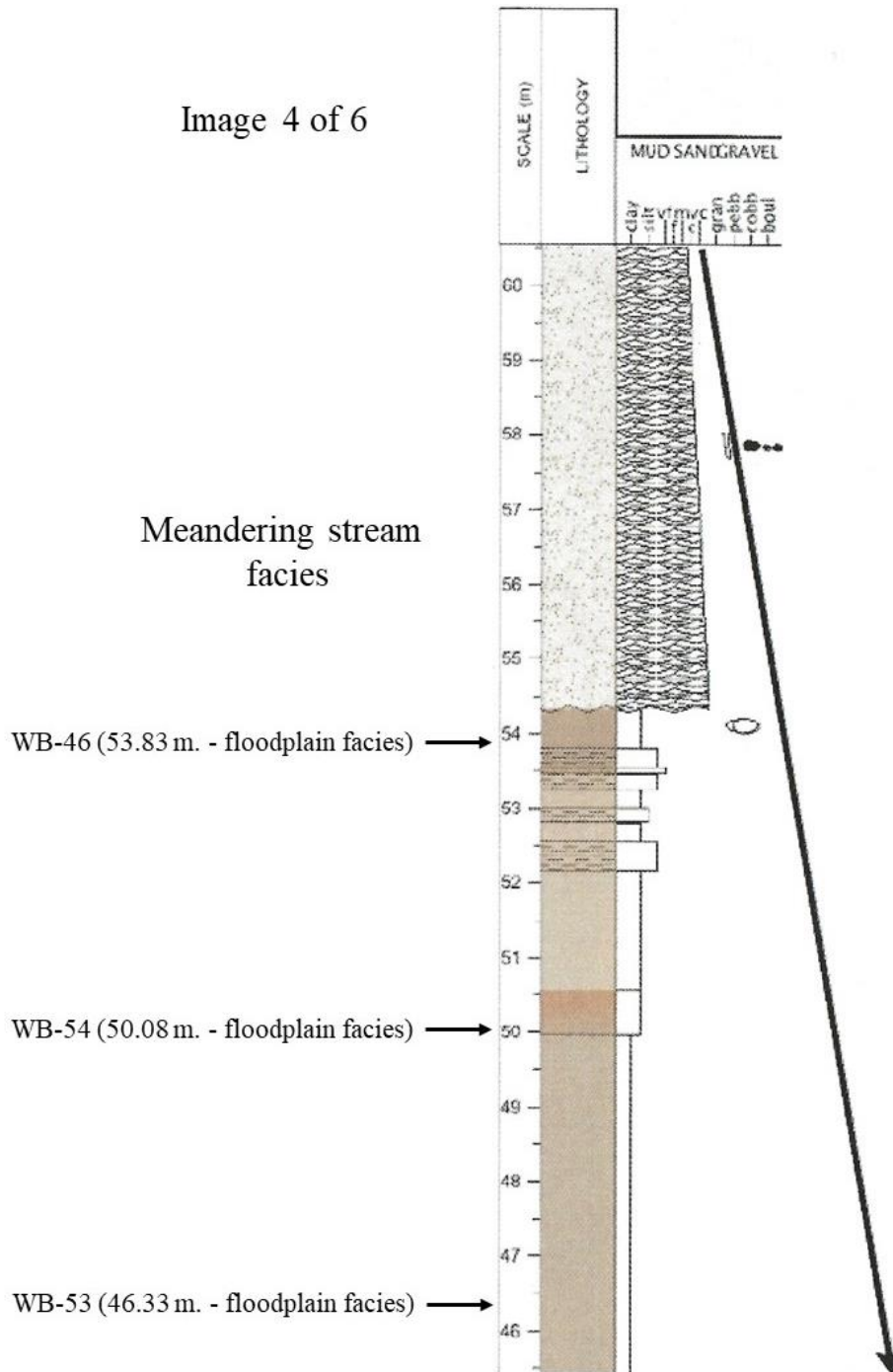


Figure 77: Stratigraphic column of a clay pit in the Wadesboro sub-basin showing the depth and depositional environment of the samples collected for this study. The depositional environments listed were, in general, based on observations by Brazell, 2013. The vertical profile is approximately 87.5 meters in length and is displayed in six consecutive images. (Modified from Brazell, 2013)

Image 5 of 6

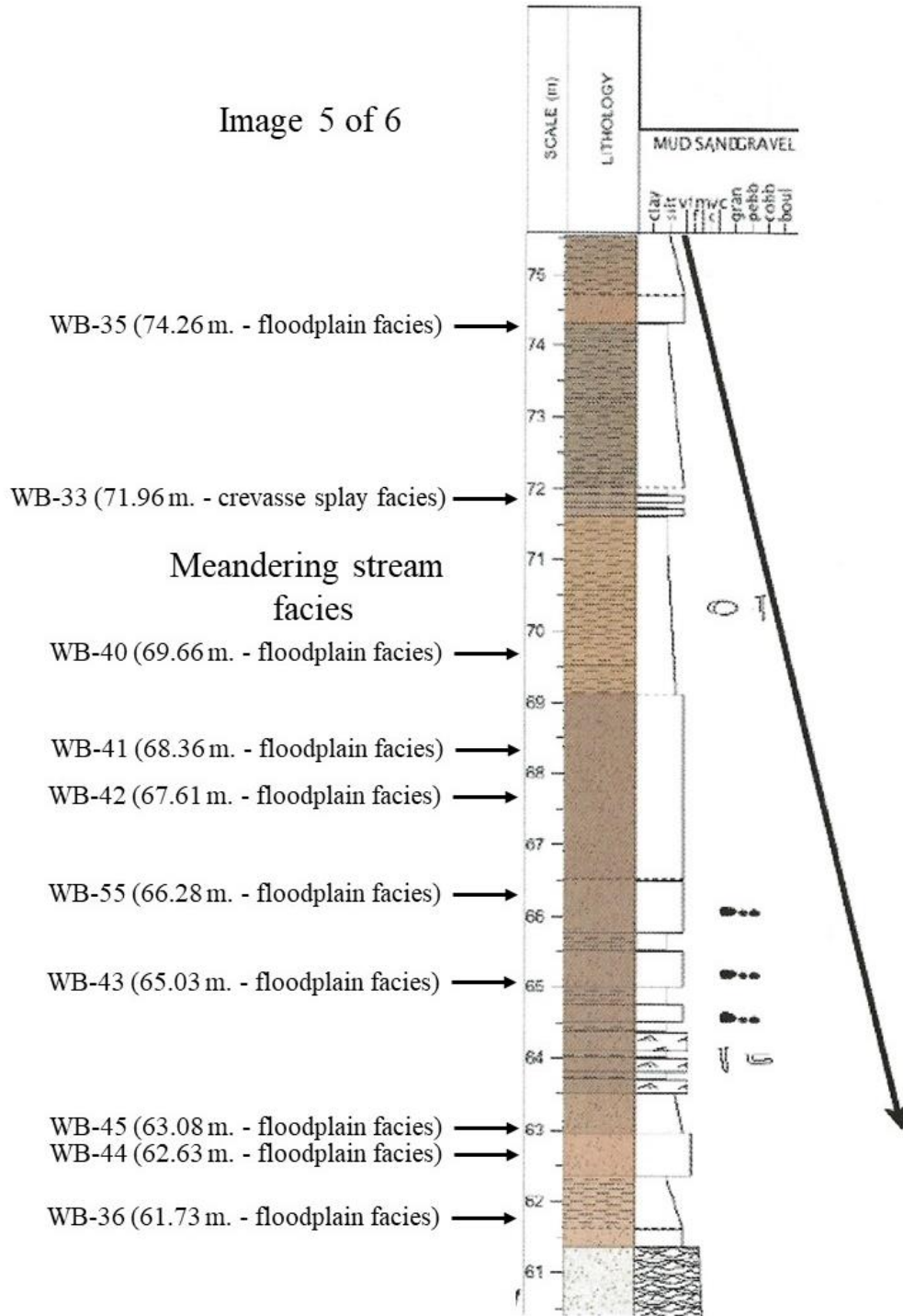


Figure 78: Stratigraphic column of a clay pit in the Wadesboro sub-basin showing the depth and depositional environment of the samples collected for this study. The depositional environments listed were, in general, based on observations by Brazell, 2013. The vertical profile is approximately 87.5 meters in length and is displayed in six consecutive images. (Modified from Brazell, 2013)

Image 6 of 6

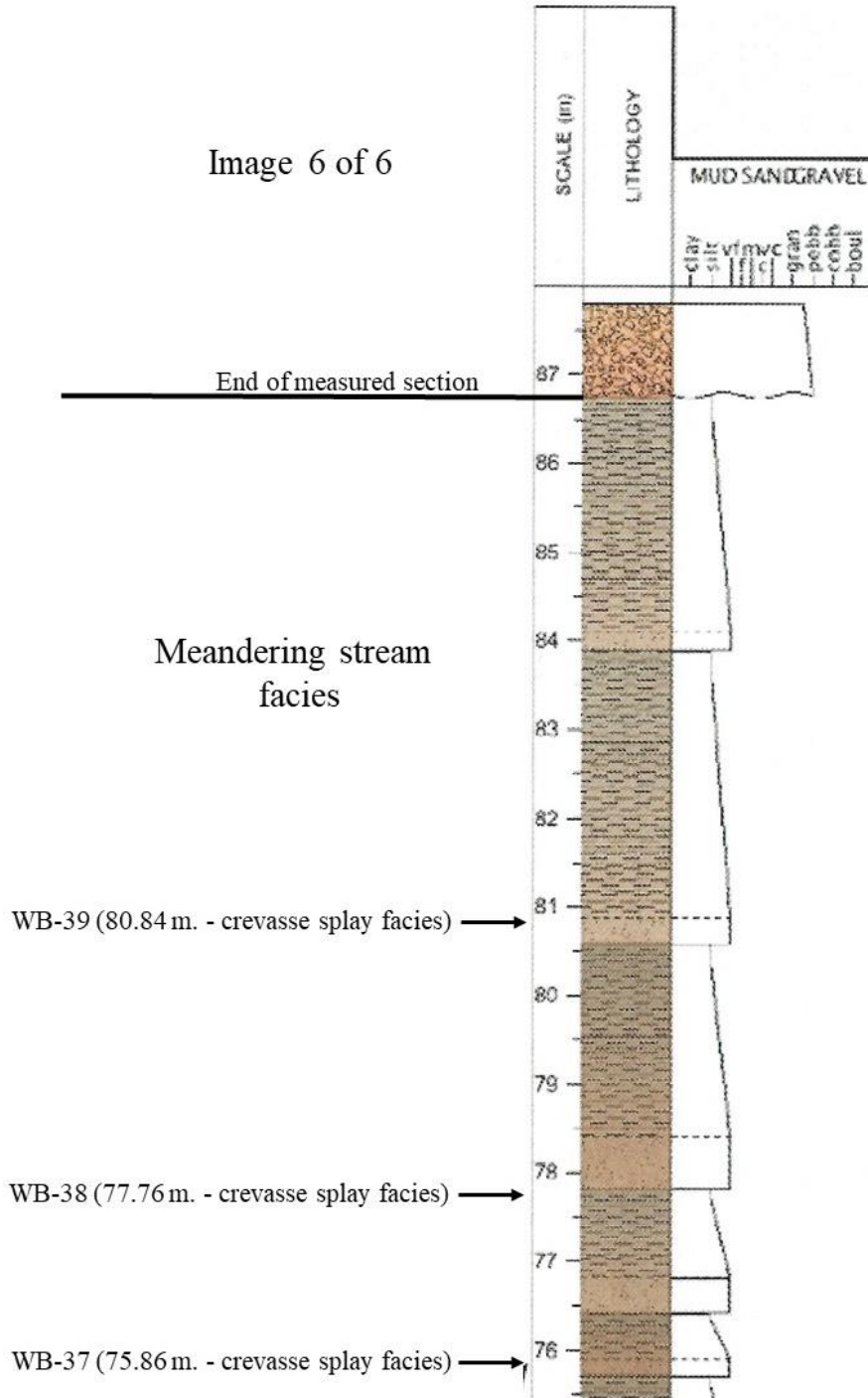


Figure 79: Stratigraphic column of a clay pit in the Wadesboro sub-basin showing the depth and depositional environment of the samples collected for this study. The depositional environments listed were, in general, based on observations by Brazell, 2013. The vertical profile is approximately 87.5 meters in length and is displayed in six consecutive images. (Modified from Brazell, 2013)

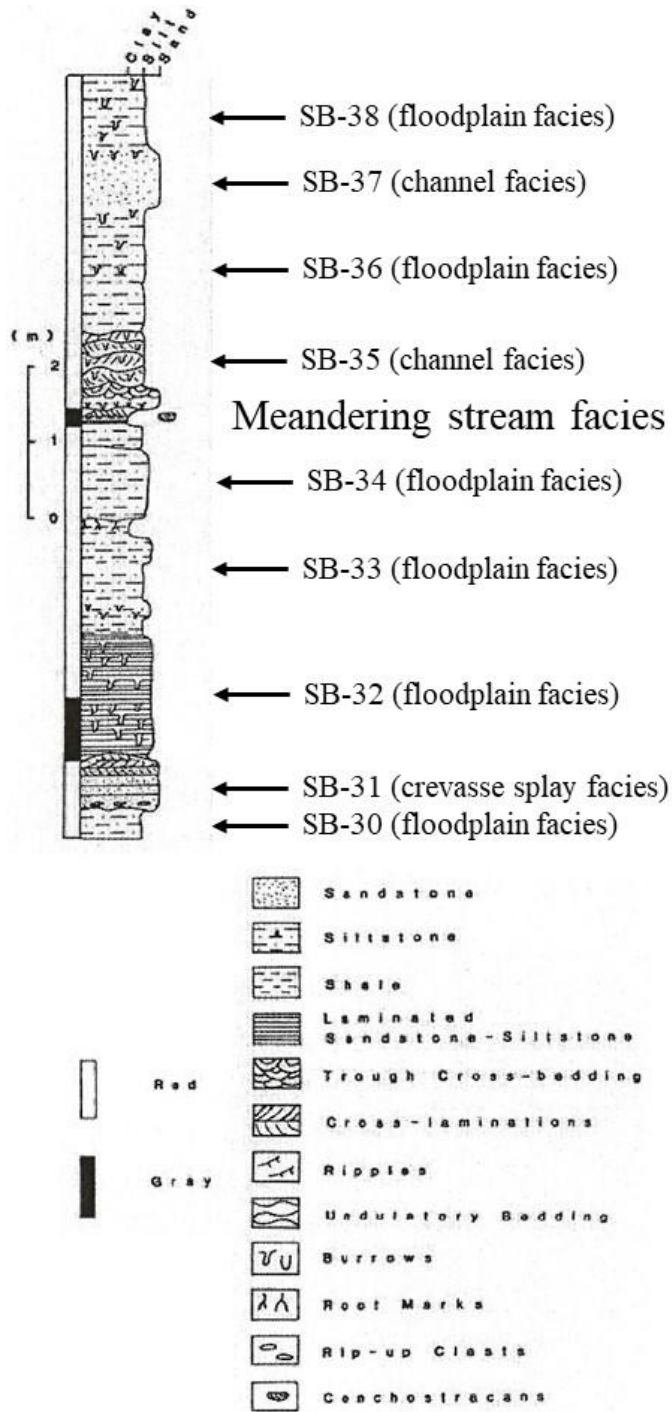


Figure 80: Vertical profile of a roadcut in the Sanford sub-basin showing the general location and depositional environment of the samples collected for this study. The depositional environments listed were, in general, based on observations by Reid et al., 2011. The vertical profile is approximately 9.5 meters in length. (Modified from Reid et al., 2011)

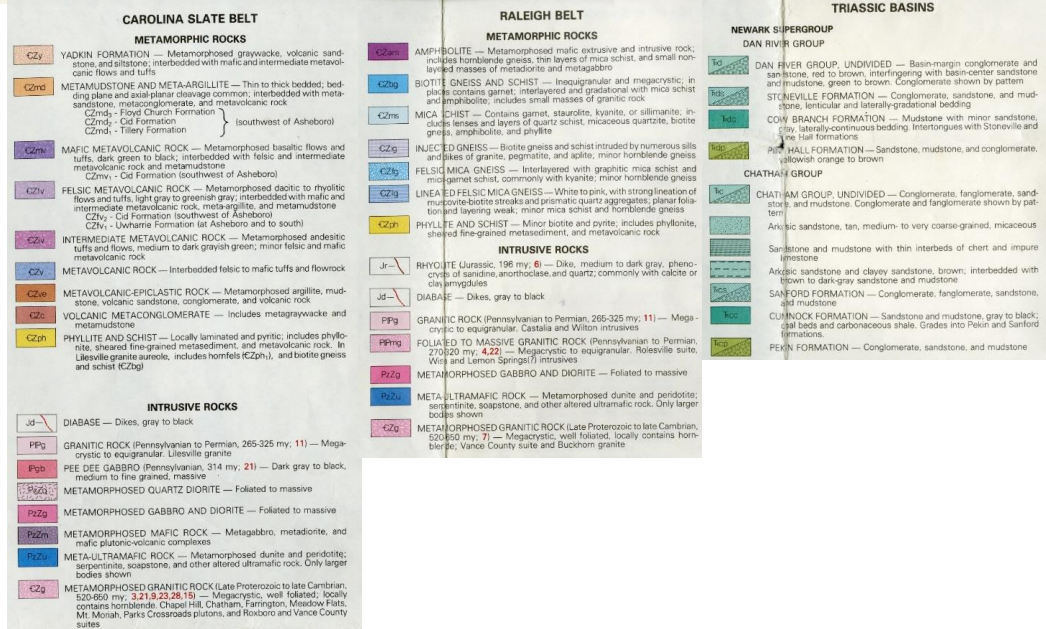
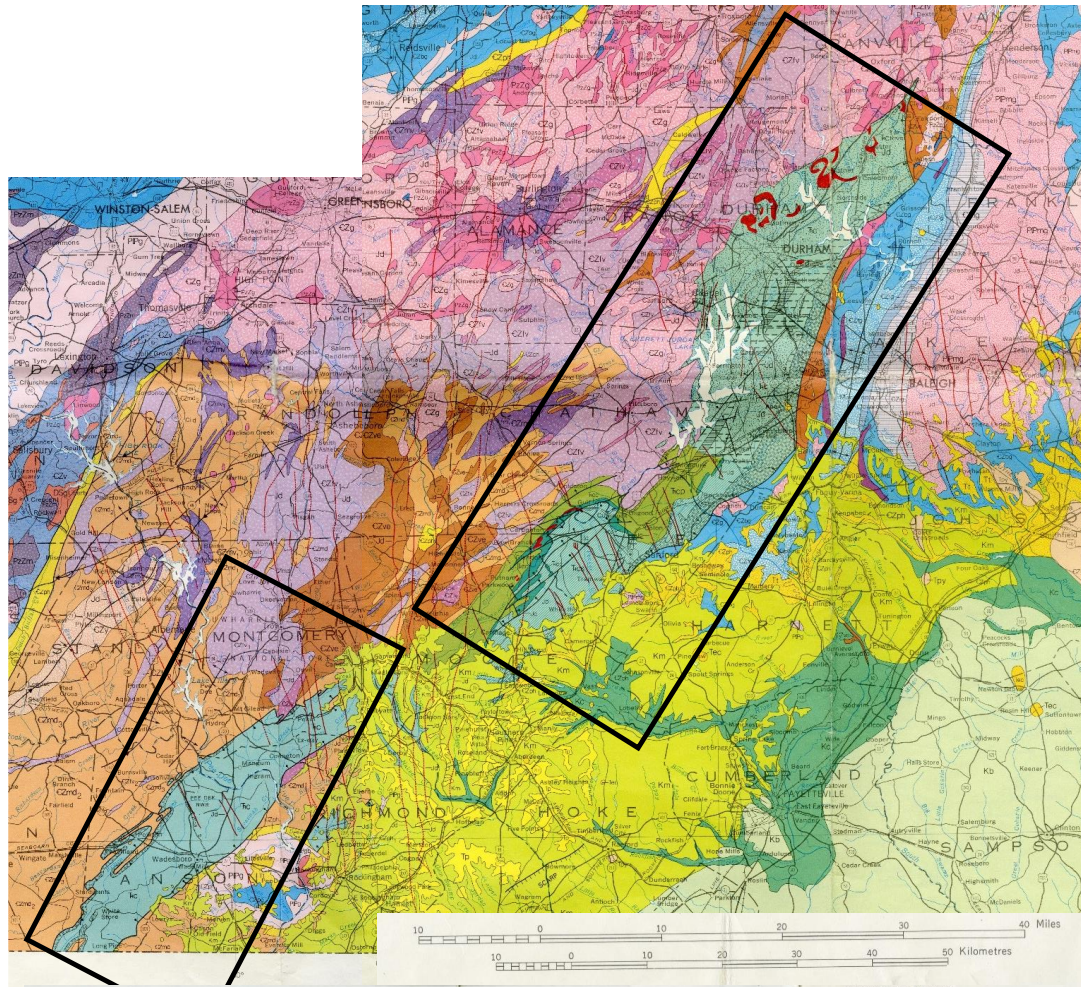


Figure 81: Geologic map of the Deep River basin, North Carolina (Modified from: NCGS, 1985). A link to the full geologic map of North Carolina is in the references.

Table 2: The results of the petrographic analysis. The mineralogy data were organized into nine mineral groups as discussed in the text.

Sample ID	Grain Size	Quartz (%)	Feldspar (%)	Mica (%)	Chlorite (%)	Carbonate (%)	Matrix (%)	Opaque (%)	Other (%)	Unknown (%)	Total (%)
WB-6	m-c-vc s.s	37.5	27.8	1.5	0.2	2.6	25.5	0.4	0.0	4.5	100.00
WB-7	m-c-vc s.s	14.1	13.1	0.0	0.2	0.0	68.9	1.7	0.2	1.8	100.00
WB-11	m-c-vc s.s	36.5	27.4	0.2	0.0	8.9	17.7	3.5	0.0	5.8	100.00
WB-13	vf-f s.s	17.3	37.3	4.3	0.0	0.0	27.2	7.9	0.0	6.0	100.00
SB-21	vf-f s.s	20.7	32.8	0.2	0.0	0.0	4.0	24.0	0.0	18.3	100.00
SB-39	gravel	31.3	30.3	0.0	0.0	0.0	23.4	6.2	0.0	8.8	100.00
SB-40	vf-f s.s	7.3	37.6	1.5	0.0	0.0	22.0	19.5	0.0	12.2	100.00
DB-3	vf-f s.s	9.4	16.4	1.0	0.0	0.0	38.0	25.5	5.7	3.9	100.00
DB-27	m-c-vc s.s	23.9	32.7	1.1	2.4	3.2	28.5	1.9	1.3	5.1	100.00
DB-34	vf-f s.s	9.1	17.3	2.7	6.7	0.0	5.1	50.9	1.3	6.9	100.00
DB-41	m-c-vc s.s	8.9	30.9	2.2	4.5	0.0	28.2	10.3	7.2	7.8	100.00
DB-45	vf-f s.s	9.1	27.9	2.3	4.4	0.0	35.4	11.5	4.2	5.2	100.00
DB-49	vf-f s.s	4.7	33.0	2.6	6.0	0.0	33.8	6.0	5.2	8.6	99.95
DB-51	vf-f s.s	8.7	24.2	2.3	6.4	0.8	40.7	8.1	2.6	6.4	100.05
DB-57	m-c-vc s.s	21.0	28.7	1.3	4.1	0.0	17.7	13.9	10.5	2.8	99.96
DB-64	vf-f s.s	8.2	11.2	2.0	3.7	0.0	63.4	9.7	1.2	0.5	100.00
DB-66	m-c-vc s.s	17.1	33.2	5.1	1.3	0.0	10.2	25.8	3.8	3.5	100.00
DB-82	m-c-vc s.s	13.2	33.9	3.2	1.9	15.7	6.1	17.0	7.7	1.3	99.96
DB-88	vf-f s.s	14.8	39.6	2.3	0.3	0.0	2.9	28.0	3.5	8.6	99.95
	<b>Average</b>	16.5	28.2	1.9	2.2	1.6	26.3	14.3	2.9	6.2	99.99

Table 3: The average percentage of plagioclase, predominantly albite, compared to the average percentage of orthoclase for all samples examined using petrographic analysis. (n=19)

<b>Average Plagioclase (%)</b>	<b>Average Orthoclase (%)</b>
6.8	21.3

Table 4: The modified categories used by this study for sandstone classification.

Quartz grains ( $Q = Q_m + Q_p$ )
Q = total quartz grains
$Q_m$ = monocrystalline quartz
$Q_p$ = polycrystalline quartz (including chert)
Feldspar grains ( $F = P + K$ )
F = total feldspar grains
P = plagioclase grains
K = potassium feldspar grains
Rock Fragments ( $RF = Mic + Chl + Ep + Zr + L + Unk$ )
RF = total rock fragments
Mic = mica grains
Chl = chlorite grains
Ep = epidote grains
Zr = zircon grains
L = lithic grains
Unk = unknown grains
Matrix ( $Ma = Mtx + Cal + Op$ )
Ma = total matrix
Mtx = matrix mineral group
Cal = carbonate mineral group
Op = opaque minerals

Table 5: The petrographic data organized in the four categories used for sandstone classification.

<b>Sample ID</b>	<b>Grain Size</b>	<b>Quartz (%)</b>	<b>Feldspar (%)</b>	<b>Rock Fragments (%)</b>	<b>Matrix (%)</b>	<b>Total (%)</b>
WB-6	m-c-vc s.s	37.5	27.8	6.2	28.5	100.00
WB-7	m-c-vc s.s	14.1	13.1	2.2	70.6	100.00
WB-11	m-c-vc s.s	36.5	27.4	6.0	30.2	100.00
WB-13	vf-f s.s	17.3	37.3	10.3	35.1	100.00
SB-21	vf-f s.s	20.7	32.8	18.5	28.0	100.00
SB-39	gravel	31.3	30.3	8.8	29.6	100.00
SB-40	vf-f s.s	7.3	37.6	13.7	41.5	100.00
DB-3	vf-f s.s	9.4	16.4	10.7	63.5	100.00
DB-27	m-c-vc s.s	23.9	32.7	9.9	33.6	100.00
DB-34	vf-f s.s	9.1	17.3	17.6	56.0	100.00
DB-41	m-c-vc s.s	8.9	30.9	21.7	38.5	100.00
DB-45	vf-f s.s	9.1	27.9	16.1	46.9	100.00
DB-49	vf-f s.s	4.7	33.0	22.5	39.8	100.00
DB-51	vf-f s.s	8.7	24.2	17.6	49.6	100.00
DB-57	m-c-vc s.s	21.0	28.7	18.7	31.6	100.00
DB-64	vf-f s.s	8.2	11.2	7.5	73.1	100.00
DB-66	m-c-vc s.s	17.1	33.2	13.7	36.0	100.00
DB-82	m-c-vc s.s	13.2	33.9	14.1	38.8	100.00
DB-88	vf-f s.s	14.8	39.6	14.7	30.8	100.00

Table 6: The essential constituents including quartz, feldspar, and rock fragments, recalculated to 100%. the percentage of matrix and chemically-precipitated cements was ignored. Equations used are located in the text. Data obtained from petrographic analyses.

<b>Sample ID</b>	<b>Grain Size</b>	<b>Quartz (%)</b>	<b>Feldspar (%)</b>	<b>Rock Fragments (%)</b>	<b>Total (%)</b>
WB-6	m-c-vc s.s	52.5	38.8	8.7	100.0
WB-7	m-c-vc s.s	48.0	44.6	7.4	100.0
WB-11	m-c-vc s.s	52.2	39.3	8.5	100.0
WB-13	vf-f s.s	26.7	57.4	15.9	100.0
SB-21	vf-f s.s	28.7	45.5	25.7	100.0
SB-39	gravel	44.5	43.0	12.5	100.0
SB-40	vf-f s.s	12.5	64.2	23.3	100.0
DB-3	vf-f s.s	25.7	45.0	29.3	100.0
DB-27	m-c-vc s.s	35.9	49.2	14.9	100.0
DB-34	vf-f s.s	20.6	39.4	40.0	100.0
DB-41	m-c-vc s.s	14.5	50.2	35.3	100.0
DB-45	vf-f s.s	17.2	52.5	30.4	100.0
DB-49	vf-f s.s	7.8	54.8	37.3	99.9
DB-51	vf-f s.s	17.2	48.0	34.9	100.1
DB-57	m-c-vc s.s	30.6	41.9	27.4	99.9
DB-64	vf-f s.s	30.6	41.7	27.8	100.0
DB-66	m-c-vc s.s	26.7	51.9	21.4	100.0
DB-82	m-c-vc s.s	21.5	55.4	23.0	99.9
DB-88	vf-f s.s	21.5	57.3	21.2	99.9

Table 7: Mineral groups applicable for the leaching analyses. Mineralogical patterns and trends with grain size and across the sub-basins of the DRB will be discussed in terms of these groups. This is relevant in order to more thoroughly understand the results of the leaching analyses.

Quartz minerals ( $Q = Q_m + Q_p$ )
Q = total quartz minerals
$Q_m$ = monocrystalline quartz
$Q_p$ = polycrystalline quartz (including chert)
Feldspar minerals ( $F = P + K$ )
F = total feldspar minerals
P = plagioclase grains
K = potassium feldspar grains
Clay minerals (Clays = $Mtx + Mic + Chl$ )
Mtx = matrix
Mic = mica grains
Chl = chlorite grains
Carbonate minerals (Cal)
Cal = carbonate minerals
Oxide minerals (Oxides = $Op$ )
$Op$ = opaque minerals
Other (Other = $Ep + Zr + L + Unk$ )
Ep = epidote grains
Zr = zircon grains
L = lithic grains
Unk = unknown grains

Table 8: Petrographic data organized in the mineral groups applicable for the sequential extraction analyses.

Sample ID	Grain Size	Quartz (%)	Feldspar (%)	Clay Minerals (%)	Carbonates (%)	Oxides (%)	Other (%)	Total (%)
WB-6	m-c-vc s.s	37.5	27.8	27.2	2.6	0.4	4.5	100.00
WB-7	m-c-vc s.s	14.1	13.1	69.1	0.0	1.7	2.0	100.00
WB-11	m-c-vc s.s	36.5	27.4	17.9	8.9	3.5	5.8	100.00
WB-13	vf-f s.s	17.3	37.3	31.5	0.0	7.9	6.0	100.00
SB-21	vf-f s.s	20.7	32.8	4.3	0.0	24.0	18.3	100.00
SB-39	gravel	31.3	30.3	23.4	0.0	6.2	8.8	100.00
SB-40	vf-f s.s	7.3	37.6	23.4	0.0	19.5	12.2	100.00
DB-3	vf-f s.s	9.4	16.4	39.1	0.0	25.5	9.6	100.00
DB-27	m-c-vc s.s	23.9	32.7	32.0	3.2	1.9	6.4	100.00
DB-34	vf-f s.s	9.1	17.3	14.4	0.0	50.9	8.3	100.00
DB-41	m-c-vc s.s	8.9	30.9	34.9	0.0	10.3	15.0	100.00
DB-45	vf-f s.s	9.1	27.9	42.2	0.0	11.5	9.4	100.00
DB-49	vf-f s.s	4.7	33.0	42.4	0.0	6.0	13.8	99.95
DB-51	vf-f s.s	8.7	24.2	49.4	0.8	8.1	9.0	100.05
DB-57	m-c-vc s.s	21.0	28.7	23.1	0.0	13.9	13.3	99.96
DB-64	vf-f s.s	8.2	11.2	69.2	0.0	9.7	1.7	100.00
DB-66	m-c-vc s.s	17.1	33.2	16.7	0.0	25.8	7.3	100.00
DB-82	m-c-vc s.s	13.2	33.9	11.2	15.7	17.0	9.0	99.96
DB-88	vf-f s.s	14.8	39.6	5.5	0.0	28.0	12.1	99.95
	<b>Average</b>	16.5	28.2	30.4	1.6	14.3	9.1	99.99

Table 9: Petrographic data of the samples from the Wadesboro sub-basin.

<b>Sample ID</b>	<b>Grain Size</b>	<b>Quartz (%)</b>	<b>Feldspar (%)</b>	<b>Clay Minerals (%)</b>	<b>Carbonates (%)</b>	<b>Oxides (%)</b>	<b>Other (%)</b>	<b>Total (%)</b>
WB-6	m-c-vc s.s	37.5	27.8	27.2	2.6	0.4	4.5	100.00
WB-7	m-c-vc s.s	14.1	13.1	69.1	0.0	1.7	2.0	100.00
WB-11	m-c-vc s.s	36.5	27.4	17.9	8.9	3.5	5.8	100.00
WB-13	vf-f s.s	17.3	37.3	31.5	0.0	7.9	6.0	100.00
	<b>Average</b>	26.4	26.4	36.4	2.9	3.4	4.6	100.00

Table 10: Petrographic data of the samples from the Sanford sub-basin.

<b>Sample ID</b>	<b>Grain Size</b>	<b>Quartz (%)</b>	<b>Feldspar (%)</b>	<b>Clay Minerals (%)</b>	<b>Carbonates (%)</b>	<b>Oxides (%)</b>	<b>Other (%)</b>	<b>Total (%)</b>
SB-21	vf-f s.s	20.7	32.8	4.3	0.0	24.0	18.3	100.00
SB-39	gravel	31.3	30.3	23.4	0.0	6.2	8.8	100.00
SB-40	vf-f s.s	7.3	37.6	23.4	0.0	19.5	12.2	100.00
	<b>Average</b>	19.8	33.5	17.0	0.0	16.6	13.1	100.00

Table 11: Petrographic data of the samples from the Durham sub-basin.

Sample ID	Grain Size	Quartz (%)	Feldspar (%)	Clay Minerals (%)	Carbonates (%)	Oxides (%)	Other (%)	Total (%)
DB-3	vf-f s.s	9.4	16.4	39.1	0.0	25.5	9.6	100.00
DB-27	m-c-vc s.s	23.9	32.7	32.0	3.2	1.9	6.4	100.00
DB-34	vf-f s.s	9.1	17.3	14.4	0.0	50.9	8.3	100.00
DB-41	m-c-vc s.s	8.9	30.9	34.9	0.0	10.3	15.0	100.00
DB-45	vf-f s.s	9.1	27.9	42.2	0.0	11.5	9.4	100.00
DB-49	vf-f s.s	4.7	33.0	42.4	0.0	6.0	13.8	99.95
DB-51	vf-f s.s	8.7	24.2	49.4	0.8	8.1	9.0	100.05
DB-57	m-c-vc s.s	21.0	28.7	23.1	0.0	13.9	13.3	99.96
DB-64	vf-f s.s	8.2	11.2	69.2	0.0	9.7	1.7	100.00
DB-66	m-c-vc s.s	17.1	33.2	16.7	0.0	25.8	7.3	100.00
DB-82	m-c-vc s.s	13.2	33.9	11.2	15.7	17.0	9.0	99.96
DB-88	vf-f s.s	14.8	39.6	5.5	0.0	28.0	12.1	99.95
	<b>Average</b>	12.3	27.4	31.7	1.6	17.4	9.6	99.99

Table 12: The average percent of identified minerals in each of the three sub-basins. These averages were calculated using the raw petrographic data from 11, 12, and 13.

<b>Sub-Basin/basin</b>	<b>Quartz (%)</b>	<b>Feldspar (%)</b>	<b>Clay Minerals (%)</b>	<b>Carbonates (%)</b>	<b>Oxides (%)</b>	<b>Other (%)</b>
Wadesboro	26.4	26.4	36.4	2.9	3.4	4.6
Sanford	19.8	33.5	17.0	0.0	16.6	13.1
Durham	12.3	27.4	31.7	1.6	17.4	9.6
Deep River Basin	16.5	28.2	30.4	1.6	14.3	9.1

Table 13: The average percent of identified minerals organized by grain size.

<b>Grain Size</b>	<b>Quartz (%)</b>	<b>Feldspar (%)</b>	<b>Clay Minerals (%)</b>	<b>Carbonates (%)</b>	<b>Oxides (%)</b>	<b>Other (%)</b>
vf-f s.s	10.9	27.7	32.1	0.1	19.1	10.0
m-c-vc s.s	21.5	28.5	29.0	3.8	9.3	7.9
gravel	31.3	30.3	23.4	0.0	6.2	8.8

Table 14: Petrographic data of samples from an alluvial fan environment.

<b>Sample ID</b>	<b>Depositional Environment</b>	<b>Grain Size</b>	<b>Quartz (%)</b>	<b>Feldspar (%)</b>	<b>Clay Minerals (%)</b>	<b>Carbonates (%)</b>	<b>Oxides (%)</b>	<b>Other (%)</b>	<b>Total (%)</b>
DB-3	Fan Fringe	vf-f s.s	9.4	16.4	39.1	0.0	25.5	9.6	100.00
DB-88	Fan Fringe	vf-f s.s	14.8	39.6	5.5	0.0	28.0	12.1	99.95
DB-57	Fan Fringe	m-c-vc s.s	21.0	28.7	23.1	0.0	13.9	13.3	99.96
SB-39	Fan Fringe	gravel	31.3	30.3	23.4	0.0	6.2	8.8	100.00
		<b>Average</b>	19.1	28.7	22.8	0.0	18.4	11.0	99.98

Table 15: Petrographic data of samples from a meandering stream environment.

Sample ID	Depositional Environment	Grain Size	Quartz (%)	Feldspar (%)	Clay Minerals (%)	Carbonates (%)	Oxides (%)	Other (%)	Total (%)
DB-27	Channel Facies	m-c-vc s.s	23.9	32.7	32.0	3.2	1.9	6.4	100.00
DB-45	Channel Facies	vf-f s.s	9.1	27.9	42.2	0.0	11.5	9.4	100.00
DB-64	Channel Facies	vf-f s.s	8.2	11.2	69.2	0.0	9.7	1.7	100.00
SB-40	Channel Facies	vf-f s.s	7.3	37.6	23.4	0.0	19.5	12.2	100.00
WB-11	Channel Facies	m-c-vc s.s	36.5	27.4	17.9	8.9	3.5	5.8	100.00
WB-13	Channel Facies	vf-f s.s	17.3	37.3	31.5	0.0	7.9	6.0	100.00
WB-6	Channel Facies	m-c-vc s.s	37.5	27.8	27.2	2.6	0.4	4.5	100.00
DB-49	Crevasse Splay Facies	vf-f s.s	4.7	33.0	42.4	0.0	6.0	13.8	99.95
DB-51	Crevasse Splay Facies	vf-f s.s	8.7	24.2	49.4	0.8	8.1	9.0	100.05
DB-66	Crevasse Splay Facies	m-c-vc s.s	17.1	33.2	16.7	0.0	25.8	7.3	100.00
DB-82	Crevasse Splay Facies	m-c-vc s.s	13.2	33.9	11.2	15.7	17.0	9.0	99.96
DB-34	Floodplain Facies	vf-f s.s	9.1	17.3	14.4	0.0	50.9	8.3	100.00
SB-21	Floodplain Facies	vf-f s.s	20.7	32.8	4.3	0.0	24.0	18.3	100.00
WB-7	Floodplain Facies	m-c-vc s.s	14.1	13.1	69.1	0.0	1.7	2.0	100.00
		<b>Average</b>	16.2	27.8	32.2	2.2	13.4	8.1	100.00

Table 16: Average composition of sub-environments in a meandering stream environment.

<b>Depositional Environment</b>	<b>Quartz (%)</b>	<b>Feldspar (%)</b>	<b>Clay Minerals (%)</b>	<b>Carbonates (%)</b>	<b>Oxides (%)</b>	<b>Other (%)</b>
Channel Facies	20.0	28.8	34.8	2.1	7.8	6.6
Crevasse Splay Facies	10.9	31.1	29.9	4.1	14.2	9.8
Floodplain Facies	14.6	21.1	29.3	0.0	25.5	9.5

Table 17: Petrographic data of samples from a lacustrine environment.

<b>Sample ID</b>	<b>Depositional Environment</b>	<b>Grain Size</b>	<b>Quartz (%)</b>	<b>Feldspar (%)</b>	<b>Clay Minerals (%)</b>	<b>Carbonates (%)</b>	<b>Oxides (%)</b>	<b>Other (%)</b>	<b>Total (%)</b>
DB-41	Lacustrine Facies	m-c-vc s.s	8.9	30.9	34.9	0.0	10.3	15.0	100.00

Table 18: Average composition of samples from alluvial fan, meandering stream, and lacustrine environments.

<b>Depositional Environment</b>	<b>Quartz (%)</b>	<b>Feldspar (%)</b>	<b>Clay Minerals (%)</b>	<b>Carbonates (%)</b>	<b>Oxides (%)</b>	<b>Other (%)</b>
Alluvial Fan	19.1	28.7	22.8	0.0	18.4	11.0
Meandering Stream	16.2	27.8	32.2	2.2	13.4	8.1
Lacustrine	8.9	30.9	34.9	0.0	10.3	15.0

Table 19: Percentage of total organic carbon (TOC) for tested samples using the Thermo Scientific Flash 2000 Organic Elemental Analyzer.

<b>Sample ID</b>	<b>TOC (%)</b>
WB-5	ND
SB-4	ND
SB-5	ND
SB-13	6.00
SB-15	0.04
SB-22	1.42
SB-24	7.85
SB-26	0.40
SB-27	29.35
SB-28	0.95

Table 20: Mineral groups identified by XRD analyses and applicable for the leaching analyses. Mineralogical trends across the sub-basins of the DRB and with grain size will be discussed in terms of these groups. This is relevant in order to more thoroughly understand the results of the leaching analyses.

Quartz minerals (Q)
Q = total quartz minerals
Feldspar minerals (F = P + K)
F = total feldspar minerals
P = plagioclase minerals
K = potassium feldspar minerals
Clay minerals (Clays = Kao + Smc + Vrm + Mic + Chl)
Kao = kaolinite minerals
Smc = smectite minerals
Vrm = vermiculite minerals
Mic = mica minerals
Chl = chlorite minerals
Carbonate minerals (Carb = Cal + Dol)
Cal = carbonate minerals
Dol = dolomite minerals
Other (Other = Hm + Cp + Px + Cpx + Spi)
Hm = Hematite minerals
Cp = chalcopyrite minerals
Px = pyroxene minerals
Cpx = clinopyroxene minerals
Spi = spinel minerals

Table 21: Relative abundance of mineral groups identified by XRD in the Deep River Basin and its sub-basins. The values in this table were obtained by converting the abbreviations such as XX in Appendix D to a numerical value as discussed in the text. These numerical values were averaged to determine the relative abundance of the mineral groups in the Deep River Basin and the individual sub-basins. Relative abundance is on a scale from 0 to 4. See text and Appendix D for details.

<b>Sub-basin/basin</b>	<b>Quartz (Rel. Abun.)</b>	<b>Feldspar (Rel. Abun.)</b>	<b>Clay Minerals (Rel. Abun.)</b>	<b>Carbonates (Rel. Abun.)</b>	<b>Other (Rel. Abun.)</b>
Wadesboro	3.8	1.9	1.6	1.5	0.2
Sanford	3.5	2.0	2.4	0.1	0.3
Durham	3.9	2.3	2.0	0.2	0.0
Deep River Basin	3.8	2.1	2.0	0.5	0.1

Table 22: Relative abundance of mineral groups identified by XRD and organized by grain size. Relative abundance is on a scale from 0 to 4. See text and Appendix D for details.

<b>Grain Size</b>	<b>Quartz (Rel. Abun.)</b>	<b>Feldspar (Rel. Abun.)</b>	<b>Clay Minerals (Rel. Abun.)</b>	<b>Carbonates (Rel. Abun.)</b>	<b>Other (Rel. Abun.)</b>
mudstone-shale	3.4	1.3	2.5	1.2	0.1
siltstone	3.9	2.2	1.9	0.6	0.1
vf-f s.s	4.0	2.0	2.2	0.5	0.2
m-c-vc s.s	3.9	2.7	1.6	0.2	0.1
gravel	4.0	1.5	1.5	0.0	0.0

Table 23: Relative abundance of mineral groups identified by XRD in samples from alluvial fan environments. The XRD data for the two lithofacies associations identified in alluvial fan deposits in the DRB are also displayed. Relative abundance is on a scale from 0 to 4. See text and Appendix D for details. The data displayed in Appendix D were used to calculate these values. The numerical values used to represent the relative abundance were averaged to obtain the overall relative abundance for the depositional environments as well as the individual lithofacies associations.

<b>Depositional Environment</b>	<b>Quartz (Rel. Abun.)</b>	<b>Feldspar (Rel. Abun.)</b>	<b>Clay Minerals (Rel. Abun.)</b>	<b>Carbonates (Rel. Abun.)</b>	<b>Other (Rel. Abun.)</b>
Distal Fan	4.0	3.0	2.0	0.0	0.0
Fan Fringe	4.0	2.7	1.8	0.0	0.0
<i>Overall depositional environment:</i>					
Alluvial Fan	4.0	2.7	1.9	0.0	0.0

Table 24: Relative abundance of mineral groups identified by XRD in samples from meandering stream environments. The XRD data for the three lithofacies associations identified in meandering stream deposits in the DRB are also displayed. Relative abundance is on a scale from 0 to 4. See text and Appendix D for details. The data displayed in Appendix D were used to calculate these values. The numerical values used to represent the relative abundance were averaged to obtain the overall relative abundance for the depositional environments as well as the individual lithofacies associations.

<b>Depositional Environment</b>	<b>Quartz (Rel. Abun.)</b>	<b>Feldspar (Rel. Abun.)</b>	<b>Clay Minerals (Rel. Abun.)</b>	<b>Carbonates (Rel. Abun.)</b>	<b>Other (Rel. Abun.)</b>
Channel Facies	4.0	2.4	1.9	0.3	0.2
Crevasse Splay Facies	4.0	2.6	1.5	0.6	0.1
Floodplain Facies	3.8	1.8	2.1	0.8	0.2
<i>Overall depositional environment:</i>					
Meandering Stream	3.9	2.0	2.0	0.7	0.2

Table 25: Relative abundance of mineral groups identified by XRD in samples from lacustrine environments. Relative abundance is on a scale from 0 to 4. See text and Appendix D for details. The data displayed in Appendix D were used to calculate these values. The numerical values used to represent the relative abundance were averaged to obtain the overall relative abundance for the depositional environment.

<b>Depositional Environment</b>	<b>Quartz (Rel. Abun.)</b>	<b>Feldspar (Rel. Abun.)</b>	<b>Clay Minerals (Rel. Abun.)</b>	<b>Carbonates (Rel. Abun.)</b>	<b>Other (Rel. Abun.)</b>
Lacustrine	3.6	1.8	2.5	0.3	0.1

Table 26: Relative abundance of mineral groups identified by XRD in samples from alluvial fan, meandering stream, and lacustrine environments. Relative abundance is on a scale from 0 to 4. See text and Appendix D for details. The data displayed in Appendix D were used to calculate these values. The numerical values used to represent the relative abundance were averaged to obtain the overall relative abundance for the depositional environment.

<b>Depositional Environment</b>	<b>Quartz (Rel. Abun.)</b>	<b>Feldspar (Rel. Abun.)</b>	<b>Clay Minerals (Rel. Abun.)</b>	<b>Carbonates (Rel. Abun.)</b>	<b>Other (Rel. Abun.)</b>
Alluvial Fan	4.0	2.7	1.9	0.0	0.0
Meandering Stream	3.9	2.0	2.0	0.7	0.2
Lacustrine	3.6	1.8	2.5	0.3	0.1

Table 27: The two mineralogical data sets, the petrographic data and XRD data, organized by sub-basin. The top table also displayed in Table 12 is the average percent of the identified mineral group in the Deep River Basin and each of the sub-basins. The lower table also illustrated in Table 21 displays the relative abundance of mineral groups identified by XRD in samples from the DRB and its sub-basins. Relative abundance is on a scale from 0 to 4. See text and Appendix D for details.

<b>Petro. Sub-basin/basin</b>	<b>Quartz (%)</b>	<b>Feldspar (%)</b>	<b>Clay Minerals (%)</b>	<b>Carbonates (%)</b>	<b>Oxides (%)</b>	<b>Other (%)</b>
Wadesboro	26.4	26.4	36.4	2.9	3.4	4.6
Sanford	19.8	33.5	17.0	0.0	16.6	13.1
Durham	12.3	27.4	31.7	1.6	17.4	9.6
Deep River Basin	16.5	28.2	30.4	1.6	14.3	9.1

<b>XRD Sub-basin/basin</b>	<b>Quartz (Rel. Abun.)</b>	<b>Feldspar (Rel. Abun.)</b>	<b>Clay Minerals (Rel. Abun.)</b>	<b>Carbonates (Rel. Abun.)</b>	<b>Other (Rel. Abun.)</b>
Wadesboro	3.8	1.9	1.6	1.5	0.2
Sanford	3.5	2.0	2.4	0.1	0.3
Durham	3.9	2.3	2.0	0.2	0.0
Deep River Basin	3.8	2.1	2.0	0.5	0.1

Table 28: The two mineralogical data sets, the petrographic data and XRD data, organized by grain size. The top table also displayed in Table 13 is the average percent of the identified mineral groups in the Deep River Basin and each of the sub-basins by grain size. The lower table also illustrated in Table 22 displays the relative abundance of mineral groups identified by XRD in samples from the DRB and its sub-basins by grain size. Relative abundance is on a scale from 0 to 4. See text and Appendix D for details.

<b>Grain Size</b>	<b>Quartz (%)</b>	<b>Feldspar (%)</b>	<b>Clay Minerals (%)</b>	<b>Carbonates (%)</b>	<b>Oxides (%)</b>	<b>Other (%)</b>
vf-f s.s	10.9	27.7	32.1	0.1	19.1	10.0
m-c-vc s.s	21.5	28.5	29.0	3.8	9.3	7.9
gravel	31.3	30.3	23.4	0.0	6.2	8.8

<b>Grain Size</b>	<b>Quartz (Rel. Abun.)</b>	<b>Feldspar (Rel. Abun.)</b>	<b>Clay Minerals (Rel. Abun.)</b>	<b>Carbonates (Rel. Abun.)</b>	<b>Other (Rel. Abun.)</b>
mudstone-shale	3.4	1.3	2.5	1.2	0.1
siltstone	3.9	2.2	1.9	0.6	0.1
vf-f s.s	4.0	2.0	2.2	0.5	0.2
m-c-vc s.s	3.9	2.7	1.6	0.2	0.1
gravel	4.0	1.5	1.5	0.0	0.0

Table 29: The two mineralogical data sets, the petrographic data and XRD data, for alluvial fan environments in the DRB. The top table, also displayed in Table 14, shows the average composition of samples from an alluvial fan. All petrographic samples analyzed were from the fan fringe lithofacies association. The lower table also displayed in Table 23 shows the relative abundance of mineral groups identified by XRD in samples from alluvial fan environments. The XRD data for the two lithofacies associations identified in alluvial fan deposits in the DRB are also displayed.

<b>Depositional Environment</b>	<b>Quartz (%)</b>	<b>Feldspar (%)</b>	<b>Clay Minerals (%)</b>	<b>Carbonates (%)</b>	<b>Oxides (%)</b>	<b>Other (%)</b>	<b>Total (%)</b>
Fan Fringe	19.1	28.7	22.8	0.0	18.4	11.0	99.98

<b>Depositional Environment</b>	<b>Quartz (Rel. Abun.)</b>	<b>Feldspar (Rel. Abun.)</b>	<b>Clay Minerals (Rel. Abun.)</b>	<b>Carbonates (Rel. Abun.)</b>	<b>Other (Rel. Abun.)</b>
Distal Fan	4.0	3.0	2.0	0.0	0.0
Fan Fringe	4.0	2.7	1.8	0.0	0.0
<i>Overall depositional environment:</i>					
Alluvial Fan	4.0	2.7	1.9	0.0	0.0

Table 30: The two mineralogical data sets, the petrographic data and XRD data, for meandering stream environments in the DRB. The top table, also displayed in Table 16, shows the average composition of samples from a meandering stream and its sub-environments. The lower table also displayed in Table 24 shows the relative abundance of mineral groups identified by XRD in samples from meandering stream environments. The XRD data for the two lithofacies associations identified in meandering stream deposits in the DRB are also displayed.

<b>Depositional Environment</b>	<b>Quartz (%)</b>	<b>Feldspar (%)</b>	<b>Clay Minerals (%)</b>	<b>Carbonates (%)</b>	<b>Oxides (%)</b>	<b>Other (%)</b>
Channel Facies	20.0	28.8	34.8	2.1	7.8	6.6
Crevasse Splay Facies	10.9	31.1	29.9	4.1	14.2	9.8
Floodplain Facies	14.6	21.1	29.3	0.0	25.5	9.5
<i>Overall depositional environment</i>						
Meandering Stream	16.2	27.8	32.2	2.2	13.4	8.1

<b>Depositional Environment</b>	<b>Quartz (Rel. Abun.)</b>	<b>Feldspar (Rel. Abun.)</b>	<b>Clay Minerals (Rel. Abun.)</b>	<b>Carbonates (Rel. Abun.)</b>	<b>Other (Rel. Abun.)</b>
Channel Facies	4.0	2.4	1.9	0.3	0.2
Crevasse Splay Facies	4.0	2.6	1.5	0.6	0.1
Floodplain Facies	3.8	1.8	2.1	0.8	0.2
<i>Overall depositional environment:</i>					
Meandering Stream	3.9	2.0	2.0	0.7	0.2

Table 31: The two mineralogical data sets, the petrographic data and XRD data, for lacustrine environments in the DRB. The top table, also displayed in Table 17, shows the average composition of lacustrine samples. The lower table also displayed in Table 25 shows the relative abundance of mineral groups identified by XRD in samples from lacustrine environments. The XRD data for the two lithofacies associations identified in lacustrine deposits in the DRB are also displayed.

<b>Depositional Environment</b>	<b>Quartz (%)</b>	<b>Feldspar (%)</b>	<b>Clay Minerals (%)</b>	<b>Carbonates (%)</b>	<b>Oxides (%)</b>	<b>Other (%)</b>
Lacustrine	8.9	30.9	34.9	0.0	10.3	15.0

<b>Depositional Environment</b>	<b>Quartz (Rel. Abun.)</b>	<b>Feldspar (Rel. Abun.)</b>	<b>Clay Minerals (Rel. Abun.)</b>	<b>Carbonates (Rel. Abun.)</b>	<b>Other (Rel. Abun.)</b>
Lacustrine	3.6	1.8	2.5	0.3	0.1

Table 32: The two mineralogical data sets, the petrographic data and XRD data, from alluvial fan, meandering stream, and lacustrine environments in the DRB.

<b>Depositional Environment</b>	<b>Quartz (%)</b>	<b>Feldspar (%)</b>	<b>Clay Minerals (%)</b>	<b>Carbonates (%)</b>	<b>Oxides (%)</b>	<b>Other (%)</b>
Alluvial Fan	19.1	28.7	22.8	0.0	18.4	11.0
Meandering Stream	16.2	27.8	32.2	2.2	13.4	8.1
Lacustrine	8.9	30.9	34.9	0.0	10.3	15.0

<b>Depositional Environment</b>	<b>Quartz (Rel. Abun.)</b>	<b>Feldspar (Rel. Abun.)</b>	<b>Clay Minerals (Rel. Abun.)</b>	<b>Carbonates (Rel. Abun.)</b>	<b>Other (Rel. Abun.)</b>
Alluvial Fan	4.0	2.7	1.9	0.0	0.0
Meandering Stream	3.9	2.0	2.0	0.7	0.2
Lacustrine	3.6	1.8	2.5	0.3	0.1

## 4. THE INORGANIC GEOCHEMISTRY OF EXTRACTABLE ELEMENTS FROM THE DEEP RIVER BASIN

### 4.1 Introduction

As a result of the rapid expansion of shale gas development in the United States, the public has become increasingly concerned about the proper management of hydraulic fracturing wastewater also referred to as produced water (sections 1.1 and 2.5). Adverse environmental and human health implications may occur should there be a release of untreated or inadequately treated produced water into the environment (Jackson et al., 2013; Vidic et al., 2013; Vengosh et al., 2014; Warner et al., 2014; EPA, 2016). Previous studies conducted in the Marcellus Shale region suggested areas of intensive unconventional gas development and associated hydraulic fracturing experienced more frequent accidental releases of produced water into the environment (Vengosh et al., 2014; Warner et al., 2014). In addition, not all of the produced water generated during shale gas development is brought to the surface. Some of the injected fluids may remain in the shale, but the fate of these unrecovered fluids is currently unknown (Vidic et al., 2013; Capo et al., 2014; Balashov et al., 2015). Produced water has the potential to impact the quality of surface and groundwater water resources in the area (Jackson et al., 2013; Vidic et al., 2013; EPA, 2016). Consequently, there is a need to be able to identify environmental signatures of produced water in the environment in order to understand the fate of unrecovered fluids and to help delineate the source and extent of accidental releases of produced water into the environment.

The chemistry of produced water reflects the original composition of the injected fluids (water and chemicals introduced during hydraulic fracturing), mobilized

constituents such as salts from the shale formation and/or adjacent units, and formation waters liberated during gas production (Gregory et al., 2011; Jackson et al., 2013; Capo et al., 2014). Produced waters are often characterized by high total dissolved solids (TDS), toxic metals, organic compounds, and naturally occurring radionuclides (Gregory et al., 2011; Jackson et al., 2013; Warner et al., 2013; Vengosh et al., 2014; Balashov et al., 2015; EPA, 2016). The inorganic chemical characteristics of produced water vary depending on the geographic location of the basin and the geologic formation from which the waters were produced (Benko and Drews, 2008). For example, the Marcellus Shale Formation was deposited in a shallow interior sea over an area presently referred to as the Appalachian basin. As a result, the produced water from the Marcellus Shale Formation is high in TDS including elevated levels of sodium, calcium, chloride, boron, lithium, strontium, barium, and bromide (Jackson et al., 2013; Brantley et al., 2014; Capo et al., 2014; Warner et al., 2014; Balashov et al., 2015; Stewart et al., 2015). Many of these constituents are found in much higher concentrations in the produced water compared to the injected hydraulic fracturing fluids. This suggests that the bulk of these constituents originated from within the Marcellus Shale either as long-lived, *in situ* formation brine that was mobilized by hydraulic fracturing or from water-rock interactions between the injected fluids with minerals and organic constituents in the shale formation and/or adjacent units (Gregory et al., 2011; Jackson et al., 2013; Vengosh et al., 2014; Stewart et al., 2015; Ziemkiewicz and He, 2015; EPA, 2016). As a result of the potential for elevated levels of contaminants such as strontium and barium, and the sheer volume of wastewater generated, the proper disposal of produced water associated with

unconventional gas development is often a challenge (Benko and Drews, 2008) (section 2.6).

The inorganic chemical characteristics of produced water may be used to identify the wastewater in the environment. Although, elevated levels of sodium, calcium, and chloride are likely to be detected if produced water from the Marcellus Shale enters surface or groundwater, these elements are already common in natural waters (Brantley et al., 2014). Although present at lower concentrations, strontium, barium, and bromide have distinctive concentrations or ratios in produced water from the Marcellus Shale (Brantley et al., 2014). Additionally, produced water generated by unconventional gas development and hydraulic fracturing across several shale plays in the United States appears to have distinct lithium and boron elemental and isotopic signatures (Warner et al., 2014). Understanding the unique geochemical fingerprint of produced water has important implications for the evaluation of hydraulic fracturing-related impacts and the identification of produced water in the environment (Jackson et al., 2013; Brantley et al., 2014; Warner et al., 2014; Johnson and Graney, 2015; Stewart et al., 2015).

Many of the distinctive chemical constituents in produced water are naturally sourced from the shale formation and/or surrounding rock units. As a result, a potential benefit exists from an improved understanding of the natural, *in situ* water-rock interactions prior to shale gas development in an area. Baseline data including the geochemical characterization of formation waters are necessary in order to address concerns regarding the potential for contamination of surface and groundwater as a result of unconventional gas development (Jackson et al., 2013). An improved understanding of the composition of formation water, and by extension, the possible characteristics of

produced water will allow industry and government agencies to have a more accurate picture of the challenges, costs, and methods of properly managing the wastewater before beginning operations in an area (Benko et al., 2008 Stewart et al., 2015).

It is possible that the shale gas in the Deep River basin, North Carolina may be developed in the future using hydraulic fracturing (section 2.2). This study provides baseline data about the natural, *in situ* water-rock interactions occurring in the basin. Several lithologic variables such as mineralogy (including the degree of post-depositional alteration), grain size, lithofacies and lithofacies association were examined to determine their influence on the water-rock interactions in the Deep River basin (sections 1.3 and 1.4). A series of sequential leaching extractions were conducted as part of this study because these extractions target different geochemical reservoirs for extractable elements such as sodium, chloride, boron, strontium, and barium (Tessier et al., 1979; Ryan, 2014; Stewart et al., 2015). The objectives of the sequential extractions were to understand: 1) the possible sources of extractable elements such exchangeable sites on clay minerals and/or carbonate minerals, and 2) the solubility and leaching potential of a suite of elements into the environment. The sources and solubility and leaching potential of boron, strontium, and barium were of particular interest to this study because the distinctive chemical ratios of these elements and others (e.g. chloride, lithium and bromide) have been used as geochemical tracers to identify Marcellus Shale produced water in the environment (Brantley et al., 2014; Capo et al., 2014; Warner et al., 2014; Balashov et al., 2015; Ziemkiewicz and He, 2015).

It was hypothesized that North Carolina Mesozoic basin formation water will exhibit different chemical characteristics than other basins because of different

depositional histories. Specifically, the fluvial, alluvial, and lacustrine (non-marine) deposits of the Deep River basin likely generate lower salinities than the marine brines of the Appalachian Basin (e.g Marcellus Shale) (Benko and Drews, 2008, Stewart et al., 2015). Thus, it is hypothesized that mineralogy will influence the composition of leachate resulting from sequential extractions. Additionally, it is hypothesized that fine-grained lithologies such as shales and fine-grained sandstones will leach trace elements such as strontium and barium more readily than coarse-grained lithologies. Lastly, it is hypothesized that post-depositional alteration will result in authigenic minerals such as carbonates and oxides that will influence the composition of leachate resulting from sequential extractions.

The purpose of this chapter is to present and discuss the geochemical data from the sequential leaching experiments that were conducted on samples collected from the Deep River basin. Background information about leaching experiments with an emphasis on the advantages of sequential extractions follows this section. The sequential extraction procedure used for this study and the resulting geochemical data are presented in subsequent sections. Additionally, a discussion about the geochemical trends present in the Deep River basin as they relate to mineralogy specifically the abundance of clay, carbonate, and oxide minerals, grain size, and depositional environment are at the end of the chapter.

#### 4.2 An Overview of Leaching Experiments and Sequential Extractions

During leaching, solid materials such as soil and rock react chemically with water and other reagents releasing constituents into solution. The rate and extent of the transfer of inorganic constituents is a function of physical and chemical processes that depend on

the properties of the solid material such as mineralogy and particle size as well as the environmental conditions present (Kosson et al., 2017). The resultant leachate records the leachability of geologically-derived components from the solid material (Hageman, 2005; Kosson et al., 2017).

Sequential extractions, a type of leaching experiment, are designed to simulate the types of elements likely to be released into solution under various environmental conditions (Tessier et al., 1979; Conklin, 2014; Kosson et al., 2017). Tessier et al. (1979) developed a series of aqueous sequential chemical extractions for partitioning particulate trace metals into five fractions. Those fractions are defined as: 1) exchangeable constituents, 2) trace metals bound to carbonates, 3) trace metals bound to iron-manganese oxides, 4) trace metals bound to organic matter, and 5) residual trace metals. Reagents were selected based on their ability to target specific geochemical phases in order to determine the speciation of trace metals (Tessier et al., 1979). The methodology used by Tessier et al. (1979) was proven satisfactory by comparing total trace metal concentrations with the sum of all the five fractions. The experimental results demonstrated by the sequential extraction procedure had a relative standard deviation generally better than +/- 10% (Tessier et al., 1979).

An advantage of sequential extractions is that they, to a certain degree, simulate various environmental conditions to which a sediment or rock may be subjected (Tessier, 1979). By doing so, sequential extractions provide “detailed information about the origin, mode of occurrence, biological and physicochemical availability, mobilization, and transport of trace metals” (Tessier, 1979, p. 844). The sequential extractions used in this study can help elucidate the sources of extractable elements in sedimentary samples from

the Deep River basin and may provide information about the potential mobility of boron, strontium, and barium during unconventional gas production (Tessier, 1979; Spivak-Birndorf et al., 2012; Stewart et al., 2015).

#### 4.3 Sequential Extraction Procedure

Sequential extractions were conducted on 183 samples from the Deep River basin (Figure 23 and 45). The methodology used for this study was adapted from the sequential extraction procedures in Tessier et al. (1979) and Stewart et al. (2015). In this study, a four-step aqueous sequential extraction procedure and appropriate reagents such as ammonium acetate and acetic acid were used to selectively target four specific geochemical phases: 1) water-soluble components, 2) exchangeable cations, 3) carbonates, and 4) strong-acid (hydrochloric acid) soluble phases (Tessier, 1979; Stewart, 2015) (Figure 45).

Approximately 0.667 g of crushed (100 mesh; 0.149 mm) sample was leached in 40 mL of deionized water (water: rock ratio of 60:1 (vol/vol)) in a polypropylene centrifuge tube. The tube was placed on an orbital shaker table for 24 hours at 250 rpm. After shaking, the tube was placed in a centrifuge for 1 hour at 2000 rpm. Upon completion of the previous step, the supernatant was decanted into a syringe equipped with a Millipore 0.45-micron syringe tip filter. The filtered sample was split roughly equally between 2 new centrifuge tubes which were labeled CAT and the other AN. The CAT sample received 4 drops of concentrated Optima Grade nitric acid and was capped, shaken, and stored at room temperature. The AN sample was stored in a refrigerator. The sediment samples were saved for subsequent sequential extractions.

Using the sample-holding centrifuge tube from the previous step, 40 mL of 1 molar ammonium acetate was added to each tube. Next, the tubes were placed on an orbital shaker table at 250 rpm for 18 hours. At the end of shaking, the tubes were centrifuged for 1 hour at 2000 rpm. Once centrifuging was completed, the supernatant was decanted into a new centrifuge tube. The supernatant of each sample received 4 drops of concentrated optima grade nitric acid and was capped, shaken and stored at room temperature. The sediment samples were saved for subsequent extractions. This step, which describes the addition of a reagent followed by shaking and decanting, was repeated two additional times, once with 8% acetic acid and once with 0.1 molar hydrochloric acid.

In summary, the samples were initially exposed to ultrapure water to extract pore water and water-soluble salts, including chlorides and sulfates (Stewart et al., 2015). The residue from the previous step was leached with ammonium acetate to extract exchangeable cations. The ammonium ions from this treatment displace interlayer cations from clay minerals and loosely bound cations on the surfaces of minerals and organic matter (Suarez, 1996; Stewart et al., 2001; Stewart et al., 2015). The residue was leached with acetic acid to target trace elements bound to carbonate minerals (Tessier et al., 1979; Stewart et al., 2015). Lastly, the residue was leached with hydrochloric acid in order to target acid-soluble phases such as iron- and manganese- oxides (Tessier et al., 1979; Stewart et al., 2015).

The leachates from the sequential extractions were analyzed for trace cations by inductively coupled plasma mass spectrometry (ICP-MS) (Appendix E). The water leachates were also analyzed for major cations and anions by ion chromatography (IC)

(Appendix F). Both the ICP-MS and IC were located at the University of North Carolina at Charlotte.

#### 4.4 The Sequential Extraction Results

Appendix E shows the amount of boron, strontium, and barium released from the Deep River basin samples during the sequential leaching by ultrapure water, ammonium acetate, acetic acid, and hydrochloric acid. Appendix F shows the amount of cations such as sodium and calcium and anions such as chloride released from the Deep River basin samples during the sequential leaching by ultrapure water.

The response of the trace elements, boron, strontium, and barium, to the sequential extraction solutions varied greatly due to the affinity of the element and the specific geochemical phase targeted by each solution (Figure 82). In general, the average extractable boron released from all of the Deep River basin samples and from all steps of the sequential extractions was notably lower ( $0.3 \mu\text{g/g}$ ) than the average extractable strontium and barium,  $11.9 \mu\text{g/g}$  and  $19.3 \mu\text{g/g}$ , respectively (Table 33). Boron was preferentially released to acetic acid from carbonate minerals (Figure 82 and Table 34). The alkaline earth metals, strontium and barium, show variation in their response to the sequential extractions (Figure 82). Both were preferentially leached from exchangeable sites by the ammonium acetate solution, but unlike strontium, barium does not appear to be released in appreciable amounts from carbonate minerals (Figure 82). In contrast, the geochemical data show that a greater quantity of barium was released by the HCl solution, possibly from oxide minerals such as hematite, compared to strontium (Figure 82 and Table 34).

#### 4.5 The Relationship between Grain Size and the Concentration of Extractable Elements

In order to examine the influence of grain size on the water-rock interactions in the Deep River basin, the leachate data from the sequential extractions were organized by the grain size of the sample prior to crushing (Figure 83 and Table 35). The samples used for the sequential extractions were powdered and passed through a sieve (100 mesh; 0.149 mm) in order to achieve a uniform grain size for the leaching analyses. In general, as grain size increases, the average concentration of extractable boron, strontium, and barium decreases (Figure 83 and Table 35). Mudstones and shales are characterized by the highest average concentrations of these trace elements while coarse-grained samples such as gravels have the lowest average concentrations.

The leaching behavior of boron and barium is comparable to that observed in the overall Deep River basin regardless of grain size (Figures 82 and 83). Boron was preferentially released to acetic acid from carbonate minerals and barium was preferentially leached from exchangeable sites by the ammonium acetate solution (Figure 83 and Table 36). Thus, while grain size influences the quantity of these elements leached to solution, it does not appear that the affinity of boron and barium vary with grain size in the Deep River basin. On the contrary, the geochemical data indicate strontium has a more complex leaching behavior depending on the grain size of the sample. Mudstones and shales tended to release more strontium from carbonate minerals, whereas more coarse-grained samples ranging from siltstones to gravels tend to release more strontium from exchangeable sites such as found on clay minerals (Figure 83). The geochemical data suggest that the affinity and/or solubility and leaching potential of strontium may vary depending on grain size.

#### 4.6 The Leaching Behavior of Extractable Elements as it Relates to the Sub-basins and Depositional Environments of the Deep River Basin

In order to identify geochemical trends in the affinity and/or solubility and leaching potential of extractable elements across the Deep River basin, the leachate data were organized by sub-basin and depositional environment. In general, boron was released in low average quantities from the Deep River basin samples ( $0.3 \mu\text{g/g}$ ) (Figure 82 and Table 33). The geochemical data also indicate little variation in the solubility and/or leaching potential of boron among the targeted mineral phases or among grain size (Figure 83 and Table 36). On the contrary, strontium and barium were released in much higher average quantities from the Deep River basin samples,  $11.9 \mu\text{g/g}$  and  $19.3 \mu\text{g/g}$ , respectively (Table 33). In addition, despite both being alkaline earth metals, the leaching behavior of strontium and barium differed, possibly due to variations in the affinity and/or the solubility and leaching potential of the trace metals (Figure 82 and 83). As a result of the low concentration and lack of variability in the leaching behavior of boron from targeted mineral phases, this study primarily focused on the more complex leaching behavior of extractable strontium and barium. The geochemical data for extractable boron may appear in many tables, but it will not be discussed in detail.

##### 4.6.1 The leaching behavior of extractable strontium and barium according to sub-basin

The highest average cumulative concentration of strontium extracted from all steps of the sequential extractions was leached from the Wadesboro sub-basin samples ( $22.5 \mu\text{g/g}$ ) (Table 33). The Durham and Sanford sub-basin samples released lower average cumulative concentrations of extractable strontium,  $7.8 \mu\text{g/g}$  and  $6.5 \mu\text{g/g}$ , respectively (Table 33). In the Durham sub-basin, strontium was preferentially leached from exchangeable sites by ammonium acetate with lesser amounts released by carbonate

minerals (Figure 84). In the Wadesboro and Sanford sub-basins, however, strontium was preferentially released from carbonate minerals followed by exchangeable sites (Figure 84 and Table 34).

Similar to strontium, the highest average cumulative concentration of barium extracted from all steps of the sequential extractions was leached from the Wadesboro sub-basin samples (23.4  $\mu\text{g/g}$ ) (Figure 84 and Table 33). The Durham and Sanford sub-basin samples leached lower average cumulative concentrations of extractable barium, 17.8  $\mu\text{g/g}$  and 16.9  $\mu\text{g/g}$ , respectively (Table 33). In the Deep River basin, barium was preferentially leached from exchangeable sites by ammonium acetate (Figure 84). Furthermore, oxide minerals which were targeted by the HCl solution appear to be an important source of extractable barium (Figure 84 and Table 34). This trend is consistent with the leaching behavior of barium in the Wadesboro and Durham sub-basins (Figure 84). In the Sanford sub-basin, however, carbonate minerals and HCl-soluble minerals released similar average concentrations of barium, 11.1  $\mu\text{g/g}$  and 10.6  $\mu\text{g/g}$ , respectively (Figure 84 and Table 33). In summary, the geochemical data suggest the affinity and/or the solubility and leaching potential of strontium and barium may vary depending on the sub-basin on the Deep River basin (Figure 84).

#### 4.6.2 The leaching behavior of extractable strontium and barium based on the depositional environment

As discussed in section 3.2, the depositional environments present in the Deep River basin included: 1) alluvial fans, 2) meandering streams, and 3) lacustrine environments (Figure 46). The geochemical data may indicate differences in the quantity, affinity, and/or solubility and leaching potential of strontium and barium depending on the depositional environment (Figure 85). For example, samples from alluvial fans

released the lowest average cumulative concentration of extractable strontium (6.4  $\mu\text{g/g}$ ), but the highest average cumulative concentration of extractable barium (22.9  $\mu\text{g/g}$ ) (Table 37). Samples from lacustrine environments released the highest average cumulative concentration of strontium (16.0  $\mu\text{g/g}$ ), but an intermediate average cumulative concentration of barium (19.6  $\mu\text{g/g}$ ) (Table 37). Samples from meandering streams leached an intermediate average cumulative concentration of strontium (12.8  $\mu\text{g/g}$ ) and the lowest average cumulative concentrations of barium, 18.3  $\mu\text{g/g}$  (Figure 85 and Table 37). Moreover, the geochemical data show similar average cumulative concentrations of strontium were released from carbonate minerals in meandering stream (22.6  $\mu\text{g/g}$ ) and lacustrine environments (21.5  $\mu\text{g/g}$ ), but significantly less strontium was leached from carbonate minerals in alluvial fan environments (3.2  $\mu\text{g/g}$ ) (Figure 85 and Table 38).

*The leaching behavior of extractable strontium and barium in alluvial fan environments*

As discussed in section 3.14, the alluvial fan environments encountered in this study are divided into two lithofacies associations: the fan fringe lithofacies association and the distal fan lithofacies association (Figure 46). In alluvial fan environments, strontium and barium were preferentially leached from exchangeable sites (Figure 86). Although this geochemical trend is consistent among the distal fan and the fan fringe lithofacies associations, the leaching behavior of strontium and barium varied between the two lithofacies associations (Figure 86 and Table 39). In general, the distal fan samples leached the highest average cumulative concentrations of strontium (7.1  $\mu\text{g/g}$ ) and barium (57.4  $\mu\text{g/g}$ ) compared to the fan fringe samples, 6.2  $\mu\text{g/g}$ , and 13.9  $\mu\text{g/g}$ , respectively (Table 39).

In addition, the geochemical data may indicate differences in the geochemical affinity of strontium and barium depending on the lithofacies association of alluvial fan samples (Figure 86). For example, the distal fan samples leached more strontium from carbonate minerals compared to the fan fringe samples, 8.9  $\mu\text{g/g}$  and 1.7  $\mu\text{g/g}$ , respectively (Figure 86 and Table 40). Furthermore, a higher average concentration of barium was released by HCl-soluble minerals from the distal fan samples compared to the fan fringe samples, 71.7  $\mu\text{g/g}$  and 9.8  $\mu\text{g/g}$ , respectively (Figure 86 and Table 40).

*The leaching behavior of extractable strontium and barium in meandering stream environments*

As discussed in section 3.15, meandering stream environments are divided into three sub-environments or lithofacies associations: the channel lithofacies association, the floodplain lithofacies association, and the crevasse splay lithofacies association. In meandering stream environments, strontium and barium were preferentially leached from exchangeable sites by ammonium acetate (Figure 87).

The geochemical data suggest variation in the leaching behavior of strontium and barium among the sub-environments of meandering streams. For example, the floodplain samples leached the highest average cumulative concentration of strontium (15.4  $\mu\text{g/g}$ ) whereas the crevasse splay and channel lithofacies associations released similar, lower average cumulative concentrations of strontium, 7.0  $\mu\text{g/g}$  and 6.9  $\mu\text{g/g}$ , respectively (Table 41). Interestingly, the channel lithofacies association leached the highest average cumulative concentration of barium (27.7  $\mu\text{g/g}$ ) and the floodplain and crevasse splay lithofacies associations released lower average cumulative concentrations of barium, 17.2  $\mu\text{g/g}$  and 15.8  $\mu\text{g/g}$ , respectively (Figure 87 and Table 41).

The geochemical data may indicate differences in the geochemical affinity of strontium depending on the sub-environment of the meandering stream samples (Figure 87). The leachate data indicate more strontium was released from carbonate minerals in floodplain lithofacies association (29.8  $\mu\text{g/g}$ ) and the crevasse splay lithofacies association (9.2  $\mu\text{g/g}$ ) compared to the channel lithofacies association (2.7  $\mu\text{g/g}$ ) (Figure 87 and Table 42).

*The leaching behavior of extractable strontium and barium in lacustrine environments*

In lacustrine environments, strontium and barium were preferentially leached by the ammonium acetate from exchangeable sites (Figure 88 and Table 43). Unlike strontium which was released secondarily from carbonate minerals, barium appears to be extracted in similar average concentrations from carbonate and HCl-soluble minerals in lacustrine samples (Figure 88 and Table 43).

#### 4.7 The Relationship between Mineral Content, Grain Size, and the Leaching Behavior of Extractable Strontium and Barium in the Deep River Basin

The results of the sequential extractions suggest the water-rock interactions in the Deep River basin are influenced by the mineralogy of a sample such as the presence or absence of clay minerals and/or carbonate minerals and grain size. As a result, statistical analyses were used to model 1) the relationship between mineral content and the concentration of extractable strontium and barium, and 2) the relationship between grain size and the concentration of extractable strontium and barium. It is hypothesized that samples with greater quantities of the targeted mineral phase such as clay minerals will release more extractable trace elements compared to samples with a lower abundance of the targeted mineral. Furthermore, where the concentration of extractable trace elements cannot be adequately explained by the abundance of the targeted mineral phase, it is

hypothesized that variations in grain size may explain the observed geochemical trends. The statistical analyses conducted for this study were performed using Microsoft Excel and JMP version 13 (JMP, 2016).

Linear regression analysis was used to model the relationship between the percent abundance of a targeted mineral phase compared to the concentration of extractable trace elements from the sequential extractions (for example, Figure 89). The r-squared ( $r^2$ ) value, also referred to as the correlation coefficient, provides a measurement, on a scale of -1 to +1, of the strength of the linear relationship between the two variables (NCSU, 2004; Nau, 2018). Commonly, the closer the value of  $r^2$  is to 1, the better the regression line describes the data (NCSU, 2004).

The semi-quantitative rank data derived from the XRD analyses describe the relative abundance of targeted mineral groups in samples from the Deep River basin (Appendix D). Relative abundance values range from the highest intensity (4) to lowest intensity (1) (section 3.21). A value of zero indicated the mineral group was not present in the sample. Thus, a higher numerical value indicates a greater relative abundance of the mineral in a sample. Due to the categorical nature of the mineralogical data, box and whisker plots, also referred to as box plots, were used to model the relationship between the relative abundance of a targeted mineral phase obtained from XRD analyses compared to the concentration of extractable trace metals from the sequential extractions (for example, Figure 89).

The statistical analyses conducted for this study focused on the mineral phases most likely to release increased concentrations of extractable trace elements. For example, the geochemical data from this study show exchangeable sites, most likely

associated with clay minerals have the potential to release cations such as strontium and barium into solution (Figure 82). As a result, the relationship between clay mineral abundance and the concentration of extractable strontium and barium were examined further. It is important to clarify the meaning of the term ‘clay mineral’ as it pertains to the category of minerals identified by petrographic analyses compared to the minerals in the ‘clay mineral’ category identified by XRD (Tables 7 and 20). For the petrographic analyses, the term clay mineral predominantly refers to the fine-grained interstitial material (matrix) located between grains. The matrix of sedimentary rocks commonly consists of clay minerals such as kaolinite and smectite and other phyllosilicates like mica and chlorite. Fine-grained quartz and feldspar may also be constituents in the matrix of sedimentary rocks (Newman and Brown, 1987; Tucker, 2001). The fine-grained minerals such as fine silt and clay composing the matrix are often too fine-grained to accurately identify using petrographic analyses (Harwood, 1988; Lynn et al., 2008). As a result, the term ‘clay mineral’ as it relates to the petrographic analyses generally refers to the clay-sized fraction composing the matrix which may include fine-grained minerals such as quartz, calcite, feldspar, smectite, and iron oxides (Table 7) (Ryan, 2014).

For the XRD analyses, the term ‘clay mineral’ refers to hydrous aluminosilicates such as clay minerals with a specific sheet-like structure (phyllosilicates) (section 3.21) (Table 20). XRD is the most common analytical method used to determine the mineralogy of fine-grained sediments, especially clays (Poppe et al., 2001). Clay minerals are typically less than 2 microns ( $\mu\text{m}$ ), but grains may reach 10  $\mu\text{m}$  or more (Tucker, 2001). XRD analyses of the samples from the Deep River basin allowed the specific mineral phases present in the fine-grained matrix to be identified (section 3.21).

Consequently, the clay mineral group as it pertains to the XRD analyses includes clay minerals such as smectite and kaolinite and other phyllosilicates such as mica and chlorite (Table 20).

#### 4.7.1 The relationship between mineral content, grain size, and concentrations of extractable strontium

Strontium was preferentially leached from exchangeable sites such as present on clay minerals with lesser amounts released by carbonate minerals (Figure 82). As a result, the analyses investigating the concentration of extractable strontium as a function of mineral content focused on the abundance of clay minerals and carbonate minerals in a sample. The influence of grain size on the concentration of extractable strontium is also more closely examined.

The low  $r^2$  value (0.18) appears to indicate a minimal correlation in the percentage of clay minerals and the concentration of ammonium acetate extractable strontium (Figure 89). As mentioned above, the term clay mineral as it relates to the petrographic analyses predominantly refers to the fine-grained and silt-sized minerals composing the matrix. As a result, the  $r^2$  value may elude to a stronger correlation between grain size and the concentration of extractable strontium from exchangeable sites. The box plot also indicates little correlation between the relative abundance of clay minerals and the median concentration of extractable strontium (Figure 89).

Unlike the abundance of clay minerals, the abundance of carbonate minerals in a sample appears to be strongly positively correlated to the concentration of extractable strontium ( $r^2=0.7248$ ) (Figure 90). In general, as the abundance of carbonate minerals in a sample increases, the concentration of acetic acid extractable strontium also increases.

Based on the geochemical data from this study, variations in grain size influence the average concentration of extractable strontium (Figure 83 and Table 35). The statistical analyses appear to support this interpretation (Figure 91). Fine-grained mudstones and shales released the highest median concentration of strontium from exchangeable sites such as on clay minerals, and from carbonate minerals; whereas more coarse-grained samples such as gravels released lower concentrations (Figure 91). In summary, for the Deep River basin, the highest concentrations of extractable strontium are likely to be generated from fine-grained deposits such as mudstones and shales and siltstones especially those with abundant exchangeable sites such as those on clay minerals; and carbonate minerals.

#### 4.7.2 The relationship between mineral content, grain size, and the concentration of extractable barium

Barium was preferentially leached from exchangeable sites such as on clay minerals and with lesser amounts released by oxide minerals (Figure 82). As a result, the analyses investigating the concentration of extractable barium as a function of mineral content focused on the abundance of clay minerals and oxide minerals in a sample.

The  $r^2$  value (0.3136) appears to indicate a slight positive correlation between the abundance of clay minerals and the concentration of ammonium acetate extractable barium (Figure 92). The box plot also indicates a minimal positive correlation between the relative abundance of clay minerals and the median concentration of extractable barium (Figure 92). In general, as the abundance of clay minerals increases, the concentration of extractable barium will likely increase. As mentioned above, the clay mineral group as it relates to the petrographic analyses predominantly refers to the fine-grained and silt-sized minerals composing the matrix. As a result, the  $r^2$  value may also

hint at a correlation between grain size and the concentration of extractable barium from exchangeable sites on clay minerals. The abundance of oxide minerals does not appear to be correlated ( $r^2 = 0.0044$ ) to the concentration of extractable barium (Figure 93).

The influence of grain size on the concentration of extractable barium is also more closely examined. Based on the geochemical data from this study, variations in grain size influence the average concentration of extractable barium (Figure 83 and Table 35). The statistical analyses appear to support this interpretation (Figure 94). Fine-grained deposits such as mudstones and shales released the highest median concentration of extractable barium whereas more coarse-grained samples such as gravels released lower median concentrations (Figure 94). In summary, for the Deep River basin, the highest concentrations of extractable barium are likely to be generated from fine-grained deposits such as mudstones and shales especially those with abundant exchangeable sites such as clay minerals.

#### 4.8. The Relationship between Mineral Content and the Concentration of Extractable Strontium and Barium in the Sub-basins

The geochemical data suggest that the affinity and/or solubility and leaching potential of strontium and barium may vary depending on the sub-basin of the Deep River basin (section 4.6) (Figure 82 and Tables 35 and 36). It is possible that differences in mineralogy between the sub-basins (Table 27) may influence the total (bulk) amount available, the affinity, and/or solubility and leaching potential of strontium and barium. Additionally, the Durham sub-basin samples were collected from cores; whereas the samples from the Sanford and Wadesboro sub-basins were surface samples. It is possible that modern climate conditions which are characterized as more humid could have modified the composition of the samples collected at the surface, but the presence of

carbonate and oxide minerals in the Sanford and Wadesboro sub-basins suggest modifications to composition are likely minimal as these minerals are unstable in humid climates. Statistical analyses were used to investigate the relationship between mineral content and the concentration of extractable strontium and barium from each of the sub-basins of the Deep River basin (Figures 95-97).

The XRD mineralogical dataset was used for the analyses related to the sub-basins. The XRD dataset was chosen because it includes the compositional data of all 183 samples collected from the Deep River Basin, whereas the petrographic dataset is a subset of 19 samples selected from overall total samples (Appendix A and C). As a result, the petrographic dataset included 4 samples from the Wadesboro sub-basin, 3 samples from the Sanford sub-basin, and 12 samples from the Durham sub-basin (Appendix A). The limited number of samples analyzed with petrography hinder the use of this mineralogical dataset for more in-depth examinations of the influence of mineralogy on the concentration of extractable trace metals.

Clay mineral abundance is minimally correlated to the concentration of extractable strontium in the Deep River basin and it is anticipated that the same general relationship may be maintained in the sub-basins (Figure 89). The statistical analyses appear to support this interpretation, but some variation in the nature of the relationship may exist (Figure 95). For example, in the Wadesboro sub-basin, there may be a slight negative correlation between the abundance of clay minerals and the concentration of extractable strontium. This means that for samples from the Wadesboro sub-basin, it appears that as the relative abundance of clay minerals increases, the median concentration of extractable strontium decreases (Figure 95). On the contrary, in the

Sanford sub-basin the abundance of clay minerals is slightly positively correlated to the concentration of extractable strontium. The analyses indicate that in the Sanford sub-basin, as the abundance of clay minerals increases, so does the concentration of extractable strontium. In general, highest mean concentration of extractable strontium from clay minerals was generated by samples in the Wadesboro sub-basin 35.99  $\mu\text{g/g}$ . The Durham sub-basin generated intermediate concentrations of extractable strontium and the Sanford sub-basin generated the lowest extractable strontium, 24.93  $\mu\text{g/g}$  and 9.23  $\mu\text{g/g}$ , respectively (Figure 95).

Carbonate mineral abundance is strongly positively correlated to the concentration of extractable strontium in the Deep River basin and it is anticipated that the same general relationship may be maintained in the sub-basins (Figure 90). As predicted, the relative abundance of carbonate minerals in each of the sub-basins is strongly positively correlated to the concentration of acetic acid extractable strontium (Figure 96). In general, as the abundance of carbonate minerals increases so does the concentration of extractable strontium. Although the relationship between carbonate mineral content and the concentration of extractable strontium is consistent among the sub-basins, the average concentration of extractable strontium from carbonate minerals varies by sub-basin (Figure 96). The highest mean concentration of extractable strontium from carbonate minerals (47.62  $\mu\text{g/g}$ ) was leached by samples from the Wadesboro sub-basin (Figure 96). The Sanford sub-basin had one sample with abundant carbonate minerals, but, in general, the Sanford sub-basin samples had a low relative abundance of carbonate minerals. As a result, the Sanford sub-basin samples leached a significantly lower mean concentration of extractable strontium from carbonate minerals (11.53  $\mu\text{g/g}$ )

compared to the Wadesboro sub-basin. The Durham sub-basin samples leached the lowest mean concentration of acetic acid extractable strontium ( $4.50 \mu\text{g/g}$ ) (Figure 96).

Clay mineral abundance is minimally correlated to the concentration of extractable barium in the Deep River basin and it is anticipated that the same general relationship may be maintained in the sub-basins (Figure 92). The box plots suggest a minimal, positive correlation between the relative abundance of clay minerals and the concentration of extractable barium in the Wadesboro and Durham sub-basins (Figure 97). In the Sanford sub-basin, the concentration of extractable barium does not appear to be correlated to clay mineral abundance.

In summary, in the Wadesboro sub-basin, the concentration of ammonium acetate extractable strontium is minimal, but slightly negatively correlated to the clay mineral content. In contrast, the concentration of ammonium acetate extractable barium shows a minimal, positive correlation to clay mineral abundance. Additionally, among the sub-basins of the Deep River basin, the Wadesboro sub-basin samples are characterized as releasing the highest average concentrations of ammonium acetate extractable strontium and barium, as well as acetic acid extractable strontium,  $35.99 \mu\text{g/g}$  (Sr),  $47.62 \mu\text{g/g}$  (Ba),  $67.93 \mu\text{g/g}$  (Sr), respectively (Figures 95-97).

In the Sanford sub-basins, the concentration of ammonium acetate extractable strontium is slightly positively correlated to the clay mineral content, whereas the concentration of ammonium acetate extractable barium does not appear to be correlated to the clay mineral content. Compared to the other sub-basins, samples from the Sanford sub-basin leached the lowest mean concentrations of ammonium acetate extractable strontium and barium,  $9.23 \mu\text{g/g}$  and  $45.24 \mu\text{g/g}$ , respectively. The Sanford sub-basin

samples leached an intermediate mean concentration acetic acid extractable strontium, 11.53  $\mu\text{g/g}$  (Figures 95-97).

In the Durham sub-basins, the concentration of ammonium acetate extractable strontium and barium may show a minimal positive correlation with the clay mineral content. Compared to the other sub-basins, the Durham sub-basin leached an intermediate average concentration of ammonium acetate extractable strontium and barium, 24.93  $\mu\text{g/g}$  and 46.53  $\mu\text{g/g}$ , respectively, and the lowest average concentration of acetic acid extractable strontium, 4.5  $\mu\text{g/g}$ . The relative abundance of carbonate minerals in each of the sub-basins is strongly positively correlated to the concentration of acetic acid extractable strontium (Figures 95-97).

#### 4.9 The Relationship between Mineral Content, Grain Size, and the Concentration of Extractable Elements in Depositional Environments

The geochemical data may indicate differences in the quantity, affinity, and/or solubility and leaching potential of strontium and barium depending on the depositional environment of the Deep River basin (Figure 85 and Tables 37 and 38). It is possible that differences in mineralogy between the depositional environments may influence the total (bulk) amount of strontium and barium available for leaching. Additionally, inherently different geologic processes occur in the different depositional environments such as different transport mechanisms, sediment diagenesis, and changes in redox conditions that may influence the affinity and/or solubility and leaching potential of strontium and barium (Tucker, 2001; Ryan, 2014). As a result, statistical analyses were used to investigate the relationship between mineral content and the concentration of extractable strontium and barium from the depositional environments of the Deep River basin. The

influence of grain size on the concentration of extractable trace metals is also considered (Figures 98-103).

Clay mineral abundance is minimally correlated to the concentration of extractable strontium, but some variation in the nature of the relationship may exist among the depositional environments (Figure 98). For example, samples from lacustrine environments appear to show a slight positive correlation between clay mineral abundance and extractable strontium, whereas the alluvial fan and meandering stream samples appear to show a slight negative correlation (Figure 98). This may suggest that as clay mineral abundance increases in lacustrine samples so will the median concentration of ammonium acetate extractable strontium. The opposite would be expected to occur in samples from alluvial fans and meandering streams (Figure 98). Samples from lacustrine environments also leached the highest average concentration of extractable strontium 32.96  $\mu\text{g/g}$ . Meandering stream and alluvial fan samples released similar, lower concentrations of strontium, 25.04  $\mu\text{g/g}$  and 21.09  $\mu\text{g/g}$ , respectively (Figure 98).

As expected based on previous analyses, the relative abundance of carbonate minerals in meandering stream and lacustrine environments is strongly correlated to the median concentration of acetic acid extractable strontium (Figure 99). In general, as the abundance of carbonate minerals increase so does the median concentration of acetic acid extractable strontium. The data set appears to contain a limited number of samples from alluvial fans that contain carbonate minerals. Consequently, a correlation between carbonate mineral content and extractable strontium in alluvial fans cannot be determined (Figure 99). Meandering stream and lacustrine samples released similar high average

concentrations of acetic acid extractable strontium, 22.55  $\mu\text{g/g}$  and 21.53  $\mu\text{g/g}$ , respectively. On the contrary, possibly as a result of low carbonate mineral abundance, alluvial fan samples leached the lowest average concentration of extractable strontium (3.19  $\mu\text{g/g}$ ) (Figure 99). Based on the geochemical data from this study, there is a consistent strong correlation between the relative abundance of carbonate minerals and the mean concentration of acetic acid extractable strontium in the Deep River basin, its sub-basins, and depositional environments. As a result, it is assumed this relationship will be maintained within the sub-environments of alluvial fans and meandering streams and, therefore, will not be examined in greater detail.

The box plots indicate that the median concentration of ammonium acetate extractable barium and the relative abundance of clay minerals among the depositional environments is not correlated (Figure 100). Additionally, the average concentration of ammonium acetate barium extractable from clay mineral is similar regardless of the depositional environment. Lacustrine and alluvial fan samples leached similar, high mean concentrations of ammonium acetate extractable barium, 59.10  $\mu\text{g/g}$  and 58.85  $\mu\text{g/g}$ , respectively, whereas meandering streams leached a slightly lower mean concentration of ammonium acetate extractable barium (48.82  $\mu\text{g/g}$ ) (Figure 100). Based on the geochemical data from this study, there is a minimal correlation between the relative abundance of clay minerals and the mean concentration of ammonium acetate extractable barium in the Deep River basin, its sub-basins, and depositional environments. As a result, it is assumed this relationship will be maintained within the sub-environments of alluvial fans and meandering streams and, therefore, will not be examined in greater detail.

#### 4.9.1 The relationship between clay mineral content, grain size, and the concentration of strontium from alluvial fan sub-environments

Clay mineral abundance is slightly negatively correlated to the concentration of ammonium acetate extractable strontium in alluvial fans. Further analyses were conducted to determine if this correlation is consistent among the sub-environments of alluvial fans (Figure 101). A slight negative correlation between clay mineral content and the concentration of ammonium acetate extractable strontium appears to be consistent in the fan fringe sub-environment (Figure 101). Similar to the overall alluvial fan environment, the geochemical data suggest that as the abundance of clay minerals increases, the median concentration of ammonium acetate extractable strontium decreases. The average concentration of ammonium acetate extractable strontium was greatest from the fan fringe samples and decreased in the distal fan samples, 22.19  $\mu\text{g/g}$  and 16.84  $\mu\text{g/g}$ , respectively (Figure 101).

Although clay mineral content is slightly negatively correlated to the median concentration of ammonium acetate extractable strontium, grain size appears to potentially play a more significant role in influencing the median concentration of ammonium acetate extractable strontium in alluvial fan sub-environments (Figure 101). Similar to other grain size trends previously established by this study (section 4.5), as grain size increases the median concentration of extractable strontium decreases. Thus, fine-grained alluvial fan deposits such as siltstones are likely to release more ammonium acetate extractable strontium compared more coarse-grained alluvial fan deposits (Figure 101).

#### 4.9.2 The relationship between clay mineral content, grain size, and the concentration of extractable strontium from meandering stream sub-environments

Clay mineral abundance is slightly negatively correlated to the concentration of ammonium acetate extractable strontium in meandering stream environments. Further analyses were conducted to determine if this correlation is consistent among the sub-environments of meandering streams (Figure 102). According to the geochemical data, clay mineral abundance and the median concentration of ammonium acetate extractable strontium in the channel and crevasse splay samples do not appear to be correlated, but a slight negative correlation may be present in the floodplain samples (Figure 102). In the floodplain samples, it appears that as the relative abundance of clay minerals increases, the concentration of ammonium acetate extractable strontium is likely to decrease (Figure 102). The floodplain samples and the channel samples leached similar high average concentration of extractable strontium, 27.50  $\mu\text{g/g}$  and 23.22  $\mu\text{g/g}$ , respectively (Figure 102). The crevasse splay samples leached a lower mean concentration of extractable strontium, 16.83  $\mu\text{g/g}$ .

An interesting pattern may be present between the concentration of ammonium acetate extractable strontium and grain size among the sub-environments of meandering streams in the Deep River basin (Figure 102). For example, in the channel and floodplain sub-environments, medium-coarse-very coarse sandstones leached a higher median concentration of ammonium acetate extractable strontium compared to very fine-fine-grain sandstones (Figure 102). As a result of different geologic processes occurring in the sub-environments, the floodplain sub-environment has more fine-grained samples such as mudstones and shales and siltstones compared to the channel and crevasse splays. Besides the aforementioned unusual leaching behavior of medium-coarse-very coarse

sandstones, the influence of grain size in the floodplain facies appears to be consistent with previously established trends. Fine-grained floodplain deposits such as mudstones and shales leached higher median concentrations of ammonium acetate extractable strontium compared to more coarse-grained deposits (Figure 102).

#### 4.9.3 The relationship between grain size and the concentration of ammonium acetate extractable strontium in lacustrine environments

Samples from lacustrine environments appear to show a slight positive correlation between clay mineral abundance and median concentration of ammonium acetate extractable strontium, whereas the alluvial fan and meandering stream samples appear to show a slight negative correlation (Figure 98). Thus, the geochemical data suggest that as the abundance of clay minerals increases in lacustrine environments, the concentration of ammonium acetate extractable strontium is likely to increase. Additional analyses of lacustrine samples appear to show a strong correlation between grain size and the concentration of ammonium acetate extractable strontium. Fine-grained lacustrine deposits such as mudstones and shales leached higher median concentrations of ammonium acetate extractable strontium compared to more coarse-grained very fine-fine sandstone deposits (Figure 103). Similar to the channel and floodplain sub-environments of meandering streams, medium-coarse-very coarse sandstones released an uncharacteristically high median concentration of ammonium acetate extractable strontium (Figure 103). It is difficult to make a more in-depth interpretation though as only one coarse sandstone sample from a lacustrine environment was analyzed (Figure 103 and Appendix D).

In summary, in the depositional environments of the Deep River basin, the concentration of ammonium acetate extractable strontium appears to be minimally

correlated with clay mineral abundance (Figure 98). The concentration of ammonium acetate extractable barium, however, does not appear to be correlated with clay mineral abundance (Figure 100). The relative abundance of carbonate minerals in each of the depositional environments is strongly positively correlated to the concentration of acetic acid extractable strontium (Figure 99). In general, samples from lacustrine environments leached the highest mean concentration of ammonium acetate extractable strontium and barium, 32.96  $\mu\text{g/g}$  and 59.10  $\mu\text{g/g}$ , respectively (Figures 98 and 100). Meandering stream and lacustrine samples released a similar, high mean concentration of acetic acid extractable strontium, 22.55  $\mu\text{g/g}$  and 21.53  $\mu\text{g/g}$ , respectively (Figure 99).

#### 4.10 A Summary of the Sequential Extraction Results: The Relationship between Mineral Content, Grain Size, and the Concentration of Extractable Elements from the Deep River Basin

The results of the sequential extractions suggest the water-rock interactions in the Deep River basin are influenced by the mineralogy of a sample such as the presence or absence of clay minerals and/or carbonate minerals and grain size. For example, sedimentary samples from the Deep River basin with clay minerals such as smectite with a specific sheet-like structure (phyllosilicates) are likely to release more strontium and barium to solution than samples without clay minerals. Clay minerals have highly reactive sites and are important in the process of ion exchange (Grim, 1953; Tucker, 2001). Additionally, the geochemical analyses show fine-grained deposits such as mudstones and shales tend to release the highest average concentration of extractable strontium and barium compared to more coarse-grained deposits.

The geochemical data also suggest that quantity, affinity and/or solubility and leaching potential of strontium and barium may vary depending on the sub-basin as well

as the depositional environment of the Deep River basin (Figures 84 and 85). For example, the highest average cumulative concentration of extractable strontium and barium were leached from the Wadesboro sub-basin, whereas, the lowest average cumulative concentration of extractable strontium and barium were leached from the Sanford sub-basin. Furthermore, samples from lacustrine environments leached the highest mean concentration of ammonium acetate extractable strontium and barium. Meandering stream and lacustrine samples released similar, high concentrations of acetic acid extractable strontium compared to alluvial fan samples.

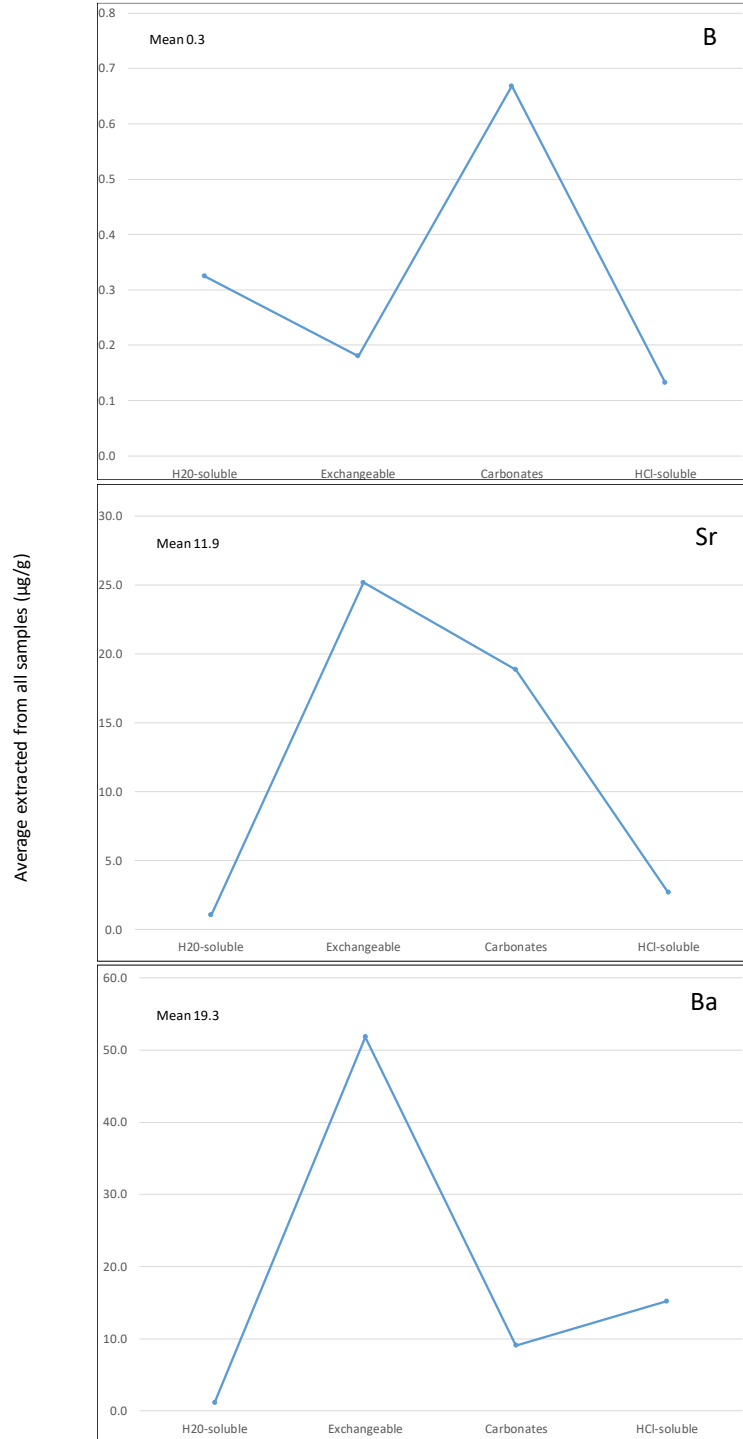


Figure 82: The average concentration of B, Sr, and Ba extracted by each extraction step from all of the samples in this study. Sequential extractions took place in the order shown (left to right). (n=183).

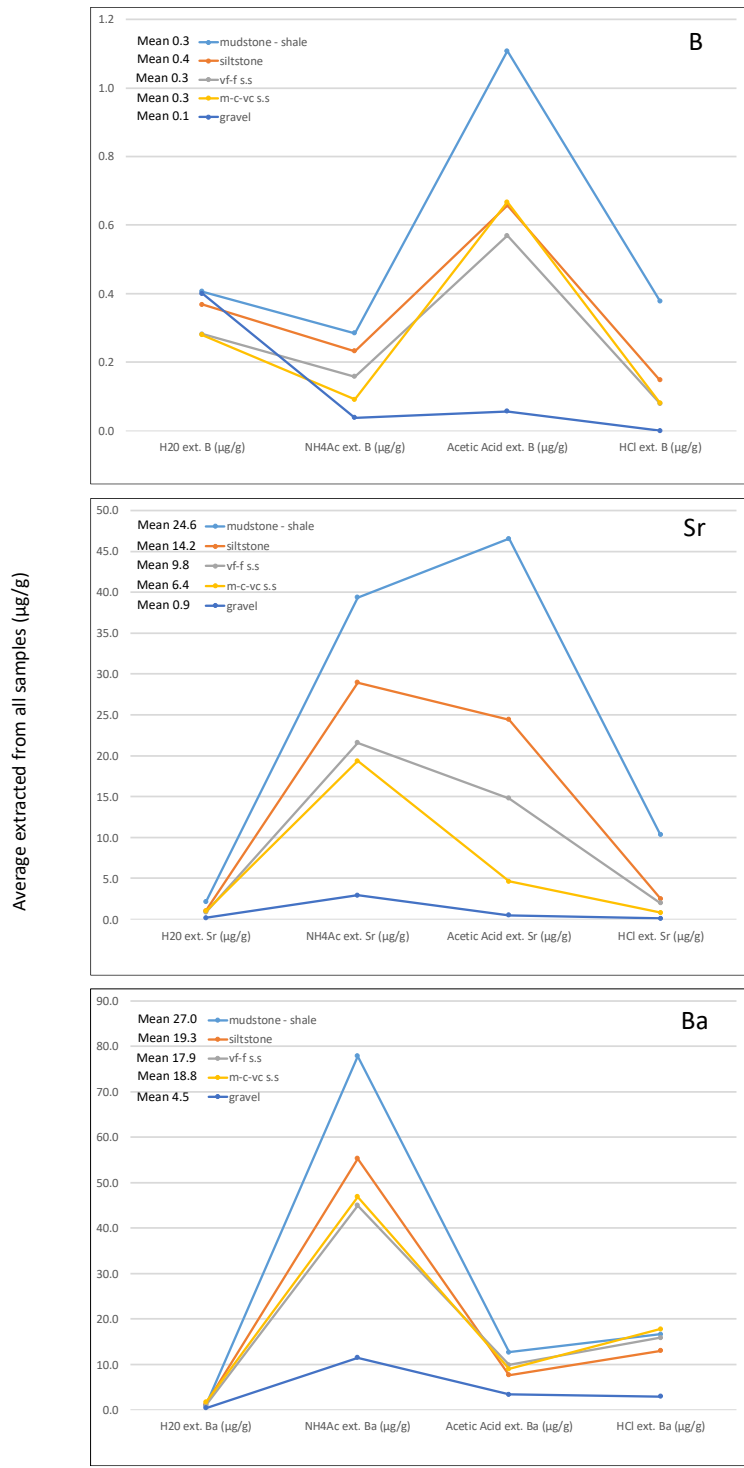


Figure 83: The average concentration of B, Sr, and Ba extracted by each extraction step from all of the samples in this study organized by the grain size of the sample. Sequential extractions took place in the order shown (left to right). (n=183)

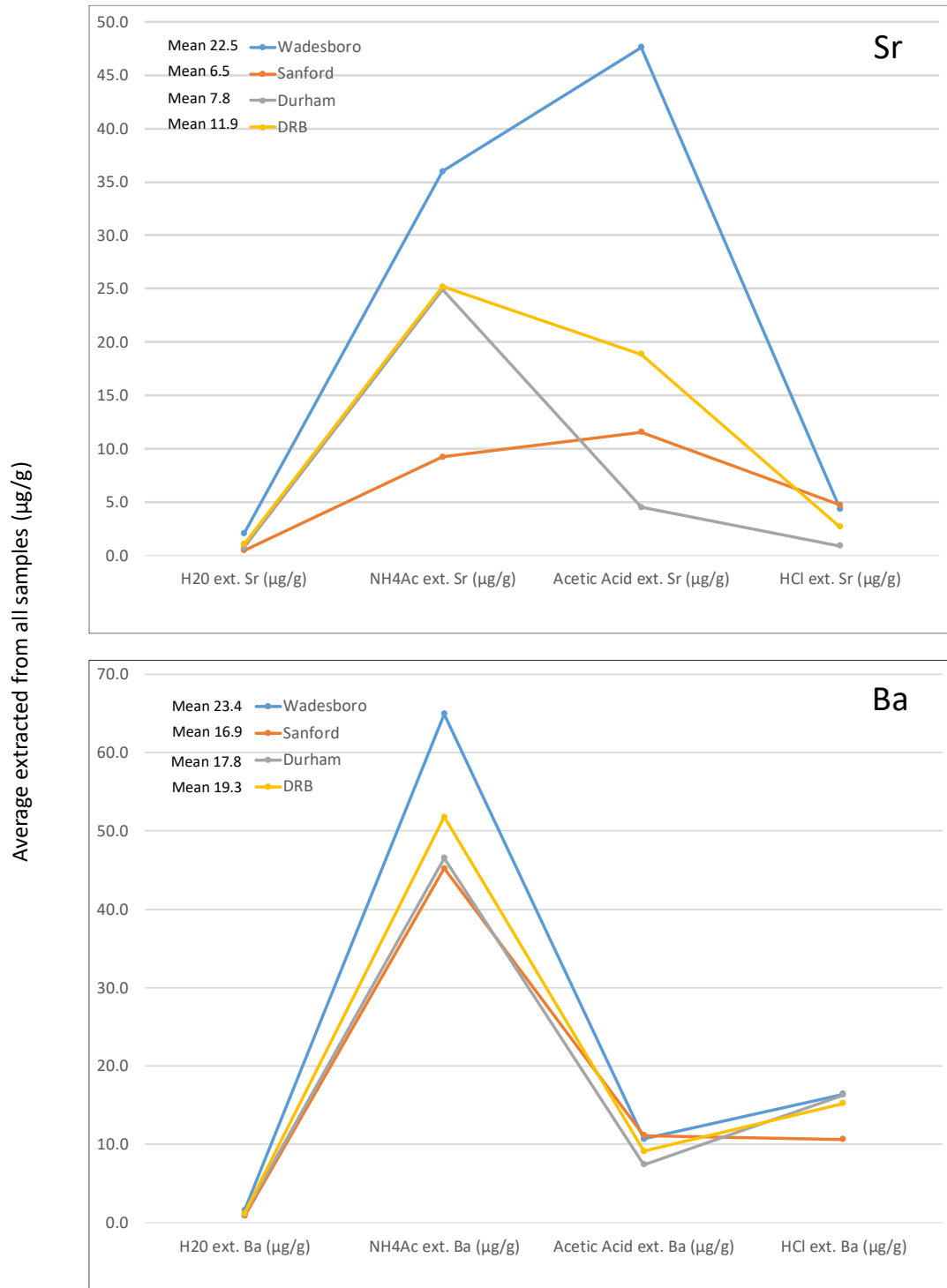


Figure 84: The average concentration of Sr and Ba extracted by each extraction step from all of the samples in this study (represented by the DRB). The data were also organized according to the appropriate sub-basin for the sample. Sequential extractions took place in the order shown (left to right). (n=183)

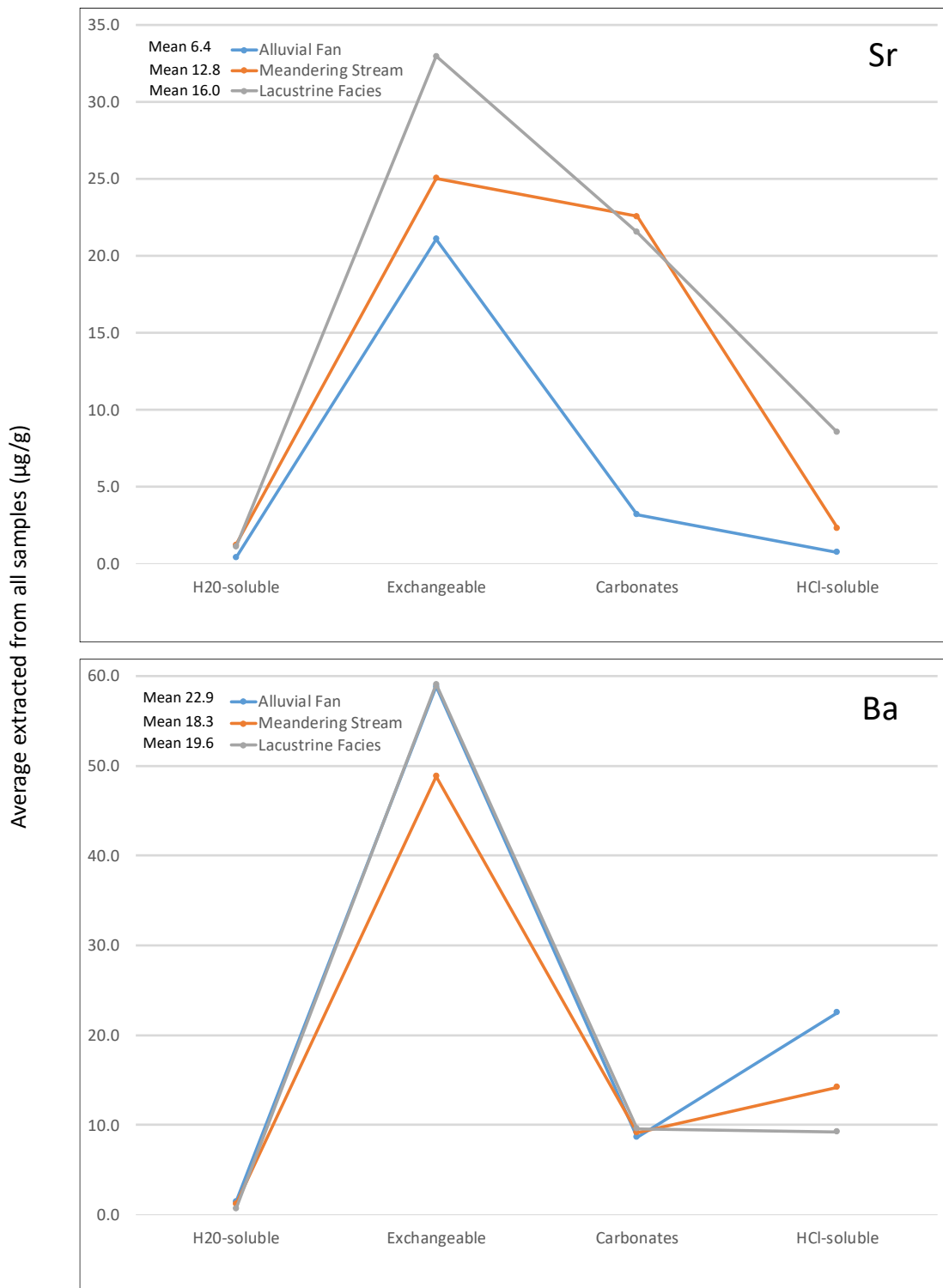


Figure 85: The average concentration of Sr and Ba extracted by each extraction step from all of the samples from this study organized by depositional environment. Sequential extractions took place in the order shown (left to right). (n=183)

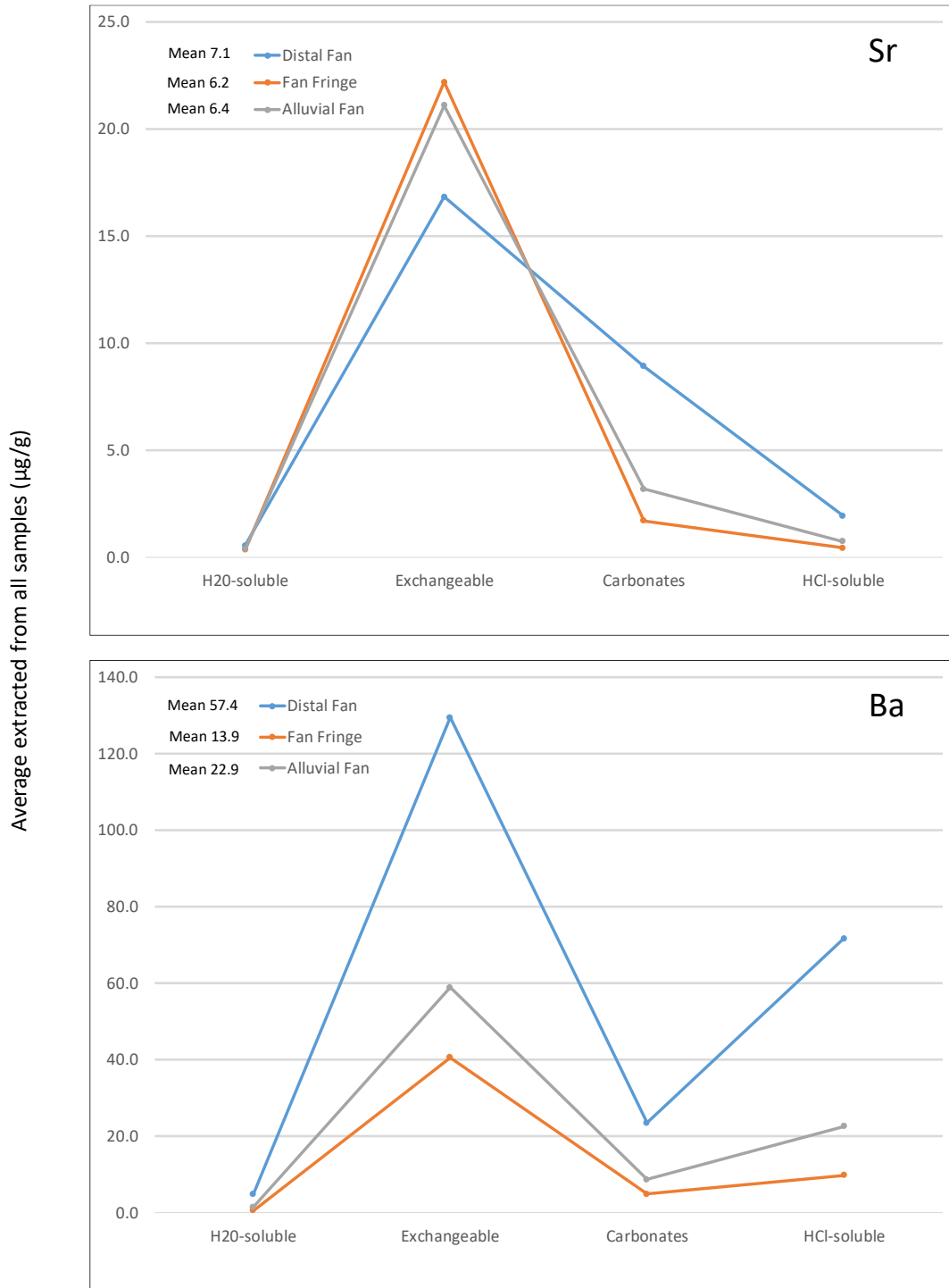


Figure 86: The average concentration of Sr and Ba extracted by each extraction step from samples from an alluvial fan environment. The alluvial fan samples were also organized by appropriate sub-environment. Sequential extractions took place in the order shown (left to right). (n=34)

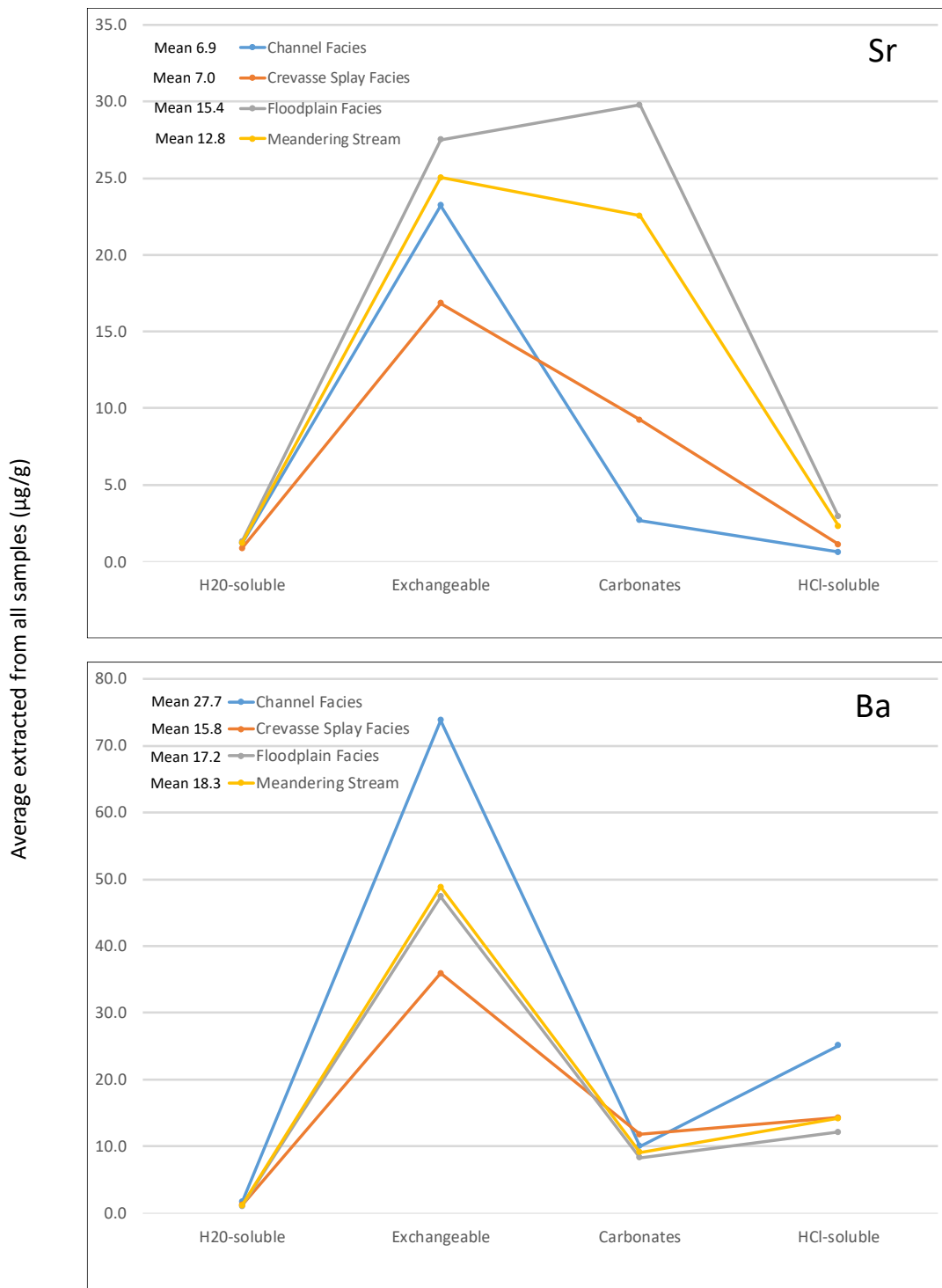


Figure 87: The average concentration of Sr and Ba extracted by each extraction step from samples from a meandering stream environment. The meandering stream samples were also organized by sub-environment. Sequential extractions took place in the order shown (left to right). (n=129)

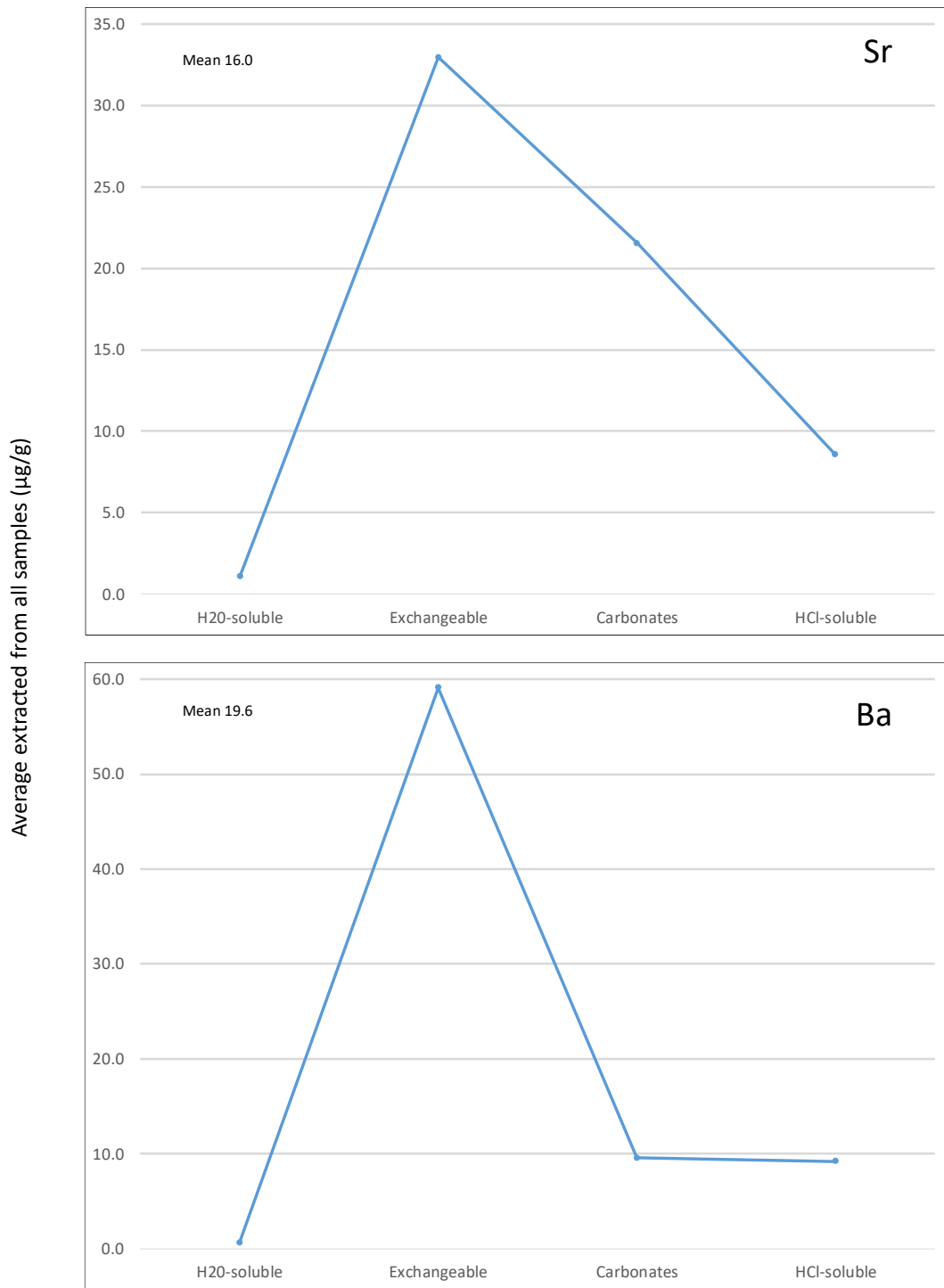


Figure 88: The average concentration of B, Sr, and Ba extracted by each extraction step from samples from a lacustrine environment. Sequential extractions took place in the order shown (left to right). (n=20)

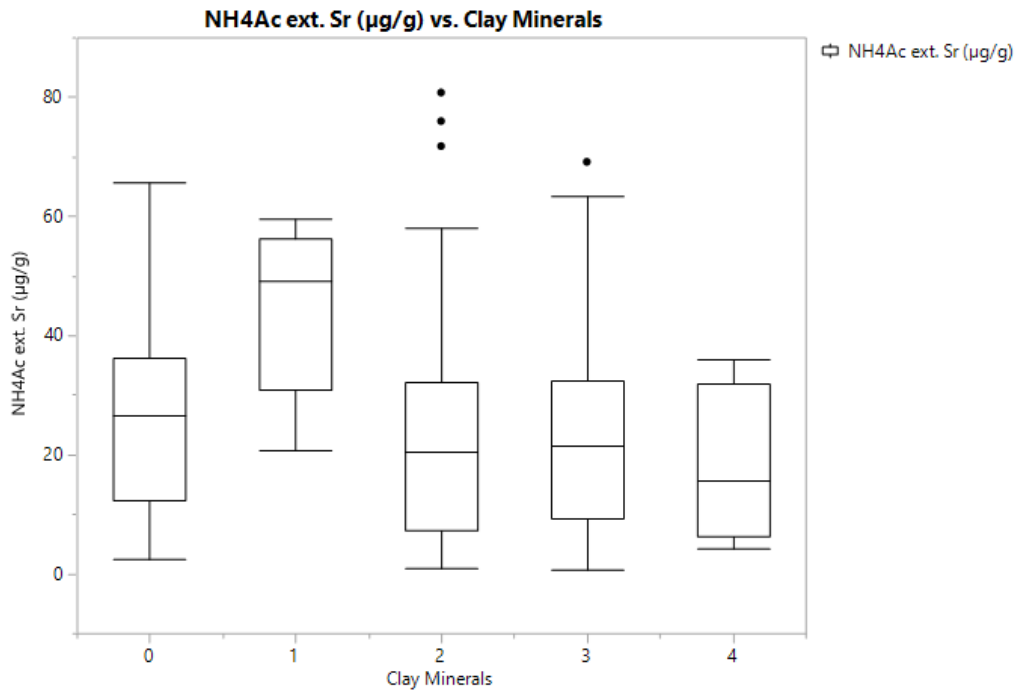
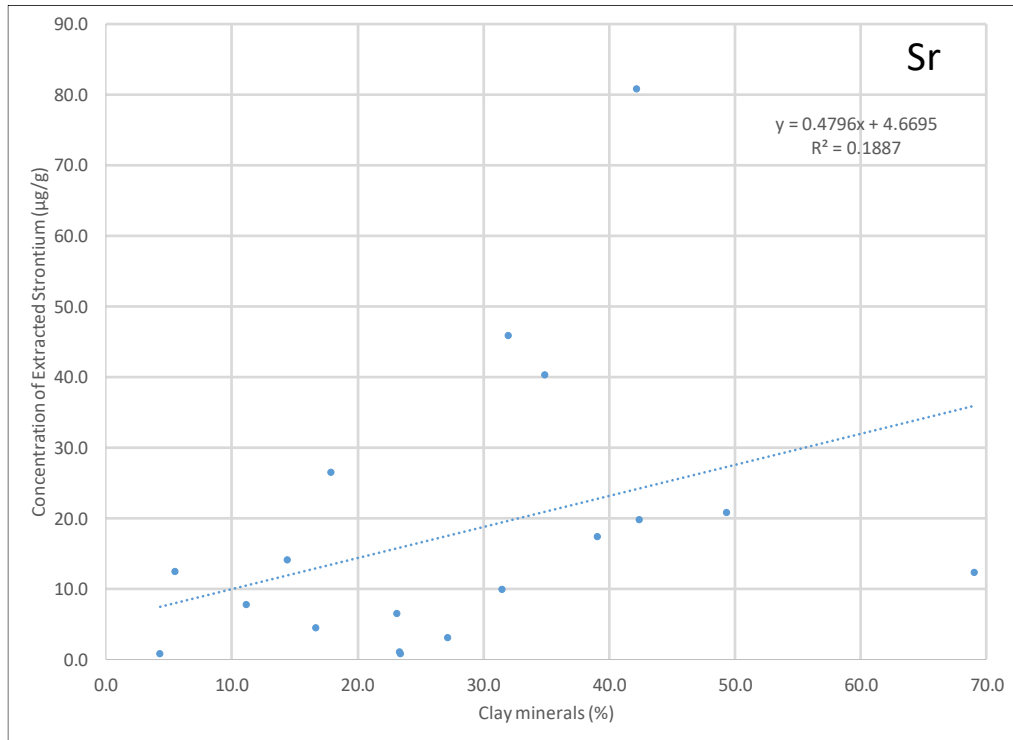


Figure 89: The concentration of ammonium acetate extracted strontium compared to the abundance of clay minerals based on petrographic analysis (top figure) and XRD (lower figure).

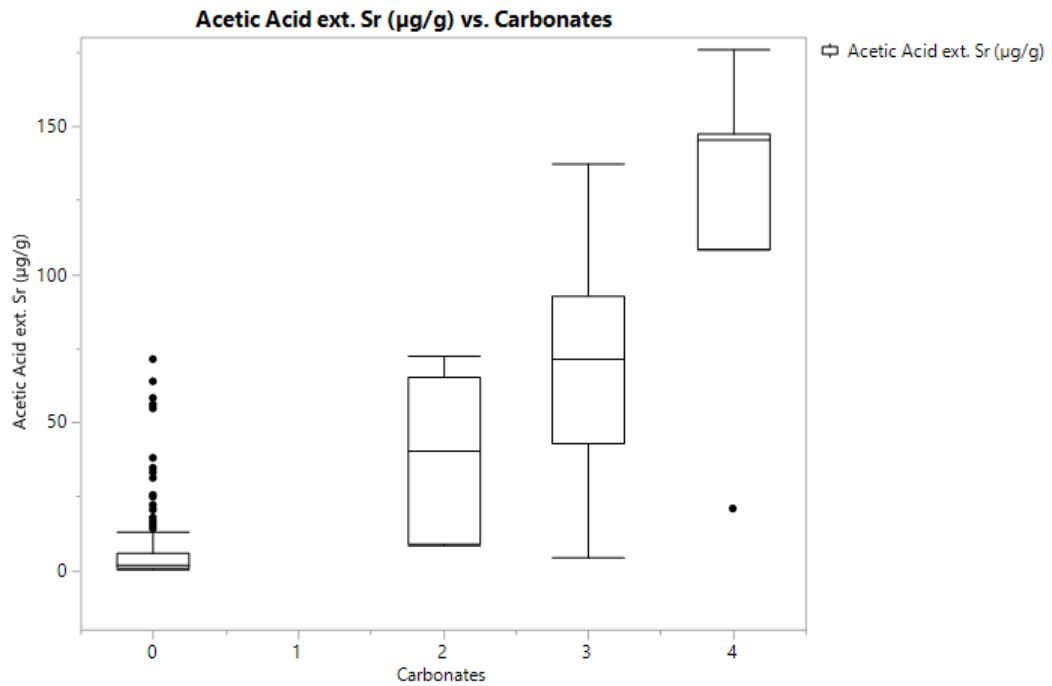
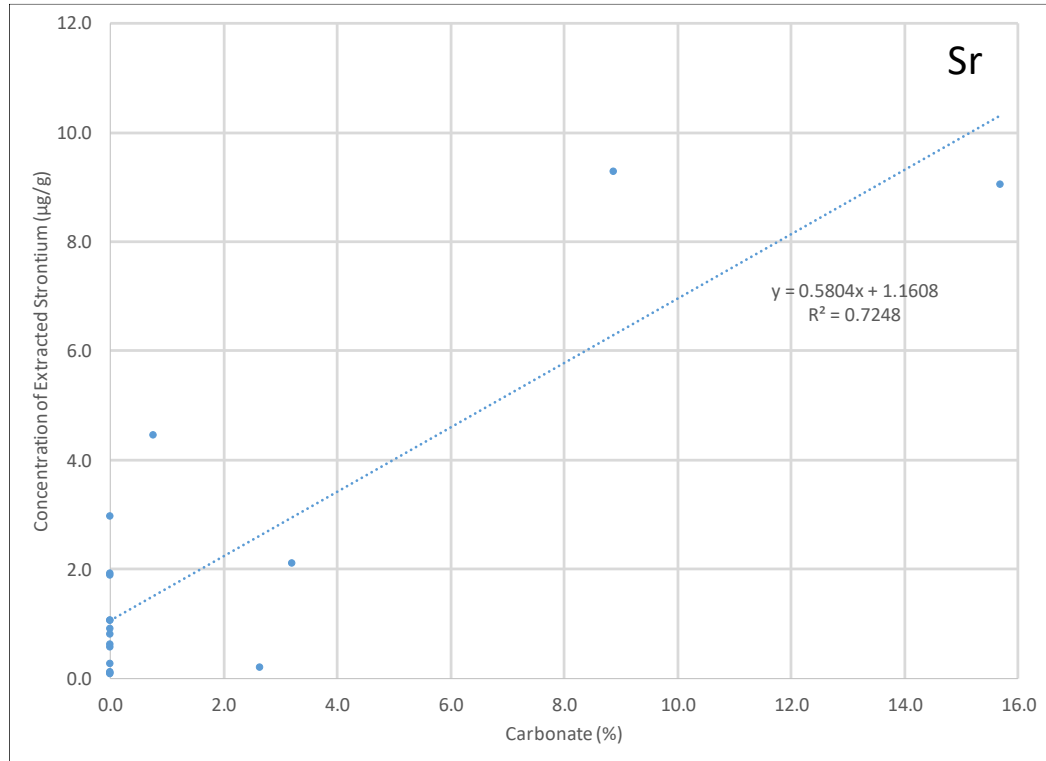


Figure 90: The concentration of acetic acid extracted strontium compared to the abundance of carbonate minerals based on petrographic analysis (top figure) and XRD (lower figure).

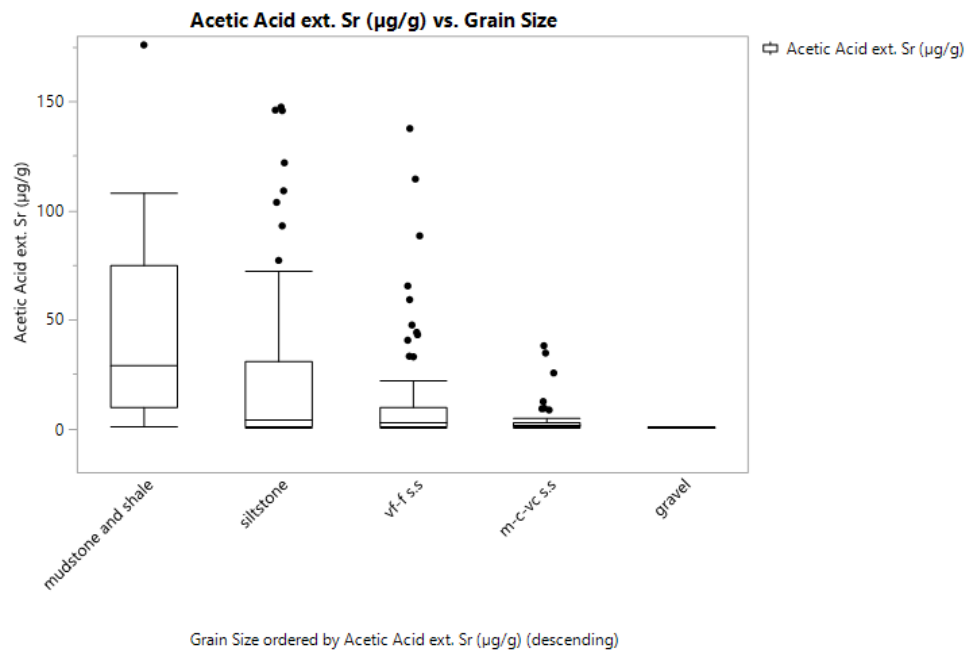
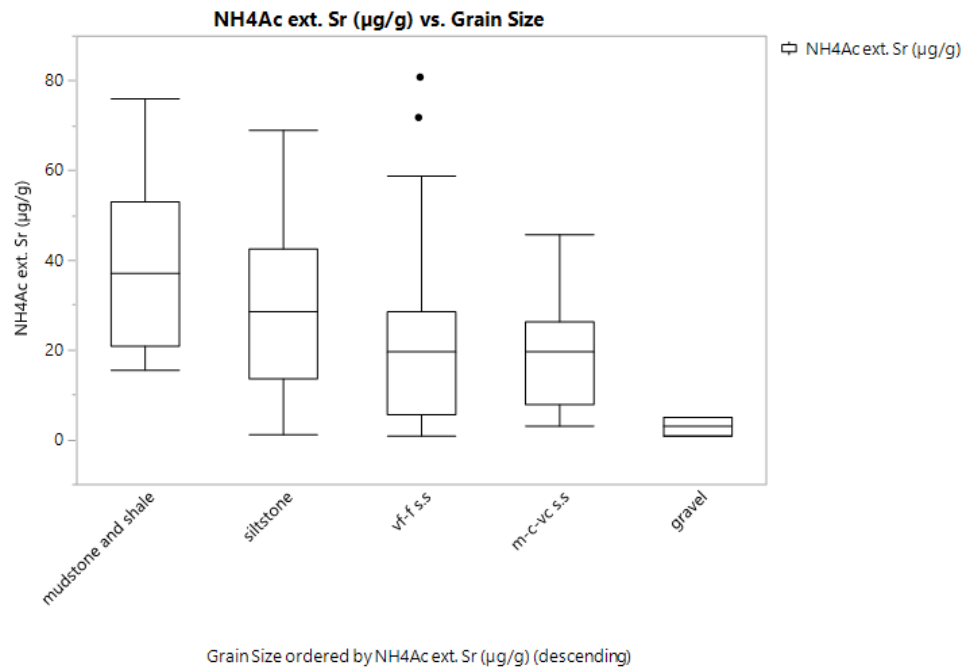


Figure 91: The range and median concentration of ammonium acetate extracted strontium based on grain size (top) and the range and mean concentration of acetic acid extracted strontium based on grain size (bottom).

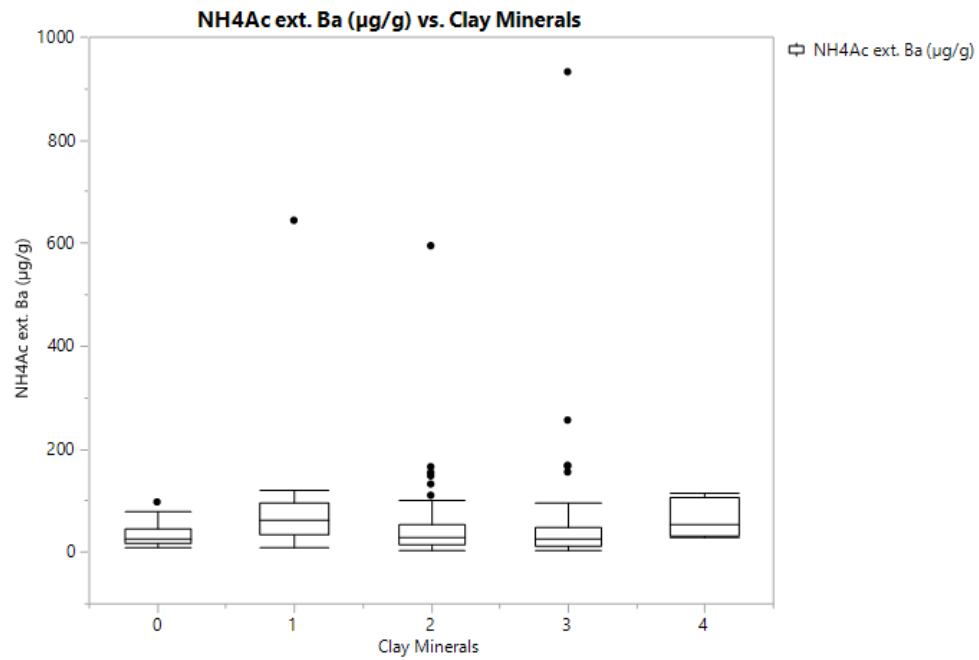
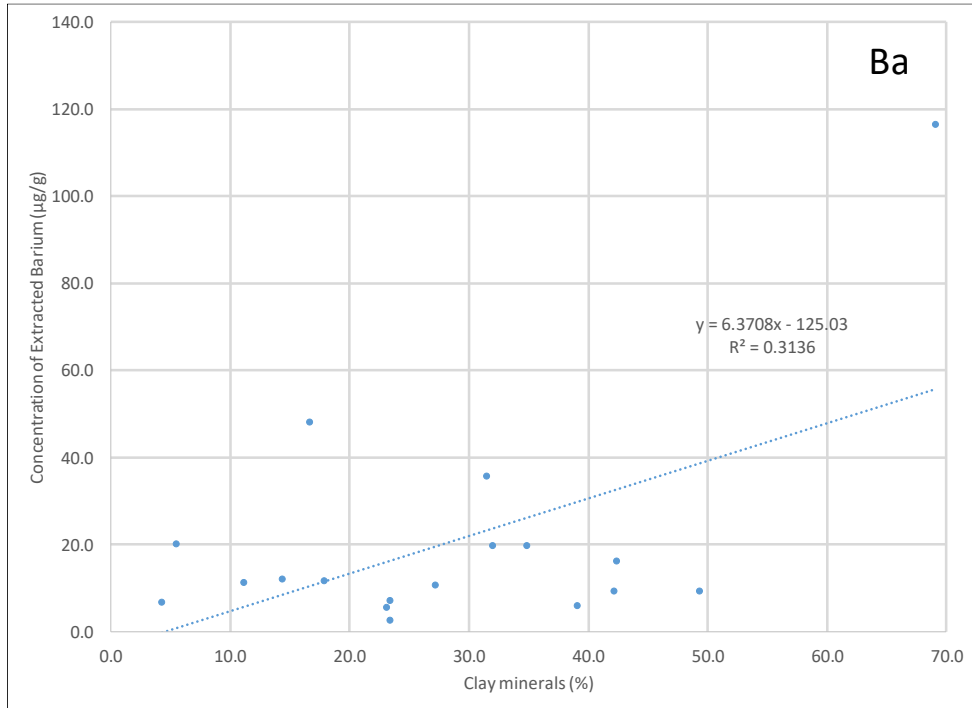


Figure 92: The concentration of ammonium acetate extracted barium compared to the abundance of clay minerals based on petrographic analysis (top figure) and XRD (lower figure).

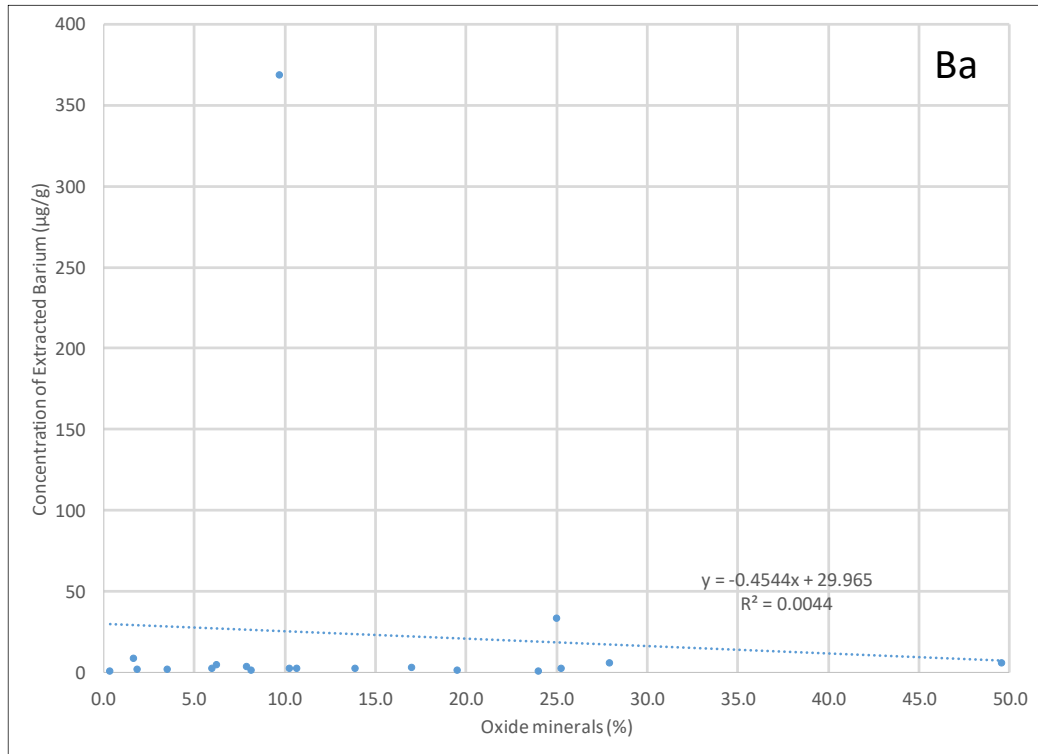
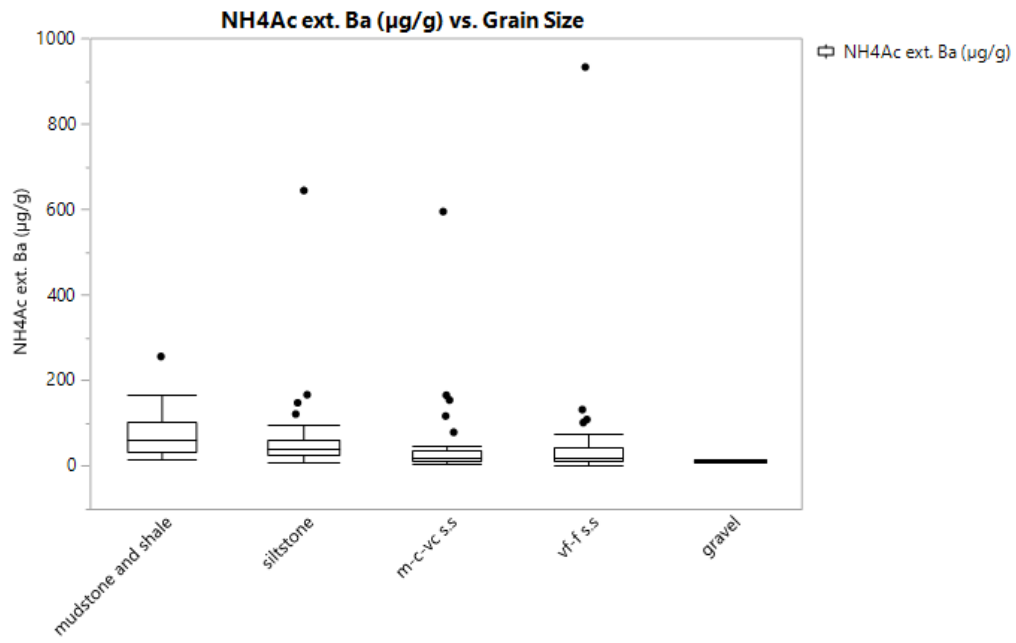
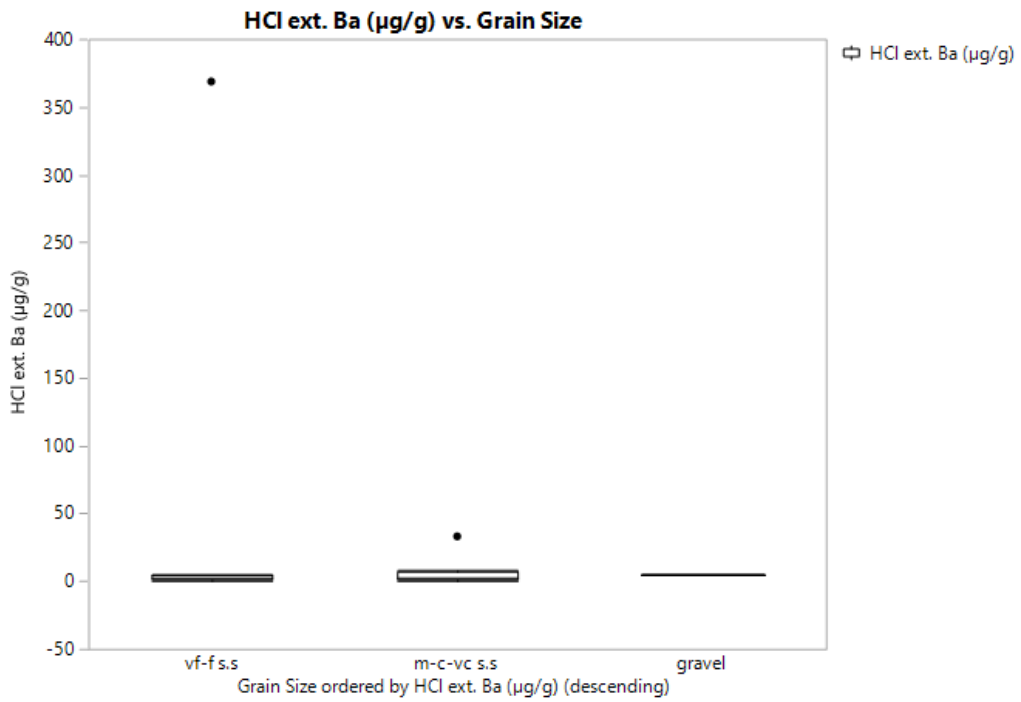


Figure 93: The concentration of hydrochloric acid extracted barium compared to the abundance of oxide minerals based on petrographic analysis.



Grain Size ordered by NH4Ac ext. Ba (µg/g) (descending)



Grain Size ordered by HCl ext. Ba (µg/g) (descending)

Figure 94: The concentration of ammonium acetate extracted barium based on grain size (top) and the concentration of HCl-extracted barium based on grain size based on petrographic analyses (bottom).

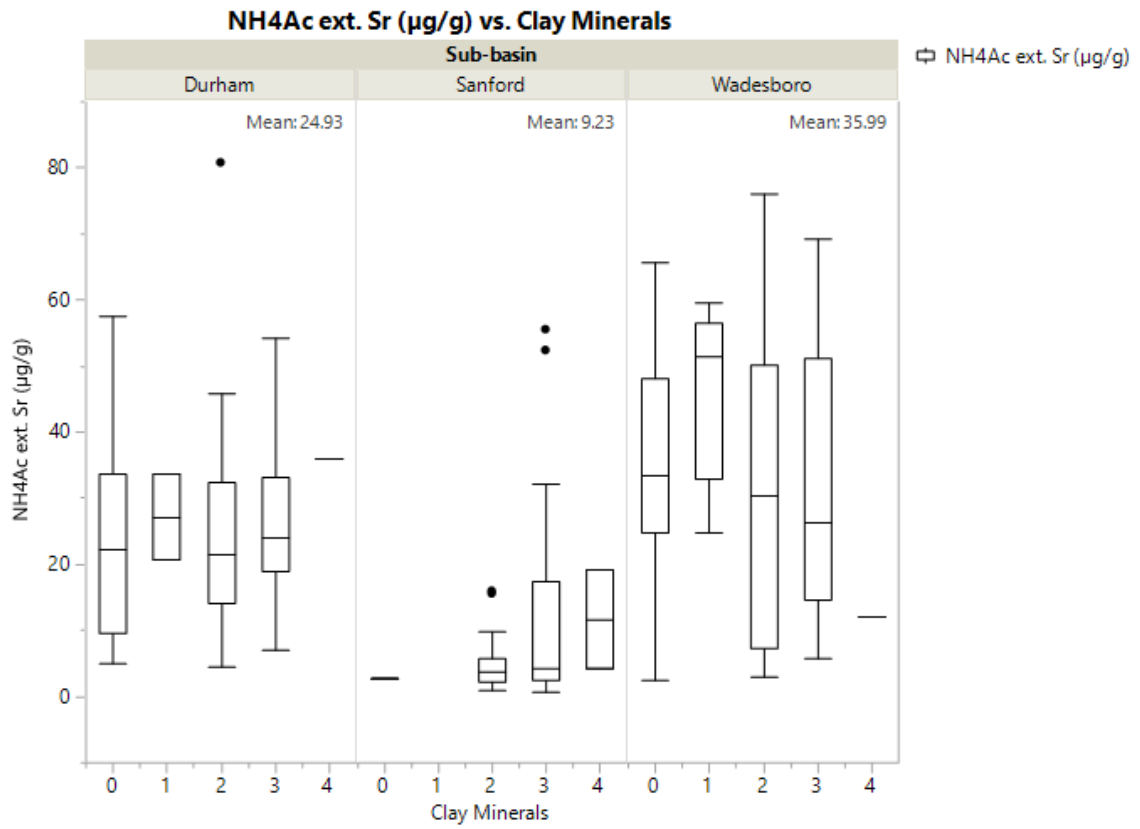


Figure 95: The range and median concentration of ammonium acetate extracted strontium compared to the abundance of clay minerals in each of the sub-basins of the Deep River basin.

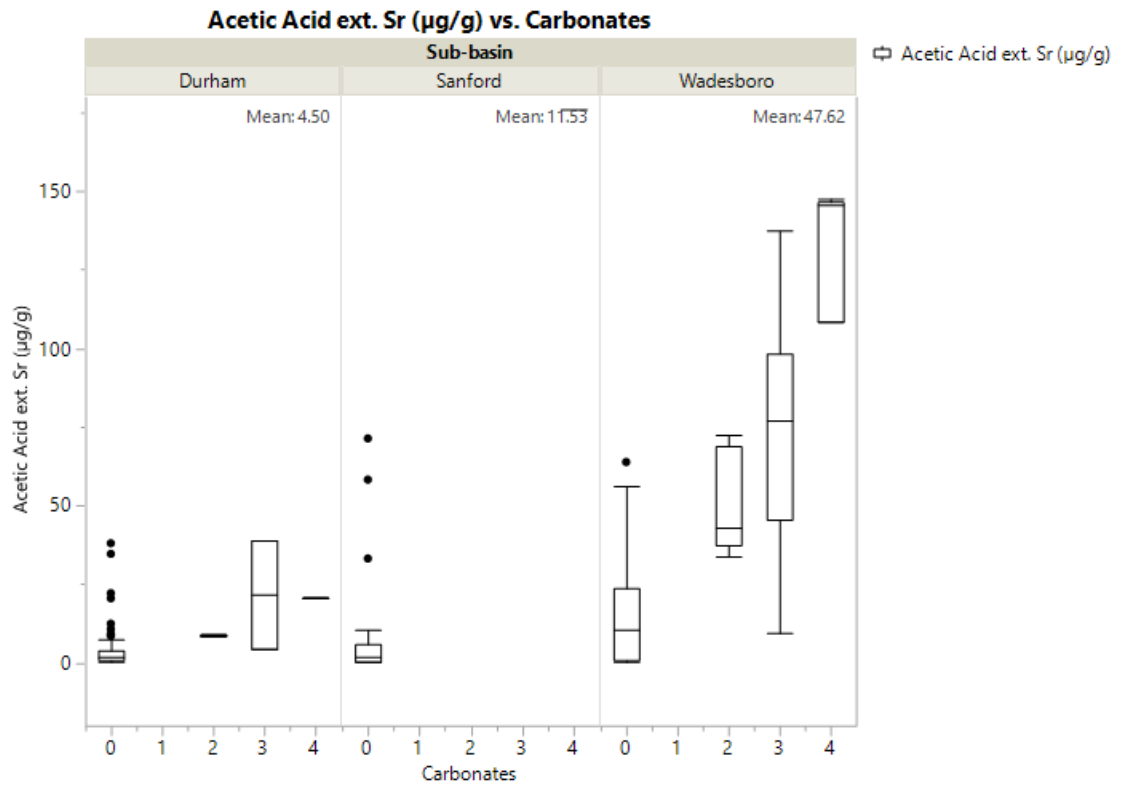


Figure 96: The range and median concentration of acetic acid extracted strontium compared to the relative abundance of carbonate minerals in each of the sub-basins of the Deep River basin.

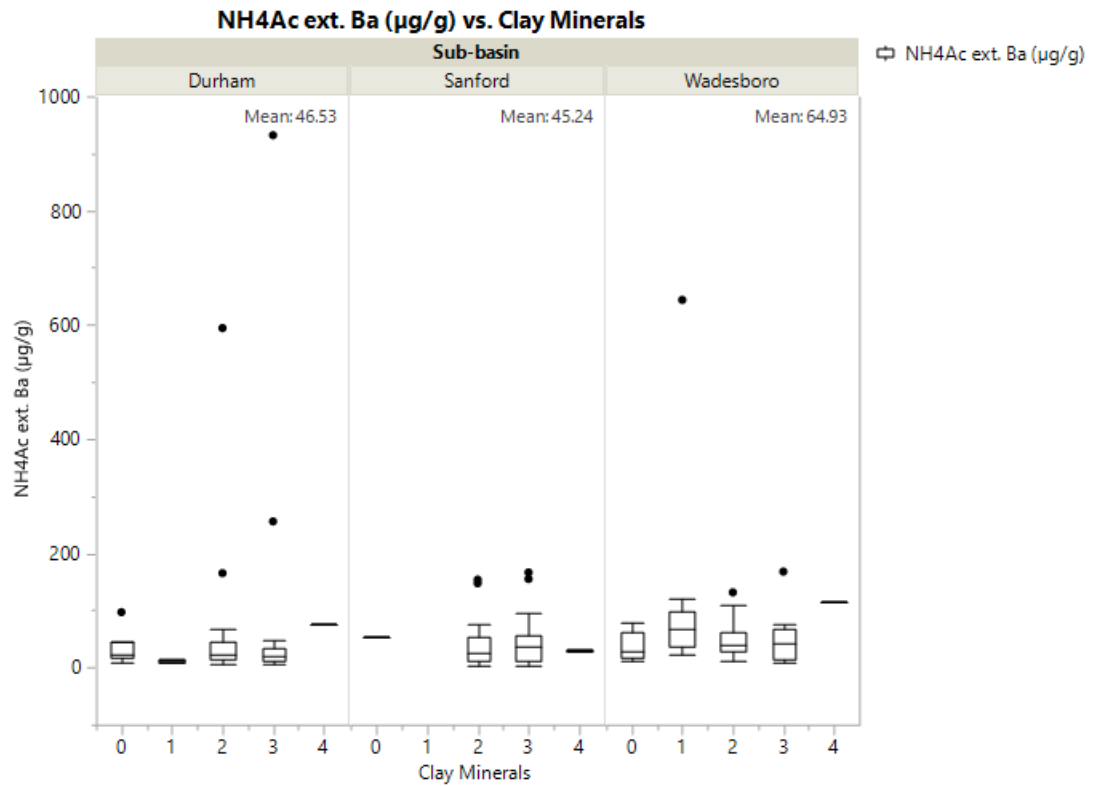


Figure 97: The range and median concentration of ammonium acetate extracted barium compared to the relative abundance of clay minerals in each of the sub-basins of the Deep River basin.

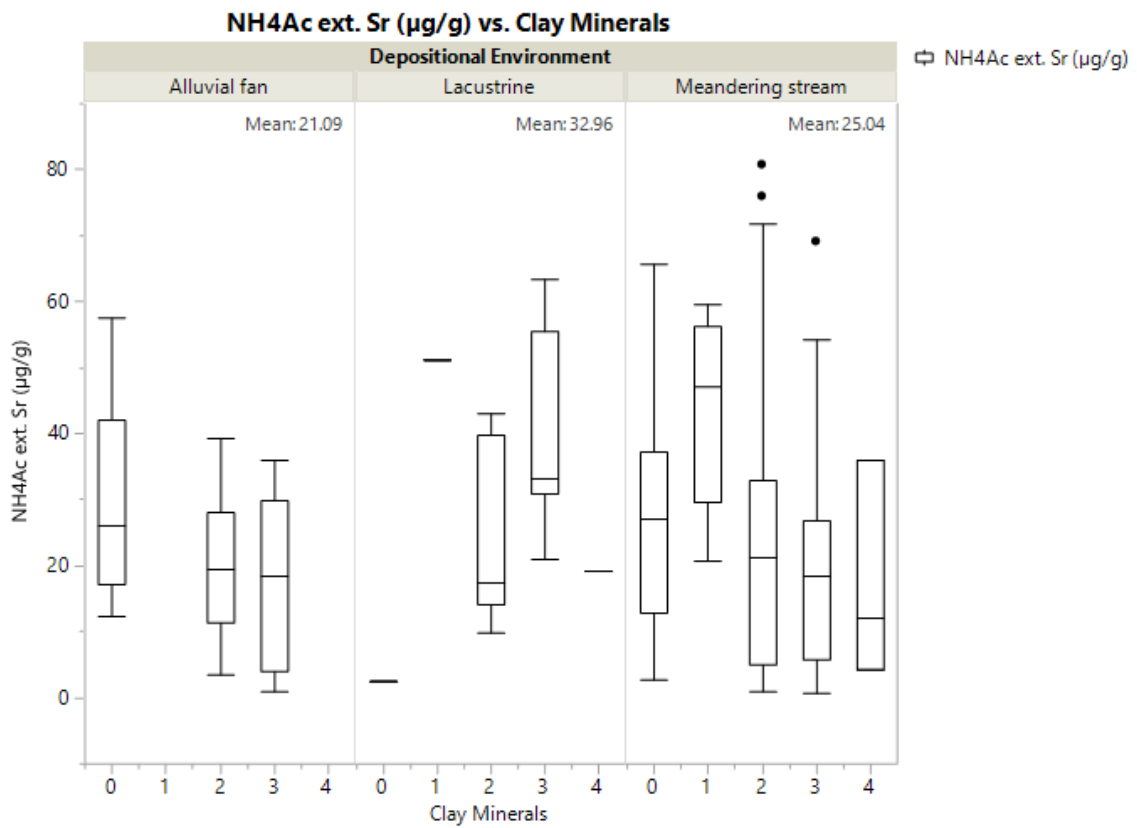


Figure 98: The range and median concentration of ammonium acetate extracted strontium compared to the relative abundance of clay minerals for the depositional environments of the Deep River basin.

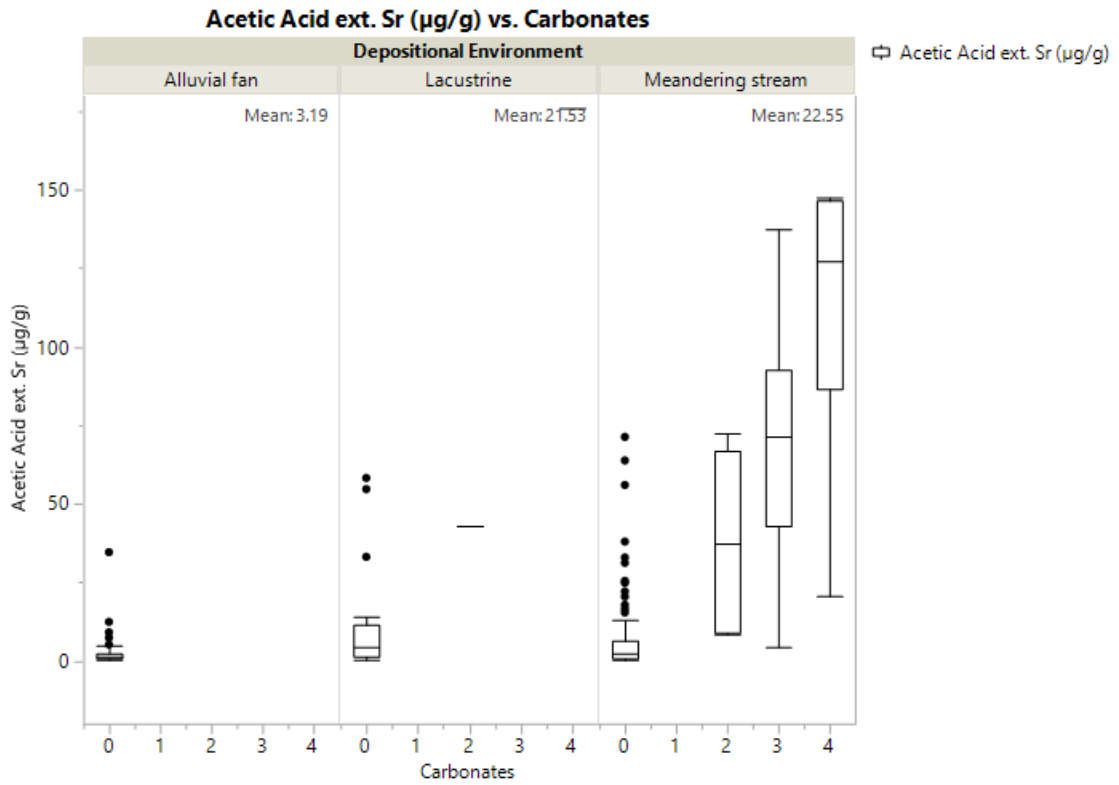


Figure 99: The range and median concentration of acetic acid extracted strontium compared to the relative abundance of carbonate minerals for the depositional environments of the Deep River basin.

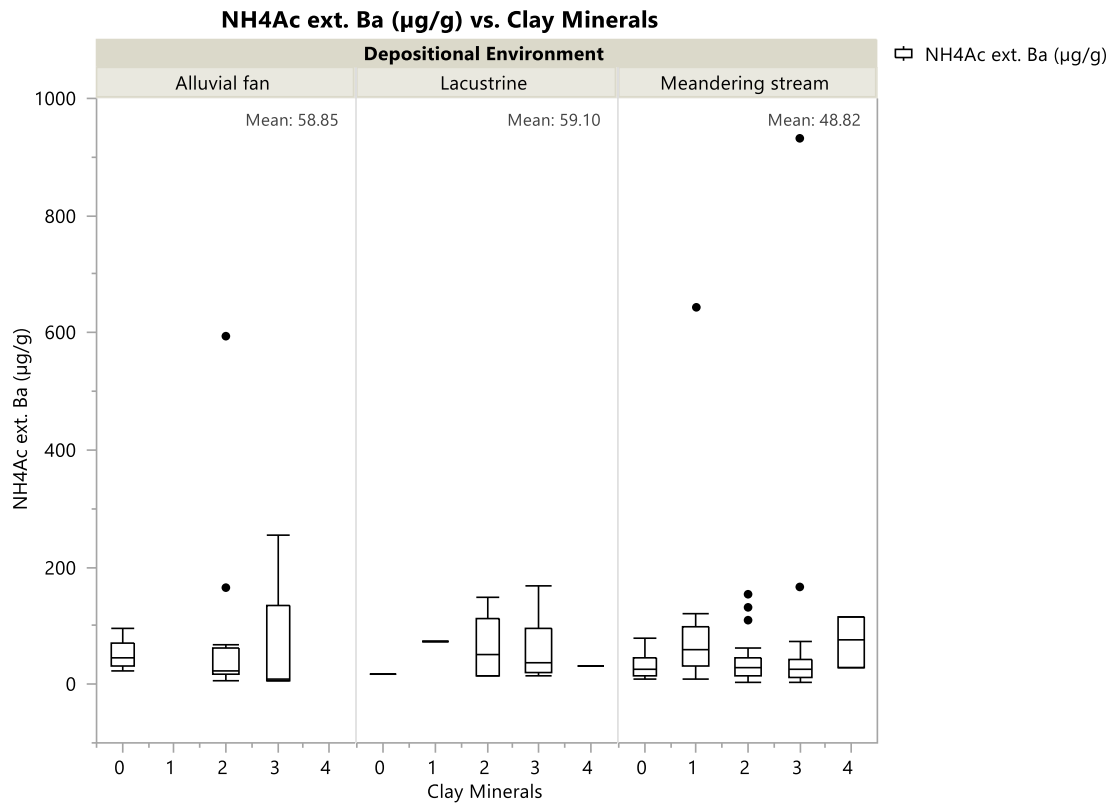


Figure 100: The range and median concentration of ammonium acetate extracted barium compared to the relative abundance of clay minerals for the depositional environments of the Deep River basin.

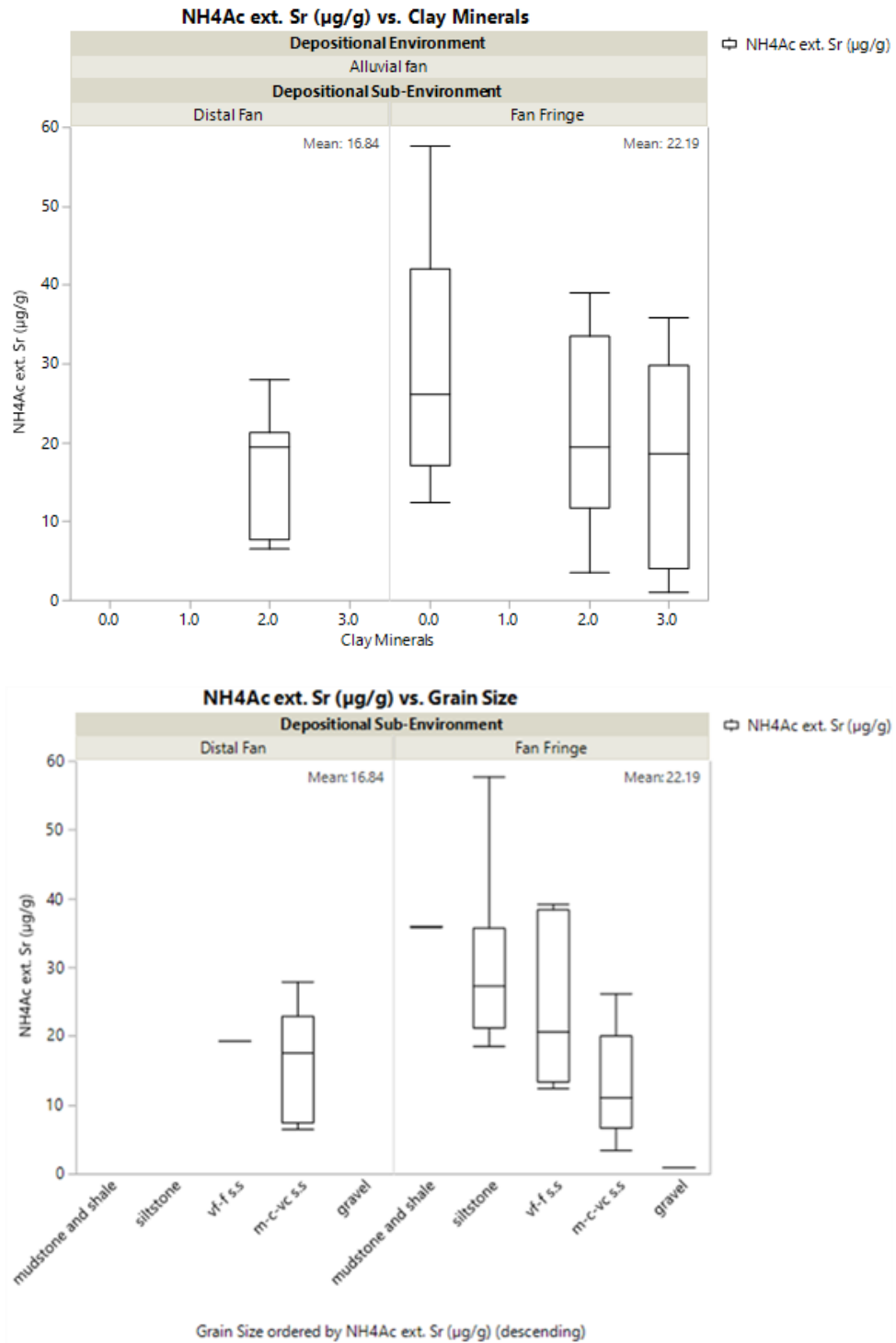


Figure 101: The range and median concentration of ammonium acetate extracted strontium compared to the relative abundance of clay minerals (top) and grain size (bottom) for alluvial fan sub-environments. Note: the grain sizes are organized by descending concentrations of extractable strontium.

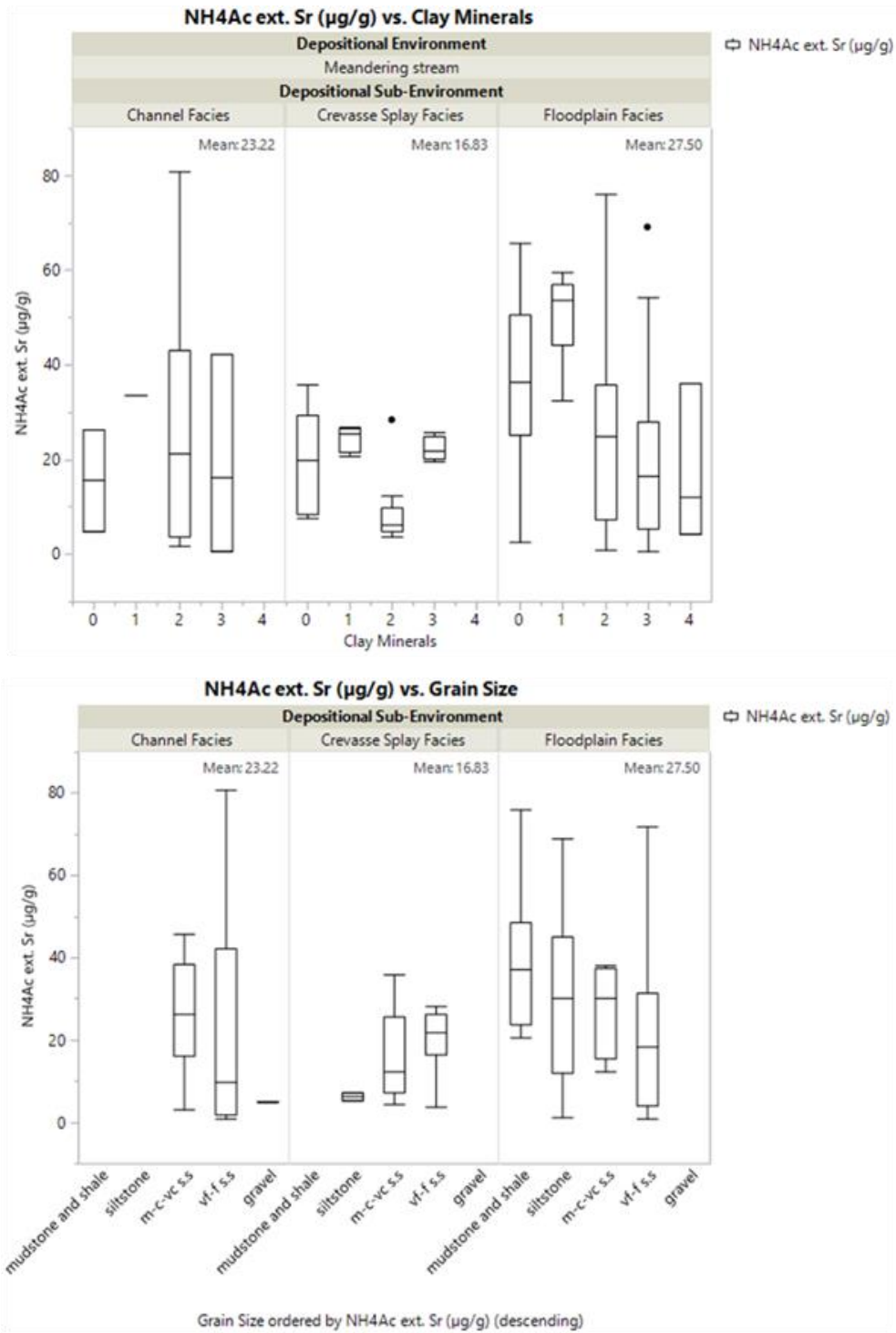


Figure 102: The range and median concentration of acetic acid extracted strontium compared to the relative abundance of carbonate minerals (top) and grain size (bottom) for meandering stream sub-environments. Note: the grain sizes are organized by descending concentrations of extractable strontium.

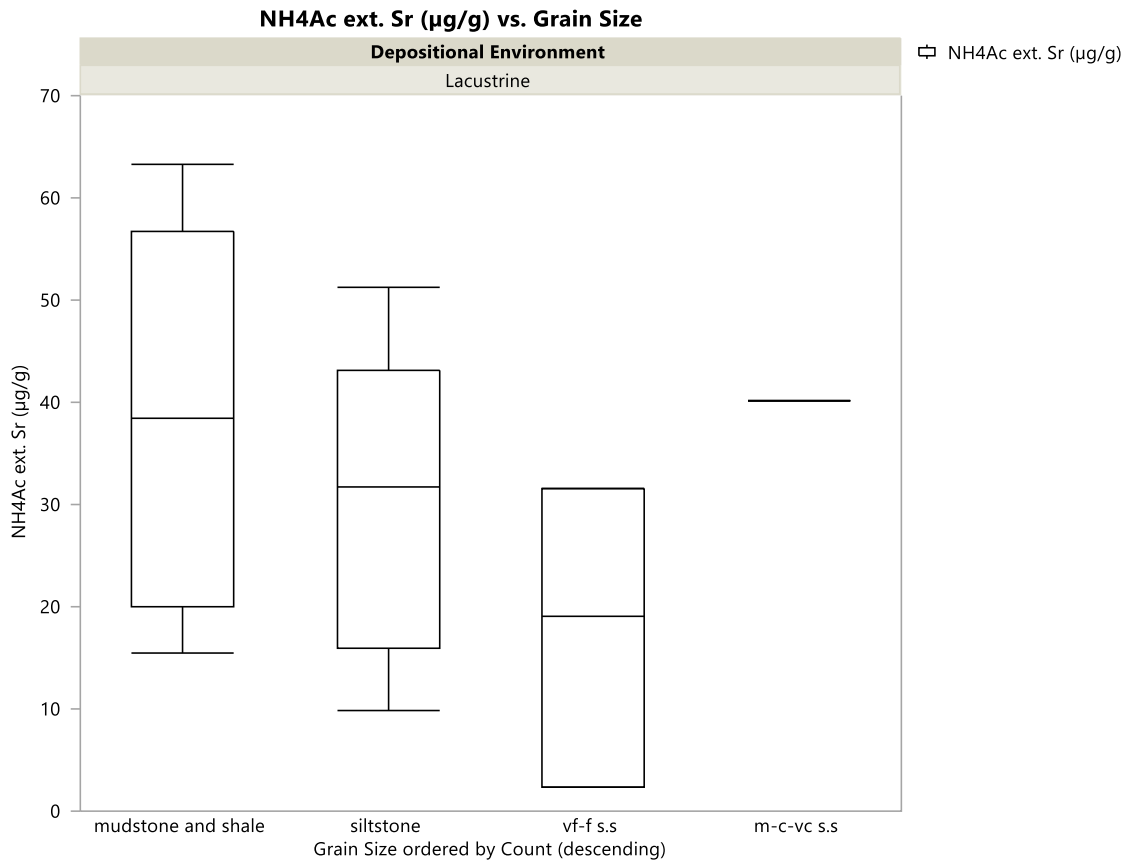


Figure 103: The range and median concentration of ammonium acetate extracted strontium compared to grain size in lacustrine environments. Note: the grain sizes are organized by number of samples (n) from each grain size.

Table 33: The average concentration of B, Sr, and Ba extracted from all steps of the sequential extractions from all of the samples organized by sub-basin. Sequential extractions took place in the order show (left to right).

<b>Sub-basin/basin</b>	<b>Average Extractable B (µg/g)</b>	<b>Average Extractable Sr (µg/g)</b>	<b>Average Extractable Ba (µg/g)</b>
Wadesboro	0.5	22.5	23.4
Sanford	0.2	6.5	16.9
Durham	0.2	7.8	17.8
Deep River Basin	0.3	11.9	19.3

Table 34: The average concentration of B, Sr, and Ba extracted by each extraction step from all of the samples in this study (represented by the DRB). The geochemical data were also organized according to the appropriate sub-basin for the sample. The column ‘n’ represents the number of samples classified in each sub-basin.

Sub-basin/basin	n	H2O ext. B (µg/g)	NH4Ac ext. B (µg/g)	Acetic Acid ext. B (µg/g)	HCl ext. B (µg/g)	H2O ext. Sr (µg/g)	NH4Ac ext. Sr (µg/g)	Acetic Acid ext. Sr (µg/g)	HCl ext. Sr (µg/g)	H2O ext. Ba (µg/g)	NH4Ac ext. Ba (µg/g)	Acetic Acid ext. Ba (µg/g)	HCl ext. Ba (µg/g)
Wadesboro	55	0.5	0.5	0.9	0.2	2.0	36.0	47.6	4.4	1.6	64.9	10.6	16.4
Sanford	36	0.4	0.1	0.3	0.2	0.4	9.2	11.5	4.7	0.8	45.2	11.1	10.6
Durham	92	0.2	0.0	0.7	0.1	0.7	24.9	4.5	0.9	1.0	46.5	7.4	16.3
DRB	183	0.3	0.2	0.7	0.1	1.0	25.2	18.8	2.7	1.2	51.8	9.1	15.2

Table 35: The average concentration of B, Sr, and Ba extracted from all steps of the sequential extractions from all of the samples organized by grain size. Sequential extractions took place in the order show (left to right).

<b>Grain Size</b>	<b>Average Extractable B (<math>\mu\text{g/g}</math>)</b>	<b>Average Extractable Sr (<math>\mu\text{g/g}</math>)</b>	<b>Average Extractable Ba (<math>\mu\text{g/g}</math>)</b>
mudstone - shale	0.5	24.6	27.0
siltstone	0.4	14.2	19.3
vf-f s.s	0.3	9.8	17.9
m-c-vc s.s	0.3	6.4	18.8
gravel	0.1	0.9	4.5

Table 36: The average concentration of B, Sr, and Ba extracted by each extraction step from all of the samples in this study organized by the grain size of the sample. Sequential extractions took place in the order show (left to right). The column 'n' represents the number of samples classified in each grain size category.

Grain Size	n	H2O ext. B (µg/g)	NH4Ac ext. B (µg/g)	Acetic Acid ext. B (µg/g)	HCl ext. B (µg/g)	H2O ext. Sr (µg/g)	NH4Ac ext. Sr (µg/g)	Acetic Acid ext. Sr (µg/g)	HCl ext. Sr (µg/g)	H2O ext. Ba (µg/g)	NH4Ac ext. Ba (µg/g)	Acetic Acid ext. Ba (µg/g)	HCl ext. Ba (µg/g)
mudstone - shale	18	0.4	0.3	1.1	0.4	2.1	39.4	46.5	10.3	1.0	77.9	12.7	16.6
siltstone	63	0.4	0.2	0.7	0.1	1.0	28.9	24.4	2.5	1.2	55.3	7.6	13.0
vf-f s.s	60	0.3	0.2	0.6	0.1	0.8	21.6	14.8	2.0	0.9	44.9	9.9	15.8
m-c-vc s.s	40	0.3	0.1	0.7	0.1	1.0	19.3	4.6	0.8	1.6	46.9	9.0	17.7
gravel	2	0.4	0.0	0.1	0.0	0.2	2.9	0.5	0.1	0.4	11.4	3.3	2.9

Table 37: The average concentration of B, Sr, and Ba extracted from all steps of the sequential extractions from all of the samples from this study organized by depositional environment. Sequential extractions took place in the order shown (left to right). (n=183)

<b>Depositional Environment</b>	<b>Average Extractable B (<math>\mu\text{g/g}</math>)</b>	<b>Average Extractable Sr (<math>\mu\text{g/g}</math>)</b>	<b>Average Extractable Ba (<math>\mu\text{g/g}</math>)</b>
Alluvial Fan	0.2	6.4	22.9
Meandering Stream	0.3	12.8	18.3
Lacustrine	0.4	16.0	19.6

Table 38: The average concentration of B, Sr, and Ba extracted by each extraction step from all of the samples from this study organized by depositional environment. Sequential extractions took place in the order shown (left to right). (n=183). The column ‘n’ represents the number of samples classified in each depositional environment.

Depositional Environment	n	H2O	NH4Ac	Acetic	HCl	H2O	NH4Ac	Acetic	HCl	H2O	NH4Ac	Acetic	HCl
		ext. B (µg/g)	ext. B (µg/g)	ext. B (µg/g)	ext. B (µg/g)	ext. Sr (µg/g)	ext. Sr (µg/g)	ext. Sr (µg/g)	ext. Sr (µg/g)	ext. Ba (µg/g)	ext. Ba (µg/g)	ext. Ba (µg/g)	ext. Ba (µg/g)
Alluvial Fan	34	0.2	0.1	0.6	0.1	0.4	21.1	3.2	0.7	1.4	58.8	8.6	22.5
Meandering Stream	129	0.4	0.2	0.7	0.1	1.2	25.0	22.6	2.3	1.2	48.8	9.1	14.2
Lacustrine	20	0.3	0.2	0.7	0.3	1.1	33.0	21.5	8.5	0.6	59.1	9.6	9.2

Table 39: The average concentration of B, Sr, and Ba extracted from all steps of the sequential extractions from samples from an alluvial fan environment. The alluvial fan samples were also organized by appropriate sub-environment.

<b>Depositional Environment</b>	<b>Average Extractable B (<math>\mu\text{g/g}</math>)</b>	<b>Average Extractable Sr (<math>\mu\text{g/g}</math>)</b>	<b>Average Extractable Ba (<math>\mu\text{g/g}</math>)</b>
Distal Fan	0.6	7.1	57.4
Fan Fringe	0.2	6.2	13.9
Alluvial Fan	0.2	6.4	22.9

Table 40: The average concentration of B, Sr, and Ba extracted by each extraction step from samples from an alluvial fan environment. The alluvial fan samples were also organized by sub-environment. Sequential extractions took place in the order shown (left to right). The column ‘n’ represents the number of samples classified in each depositional environment.

Depositional Environment	n	H2O	NH4Ac	Acetic Acid	HCl	H2O	NH4Ac	Acetic Acid	HCl	H2O	NH4Ac	Acetic Acid	HCl
		ext. B (µg/g)	ext. B (µg/g)	ext. B (µg/g)	ext. B (µg/g)	ext. Sr (µg/g)	ext. Sr (µg/g)	ext. Sr (µg/g)	ext. Sr (µg/g)	ext. Ba (µg/g)	ext. Ba (µg/g)	ext. Ba (µg/g)	ext. Ba (µg/g)
Distal Fan	7	0.2	0.0	2.0	0.2	0.5	16.8	8.9	1.9	4.8	129.5	23.4	71.7
Fan Fringe	27	0.2	0.1	0.2	0.1	0.3	22.2	1.7	0.4	0.6	40.5	4.8	9.8
<i>Overall depositional environment:</i>													
Alluvial Fan	34	0.2	0.1	0.6	0.1	0.4	21.1	3.2	0.7	1.4	58.8	8.6	22.5

Table 41: The average concentration of B, Sr, and Ba extracted from all steps of the sequential extractions from samples from a meandering stream environment. The meandering samples were also organized by appropriate sub-environment.

<b>Depositional Environment</b>	<b>Average Extractable B (<math>\mu\text{g/g}</math>)</b>	<b>Average Extractable Sr (<math>\mu\text{g/g}</math>)</b>	<b>Average Extractable Ba (<math>\mu\text{g/g}</math>)</b>
Channel	0.1	6.9	27.7
Crevasse Splay	0.2	7.0	15.8
Floodplain	0.4	15.4	17.2
Meandering Stream	0.3	12.8	18.3

Table 42: The average concentration of B, Sr, and Ba extracted by each extraction step from samples from a meandering stream environment. The meandering samples were also organized by appropriate sub-environment. Sequential extractions took place in the order show (left to right). The column ‘n’ represents the number of samples classified in each depositional environment.

Depositional Environment	n	H2O ext. B (µg/g)	NH4Ac ext. B (µg/g)	Acetic Acid ext. B (µg/g)	HCl ext. B (µg/g)	H2O ext. Sr (µg/g)	NH4Ac ext. Sr (µg/g)	Acetic Acid ext. Sr (µg/g)	HCl ext. Sr (µg/g)	H2O ext. Ba (µg/g)	NH4Ac ext. Ba (µg/g)	Acetic Acid ext. Ba (µg/g)	HCl ext. Ba (µg/g)
Channel	17	0.3	0.1	0.1	0.0	1.2	23.2	2.7	0.6	1.7	73.8	10.0	25.1
Crevasse Splay	23	0.4	0.2	0.4	0.0	0.9	16.8	9.2	1.1	1.2	35.9	11.8	14.3
Floodplain	89	0.4	0.2	0.9	0.1	1.3	27.5	29.8	2.9	1.1	47.4	8.3	12.1
<i>Overall depositional environment</i>													
Meandering Stream	129	0.4	0.2	0.7	0.1	1.2	25.0	22.6	2.3	1.2	48.8	9.1	14.2

Table 43: The average concentration of B, Sr, and Ba extracted by each extraction step from samples from a lacustrine environment. Sequential extractions took place in the order show (left to right). The column ‘n’ represents the number of samples classified in each grain size category.

Depositional Environment	n	H2O ext. B (µg/g)	NH4Ac ext. B (µg/g)	Acetic Acid ext. B (µg/g)	HCl ext. B (µg/g)	H2O ext. Sr (µg/g)	NH4Ac ext. Sr (µg/g)	Acetic Acid ext. Sr (µg/g)	HCl ext. Sr (µg/g)	H2O ext. Ba (µg/g)	NH4Ac ext. Ba (µg/g)	Acetic Acid ext. Ba (µg/g)	HCl ext. Ba (µg/g)
Lacustrine	20	0.3	0.2	0.7	0.3	1.1	33.0	21.5	8.5	0.6	59.1	9.6	9.2

Table 44: The average concentration of B, Sr, and Ba extracted from all steps of the sequential extractions from samples from a lacustrine environment

<b>Depositional Environment</b>	<b>Average Extractable B (<math>\mu\text{g/g}</math>)</b>	<b>Average Extractable Sr (<math>\mu\text{g/g}</math>)</b>	<b>Average Extractable Ba (<math>\mu\text{g/g}</math>)</b>
Lacustrine	0.4	16.0	19.6

## CHAPTER 5: DISCUSSION AND CONCLUSIONS

### 5.1 Discussion

The mineralogical data from this study show the deposits of the Deep River basin are characterized as compositionally immature consisting of quartz- and feldspar-bearing siliciclastics containing abundant clay minerals and lesser amounts of carbonate and oxide minerals (Chapter 3). The geochemical data from the sequential extractions conducted for this study suggest that the mineralogy and degree of post-depositional alteration of a sample, such as the presence or absence of carbonate minerals, and grain size influence the leaching behavior of extractable boron, strontium, and barium from samples from the Deep River basin (Chapter 4). The compositional and grain size trends within the Deep River basin may account for the abundance of extractable strontium and barium from exchangeable sites such as on clay minerals with lesser amounts of strontium leached from carbonate and barium released from oxide minerals.

A study conducted in the Marcellus Shale region on produced water suggested that exchangeable boron was released from adsorption sites on clay mineral surfaces as a result of interactions with injected fluids (Warner et al., 2014). The present study found boron was preferentially leached from carbonate minerals with lesser amounts released from exchangeable sites (Figure 82). It may be possible that the differences in depositional environments between the Marcellus Shale and the Deep River basin (marine vs. non-marine) caused the affinity of boron to vary. The geochemical data from this study show the leaching behavior of strontium and barium is consistent with the geochemical trends from the sequential extractions conducted by Stewart et al., (2015) on

drill cuttings from the Marcellus Shale and adjacent units (Figure 82). Stewart et al. (2015) suggested, and this study confirms, that strontium and barium were preferentially leached from exchangeable sites by ammonium acetate, but unlike strontium, barium was not released in appreciable amounts from carbonate minerals.

As expected from published literature (e.g. Hageman, 2005; Kosson et al., 2017), in general, as grain size increases, the average concentration of extractable boron, strontium, and barium decreases (Figure 83). Fine-grained sediments, often referred to as the clay-sized fraction, tend to be highly reactive due to their high ratio of surface area to volume (Ryan, 2014). As discussed in section 4.5, mudstones and shales released more strontium from carbonate minerals, whereas more coarse-grained samples released more strontium from exchangeable sites (Figure 83). This is likely a result of the abundance of carbonate minerals in mudstone and shale samples compared to other grain sizes (Table 28).

Although strontium and barium were preferentially leached from exchangeable sites by the ammonium acetate solution, the median concentrations of extractable strontium and barium from all of the Deep River basins samples were only minimally correlated to the abundance of clay (phyllosilicate) minerals (Figures 89 and 92). The median concentration of HCl- acid extractable barium is not correlated to the abundance of oxide minerals (Figure 93). It is possible that grain size plays a more influential role compared to clay mineral abundance in determining the solubility of extractable strontium and barium (Figures 91 and 94). As a result, should hydraulic fracturing occur in the Deep River basin, the produced water generated by fine-grained deposits such as mudstones and shales are likely to generate increased concentrations of extractable

strontium and barium. Carbonate mineral content as well as grain size appear to be strongly correlated to the concentration of extractable strontium (Figure 90). As a result, carbonate-rich deposits, especially fine-grained mudstones and shales which are characterized by the most carbonate minerals in the Deep River basin, are likely to release high concentrations of strontium into the environment.

## 5.2 The Inorganic Geochemistry of Extractable Strontium and Barium Compared to the Mineralogy of the Sub-basins

The geochemical data show a minimal correlation between the median concentration of ammonium acetate-extractable strontium and barium and the relative abundance of clay minerals present in the sub-basins (Figures 95 and 97). Although the correlation is consistent among the sub-basins, there are differences in the leaching behavior of ammonium acetate extractable strontium and barium that may be related to differences in the clay mineral assemblage among the sub-basins. For example, the highest average concentrations of ammonium acetate extractable strontium and barium were leached from the Wadesboro sub-basin samples, 35.99  $\mu\text{g/g}$  and 64.93  $\mu\text{g/g}$ , respectively, despite the sub-basin having the lowest relative abundance (1.6) of clay minerals (Table 27; Figures 95 and 97). The Sanford sub-basin, however, is characterized as having the highest relative abundance of clay minerals (2.4), but released the lowest average concentrations of ammonium acetate extractable strontium and barium, 9.23  $\mu\text{g/g}$  and 45.24  $\mu\text{g/g}$ , respectively (Table 27; Figures 95 and 97). These differences in clay mineral abundance and the mean concentration of ammonium acetate extractable strontium and barium may be a result of differences in the types of clay minerals present in the sub-basins (Table 45).

Due to differences in cation exchange capacities, smectite minerals such as montmorillonite are much more likely to release ions to solution than kaolinite and related minerals such as halloysite and dickite (Figure 69) (Ryan, 2014). As a result, deposits containing smectite are more likely to release high concentrations of strontium and barium into the environment. Differences in the clay mineral assemblage among the sub-basins may help explain the variation in the leaching behavior of strontium and barium among the sub-basins (Figure 84). For example, the Wadesboro sub-basin is characterized by the lowest relative abundance of clay minerals, but leached the highest average cumulative concentrations of strontium and barium extracted from all steps of the sequential extraction, 22.5  $\mu\text{g/g}$  and 23.4  $\mu\text{g/g}$ , respectively (Table 27 and Figure 84). However, the Sanford sub-basin has the highest relative abundance of clay minerals, but leached the lowest average cumulative concentration of strontium and barium extracted from all steps of the sequential extractions, 6.5  $\mu\text{g/g}$  and 16.9  $\mu\text{g/g}$ , respectively (Table 27 and Figure 84). The Sanford sub-basin appears to contain more kaolinite minerals; whereas the Wadesboro sub-basins appears to contain more smectite minerals (Table 45). Thus, the data from this study suggest deposits with smectite minerals such as those present in the Wadesboro sub-basin are likely to leach high concentrations of strontium and barium to the environment.

This study examined all three of the sub-basins of the Deep River basin to provide baseline data about the water-rock interactions likely to influence the composition of formation water in the basin. As previously discussed, a similar stratigraphy is displayed in all three sub-basins, but the Sanford sub-basin contains the best developed middle clay-shale and mudstone interval. The coal-bearing Cumnock Formation in the Sanford

sub-basin is of particular interest because it is the known target formation for shale gas development in the sub-basin. Due to the apparent absence of the Cumnock Formation or its equivalents in the Wadesboro and Durham sub-basins, it is unlikely that these sub-basins would be a focus of shale gas development.

The Sanford sub-basin is characterized by a high relative abundance of clay minerals, but a low relative abundance of carbonate minerals. The sub-basin released the lowest concentration of extractable strontium and barium. Despite a low abundance of carbonate minerals in the Sanford sub-basin, strontium was preferentially leached from carbonate minerals and statistical analyses indicate carbonate mineral content is strongly correlated to the median concentration of extractable strontium. The XRD data show dolomite was present in one sample, SB-23, from the Sanford sub-basin (Appendix C). Figure 19 shows this sample was collected from a large displacive nodule that likely formed in the sediments while they were still soft and not compacted. As a result, the kaolinite minerals in the Sanford sub-basin are unlikely to release abundant strontium to the environment, but carbonate nodules and cements found in paleosols which are pervasive throughout the sub-basin could contribute significant quantities of strontium to the environment should hydraulic fracturing begin.

### 5.3 The Inorganic Geochemistry of Extractable Strontium and Barium Compared to the Mineralogy of the Depositional Environments

The geochemical data show a minimal correlation between the median concentration of ammonium acetate extractable strontium and barium and the relative abundance of clay minerals present in a depositional environment (Figures 98 and 100). Although the correlation is consistent among the depositional environments, there are differences in the leaching behavior of ammonium acetate extractable strontium and

barium that may be related to the overall abundance and/or type of clay minerals present as well as inherent differences in grain size among the depositional environments. For example, lacustrine environments are characterized by the highest relative abundance of clay minerals (2.5) and leached the highest mean concentration of ammonium acetate extractable strontium and barium, 32.96  $\mu\text{g/g}$  and 59.10  $\mu\text{g/g}$ , respectively (Table 29; Figure 98 and 100). Furthermore, in lacustrine environments, clay mineral abundance while minimally correlated to the median concentration of ammonium extractable strontium, shows a slight positive correlation, whereas, the alluvial fan and meandering stream depositional environments exhibit a slight negative correlation (Figure 98). As discussed above, the variability in leaching behavior of strontium and barium among the depositional environments may be related to differences in the predominant clay mineral such as smectite or kaolinite present.

The geochemical data show a strong positive correlation between the median concentration of acetic extractable strontium and the relative abundance of carbonate minerals present in a depositional environment (Figure 96). For example, the meandering stream samples were characterized as having the highest relative abundance of carbonate minerals (0.7) and released the highest mean concentration of acetic acid extractable strontium (Table 32).

#### 5.4 Conclusions

The purpose of this research was to 1) provide baseline data of water-rock interactions in an undisturbed Mesozoic basin in advance of drilling and hydraulic fracturing, 2) to simulate the formation water that may be brought to the surface during shale gas development, and 3) to examine the geochemical fingerprint that could be used

to identify this formation water in the environment. The sequential extractions conducted as part of this study targeted specific mineral phases such as clay minerals to identify possible sources of extractable elements (Figure 52). The geochemical data indicate the water-rock interactions in the Deep River basin are influenced by variations in mineralogy and grain size (Figures 82 and 83). The average concentration of boron, strontium, and barium extracted from a specific mineral phase may be representative of the solubility of the element during water-rock interactions in the Deep River basin (Table 34). For example, the highest average concentration of strontium (25.2  $\mu\text{g/g}$ ) and barium (51.8  $\mu\text{g/g}$ ) from the Deep River basin samples were leached from exchangeable sites on clay minerals (Table 34). Thus, deposits with abundant clay minerals are likely to leach more strontium and barium compared to deposits with fewer clay minerals. Additionally, fine-grained samples ranging from mudstones and shales to very fine to fine-grained sandstones are likely to release more strontium to solution from carbonate minerals compared to boron and barium (Table 36). Thus, carbonate minerals likely represent an important source of extractable strontium in the Deep River basin.

It was hypothesized that the geochemical characteristics of formation water in North Carolina would likely be different than those of the Marcellus Shale because of different depositional environments (section 1.4). Comparing the geochemical analyses conducted for this study with studies conducted by Warner et al. (2014) and Stewart et al., (2015) on samples from the Marcellus Shale, the leaching behavior of boron differs, but the leaching behavior of strontium and barium is consistent among marine and non-marine basins. It may be possible that the differences in depositional environments

between the Marcellus Shale and the Deep River basin (marine vs. non-marine) caused the affinity of boron to vary.

The marine brines of the Marcellus Shale generate produced water with high TDS (Warner et al., 2013; Brantley et al., 2014; Vengosh et al., 2014). For example, chloride concentrations in wastewater effluent associated with Marcellus Shale produced water ranged between 55,000 and 98,000 mg/L (Warner et al., 2013). The low concentrations of chloride and other dissolved cations and anions extracted by the water step of the sequential extractions conducted for this study show the non-marine lacustrine deposits of the Deep River basin will likely generate significantly lower concentrations of TDS compared to the Marcellus Shale (Appendix F).

#### 5.5 Recommendations for Future Geochemical Studies in Non-Marine Basins

The analytical methods and interpretations of the present study could be applied to other studies occurring in non-marine basins, especially rift basins. As a result, this section provides recommendations to guide similar basin-wide geochemical studies of non-marine basins. The geochemical data of the present study suggest that the mineralogy and grain size of a deposit are likely to influence the water-rock interactions and the composition of formation water. Thus, it is recommended that core samples be obtained to characterize the basin fill material. Mineralogical studies should include grain size observations and the qualitative and quantitative analysis of mineral occurrences, especially clay, carbonate, and oxide minerals. The present study indicated that the clay mineral assemblage of a deposit may influence the leaching behavior of extractable strontium and barium. Thus, scanning electron microscope (SEM) and XRD technology

should be used to identify fine-grained sediments and sedimentary rocks and specifically, the species of clay minerals present in a deposit.

The episodic nature of tectonic activity in rift basins such as the Deep River basin is often recorded as characteristic and recurrent lithofacies associations and vertical successions within the basins (Figure 46). These recurrent lithofacies associations and vertical successions create complex sedimentary deposits with lateral and vertical changes in mineralogy and grain size (Figure 46 and 104). Additionally, the presence of authigenic minerals such as carbonate and oxide minerals suggest that periods of tectonic stability and quiescence allowed pedogenesis and diagenesis to occur. In the Deep River basin, clay, carbonate, and oxide minerals are largely the result of post-depositional alteration and represent important sources of extractable strontium and barium. As a result, it may be useful to understand the depositional history of a deposit to anticipate possible heterogeneity associated with post-depositional alteration which may influence the composition of formation water.

The sequential extractions conducted as part of this study provide baseline data about the *in situ* water-rock interactions that may influence the composition of formation water in the Deep River basin. This study focused primarily on understanding the sources of extractable boron, strontium, and barium because they have been used as geochemical tracers to identify Marcellus Shale produced water in the environment. It is recommended that the leachate resulting from the sequential extractions of future studies of non-marine basins also be analyzed for components such as bromide and lithium. In addition to boron, strontium, and barium, bromide and lithium are present in distinctive chemical ratios in Marcellus Shale produced water and may be used as geochemical tracers to

identify the wastewater in the environment (Brantley et al., 2014; Warner et al., 2014).

It is recommended that future geochemical studies collect *in situ* formation water and groundwater. These water samples should be analyzed for similar chemical constituents such as strontium and barium as the leachate from the sequential extractions. Where possible, formation water should be collected from representative stratigraphic units. Groundwater samples should be collected from various depths ranging from relatively shallow depths near where the stratigraphic units outcrop as well as along the contacts as they dip toward the bounding fault (Figure 104). This sampling strategy may help understand the influence of the surface on the composition of formation water and should help capture the influence of heterogeneity in grain size and mineralogy on the composition of formation water (Figure 104). Similar to other rift basins, the Deep River basin is intruded by through-going diabase dikes and major and minor faults (Figure 104) (Olsen et al., 1991). Future geochemical and subsurface hydrology studies should explore the influence of fluid migration along these structural features and the influence of the fluid migration on the composition of formation water. As a result, groundwater samples should be collected from wells that are in close proximity to the dikes and faults as well as farther away.

In summary, the analytical methods and interpretations of the present study may provide valuable insight into the development of comprehensive basin-wide studies of the water-rock interactions that likely influence the composition of formation water in non-marine basins. Thus, these geochemical studies may provide insight into the naturally-sourced components of produced water.

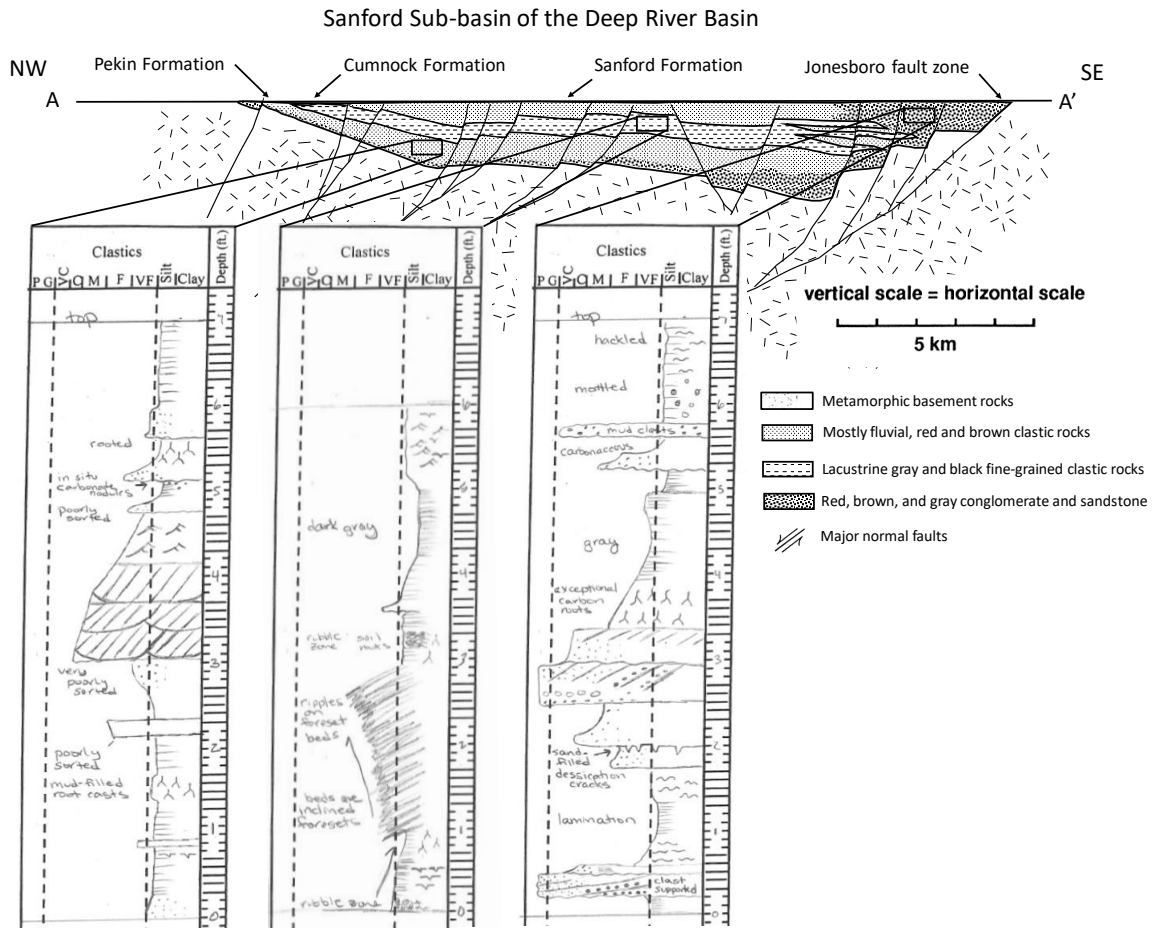


Figure 104: Cross section of the Sanford sub-basin of the Deep River basin. Representative core logs of each lithofacies association are included. (Modified from: Olsen et al., 1991; Chem-Nuclear Systems, 1993).

Table 45: The average relative abundance of clay minerals phases present in the sub-basins of the Deep River basin.

<b>Sub-basin</b>	<b>Kaolinite</b>	<b>Smectite</b>	<b>Mica</b>	<b>Chlorite</b>	<b>Mixed-Layer Clay</b>
Wadesboro	0.0	0.1	0.3	0.5	0.0
Sanford	0.1	0.0	0.7	0.2	0.0
Durham	0.0	0.0	0.6	0.2	0.1

## 6. REFERENCES

Ake, J., Mahrer, K., O'Connell, D., and Block, L. 2005. Deep-injection and closely monitored induced seismicity at Paradox Valley, Colorado. *Bulletin of the Seismological Society of America* 95: 664-683.

American Association of Petroleum Geologists (AAPG) Wiki, 2019. Sandstone. <https://wiki.aapg.org/Sandstone> (June 27, 2019).

Arthur, J. D., Bohm, B., and Layne, M. 2008. Hydraulic fracturing considerations for natural gas wells of the Marcellus Shale. The Ground Water Protection Council: Annual Forum, Cincinnati, Ohio, September 21-24, 2008: 16 pp.

Ayers, W.B. 1986. Lacustrine and fluvial-deltaic depositional systems, Fort Union Formation (Paleocene), Powder River Basin, Wyoming and Montana. *The American Association of Petroleum Geologists (AAPG) Bulletin* 70 (11): 1651-1673.

Ayers, W.B., and Kaiser, W.R. 1984. Lacustrine-interdeltaic coal in the Fort Union Formation (Paleocene), Powder River Basin, Wyoming and Montana, U.S.A. In: *Sedimentology of Coal and Coal-bearing Sequences*, edited by R.A. Rahmani and R.M. Flores, 61-84. Special Publication of International Association of Sedimentologists 7.

Balashov, V.N., Engelder T., Gu, X, Fantle, M.S. and Brantley, S.L. 2015. A model describing flowback chemistry changes with time after Marcellus hydraulic fracturing. *The American Association of Petroleum Geologists (AAPG) Bulletin* 99 (1): 143-154.

Barker, D.S. 1970. Compositions of granophyre, myrmekite, and graphic granite. *Geological Society of America Bulletin* 81: 3339-3350.

Baron, A. 1997. Linear regression. <http://www.stat.yale.edu/Courses/1997-98/101/linreg.htm> (April 11, 2019).

Benko, K.L. and Drews, J.E. 2008. Produced water in the western United States: geographic distribution, occurrence, and composition. *Environmental Engineering Science* 25 (2): 239-246.

Berendsen, P., Borcharding, R.M., Doveton, J., Gerhard, L., Newell, K.D., Steeples, D., and Watney, W.L. 1988. Texaco Poersch #1, Washington County, Kansas--Preliminary geologic report of the pre-Phanerozoic rocks: Kansas Geological Survey, Open-file Report 88-22, 1-5.

Bohacs, K.M., Carroll, A.R., Neal, J.E., and Mankiewicz, P.J. 2000. Lake-basin type, source potential, and hydrocarbon character: An integrated-sequence-stratigraphic-geochemical framework. In: *Lake Basins Through Space and Time*, edited by E.H. Gierlowski-Kordesch and K.R. Kelts, K.R. AAPG Studies in Geology: 46: 3-33.

- Brantley, S., Yoxtheimer, D., Arjmand, S., Grieve, P., Vidic, R., Pollak, J., Llewellyn, G., Abad, J., and Simon, C. 2014. Water resources impacts during unconventional shale gas development: The Pennsylvania experience. *International Journal Coal Geology* 126: 140-156.
- Brazell, S.J. 2013. Sedimentology and depositional environments of the Wadesboro sub-basin, eastern Piedmont, North Carolina. Master's project report, University of North Carolina at Charlotte.
- Brazell, S.J., and Diemer, J.A. 2012. A field guide to the sedimentology of the Triassic Wadesboro sub-basin, North Carolina. Unpublished field guide, University of North Carolina at Charlotte.
- Brinck, E.L., Drever, J.L., and Frost, C.D. 2008. The geochemical evolution of water coproduced with coalbed natural gas in the Powder River Basin, Wyoming. *Environmental Geosciences*. 15 (4): 153-171.
- Brown, J. 1993. Sedimentology and depositional history of the Lower Paleocene Tullock Member of the Fort Union Formation, Powder River Basin, Wyoming and Montana. *U.S. Geological Survey Bulletin* 1917, 50 p.
- Burdge, J. 2014. *Chemistry*. United States of America: McGraw-Hill Education. pp. 231-242.
- Campbell, M.R, and Kimball, K.W. 1923. The Deep River coal field of North Carolina. *North Carolina Geological and Economic Survey Bulletin* 33, 95 p.
- Cant, D.J. and Walker R.G. 1978. Fluvial processes and facies sequences in the sandy braided South Saskatchewan River, Canada. *Sedimentology* 25, 625-648.
- Capo, R.C., Stewart, B.W., Rowan, E.L., Kohl, C.A., Wall, A.J., Chapman, E.C., Hammack, R.W., and Schroeder, K.T. 2014. The strontium isotopic evolution of Marcellus Formation produced water, southeastern Pennsylvania. *International Journal of Coal Geology* 126, 57-63.
- Carroll, D. 1959. Ion exchange in clays and other minerals. *Geological Society of America Bulletin*. 70, 749-780.
- Chem-Nuclear Systems, Inc. 1993. Characterization report of the Wake/Chatham county site.
- Clark, T., Gore, P., Watson, M. 2001. Deposition and structural framework of the Deep River Triassic Basin, NC. *Field Trip Guide*, Raleigh: Southeastern Geological Society of America.
- Clark, T., Taylor, K., Bradley, P. 2011. Geology, natural gas potential, and mineral resources of Lee, Chatham, and Moore Counties, North Carolina. *Field Trip Guide*, Carolina Geological Society.

- Coffey, B.P. and Textoris, D.A. 2003. Palesols and paleoclimate evolution, Durham sub-basin, North Carolina. In: *The Great Rift Valleys of Pangea in Eastern North America*, edited by P.M. LeTourneau and P.E. Olsen. New York: Columbia University Press 2, 78-87.
- Conklin, A. R, Jr. 2014. *Introduction to Soil Chemistry: Analysis and Instrumentation*. Hoboken, NJ: Wiley.
- Dickinson, W.R. 1970. Interpreting detrital modes of greywacke and arkose. *Journal of Sedimentary Petrology* 40: 695-707.
- Dott, R.H. 1964. Wacke, greywacke and matrix—what approach to immature sandstone classification? *Journal of Sedimentary Petrology* 34: 625-632.
- Drever, J. I. 1982. *The Geochemistry of Natural Waters*. Englewood, NJ: Prentice-Hall, Inc.
- Dutrow, B.L., and Clark, C.M., 2015. X-ray powder diffraction (XRD): [http://serc.carleton.edu/research\\_education/geochemsheets/techniques/XRD.html](http://serc.carleton.edu/research_education/geochemsheets/techniques/XRD.html) (accessed June 2015)
- Ellsworth, W. 2013. Injection-induced earthquakes. *Science*. 341(6412): 142-148.
- Emmons, E. 1852. Report of Professor Emmons on his geological survey of North Carolina. Executive Document 13, Seaton Gales, Raleigh, North Carolina, 181 p.
- Energy Information Administration (EIA). 2007. U.S. coalbed methane: past, present, and future. Panel 2 of 2. Washington, DC: U.S. Department of Energy. Available at [www.eia.doe.gov/oil\\_gas/rpd/cbmusa2.pdf](http://www.eia.doe.gov/oil_gas/rpd/cbmusa2.pdf) (February 14, 2018).
- Energy Information Administration (EIA). 2017a. Natural gas explained: where our natural gas comes from. [https://www.eia.gov/energy\\_in\\_brief/article/shale\\_in\\_the\\_united\\_states.cfm](https://www.eia.gov/energy_in_brief/article/shale_in_the_united_states.cfm) (April 4, 2017).
- Engelder, T., and Lash, G.G. 2008. Marcellus Shale play's vast resource potential creating stir in Appalachia. *The American Oil and Gas Reporter*: 7.
- Engle, M.A. and Rowan, E.L. 2014. Geochemical evolution of produced waters from hydraulic fracturing of the Marcellus Shale, northern Appalachian Basin: A multivariate compositional data analysis approach. *International Journal Coal Geology* 126: 45-56.
- Folk, R.L. 1980. *Petrology of Sedimentary Rocks*: Austin: Hemphill Publishing Company.

Gilmer, J.P., Textoris, D.A., Watson, M.E. 2003. Provenance of upper Triassic fluvial redbeds in the center of the Durham sub-basin, North Carolina. In: *The Great Rift Valleys of Pangea in Eastern North America*, edited by P.M. LeTourneau and P.E. Olsen. New York: Columbia University Press 2, 69-77.

Gregory, K.B., Vidic, R.D., and Dzombak, D.A. 2011. Water management challenges associated with the production of shale gas by hydraulic fracturing. *Elements* 7 (3): 181-186.

Grim, R. E. 1953. *Clay Mineralogy*. New York McGraw-Hill Book Company, Inc.

Ground Water Protection Council and All Consulting. 2009. *Modern Shale Gas Development in the United States: A Primer*. Department of Energy: 116 p.

Hageman, P.L. 2005. A simple field leach test to assess potential leaching of soluble constituents from mine wastes, soils, and other geologic materials. *U.S.G.S Fact Sheet 2005-3100*.

Harwood, G. 1988. Microscopic techniques: II. Principles in sedimentary petrography. In: *Techniques in Sedimentology*, edited by M. Tucker, M., 108-173. Oxford: Blackwell Scientific Publications.

Healy, J., Rubey, W., Griggs, D., and Raleigh, C. 1968. The Denver earthquakes. *Science* 161: 1301-1310.

Horton, S. 2012. Disposal of hydrofracking waste fluid by injection into subsurface aquifers triggers earthquake swarm in central Arkansas with potential for damaging earthquake. *Seismological Research Letters* 83 (2): 250-260.

Horton, J.W., Jr., and Zullo, V.A. 1991. An introduction to the geology of the Carolinas. In: *The Geology of the Carolinas*, edited by J.W. Horton, Jr., and V.A. Zullo, 1-10. Knoxville: The University of Tennessee Press.

Hudson Institute of Mineralogy. 1993-2018. Mindat. <https://www.mindat.org/> (Sept 3 2018).

Hu, L.N and Textoris, D.A. 1994. Cycles in lake bed of the Triassic Sanford sub-basin of North Carolina. *Concepts in Sedimentology and Paleontology* 4: 5-23.

Ingersoll, R.V., Bullard, T.F., Ford, R.L., Grimm, J.P., Pickle, J.D., and Sares, S.W. 1984. The effect of grain size on detrital modes: A test of the Gazzi-Dickinson point-counting method. *Journal of Sedimentary Petrology* 54: 103-116.

Jackson, R.E., Gorody, A.W., Mayer, B., Roy, J.W., Ryan, M.C., Van Stempvoort D.R. 2013. Groundwater protection and the unconventional gas extraction: The critical need for field-based hydrogeological research. *Groundwater* 51 (4): 488-510.

JMP Pro. 2016. Statistical Discovery: Release 13.0.0. SAS Institute, Inc.

- Johnson, J.D., and Graney, J.R. 2015. Fingerprinting Marcellus Shale waste products from Pb isotope and trace metal perspectives. *Applied Geochemistry* 60: 104-115.
- Karathanasis, A.D., and Hajek, B.F. 1996. Elemental analysis by X-ray fluorescence spectroscopy. *Methods of Soil Analysis Part 3 Chemical Methods-SSSA Book Series*. 5: 161-220.
- Kargo, D.M., Wilhelm, R.G, and Campbell, D.J. 2010. Natural gas plays in the Marcellus Shale: Challenges and potential opportunities. *Environmental Science & Technology* 44 (15): 5679-5684.
- Keren, R. 1996. Boron. *Methods of Soil Analysis Part 3 Chemical Methods-SSSA Book Series*. 5: 603-626.
- Kahn Academy. 2019. Summarizing quantitative data. <https://www.khanacademy.org/math/statistics-probability/summarizing-quantitative-data/box-whisker-plots/a/box-plot-review> (April 13, 2019).
- Knippenberg, L. 2011. NOAA Teacher at Sea. <http://teacheratsea.wordpress.com/tag/pycnocline/> (Sept. 19, 2012)
- Kosson, D.S., Garrabrants, A., Thorneloe, S., Fagnant, D., Helms, G., Connolly, K., and Rodgers, M. 2017. *Leaching Environmental Assessment Framework (LEAF) How-to Guide*. Environmental Protection Agency. 122 p.
- Learn, S. 2012. “Coal clash: The Powder River Basin, where coal is king”. [http://www.oregonlive.com/environment/index.ssf/2012/06/coal\\_clash\\_out\\_of\\_the\\_gigantic.html](http://www.oregonlive.com/environment/index.ssf/2012/06/coal_clash_out_of_the_gigantic.html) (February 14, 2018)
- Lorenz, J.C. 1988. *Triassic-Jurassic Rift-Basin Sedimentology*. New York: Van Nostrand Reinhold Company.
- Luppens, J.A., Scott, D.C., Osmonson, L.M., Haacke, J.E., Pierce, P.E. 2013. Assessment of coal geology, resources, and reserve base in the Powder River Basin, Wyoming and Montana. *U.S.G.S Fact Sheet 2012-3143*.
- Lynn, W., Thomas, J.E., Moody, L.E. 2008. Petrographic microscope techniques for identifying soil minerals in grain mounts. *Methods of Soil Analysis Part 5 Mineralogical Methods-SSSA Book Series*. 5: 161-189.
- Malaza, N., Liu, K., and Zhao, B. 2013. Facies analysis and depositional environments of the late Paleozoic coal-bearing Madzaringwe Formation in the Tshipise-Pafuri basin, South Africa. *ISRP Geology*. 2013: 1-11.
- Maley, T.S. 2005. *Field Geology Illustrated*. Ann Arbor, MI: Sheridan Books.
- Marshak, S. 2012. *Earth: Portrait of a Planet*. New York: W.W. Norton & Company, Inc.

Miall, A.D. 1977. Lithofacies types and vertical profile models in braided river deposits: A summary. In: *Fluvial Sedimentology*, edited by A.D. Miall, 597-604. Geological Survey of Canada, Calgary.

Miall, A.D. 1996. *The Geology of Fluvial Deposits: Sedimentary Facies, Basin Analysis, and Petroleum Geology*. New York: Springer.

Milici, R.C., Coleman, J.L., Rowan, E. L., Cook, T.A., Charpentier, R.R., Kirschbaum, M. A., Klett, T.R., Pollastro, R. M., and Schenk, C. J., 2012. Assessment of undiscovered oil and gas resources of the East Coast Mesozoic Basins of the Piedmont, Blue Ridge Thrust Belt, Atlantic Coastal Plain, and New England provinces, 2011: *U.S.G.S Fact Sheet 2012-3075*.

Mineralogical Society of America, 2004-2018. *Handbook of Mineralogy*. <http://www.handbookofmineralogy.org/search.html?p=all>. (Sept 3, 2018).

Moore, D.M., and Reynolds Jr., R.C. 1997. *X-Ray Diffraction and the Identification and Analysis of Clay Minerals*. New York: Oxford University Press.

Moss, K. 2009. Development of the natural gas resources in the Marcellus Shale. Denver: National Park Service.

National Energy Technology Laboratory (NETL). 2013. Modern shale gas development in the United States: An update. United States Department of Energy.

Natural Gas Supply Association. 2010. *Natural Gas*. [www.naturalgas.org/overview/background/](http://www.naturalgas.org/overview/background/) (July 1, 2016).

National Research Council (NRC). 2010. *Management and Effects of Coalbed Methane Produced Water in the Western United States*. Washington, DC: The National Academies Press. <https://doi.org/10.17226/12915>. (Feb. 14, 2018).

Nau, R. 2018. Statistical forecasting: notes on regression and time series analysis. <https://people.duke.edu/~rnau/rsquared.htm> (April 13, 2019).

Nave, C.R. 2017. *Bragg's Law*. HyperPhysics. <http://hyperphysics.phy-astr.gsu.edu/hbase/quantum/bragg.html> (Sept. 14, 2018).

Nesse, W. D. 2004. *Introduction to Optical Microscopy*. New York: Oxford University Press.

Newman, A.C., and Brown, G. 1987. The chemical constitution of clays. In: *Chemistry of Clays and Clay Minerals*, edited by A.C. Newman, 1-128. New York: Wiley-Interscience.

North Carolina Geological Survey (NCGS). 1985. North Carolina geologic map. Plate 1. <https://deq.nc.gov/about/divisions/energy-mineral-land-resources/north-carolina-geological-survey/ncgs-maps/1985-geologic-map-of-nc> (October 22, 2019).

- North Carolina State University (NCSU). 2004. Linear regression with Excel. <https://projects.ncsu.edu/labwrite/res/gt/gt-reg-home.html> (April 13, 2019).
- Olsen, P.E., 1997. Stratigraphic record of the early Mesozoic breakup of Pangea in the Laurasia-Gondwana rift system. *Annual Reviews of Earth and Planetary Science* 25: 337-401.
- Olsen, P.E., Froelich, A.J, Daniels, D.L., Smoot, J.P., and Gore, P.J.W. 1991. Rift basins of early Mesozoic age. In: *The Geology of the Carolinas*, edited by J.W. Horton, Jr. and V.A. Zullo, 142-170. Knoxville: The University of Tennessee Press.
- Pennsylvania Department of Conservation and Natural Resources (PA DCNR). 2009. *Quantity of Organic Matter*. [http://www.dcnr.state.pa.us/topogeo/econresource/oilandgas/marcellus/sourcerock\\_index/sourcerock\\_quantity/index.htm](http://www.dcnr.state.pa.us/topogeo/econresource/oilandgas/marcellus/sourcerock_index/sourcerock_quantity/index.htm) (July 1, 2016)
- Pettijohn, F.J., Potter, P.E., Siever, R. 1987. *Sand and Sandstone*. New York: Springer-Verlag.
- Poppe, L.J., Paskevich, V.F., Hathaway, J.C., and Blackwood, D.S. 2001. A laboratory manual for X-Ray powder diffraction. *USGS Open-File Report 01-041*. <http://pubs.usgs.gov/of/2001/of01-041/index.htm> (accessed June 2015).
- Prothero, D.A., Schwab, F., 2014. *Sedimentary Geology: An Introduction to Sedimentary Rocks and Stratigraphy*. New York: W.H. Freeman and Company.
- Raith, M.M., Raase, R., and Reinhardt, J., 2011. *Guide to Thin Section Microscopy*. [http://d32ogoqmya1dw8.cloudfront.net/files/NAGTWorkshops/mineralogy/thin\\_section\\_microscopy.pdf](http://d32ogoqmya1dw8.cloudfront.net/files/NAGTWorkshops/mineralogy/thin_section_microscopy.pdf) (accessed June 2015).
- Randazzo, A.F., Swe, W., and Wheeler, W.H., 1970. A study of tectonic influence on Triassic sedimentation – the Wadesboro sub-basin, Central Piedmont: *Journal of Sedimentary Petrology*, v. 40, n. 3, p.998-1006.
- Reid, J.C., Milici, R.C. 2008. Hydrocarbon source rocks in the Deep River and Dan River Triassic Basins, North Carolina. *United States Geological Survey, Open-file Report 2008-1108*.
- Reid, J.C., and Taylor, K.B. 2009. Shale gas potential in Triassic strata of the Deep River Basin, Lee and Chatham counties, N.C., with pipeline and infrastructure data. *North Carolina Geological Survey, Open-file Report 2009-01*.
- Reid, J.C., Taylor, K.B., Olsen, P.E., Patterson, O.F. 2011. Natural gas potential of the Sanford sub-basin, Deep River Basin, North Carolina. *American Association of Petroleum Geologists (AAPG) Search and Discovery Article 10366*: 1-73.
- Reinemund, J.A., 1955. Geology of the Deep River coal field, North Carolina. *U.S. Geological Survey Professional Paper 246*: 1-159.

- Rigaku Corporation. 2010. Integrated X-ray powder diffraction software. *The Rigaku Journal*, 26 (1): 23-27.
- Roen, J. B. 1984. Geology of the Devonian black shales of the Appalachian Basin. *Organic Geochemistry* 5(44): 241-254.
- Rust, B.R., and Koster, E.H. 1984. Coarse alluvial deposits. In: *Facies Models*, edited by R.G. Walker, 53-69. Geosciences Canada, 2.
- Ryan, P. C. 2014. *Environmental and Low Temperature Geochemistry*: Oxford: Wiley Blackwell.
- Sageman, B.B., and Lyons, T.W. 2003. Geochemistry of fine-grained sediments and sedimentary rocks. In: *Treatise on Geochemistry: Sediments, Diagenesis, and Sedimentary Rocks*, edited by F.T. Mackenzie, 115-158. Oxford: Elsevier Ltd.
- Schlische, R.W., 1992. Structural and stratigraphic development of the Newark extensional basin, eastern North America: Evidence for the growth of the basin and its bounding structures: *Geological Society of America Bulletin*, v. 104, p. 1246-1263.
- Schlische, R. W. 1993. Anatomy and evolution of the Triassic-Jurassic continental rift system, eastern North America. *Tectonics* 12 (4): 1026-1042.
- Science Applications International Corporation. 2003. An assessment of laboratory leaching tests for predicting the impacts of fill material on groundwater and surface water quality. 173 p.
- Sladen, C.P. 1994. Key elements during the search for hydrocarbons in lake systems. In: *Global Geological Record of Lake Basins*, edited by E.H. Gierlowski-Kordesch and K.R. Kelts, K.R., 3-17. Cambridge: Cambridge University Press.
- Smith, R., Ozer, T. 2012. *NC Oil and Gas Study under Session Law 2011-276*. Raleigh: NC DENR., NC Department of Commerce.
- Smoot, J.P, 1991. Sedimentary facies and depositional environments of early Mesozoic Newark Supergroup basins, eastern North America: *Palaeogeography, Palaeoclimatology, Palaeoecology* 84, p. 369-423.
- Soeder D.J., and Kappel, W.M. 2009. Water resources and natural gas production from the Marcellus Shale. *U.S.G.S Fact Sheet (3032)*.
- Soil Science Society of America (SSSA), 2019. Soil mineralogy. <https://www.soils4teachers.org/mineralogy> (June 11, 2019).
- Speakman, Scott. 2015. *X-Ray Diffraction*. <http://prism.mit.edu/xray/oldsite/tutorials.htm> (June 6, 2015).

Spivak-Birndorf, L.J., Stewart, B.W., Capo, R.C., Chapman, E.C., Schroeder, K.T., and Brubaker, T.M. 2012. Strontium isotope study of coal utilization by-products interacting with environmental water. *Journal of Environmental Quality*. 41, 144-154.

Stewart, B.W., Capo, R.C., and Chadwick, O.A. 2001. Effects of rainfall on weathering rate, base cation provenance, and Sr isotope composition of Hawaiian soils. *Geochimica et Cosmochimica Acta* 65: 1087-1099.

Stewart, B.W., Chapman, E.C., Capo, R.C., Johnson, J.D., Graney, J.R., Kirby, C.S., and Schroeder, K.T. 2015. Origin of brines, salts and carbonate from shales of the Marcellus Formation: Evidence from geochemical and Sr isotope study of sequentially extracted fluids. *Applied Geochemistry* 60: 78-88.

Suarez, D.L. 1996. Beryllium, magnesium, calcium, strontium, and barium. *Methods of Soil Analysis Part 3 Chemical Methods-SSSA Book Series*. 5: 575-601.

Taylor, K.B., and Reid, J.C. 2011. *Natural Gas Potential of the Sanford Sub-basin, Deep River Basin, North Carolina, Field Trip Guide*. Wilmington, NC: Southeastern Section of the Geological Society of America.

Tessier, A., Campbell, P.G., and Bisson, M. 1979. Sequential extraction procedure for the speciation of particulate trace metals. *Analytical Chemistry* 51 (7): 844-851.

Textoris, D.A. 1994. Upper Triassic playa, Durham sub-basin, North Carolina, USA. In: *Global Geological Record of Lake Basins*, edited by Gierlowski-Kordesch, E. and Kelts, K. eds., 179-183. Cambridge, Cambridge University Press, 9.

Tucker, M.E. 2001. *Sedimentary Petrology*. Oxford: Blackwell Science.

United States Geological Survey (USGS). 2012. Assessment of undiscovered oil and gas resources of the east coast Mesozoic basins of the Piedmont, Blue Ridge thrust belt, Atlantic Coastal Plain and New England provinces, 2011." *U.S.G.S Fact Sheet (3075)*.

U.S. Energy Information Administration, 2017. Marcellus Shale play: geology review. [https://www.eia.gov/maps/pdf/MarcellusPlayUpdate\\_Jan2017.pdf](https://www.eia.gov/maps/pdf/MarcellusPlayUpdate_Jan2017.pdf). (June 9, 2019).

United States Environmental Protection Agency (EPA). 2016. Hydraulic fracturing for oil and gas: impacts from the hydraulic fracturing water cycle on drinking water resources in the United States. U.S. EPA, Washington, DC.

Van Voast, W. 2003. Geochemical signature of formation waters associated with coalbed methane. *AAPG Bulletin* 87 (4): 667-676.

Vengosh, A., Warner, N., Jackson, R., Darrah, T. 2013. The effects of shale gas exploration and hydraulic fracturing on the quality of water resources in the United States. *Procedia Earth and Planetary Science* 7: 863-866.

- Vengosh, A., Jackson, R., Warner, N., Darrah, T., and Kondash, A. 2014. A critical review of the risks to water resources from unconventional shale gas development and hydraulic fracturing in the US. *Environmental Science and Technology* 48: 8334–8348.
- Vidic, R., Brantley, S., Vandenbossche, J., Yoxtheimer, D., Abad, J. 2013. Impact of shale gas development on regional water quality. *Science* 340: 823-835.
- Walker, R.G., and Cant, D.J. 1984. Sandy fluvial systems. In: *Facies Models*, edited by R.G. Walker, 71-89. Geosciences Canada, 2.
- Warner, N., Christie, C., Jackson, R., Vengosh, A. 2013. Impacts of shale gas wastewater disposal on water quality in western Pennsylvania. *Environmental Science and Technology* 47: 11849-11857.
- Warner N. R., Darrah, T.H. Jackson, R.B., Millot, R., Kloppmann, W. and Vengosh, A. 2014. New tracers identify hydraulic fracturing fluids and accidental releases from oil and gas operations. *Environmental Science & Technology* 48: 12552-12560.
- Xenometrix Ltd. 2014. *Next Series Operation Manual: X-2600 XRF Series System*, 4.
- Ziemkiewicz, P.F., and He, Y.T. 2015. Evolution of water chemistry during Marcellus Shale gas development: A case study in West Virginia. *Chemosphere* 134: 224-231.

## Appendix A: Petrographic Data

Appendix A: Results of the petrographic analysis using a minimum of 300 point counts per sample. Compositions of samples are displayed in percents.

Sample ID	Grain Size	Quartz (%)	Feldspar (%)	Mica (%)	Chlorite (%)	Carbonate (%)	Matrix (%)	Opaque (%)	Hematite (%)	Epidote (%)	Lithic Grains (%)	Zircon (%)	Unknown (%)	Total (%)
WB-6	m-c-vc s.s	37.5	27.8	1.5	0.2	2.6	25.5	0.4	0.0	0.0	0.0	0.0	4.5	100.00
WB-7	m-c-vc s.s	14.1	13.1	0.0	0.2	0.0	68.9	1.7	0.0	0.0	0.2	0.0	1.8	100.00
WB-11	m-c-vc s.s	36.5	27.4	0.2	0.0	8.9	17.7	3.5	0.0	0.0	0.0	0.0	5.8	100.00
WB-13	vf-f s.s	17.3	37.3	4.3	0.0	0.0	27.2	7.9	0.0	0.0	0.0	0.0	6.0	100.00
SB-21	vf-f s.s	20.7	32.8	0.2	0.0	0.0	4.0	24.0	0.0	0.0	0.0	0.0	18.3	100.00
SB-39	gravel	31.3	30.3	0.0	0.0	0.0	23.4	6.2	0.0	0.0	0.0	0.0	8.8	100.00
SB-40	vf-f s.s	7.3	37.6	1.5	0.0	0.0	22.0	19.5	0.0	0.0	0.0	0.0	12.2	100.00
DB-3	vf-f s.s	9.4	16.4	1.0	0.0	0.0	38.0	25.3	0.3	5.7	0.0	0.0	3.9	100.00
DB-27	m-c-vc s.s	23.9	32.7	1.1	2.4	3.2	28.5	1.9	0.0	1.1	0.3	0.0	5.1	100.00
DB-34	vf-f s.s	9.1	17.3	2.7	6.7	0.0	5.1	49.6	1.3	1.3	0.0	0.0	6.9	100.00
DB-41	m-c-vc s.s	8.9	30.9	2.2	4.5	0.0	28.2	10.3	0.0	6.9	0.0	0.2	7.8	100.00
DB-45	vf-f s.s	9.1	27.9	2.3	4.4	0.0	35.4	10.7	0.8	4.2	0.0	0.0	5.2	100.00
DB-49	vf-f s.s	4.7	33.0	2.6	6.0	0.0	33.8	6.0	0.0	4.2	1.0	0.0	8.6	99.95
DB-51	vf-f s.s	8.7	24.2	2.3	6.4	0.8	40.7	8.1	0.0	2.3	0.0	0.3	6.4	100.05
DB-57	m-c-vc s.s	21.0	28.7	1.3	4.1	0.0	17.7	13.9	0.0	10.5	0.0	0.0	2.8	99.96
DB-64	vf-f s.s	8.2	11.2	2.0	3.7	0.0	63.4	9.7	0.0	1.2	0.0	0.0	0.5	100.00
DB-66	m-c-vc s.s	17.1	33.2	5.1	1.3	0.0	10.2	25.0	0.8	3.8	0.0	0.0	3.5	100.00
DB-82	m-c-vc s.s	13.2	33.9	3.2	1.9	15.7	6.1	17.0	0.0	7.7	0.0	0.0	1.3	99.96
DB-88	vf-f s.s	14.8	39.6	2.3	0.3	0.0	2.9	28.0	0.0	3.5	0.0	0.0	8.6	99.95
	<b>Average (%)</b>	16.5	28.2	1.9	2.2	1.6	26.3	14.1	0.2	2.8	0.1	0.0	6.2	

## Appendix B: Occurrence of Intergrowths of Quartz and Feldspar

Appendix B: Results of the petrographic analysis using a minimum of 300 point counts per sample. The occurrence of myrmekites and granophyres, intergrowths of quartz and feldspars. Compositions of samples are displayed in percents.

<b>Sample ID</b>	<b>Myrmekite (%)</b>	<b>Granophyre (%)</b>
WB-6	0.0	0.0
WB-7	0.0	0.0
WB-11	0.0	0.0
WB-13	0.0	0.0
SB-21	0.0	0.0
SB-39	0.0	0.0
SB-40	0.0	0.0
DB-3	0.0	0.0
DB-27	0.3	0.0
DB-34	0.0	0.0
DB-41	0.4	0.0
DB-45	0.0	0.0
DB-49	0.0	0.0
DB-51	0.0	0.0
DB-57	0.0	0.3
DB-64	0.0	0.0
DB-66	0.5	0.8
DB-82	0.0	0.3
DB-88	0.0	0.9

## Appendix C: XRD Data

Appendix C: Results of the X-ray diffraction analyses. The color scheme and abbreviations used for the semi-quantitative data are as follows: green, XX = highest intensity; yellow, X = high intensity; red, xx = medium intensity; orange, x = lowest intensity. These intensities were determined using the PDXL2 software. As the software identified candidate phases of minerals, they were presented in order of decreasing occurrence.

Sample ID	Quartz	Albite	Anorthite	Orthoclase	Sanidine	Calcite	Dolomite	Muscovite	Illite	Annite	Clinchlore	Halloysite	Dickite	Lizardite	Guidottite	Montmorillonite	Nontronite	Yakhontovite	Vermiculite	Tosudite	Hematite	Franklinite	Lintisite	Roquesite	Grossmanite	Hedenbergite	Clinostatite
WB-1	XX							X																			
WB-2	XX	X										xx															
WB-3	XX	X						xx																			
WB-5	XX	X																									
WB-6	XX												xx									x		X			
WB-7								XX										X									
WB-8	XX	X																									
WB-9	XX	xx						X																			
WB-10	XX	xx						x		X																	
WB-11	XX	xx				X																					
WB-12	XX	x															xx									X	
WB-13	XX	X									xx																
WB-14	XX	X															xx										
WB-15	XX	X																									
WB-16	XX							X																			
WB-17	XX	x				X											xx										
WB-18	XX					X		x																xx			
WB-19	XX	xx				X				x																	
WB-20	XX	xx				X											x										
WB-21	XX	X						xx															x				
WB-22	XX	xx				X		x																			
WB-23	XX	X				xx		x																			
WB-24	XX	xx				X					x																
WB-25	XX	X																xx									
WB-26	XX		X			xx												x									
WB-27	XX	xx				X												x									
WB-28	XX					X					xx																
WB-29	XX	x						xx			X																
WB-30	XX	xx						X			x																
WB-31	XX	X						xx																			
WB-32	XX							X			xx																
WB-33	XX	X															xx										
WB-34	XX	xx				X					x																
WB-35	XX	xx				X					x																
WB-36	XX	x						xx			X																
WB-37	XX	xx				X					x																
WB-38	XX	xx				X					x																
WB-39	XX	X						xx										x									
WB-40	XX	X				xx																					

Appendix C: Continued

Sample ID	Quartz	Albite	Anorthite	Orthoclase	Sanidine	Calcite	Dolomite	Muscovite	Illite	Annite	Clinocllore	Halloysite	Dickite	Lizardite	Guidottite	Montmorillonite	Nontronite	Yakhontovite	Vermiculite	Tosudite	Hematite	Franklinite	Lintisite	Roquesite	Grossmanite	Hedenbergite	Clinostatite
WB-41	XX	X				xx																					
WB-42	XX					X		xx																			
WB-43	XX	X				xx																	x				
WB-44	XX	xx				X					x																
WB-45	XX	x							X		xx																
WB-46	XX							X																			
WB-47	X	xx				XX																					
WB-48	X	xx				XX																					
WB-49	X	xx				XX										x											
WB-50	XX	X																									
WB-51	X	xx				XX										x											
WB-52	X					XX		xx																			
WB-53	XX	xx				X		x																			
WB-54	XX	xx							X																		
WB-55	XX							X																			
WB-56	XX	xx				X			x																		
SB-1	XX	X							xx																		
SB-2	XX	X							xx														x				
SB-3	XX	xx							x																X		
SB-4	XX	X						xx																			
SB-5	XX	X						xx														x					
SB-6	XX	x						X			xx																
SB-7	XX	X						xx																			
SB-8	XX	X							xx																		
SB-9	XX	xx						X																			
SB-10	XX	X						xx																			
SB-11	XX	xx						X																			
SB-12	XX	X						xx															x				
SB-13	XX							X																			
SB-14		XX																									X
SB-15			XX											X													
SB-16	XX							xx												x		X					
SB-17	XX	x						xx					X														
SB-18	XX							X																			
SB-19	XX							X																			
SB-20	XX							X																			
SB-21	XX	x						X			xx																
SB-22	XX							xx							X												
SB-23	X						XX						xx														
SB-24																											

Appendix C: Continued

Sample ID	Quartz	Albite	Anorthite	Orthoclase	Sanidine	Calcite	Dolomite	Muscovite	Illite	Annite	Clinchlore	Halloysite	Dickite	Lizardite	Guidottite	Montmorillonite	Nontronite	Yakhontovite	Vermiculite	Tosudite	Hematite	Franklinite	Lintisite	Roquesite	Grossmanite	Hedenbergite	Clinoenstatite
SB-25	XX							X											xx								
SB-26	XX							X																			
SB-27																											
SB-28			X							XX																	
SB-29				XX							X																
SB-30	XX	xx			X																						
SB-31	XX	X						xx																			
SB-32	XX	X						xx																			
SB-33	X	xx						XX																			
SB-34	XX	xx						X																			
SB-35	XX	xx						X																			
SB-36	XX	X						xx																			
SB-37	XX	X							xx																		
SB-38	XX	X						xx																			
SB-39	XX											X															
SB-40	XX							X																			
DB-1	XX	X																									
DB-2	XX	X						x				xx															
DB-3	XX	X						xx																			
DB-4	XX	xx						X																			
DB-5	XX	X						xx																			
DB-6	XX	X																									
DB-7	XX	X						xx																			
DB-8	XX	X						x											xx								
DB-9	XX	X							xx																		
DB-10	XX	X						xx																			
DB-11	XX	X						xx																			
DB-12	XX	X						xx																			
DB-13	XX	X						xx																			
DB-14	XX	X						xx																			
DB-15	XX	X						xx																			
DB-16	XX	X																									
DB-17	XX	X						xx																			
DB-18	XX	X						xx																			
DB-19	XX	x							xx			X															
DB-20	XX	X						xx																			
DB-21	XX	X						xx																			
DB-22	XX	X						x											xx								
DB-23	XX	X							xx																		
DB-24	XX	xx						X																			

Appendix C: Continued

Sample ID	Quartz	Albite	Anorthite	Orthoclase	Sanidine	Calcite	Dolomite	Muscovite	Illite	Annite	Clinchlore	Halloysite	Dickite	Lizardite	Guidottiite	Montmorillonite	Nontronite	Yakhontovite	Vermiculite	Tosudite	Hematite	Franklinite	Lintisite	Roquesite	Grossmanite	Hedenbergite	Clinoenstatite
DB-25	XX	xx							X																		
DB-26	XX							X																			
DB-27	XX	X																		xx							
DB-28	X					XX		xx																			
DB-29	XX	X				xx		x																			
DB-30	XX	X						xx																			
DB-31	XX							X			xx																
DB-32	XX	X																									
DB-33	XX	X						xx																			
DB-34	XX	xx						X			x																
DB-35	XX	x						X			xx																
DB-36	XX							X																			
DB-37	XX	X							xx												x						
DB-38	XX	xx						X																			
DB-39	XX	xx						X																			
DB-40	XX	X						xx																			
DB-41	XX	x						xx			X																
DB-42	XX							X																			
DB-43	XX	xx						X																			
DB-44	XX								X		xx																
DB-45	XX	X						x								xx											
DB-46	XX	X						x													xx						
DB-47								XX												X							
DB-48	XX	xx						X																			
DB-49	XX	xx						X																			
DB-50	XX	X						xx			x																
DB-51	XX	xx				X			x																		
DB-52	XX					X		xx			x																
DB-53	XX							X			xx																
DB-54	XX	xx						X																			
DB-55	XX							xx			X																
DB-56	XX	xx							X																		
DB-57	XX	X						xx																			
DB-58	XX	X																									
DB-59	XX								X															xx			
DB-60	XX	X						xx																			
DB-61	XX	X						x				xx															
DB-62	XX	X						xx																			
DB-63	XX	xx						X																			
DB-64	XX							X																			

Appendix C: Continued

Sample ID	Quartz	Albite	Anorthite	Orthoclase	Sandine	Calcite	Dolomite	Muscovite	Illite	Annite	Clinchlore	Halloysite	Dickite	Lizardite	Guidottiite	Montmorillonite	Nontronite	Yakhontovite	Vermiculite	Tosudite	Hematite	Franklinite	Lintisite	Roquesite	Grossmanite	Hedenbergite	Clinoenstatite
DB-65	XX	X																									
DB-66	XX	X						xx																			
DB-67	XX							X																			
DB-68	XX	X						xx												x							
DB-69	XX	X						xx																			
DB-70	XX	X																									
DB-71	XX	X																									
DB-72	XX	X														xx											
DB-73	XX	X						xx																			
DB-74	XX	X						xx																			
DB-75	XX	xx						X			x																
DB-76	XX	X																									
DB-77	XX	xx							X																		
DB-78	XX							X															xx				
DB-79	XX	X											xx														
DB-80	XX	X						xx																			
DB-81	XX	X						xx																			
DB-82	XX	X				xx																					
DB-83	XX	X						xx																			
DB-84	XX	X																									
DB-85	XX	X																		xx							
DB-86	XX	X						xx																			
DB-87	XX	X						xx																			
DB-88	XX	X							xx																		
DB-89	XX	X																									
DB-90	XX	X								xx																	
DB-91	XX	X						xx																			
DB-92	XX	X														xx											

## Appendix D: Relative Abundance of Mineral Groups

Appendix D: Results of the X-ray diffraction analyses showing the relative abundance of the mineral groups identified in each sample and the overall relative abundance of the mineral groups in the DRB (located at the bottom of the table). The mineral groups were based on the sequential extractions. The color scheme and abbreviations used for the semi-quantitative data are as follows: green, XX, 4 = highest intensity; yellow, X, 3 = high intensity; red, xx, 2 = medium intensity; orange, x, 1 = lowest intensity. These intensities were determined using the PDXL2 software. As the software identified candidate phases of minerals, they were presented in order of decreasing occurrence.

Sample ID	Grain Size	Depositional Environment	Quartz (Rel. Abun.)	Feldspar (Rel. Abun.)	Clay Minerals (Rel. Abun.)	Carbonates (Rel. Abun.)	Other (Rel. Abun.)
WB-1	siltstone	Floodplain Facies	XX		X		
WB-2	m-c-vc s.s	Channel Facies	XX	X	xx		
WB-3	m-c-vc s.s	Fan Fringe	XX	X	xx		
WB-5	vf-f s.s	Lacustrine Facies	XX	X			
WB-6	m-c-vc s.s	Channel Facies	XX		xx		X
WB-7	m-c-vc s.s	Floodplain Facies			XX		
WB-8	siltstone	Floodplain Facies	XX	X			
WB-9	m-c-vc s.s	Crevasse Splay Facies	XX	xx	X		
WB-10	vf-f s.s	Floodplain Facies	XX	xx	X		
WB-11	m-c-vc s.s	Channel Facies	XX	xx		X	
WB-12	vf-f s.s	Floodplain Facies	XX	x	xx		X
WB-13	vf-f s.s	Channel Facies	XX	X	xx		
WB-14	m-c-vc s.s	Crevasse Splay Facies	XX	X	xx		
WB-15	m-c-vc s.s	Crevasse Splay Facies	XX	X			
WB-16	mudstone-shale	Lacustrine Facies	XX		X		
WB-17	vf-f s.s	Floodplain Facies	XX	x	xx	X	
WB-18	mudstone-shale	Floodplain Facies	XX		x	X	xx
WB-19	mudstone-shale	Floodplain Facies	XX	xx	x	X	
WB-20	vf-f s.s	Floodplain Facies	XX	xx	x	X	
WB-21	siltstone	Floodplain Facies	XX	X	xx		x
WB-22	siltstone	Floodplain Facies	XX	xx	x	X	
WB-23	vf-f s.s	Floodplain Facies	XX	X	x	xx	
WB-24	siltstone	Floodplain Facies	XX	xx	x	X	
WB-25	mudstone-shale	Lacustrine Facies	XX	X	xx		
WB-26	siltstone	Lacustrine Facies	XX	X	x	xx	
WB-27	siltstone	Floodplain Facies	XX	xx	x	X	

Appendix D: continued

Sample ID	Grain Size	Depositional Environment	Quartz (Rel. Abun.)	Feldspar (Rel. Abun.)	Clay Minerals (Rel. Abun.)	Carbonates (Rel. Abun.)	Other (Rel. Abun.)
WB-28	mudstone-shale	Floodplain Facies	XX		xx	X	
WB-29	mudstone-shale	Floodplain Facies	XX	xx	X		
WB-30	mudstone-shale	Floodplain Facies	XX	xx	X		
WB-31	mudstone-shale	Floodplain Facies	XX	X	xx		
WB-32	mudstone-shale	Lacustrine Facies	XX		X		
WB-33	vf-f s.s	Crevasse Splay Facies	XX	X	xx		
WB-34	vf-f s.s	Floodplain Facies	XX	xx	x	X	
WB-35	vf-f s.s	Crevasse Splay Facies	XX	xx	x	X	
WB-36	siltstone	Floodplain Facies	XX	xx	X		
WB-37	vf-f s.s	Crevasse Splay Facies	XX	xx	x	X	
WB-38	vf-f s.s	Crevasse Splay Facies	XX	xx	x	X	
WB-39	siltstone	Crevasse Splay Facies	XX	X	xx		
WB-40	siltstone	Floodplain Facies	XX	X		xx	
WB-41	siltstone	Floodplain Facies	XX	X		xx	
WB-42	vf-f s.s	Floodplain Facies	XX		xx	X	
WB-43	vf-f s.s	Floodplain Facies	XX	X		xx	x
WB-44	siltstone	Floodplain Facies	XX	xx	x	X	
WB-45	siltstone	Floodplain Facies	XX	xx	X		
WB-46	siltstone	Floodplain Facies	XX		X		
WB-47	siltstone	Floodplain Facies	X	xx		XX	
WB-48	siltstone	Floodplain Facies	X	xx	x	XX	
WB-49	siltstone	Floodplain Facies	X	xx		XX	
WB-50	siltstone	Floodplain Facies	XX	X			
WB-51	siltstone	Floodplain Facies	X	xx	x	XX	
WB-52	mudstone-shale	Floodplain Facies	X		xx	XX	
WB-53	vf-f s.s	Floodplain Facies	XX	xx	x	X	
WB-54	siltstone	Floodplain Facies	XX	xx	X		
WB-55	vf-f s.s	Floodplain Facies	XX		X		
WB-56	siltstone	Floodplain Facies	XX	xx	x	X	

Appendix D: continued

Sample ID	Grain Size	Depositional Environment	Quartz (Rel. Abun.)	Feldspar (Rel. Abun.)	Clay Minerals (Rel. Abun.)	Carbonates (Rel. Abun.)	Other (Rel. Abun.)
SB-1	vf-f s.s	Floodplain Facies	XX	X	xx		
SB-2	vf-f s.s	Floodplain Facies	XX	X	xx		x
SB-3	vf-f s.s	Floodplain Facies	XX	xx	x		X
SB-4	siltstone	Lacustrine Facies	XX	X	xx		
SB-5	siltstone	Lacustrine Facies	XX	X	xx		x
SB-6	siltstone	Floodplain Facies	XX	xx	X		
SB-7	vf-f s.s	Crevasse Splay Facies	XX	X	xx		
SB-8	vf-f s.s	Channel Facies	XX	X	xx		
SB-9	vf-f s.s	Floodplain Facies	XX	xx	X		
SB-10	siltstone	Floodplain Facies	XX	X	xx		
SB-11	siltstone	Floodplain Facies	XX	xx	X		
SB-12	siltstone	Crevasse Splay Facies	XX	X	xx		x
SB-13	mudstone-shale	Lacustrine Facies	XX		X		
SB-14	igneous			XX			X
SB-15	mudstone-shale	Lacustrine Facies		XX	X		
SB-16	siltstone	Floodplain Facies	XX		xx		X
SB-17	siltstone	Floodplain Facies	XX	xx	X		
SB-18	vf-f s.s	Floodplain Facies	XX		X		
SB-19	vf-f s.s	Floodplain Facies	XX		X		
SB-20	vf-f s.s	Floodplain Facies	XX		X		
SB-21	vf-f s.s	Floodplain Facies	XX	xx	X		
SB-22	mudstone-shale	Lacustrine Facies	XX		X		
SB-23	carbonate	Lacustrine Facies	X		xx	XX	
SB-25	siltstone	Floodplain Facies	XX		X		
SB-26	siltstone	Floodplain Facies	XX		X		
SB-28	mudstone-shale	Lacustrine Facies		X	XX		
SB-29	igneous			XX	X		
SB-30	siltstone	Floodplain Facies	XX	X			

Appendix D: Continued

Sample ID	Grain Size	Depositional Environment	Quartz (Rel. Abun.)	Feldspar (Rel. Abun.)	Clay Minerals (Rel. Abun.)	Carbonates (Rel. Abun.)	Other (Rel. Abun.)
SB-31	m-c-vc s.s	Crevasse Splay Facies	XX	X	xx		
SB-32	vf-f s.s	Floodplain Facies	XX	X	xx		
SB-33	siltstone	Floodplain Facies	X	xx	XX		
SB-34	siltstone	Floodplain Facies	XX	xx	X		
SB-35	vf-f s.s	Channel Facies	XX	xx	X		
SB-36	siltstone	Floodplain Facies	XX	X	xx		
SB-37	vf-f s.s	Channel Facies	XX	X	xx		
SB-38	vf-f s.s	Floodplain Facies	XX	X	xx		
SB-39	gravel	Fan Fringe	XX		X		
SB-40	vf-f s.s	Channel Facies	XX		X		
DB-1	siltstone	Fan Fringe	XX	X			
DB-2	m-c-vc s.s	Fan Fringe	XX	X	xx		
DB-3	vf-f s.s	Fan Fringe	XX	X	xx		
DB-4	siltstone	Fan Fringe	XX	xx	X		
DB-5	siltstone	Fan Fringe	XX	X	xx		
DB-6	siltstone	Fan Fringe	XX	X			
DB-7	siltstone	Fan Fringe	XX	X	xx		
DB-8	vf-f s.s	Fan Fringe	XX	X	xx		
DB-9	m-c-vc s.s	Distal Fan	XX	X	xx		
DB-10	vf-f s.s	Distal Fan	XX	X	xx		
DB-11	m-c-vc s.s	Distal Fan	XX	X	xx		
DB-12	m-c-vc s.s	Distal Fan	XX	X	xx		
DB-13	m-c-vc s.s	Distal Fan	XX	X	xx		
DB-14	m-c-vc s.s	Distal Fan	XX	X	xx		
DB-15	m-c-vc s.s	Distal Fan	XX	X	xx		
DB-16	m-c-vc s.s	Fan Fringe	XX	X			
DB-17	siltstone	Fan Fringe	XX	X	xx		
DB-18	siltstone	Fan Fringe	XX	X	xx		
DB-19	mudstone-shale	Fan Fringe	XX	xx	X		

Appendix D: Continued

Sample ID	Grain Size	Depositional Environment	Quartz (Rel. Abun.)	Feldspar (Rel. Abun.)	Clay Minerals (Rel. Abun.)	Carbonates (Rel. Abun.)	Other (Rel. Abun.)
DB-20	siltstone	Fan Fringe	XX	X	xx		
DB-21	vf-f s.s	Crevasse Splay Facies	XX	X	xx		
DB-22	siltstone	Floodplain Facies	XX	X	xx		
DB-23	vf-f s.s	Floodplain Facies	XX	X	xx		
DB-24	vf-f s.s	Floodplain Facies	XX	xx	X		
DB-25	vf-f s.s	Floodplain Facies	XX	xx	X		
DB-26	vf-f s.s	Floodplain Facies	XX		X		
DB-27	m-c-vc s.s	Channel Facies	XX	X	xx		
DB-28	mudstone-shale	Floodplain Facies	X		xx	XX	
DB-29	m-c-vc s.s	Channel Facies	XX	X	x	xx	
DB-30	m-c-vc s.s	Channel Facies	XX	X	xx		
DB-31	siltstone	Floodplain Facies	XX		X		
DB-32	m-c-vc s.s	Floodplain Facies	XX	X			
DB-33	m-c-vc s.s	Channel Facies	XX	X	xx		
DB-34	vf-f s.s	Floodplain Facies	XX	xx	X		
DB-35	mudstone-shale	Lacustrine Facies	XX	xx	X		
DB-36	siltstone	Lacustrine Facies	XX		X		
DB-37	vf-f s.s	Lacustrine Facies	XX	X	xx		
DB-38	siltstone	Lacustrine Facies	XX	xx	X		
DB-39	siltstone	Lacustrine Facies	XX	xx	X		
DB-40	siltstone	Lacustrine Facies	XX	X	xx		
DB-41	m-c-vc s.s	Lacustrine Facies	XX	xx	X		
DB-42	vf-f s.s	Lacustrine Facies	XX		X		
DB-43	siltstone	Floodplain Facies	XX	xx	X		
DB-44	vf-f s.s	Floodplain Facies	XX		X		
DB-45	vf-f s.s	Channel Facies	XX	X	xx		
DB-46	m-c-vc s.s	Channel Facies	XX	X	xx		

Appendix D: Continued

Sample ID	Grain Size	Depositional Environment	Quartz (Rel. Abun.)	Feldspar (Rel. Abun.)	Clay Minerals (Rel. Abun.)	Carbonates (Rel. Abun.)	Other (Rel. Abun.)
DB-47	siltstone	Floodplain Facies			XX		
DB-48	vf-f s.s	Floodplain Facies	XX	xx	X		
DB-49	vf-f s.s	Crevasse Splay Facies	XX	xx	X		
DB-50	siltstone	Floodplain Facies	XX	X	xx		
DB-51	vf-f s.s	Crevasse Splay Facies	XX	xx	x	X	
DB-52	siltstone	Floodplain Facies	XX		xx	X	
DB-53	siltstone	Floodplain Facies	XX		X		
DB-54	vf-f s.s	Crevasse Splay Facies	XX	xx	X		
DB-55	m-c-vc s.s	Fan Fringe	XX		X		
DB-56	vf-f s.s	Fan Fringe	XX	xx	X		
DB-57	m-c-vc s.s	Fan Fringe	XX	X	xx		
DB-58	m-c-vc s.s	Crevasse Splay Facies	XX	X			
DB-59	vf-f s.s	Floodplain Facies	XX		X		xx
DB-60	siltstone	Floodplain Facies	XX	X	xx		
DB-61	siltstone	Floodplain Facies	XX	X	xx		
DB-62	m-c-vc s.s	Channel Facies	XX	X	xx		
DB-63	siltstone	Floodplain Facies	XX	xx	X		
DB-64	vf-f s.s	Channel Facies	XX		X		
DB-65	gravel	Channel Facies	XX	X			
DB-66	m-c-vc s.s	Crevasse Splay Facies	XX	X	xx		
DB-67	vf-f s.s	Floodplain Facies	XX		X		
DB-68	vf-f s.s	Floodplain Facies	XX	X	xx		
DB-69	m-c-vc s.s	Crevasse Splay Facies	XX	X	xx		
DB-70	m-c-vc s.s	Crevasse Splay Facies	XX	X			
DB-71	m-c-vc s.s	Crevasse Splay Facies	XX	X			
DB-72	siltstone	Floodplain Facies	XX	X	xx		
DB-73	siltstone	Floodplain Facies	XX	X	xx		
DB-74	vf-f s.s	Floodplain Facies	XX	X	xx		
DB-75	vf-f s.s	Floodplain Facies	XX	xx	X		

Appendix D: Continued

Sample ID	Grain Size	Depositional Environment	Quartz (Rel. Abun.)	Feldspar (Rel. Abun.)	Clay Minerals (Rel. Abun.)	Carbonates (Rel. Abun.)	Other (Rel. Abun.)
DB-76	m-c-vc s.s	Crevasse Splay Facies	XX	X			
DB-77	siltstone	Floodplain Facies	XX	xx	X		
DB-78	vf-f s.s	Crevasse Splay Facies	XX		X		xx
DB-79	m-c-vc s.s	Floodplain Facies	XX	X	xx		
DB-80	m-c-vc s.s	Floodplain Facies	XX	X	xx		
DB-81	vf-f s.s	Floodplain Facies	XX	X	xx		
DB-82	m-c-vc s.s	Crevasse Splay Facies	XX	X		xx	
DB-83	siltstone	Floodplain Facies	XX	X	xx		
DB-84	m-c-vc s.s	Fan Fringe	XX	X			
DB-85	m-c-vc s.s	Fan Fringe	XX	X	xx		
DB-86	siltstone	Fan Fringe	XX	X	xx		
DB-87	vf-f s.s	Fan Fringe	XX	X	xx		
DB-88	vf-f s.s	Fan Fringe	XX	X	xx		
DB-89	siltstone	Fan Fringe	XX	X			
DB-90	m-c-vc s.s	Fan Fringe	XX	X	xx		
DB-91	m-c-vc s.s	Fan Fringe	XX	X	xx		
DB-92	vf-f s.s	Fan Fringe	XX	X	xx		
<b>Relative Abundance</b>			3.8	2.1	2.0	0.5	0.1

## Appendix E: Geochemical data

Appendix E: The results of the sequential extractions conducted on 183 samples including duplicates from the DRB. The concentration of B, Sr, and Ba leached from each sample by each step of the sequential extractions is shown. Concentrations reported as  $\mu\text{g}$  of element extracted per g of unleached starting material.

Sample ID	H <sub>2</sub> O ext. B ( $\mu\text{g/g}$ )	NH <sub>4</sub> Ac ext. B ( $\mu\text{g/g}$ )	Acetic Acid ext. B ( $\mu\text{g/g}$ )	HCl ext. B ( $\mu\text{g/g}$ )	H <sub>2</sub> O ext. Sr ( $\mu\text{g/g}$ )	NH <sub>4</sub> Ac ext. Sr ( $\mu\text{g/g}$ )	Acetic Acid ext. Sr ( $\mu\text{g/g}$ )	HCl ext. Sr ( $\mu\text{g/g}$ )	H <sub>2</sub> O ext. Ba ( $\mu\text{g/g}$ )	NH <sub>4</sub> Ac ext. Ba ( $\mu\text{g/g}$ )	Acetic Acid ext. Ba ( $\mu\text{g/g}$ )	HCl ext. Ba ( $\mu\text{g/g}$ )
DB-1	0.2	0.0	0.1	0.0	0.0	26.7	0.8	0.3	0.3	46.0	3.4	6.3
DB-2	0.8	0.0	0.1	0.7	0.1	21.4	0.6	0.3	0.3	25.3	2.3	4.8
DB-3	0.4	0.0	0.1	0.3	0.0	17.3	0.6	0.2	0.2	5.8	1.0	1.9
DB-3 Dup	0.1	0.0	0.1	0.1	0.0	17.7	0.6	0.2	0.2	5.9	1.0	1.9
DB-4	0.3	0.0	0.1	0.2	0.1	18.5	1.2	0.4	0.3	8.5	1.5	1.9
DB-5	0.3	0.0	1.0	0.3	0.1	19.5	7.3	1.5	0.4	12.1	4.5	5.5
DB-6	0.3	0.0	0.0	0.2	0.0	21.8	1.0	0.4	0.2	46.3	12.8	55.2
DB-7	0.2	0.0	0.1	0.2	0.1	25.4	1.0	0.5	0.3	15.2	1.3	1.3
DB-8	0.2	0.1	1.8	0.2	0.1	13.7	9.0	1.3	0.2	14.8	2.4	1.3
DB-9	0.1	0.0	2.5	0.2	0.3	20.4	12.3	2.5	0.4	23.1	7.3	9.7
DB-10	0.2	0.0	0.8	0.1	0.1	19.4	4.8	1.0	0.4	18.7	5.8	9.3
DB-11	0.1	0.0	0.8	0.1	0.7	14.6	5.1	0.9	0.6	22.1	6.6	11.4
DB-12	0.2	0.0	0.4	0.1	0.1	21.3	2.8	0.6	0.6	36.7	7.3	15.3
DB-13	0.0	0.0	0.0	0.1	1.4	7.7	1.6	2.6	24.9	594.2	100.8	421.4
DB-13 Dup	0.0	0.0	0.0	0.0	1.4	7.9	1.6	2.7	24.8	617.7	101.4	430.2
DB-14	0.2	0.1	0.2	0.2	1.1	6.5	1.2	0.4	6.3	165.0	20.0	18.1
DB-15	0.3	0.1	9.2	0.3	0.1	27.9	34.5	5.6	0.7	46.6	16.1	16.5
DB-16	0.1	0.0	0.3	0.0	0.0	26.1	2.3	0.6	0.3	40.2	6.8	13.9
DB-17	0.1	0.0	0.1	0.0	0.1	35.2	0.8	0.4	0.5	61.4	4.0	4.3
DB-18	0.1	0.2	0.1	0.0	0.1	32.0	0.8	0.4	0.5	56.3	2.7	2.7
DB-18 Dup	0.0	0.0	0.1	0.0	0.1	32.4	1.0	0.4	0.6	56.4	3.0	2.4
DB-19	0.1	0.1	0.0	0.0	0.1	35.9	0.8	1.1	0.7	255.5	27.7	92.7
DB-20	0.2	0.1	0.1	0.0	0.1	28.0	1.1	0.4	0.7	62.4	2.4	2.7
DB-21	0.1	0.1	0.2	0.0	0.1	6.3	2.4	0.5	0.1	13.9	3.4	7.4
DB-22	0.0	0.0	0.1	0.0	0.0	13.1	1.2	0.9	0.2	27.1	1.2	4.7
DB-23	0.0	0.1	0.1	0.0	1.2	10.7	1.6	0.5	0.3	12.0	1.3	2.0
DB-24	0.1	0.1	0.8	0.0	0.2	9.9	5.2	0.8	0.2	13.7	5.7	7.7
DB-24 Dup	0.0	0.1	0.8	0.0	0.2	9.6	5.1	0.8	0.2	13.7	5.5	7.8
DB-25	0.1	0.1	0.2	0.0	0.2	9.4	2.9	0.4	0.1	11.2	3.0	3.9
DB-26	0.1	0.3	0.6	0.1	0.6	18.4	0.8	0.4	0.3	19.7	3.3	8.0
DB-27	0.0	0.1	0.3	0.0	2.6	45.8	2.1	0.4	0.7	19.6	0.6	1.4
DB-27 Dup	0.0	0.0	0.1	0.0	2.7	48.8	2.2	0.4	0.7	21.2	0.7	1.4
DB-28	0.1	0.1	0.1	0.0	3.9	20.7	20.8	2.3	0.9	24.1	1.5	2.1
DB-29	0.0	0.1	0.3	0.0	3.0	33.6	8.5	0.7	0.7	15.4	2.5	1.6
DB-30	0.0	0.1	0.2	0.0	2.6	43.0	1.4	0.3	0.7	21.2	0.9	1.5

Appendix E: Continued

Sample ID	H <sub>2</sub> O ext. B (µg/g)	NH <sub>4</sub> Ac ext. B (µg/g)	Acetic Acid ext. B (µg/g)	HCl ext. B (µg/g)	H <sub>2</sub> O ext. Sr (µg/g)	NH <sub>4</sub> Ac ext. Sr (µg/g)	Acetic Acid ext. Sr (µg/g)	HCl ext. Sr (µg/g)	H <sub>2</sub> O ext. Ba (µg/g)	NH <sub>4</sub> Ac ext. Ba (µg/g)	Acetic Acid ext. Ba (µg/g)	HCl ext. Ba (µg/g)
DB-31	0.0	0.1	0.6	0.0	0.7	22.5	4.0	0.7	0.3	26.0	9.4	12.0
DB-32	0.0	0.0	0.2	0.0	0.3	38.1	2.0	0.4	0.3	24.7	2.3	5.4
DB-33	0.0	0.0	0.2	0.0	2.6	26.2	1.8	0.4	0.6	15.5	1.9	1.9
DB-34	0.0	0.0	0.1	0.0	0.3	14.1	0.8	0.2	0.3	11.9	3.9	5.3
DB-34 Dup	0.0	0.0	0.0	0.0	0.3	16.4	0.7	0.2	0.3	13.1	3.6	5.3
DB-35	0.0	0.0	0.2	0.0	1.0	30.8	1.0	0.6	0.4	34.7	3.4	2.6
DB-36	0.0	0.0	0.1	0.0	1.0	31.8	2.2	0.6	0.5	36.1	9.1	6.9
DB-37	0.0	0.0	0.0	0.0	0.2	19.1	1.3	0.2	0.2	14.8	4.4	4.4
DB-38	0.2	0.1	0.7	0.0	0.1	33.3	4.8	0.9	0.2	25.6	4.6	5.0
DB-38 Dup	0.0	0.0	0.5	0.0	0.2	30.5	4.6	0.9	0.2	23.3	4.5	4.8
DB-39	0.0	0.0	0.2	0.0	0.4	27.1	1.9	0.5	0.2	21.4	1.6	1.2
DB-40	0.1	0.0	0.4	0.0	0.1	43.1	3.7	1.1	0.3	28.4	2.5	3.2
DB-41	0.1	0.0	0.1	0.0	0.1	40.2	1.1	0.6	0.3	19.6	1.6	2.3
DB-42	0.0	0.0	0.1	0.0	0.1	31.6	1.6	0.4	0.3	14.7	2.8	2.6
DB-43	0.0	0.0	1.3	0.0	0.1	32.4	10.6	2.1	0.4	11.9	6.4	9.6
DB-44	0.0	0.0	1.2	0.0	0.1	33.4	7.5	1.2	0.3	10.6	6.7	10.7
DB-45	0.0	0.0	0.0	0.0	1.9	80.7	1.9	0.5	0.2	9.1	0.6	2.1
DB-46	0.0	0.0	0.0	0.0	0.1	24.4	0.6	0.3	0.2	13.3	1.3	2.7
DB-47	0.0	0.0	0.1	0.0	0.4	36.0	1.1	1.5	0.3	76.5	8.5	38.0
DB-48	0.0	0.0	0.0	0.0	0.4	17.4	0.3	0.3	0.2	18.0	1.0	1.5
DB-49	0.0	0.0	0.4	0.0	0.6	19.7	3.0	0.9	0.2	16.0	1.3	2.1
DB-49 Dup	0.0	0.0	0.5	0.0	0.6	19.8	3.1	0.9	0.3	16.3	1.4	2.2
DB-50	0.7	0.1	2.0	0.6	0.6	21.6	8.5	1.2	0.3	13.5	3.7	2.3
DB-51	0.3	0.0	0.1	0.2	2.6	20.7	4.5	0.6	0.3	9.1	1.3	1.0
DB-52	0.4	0.0	3.4	1.1	3.6	25.1	39.0	8.0	0.3	14.2	4.2	7.8
DB-53	0.3	0.1	5.1	0.3	0.7	24.1	20.4	3.0	0.5	16.9	11.8	15.1
DB-53 Dup	0.2	0.1	4.9	0.2	0.7	22.7	19.8	2.9	0.4	16.2	11.7	15.1
DB-54	0.3	0.0	0.5	0.0	0.1	21.5	3.7	0.4	0.4	10.8	5.8	9.7
DB-55	0.2	0.0	0.1	0.0	0.7	7.0	1.9	0.3	0.3	5.5	3.9	4.0
DB-56	0.2	0.0	0.6	0.0	0.2	23.9	4.2	0.5	0.3	11.7	6.2	8.8
DB-57	0.3	0.0	0.0	0.0	1.4	6.4	1.1	0.2	0.3	5.5	3.0	2.1
DB-58	0.2	0.0	0.0	0.0	0.2	35.9	1.3	0.4	0.6	20.0	4.3	4.7
DB-59	0.2	0.0	0.0	0.0	0.1	20.9	1.5	0.2	0.4	9.1	3.8	5.3
DB-60	0.2	0.0	0.1	0.0	0.1	24.7	2.0	0.3	0.3	10.1	2.3	1.6
DB-61	0.5	0.0	0.1	0.1	0.2	42.5	1.5	0.5	0.6	27.2	4.3	3.3
DB-61 Dup	0.5	0.0	0.2	0.1	0.1	41.8	1.3	0.5	0.7	26.9	4.0	3.4

Appendix E: Continued

Sample ID	H <sub>2</sub> O ext. B (µg/g)	NH <sub>4</sub> Ac ext. B (µg/g)	Acetic Acid ext. B (µg/g)	HCl ext. B (µg/g)	H <sub>2</sub> O ext. Sr (µg/g)	NH <sub>4</sub> Ac ext. Sr (µg/g)	Acetic Acid ext. Sr (µg/g)	HCl ext. Sr (µg/g)	H <sub>2</sub> O ext. Ba (µg/g)	NH <sub>4</sub> Ac ext. Ba (µg/g)	Acetic Acid ext. Ba (µg/g)	HCl ext. Ba (µg/g)
DB-62	0.6	0.0	0.2	0.0	0.1	21.2	1.0	0.2	0.5	12.8	2.3	2.3
DB-63	0.5	0.0	0.2	0.1	0.2	54.3	1.3	0.7	0.8	39.6	3.4	3.6
DB-64	0.2	0.0	0.1	0.0	2.5	42.2	2.7	4.9	18.6	931.9	110.6	368.6
DB-64 Dup	0.2	0.0	0.0	0.0	2.6	41.5	2.5	5.8	19.8	919.9	105.5	436.6
DB-65	0.3	0.0	0.0	0.0	0.2	4.9	0.8	0.2	0.5	15.9	2.6	1.4
DB-66	0.3	0.0	0.0	0.0	0.3	4.4	1.9	0.4	0.5	48.0	42.8	32.9
DB-67	0.3	0.0	1.6	0.0	0.2	26.9	8.9	1.4	0.6	20.2	2.3	3.8
DB-68	0.4	0.0	2.5	0.0	0.1	21.5	8.7	1.3	0.7	16.7	6.2	15.0
DB-69	0.1	0.0	0.0	0.0	0.1	12.4	0.6	0.1	0.3	9.7	1.1	0.9
DB-70	0.1	0.0	0.0	0.0	0.3	16.9	1.2	0.2	0.5	17.8	2.8	4.0
DB-71	0.2	0.0	0.0	0.0	0.1	22.9	0.7	0.2	0.8	28.7	5.8	10.0
DB-72	0.1	0.0	0.2	0.0	0.2	36.3	2.2	0.5	0.8	52.6	6.0	11.9
DB-73	0.3	0.0	0.9	0.0	0.1	29.9	5.0	0.7	0.9	44.8	6.6	10.1
DB-73 Dup	0.3	0.0	0.8	0.0	0.2	30.6	4.8	0.6	0.8	45.8	7.1	9.4
DB-74	0.2	0.0	0.3	0.0	0.1	20.7	2.7	0.3	0.7	26.0	4.6	4.6
DB-75	0.3	0.0	0.4	0.0	0.1	23.3	3.7	0.5	0.8	34.0	2.9	2.6
DB-76	0.2	0.0	0.0	0.0	2.5	8.6	1.4	0.2	0.7	9.5	3.6	2.1
DB-77	0.4	0.0	0.5	0.1	0.1	33.7	3.6	0.5	0.6	47.0	4.3	5.3
DB-78	0.3	0.0	0.5	0.0	0.1	22.3	3.3	0.4	0.8	28.7	6.7	9.6
DB-79	0.2	0.0	0.3	0.0	0.1	25.0	3.1	0.5	0.8	36.0	3.0	3.1
DB-80	0.2	0.1	8.8	0.4	4.2	35.5	37.9	5.1	1.3	43.6	14.5	11.3
DB-80 Dup	0.2	0.1	8.8	0.5	4.5	35.7	38.5	5.4	1.5	43.7	15.0	11.4
DB-81	0.2	0.0	2.8	0.2	3.6	28.6	22.0	2.4	1.1	40.7	10.6	9.5
DB-82	0.1	0.0	0.2	0.0	2.4	7.7	9.0	0.5	0.6	11.2	4.4	2.7
DB-83	0.4	0.0	0.6	0.0	0.2	32.7	4.1	0.6	1.1	52.4	6.9	12.8
DB-84	0.3	0.0	0.2	0.0	2.5	12.4	1.8	0.3	1.4	22.7	6.7	10.5
DB-85	0.3	0.0	0.0	0.0	0.1	18.8	0.7	0.2	0.7	29.5	5.5	7.5
DB-86	0.2	0.0	0.1	0.1	0.2	37.7	1.0	0.4	1.5	66.3	2.8	3.2
DB-87	0.2	0.0	0.0	0.0	0.1	38.1	1.6	0.3	0.6	60.1	3.8	5.8
DB-88	0.1	0.3	0.5	0.0	0.1	12.4	0.9	0.2	0.6	20.0	4.1	5.3
DB-89	0.3	0.1	0.5	0.1	0.2	57.6	1.8	0.6	1.5	96.6	2.7	3.9
DB-90	0.2	0.1	0.2	0.0	0.1	9.0	0.5	0.2	0.4	17.0	4.9	6.4
DB-91	0.1	0.1	0.1	0.0	2.9	11.1	1.0	0.2	1.1	16.7	2.2	1.7
DB-92	0.2	0.0	0.1	0.1	0.1	39.1	1.7	0.4	0.8	66.9	3.8	4.3
DB-92 Dup	0.2	0.0	0.2	0.1	0.1	39.4	1.8	0.4	0.8	67.6	4.2	4.1
SB-1	0.3	0.4	0.1	0.1	0.0	2.3	1.0	0.2	0.0	4.1	1.6	2.6
SB-1 Dup	0.3	0.3	0.0	0.0	0.0	2.4	1.1	0.2	0.1	4.2	1.6	2.6
SB-2	0.2	0.3	0.0	0.0	0.0	2.4	0.1	0.1	0.1	16.0	2.2	3.2
SB-3	0.1	0.3	0.0	0.0	0.0	2.3	0.1	0.1	0.1	4.1	1.8	3.4

Appendix E: Continued

Sample ID	H <sub>2</sub> O ext. B (µg/g)	NH <sub>4</sub> Ac ext. B (µg/g)	Acetic Acid ext. B (µg/g)	HCl ext. B (µg/g)	H <sub>2</sub> O ext. Sr (µg/g)	NH <sub>4</sub> Ac ext. Sr (µg/g)	Acetic Acid ext. Sr (µg/g)	HCl ext. Sr (µg/g)	H <sub>2</sub> O ext. Ba (µg/g)	NH <sub>4</sub> Ac ext. Ba (µg/g)	Acetic Acid ext. Ba (µg/g)	HCl ext. Ba (µg/g)
SB-4	0.2	0.3	0.0	0.0	0.0	9.8	0.5	0.2	0.5	75.0	6.3	10.5
SB-5	0.2	0.3	0.3	0.3	0.0	15.9	7.1	16.2	0.5	147.2	9.5	14.2
SB-6	0.8	0.3	0.6	0.1	0.7	3.8	6.0	0.8	0.3	11.6	5.4	3.9
SB-7	0.4	0.1	0.1	0.0	0.6	3.7	2.8	0.3	1.8	42.5	3.5	2.6
SB-7 Dup	0.2	0.0	0.1	0.0	0.6	3.9	3.0	0.3	1.8	44.1	4.1	2.4
SB-8	0.3	0.0	0.0	0.0	0.1	3.8	3.2	0.4	0.2	16.2	2.8	3.8
SB-9	0.2	0.0	0.3	0.0	0.4	4.7	5.7	0.7	0.5	35.1	12.4	21.8
SB-10	0.5	0.1	0.0	0.0	0.0	4.1	1.9	0.2	0.1	25.8	2.4	4.5
SB-11	0.4	0.1	1.7	0.1	1.2	32.2	71.2	12.6	0.4	23.3	13.3	8.1
SB-12	0.3	0.1	0.2	0.1	0.4	5.4	5.4	0.5	0.7	53.1	9.5	13.0
SB-13	0.6	0.2	1.6	0.7	2.2	52.3	58.2	24.1	0.7	94.4	33.0	18.4
SB-13 Dup	0.6	0.1	1.5	0.7	2.2	52.2	61.0	23.6	0.7	94.7	34.5	18.7
SB-14	0.4	0.1	0.1	0.0	0.2	6.2	2.4	5.1	0.2	29.9	6.6	3.1
SB-15	0.7	0.4	1.8	1.4	0.7	20.9	10.3	12.2	1.3	154.7	28.8	26.4
SB-16	0.2	0.1	0.0	0.0	0.1	3.5	0.7	0.3	0.3	54.7	7.2	9.4
SB-17	0.3	0.0	0.0	0.0	0.0	2.7	0.2	0.1	0.2	40.3	10.0	17.4
SB-18	0.4	0.1	0.1	0.1	0.1	5.2	1.9	1.3	0.3	37.2	31.7	43.2
SB-19	0.3	0.0	0.0	0.0	0.5	3.0	0.7	0.4	0.4	56.1	46.7	32.7
SB-20	0.4	0.0	0.0	0.0	0.2	3.3	0.5	0.3	0.3	47.2	28.6	22.4
SB-21	0.3	0.0	0.0	0.0	0.1	0.7	0.1	0.0	0.2	6.6	1.0	0.5
SB-22	0.7	0.2	1.7	0.5	1.4	55.5	33.1	6.6	0.2	36.1	9.7	5.0
SB-23	0.3	0.1	0.7	0.3	2.4	15.5	175.8	48.1	0.3	14.5	20.0	10.6
SB-25	0.2	0.0	0.0	0.0	0.1	9.4	0.3	0.1	0.2	166.2	5.4	4.8
SB-26	0.2	0.0	0.0	0.1	0.0	11.4	0.4	0.2	0.1	36.6	1.4	1.2
SB-28	0.4	0.1	0.8	1.5	0.3	19.1	8.9	42.0	0.4	30.7	8.1	15.9
SB-28 Dup	0.4	0.1	0.7	1.4	0.2	18.6	8.7	40.6	0.4	29.8	8.0	15.2
SB-29	0.9	0.4	1.2	0.7	0.5	9.9	3.7	3.4	0.2	20.2	7.7	3.9
SB-30	0.4	0.1	0.6	0.1	0.1	2.7	1.7	0.2	0.4	53.3	8.4	8.5
SB-31	0.7	0.2	0.4	0.0	1.8	5.7	1.5	0.3	13.6	153.7	42.6	37.0
SB-32	0.2	0.0	0.2	0.0	0.0	2.6	2.4	0.3	0.2	11.0	1.4	1.9
SB-33	0.3	0.0	0.2	0.0	0.0	4.2	0.2	0.0	0.2	29.8	2.1	2.2
SB-33 Dup	0.3	0.1	0.1	0.0	0.0	4.3	0.1	0.0	0.1	30.7	1.9	2.2
SB-34	0.5	0.1	0.1	0.0	0.0	1.3	0.1	0.0	0.1	12.2	1.8	1.0
SB-35	0.4	0.1	0.4	0.0	1.5	16.2	7.9	0.5	1.4	32.0	10.8	4.7
SB-36	0.4	0.1	0.1	0.0	0.0	2.4	2.4	0.2	0.2	37.5	4.3	5.1
SB-37	0.2	0.0	0.1	0.0	0.5	1.8	2.8	0.3	3.0	54.7	20.4	17.3
SB-38	0.3	0.1	0.1	0.0	0.1	0.8	0.1	0.0	0.1	5.7	0.6	0.4
SB-39	0.5	0.1	0.1	0.0	0.2	1.0	0.1	0.0	0.3	7.0	4.0	4.4
SB-39 Dup	0.5	0.1	0.1	0.0	0.2	0.9	0.1	0.0	0.2	7.0	4.1	4.5
SB-40	0.6	0.1	0.1	0.0	0.0	0.7	0.1	0.1	0.1	2.6	0.7	1.0

Appendix E: Continued

Sample ID	H <sub>2</sub> O ext. B (µg/g)	NH <sub>4</sub> Ac ext. B (µg/g)	Acetic Acid ext. B (µg/g)	HCl ext. B (µg/g)	H <sub>2</sub> O ext. Sr (µg/g)	NH <sub>4</sub> Ac ext. Sr (µg/g)	Acetic Acid ext. Sr (µg/g)	HCl ext. Sr (µg/g)	H <sub>2</sub> O ext. Ba (µg/g)	NH <sub>4</sub> Ac ext. Ba (µg/g)	Acetic Acid ext. Ba (µg/g)	HCl ext. Ba (µg/g)
WB-1	1.8	1.5	1.5	1.5	0.1	13.6	0.5	0.8	0.8	64.0	5.4	14.5
WB-2	0.9	0.4	0.3	0.3	0.0	10.8	0.6	0.4	0.3	37.0	7.9	11.2
WB-3	0.3	0.3	0.2	0.2	0.0	3.5	0.3	0.1	0.2	18.8	3.6	1.0
WB-3 Dup	0.3	0.2	0.1	0.1	0.0	4.2	0.3	0.1	0.2	22.2	3.3	1.0
WB-5	0.5	0.2	0.2	0.2	0.0	2.4	0.1	0.1	0.1	16.9	1.9	2.5
WB-6	0.8	0.2	0.1	0.2	0.8	3.0	0.2	0.1	0.5	10.7	0.9	0.4
WB-7	0.4	0.2	0.1	0.1	0.1	12.2	0.3	0.2	0.4	116.3	3.3	8.5
WB-8	0.4	0.2	0.2	0.1	1.0	19.8	16.4	1.7	0.5	13.9	2.3	1.3
WB-9	0.5	0.2	0.2	0.1	1.1	25.7	25.4	1.9	0.4	11.7	4.2	2.8
WB-10	0.3	0.4	0.3	0.2	0.6	10.3	17.7	13.9	0.2	7.5	5.3	5.3
WB-11	0.3	0.2	0.2	0.0	1.0	26.4	9.3	0.5	0.2	11.6	1.9	1.5
WB-12	0.2	0.2	0.1	0.0	1.2	26.4	32.8	3.5	0.3	15.7	4.0	3.3
WB-12 Dup	0.1	0.2	0.1	0.1	0.1	26.3	32.1	3.5	0.1	14.7	3.9	3.3
WB-13	0.2	0.2	0.1	0.0	0.3	9.9	0.6	0.2	0.2	35.6	1.9	3.3
WB-14	1.3	0.7	0.2	0.1	0.3	7.2	0.9	0.6	0.1	20.4	1.5	3.7
WB-15	0.4	0.2	0.0	0.0	0.2	27.1	3.2	1.1	0.1	78.4	3.5	9.6
WB-16	0.7	0.4	1.5	0.4	2.9	58.0	54.6	7.5	1.5	74.5	11.6	10.2
WB-17	0.8	0.4	1.9	0.5	3.6	71.7	42.9	8.1	2.4	131.3	12.0	11.6
WB-17 Dup	0.7	0.5	1.8	0.5	3.8	67.9	76.3	8.6	2.1	116.9	9.4	8.5
WB-18	0.3	0.3	0.4	0.2	2.5	33.1	71.3	6.5	0.5	28.1	3.4	3.0
WB-19	0.4	0.3	0.4	0.2	1.9	34.6	92.1	6.3	1.7	66.9	5.4	6.5
WB-20	0.5	0.4	1.6	0.3	3.1	56.0	88.3	10.3	2.3	101.0	12.9	10.2
WB-21	0.4	0.4	1.1	0.1	1.8	30.4	63.7	4.1	0.9	32.0	10.1	13.9
WB-22	0.4	0.4	0.7	0.1	4.8	51.9	53.4	2.8	2.5	59.7	7.9	4.6
WB-23	0.4	0.4	1.1	0.2	2.9	55.7	65.3	5.4	2.9	108.2	11.3	10.1
WB-24	0.4	0.4	0.4	0.2	4.2	51.7	103.6	8.1	5.6	121.0	5.7	9.6
WB-24 Dup	0.4	0.4	0.4	0.2	4.2	53.5	115.4	7.7	5.8	125.5	6.6	10.1
WB-25	0.3	0.4	1.0	0.1	2.9	38.5	7.3	1.6	1.7	101.0	11.2	19.0
WB-26	0.8	0.5	0.8	0.1	2.8	51.2	43.1	3.7	1.5	73.9	13.2	13.5
WB-27	1.5	0.6	1.0	0.2	4.1	56.7	77.0	4.9	2.2	68.5	8.4	5.1
WB-28	0.6	0.4	1.1	0.4	5.5	75.9	85.0	6.8	2.7	109.4	8.6	6.2

Appendix E: Continued

Sample ID	H <sub>2</sub> O ext. B (µg/g)	NH <sub>4</sub> Ac ext. B (µg/g)	Acetic Acid ext. B (µg/g)	HCl ext. B (µg/g)	H <sub>2</sub> O ext. Sr (µg/g)	NH <sub>4</sub> Ac ext. Sr (µg/g)	Acetic Acid ext. Sr (µg/g)	HCl ext. Sr (µg/g)	H <sub>2</sub> O ext. Ba (µg/g)	NH <sub>4</sub> Ac ext. Ba (µg/g)	Acetic Acid ext. Ba (µg/g)	HCl ext. Ba (µg/g)
WB-29	0.2	0.4	1.3	0.1	1.9	20.7	15.3	1.8	0.6	40.4	11.3	19.2
WB-30	0.5	0.4	3.1	0.4	1.6	44.2	24.8	4.7	0.7	72.5	15.7	27.0
WB-30 Dup	0.5	0.4	3.2	0.4	1.6	46.7	27.1	4.5	0.9	77.7	16.5	26.3
WB-31	0.3	0.4	1.9	0.2	1.5	39.5	55.9	4.0	0.7	39.0	10.4	8.7
WB-32	0.4	0.4	1.8	0.3	3.1	63.3	14.1	3.5	1.4	167.7	8.0	9.9
WB-33	0.3	0.4	1.9	0.2	1.6	28.3	11.0	2.3	0.9	45.7	12.7	22.2
WB-34	0.5	0.4	0.5	0.1	2.5	32.3	59.0	5.2	0.9	30.2	10.1	17.1
WB-35	0.4	0.4	0.4	0.1	1.6	26.8	44.0	4.4	0.8	22.3	10.1	17.9
WB-36	0.4	0.5	2.1	0.2	2.1	28.4	13.0	1.8	0.6	42.9	9.8	11.0
WB-36 Dup	0.3	0.5	2.1	0.2	2.1	28.4	13.4	1.7	0.7	42.7	10.2	10.9
WB-37	0.4	0.4	1.8	0.1	1.5	24.7	47.4	4.5	0.9	37.2	18.5	30.5
WB-38	1.0	0.5	0.7	0.1	1.3	26.1	33.1	4.1	0.7	74.5	61.6	70.4
WB-39	0.4	0.5	0.3	0.0	0.0	7.2	4.6	0.6	1.4	63.2	19.5	31.8
WB-40	0.3	0.5	1.1	0.1	1.6	45.7	33.8	2.8	0.7	35.4	11.3	15.1
WB-41	0.3	0.5	0.8	0.1	1.6	35.9	72.1	3.9	0.6	25.1	9.4	12.6
WB-42	0.5	0.5	2.9	0.4	2.0	58.1	114.3	14.1	0.9	62.2	14.3	15.6
WB-43	0.4	0.5	0.7	0.0	1.8	30.7	40.4	3.4	0.7	24.6	10.0	15.0
WB-44	0.5	0.6	1.6	0.1	2.5	57.3	121.7	6.2	0.7	33.6	9.1	9.3
WB-44 Dup	0.5	0.5	1.6	0.2	2.6	55.4	124.7	8.4	0.7	33.0	9.8	9.4
WB-45	0.4	0.5	1.0	0.1	1.8	15.8	6.9	0.8	0.5	29.9	10.4	13.1
WB-46	0.5	0.6	3.2	0.3	2.5	69.1	31.1	4.5	0.9	63.2	10.1	8.2
WB-47	0.6	0.7	0.3	0.3	5.1	55.6	108.9	13.2	2.6	66.5	3.8	3.8
WB-48	0.4	0.4	0.3	0.1	5.1	59.5	147.3	8.7	27.8	643.5	74.1	237.3
WB-49	0.7	0.5	0.5	0.4	4.1	65.7	145.7	10.4	1.4	61.5	5.7	12.1
WB-49 Dup	0.7	0.5	0.5	0.4	4.0	67.5	158.8	10.7	1.2	64.1	6.3	12.3
WB-50	0.7	0.7	0.7	0.5	1.7	36.3	20.2	2.1	0.7	34.4	16.0	21.1
WB-51	0.3	0.5	0.3	0.3	2.3	43.3	145.9	7.1	0.7	35.5	6.1	17.3
WB-51 Dup	0.2	0.3	0.3	0.1	2.2	38.7	149.6	7.9	0.7	37.2	6.3	16.6
WB-52	0.5	0.5	0.9	0.4	1.8	50.1	108.3	6.2	0.6	57.3	9.7	15.4
WB-53	0.9	0.8	0.6	0.4	4.0	58.7	137.5	8.9	1.4	56.9	8.0	10.7
WB-54	0.5	0.9	0.3	0.1	1.2	5.8	3.4	0.5	0.3	13.7	8.0	9.8
WB-55	0.5	0.5	1.5	0.4	1.8	39.4	9.9	2.5	0.8	64.9	11.6	18.5
WB-56	0.3	0.4	0.6	0.2	2.0	47.0	92.8	6.4	1.6	93.0	10.6	8.2

Appendix F: Cation and anion data

Appendix F: The results of the sequential extractions conducted on 183 samples including duplicates from the DRB. The concentration of the cations including sodium, potassium, magnesium, calcium, and anions including fluoride, chloride, and sulfate leached from each sample by the water step of the sequential extractions is shown.

Sample Name	Sodium (mg/L)	Potassium (mg/L)	Magnesium (mg/L)	Calcium (mg/L)	Fluoride (mg/L)	Chloride (mg/L)	Sulfate (mg/L)
DB-1	2.7	0.1	n.a.	0.3	0.1	1.6	0.1
DB-10	3.6	0.4	0.4	0.4	0.1	0.3	0.1
DB-11	3.8	0.9	0.6	1.0	0.0	0.2	0.1
DB-12	4.2	0.4	0.4	0.3	0.0	0.2	0.1
DB-13	2.1	1.0	0.7	2.3	0.0	0.3	2.5
DB-13 DUP	2.1	1.0	0.7	2.2	0.0	0.3	2.4
DB-14	2.2	0.8	0.6	2.0	0.0	0.3	1.1
DB-15	4.7	0.4	0.4	0.4	0.3	0.2	0.2
DB-16	3.6	0.2	n.a.	0.3	0.1	0.2	0.2
DB-17	5.0	0.4	0.4	0.3	0.0	0.3	0.5
DB-18	4.9	0.5	0.4	0.3	0.0	0.3	0.2
DB-18 DUP	4.8	0.5	0.4	0.3	0.0	0.2	0.2
DB-19	5.7	0.6	0.4	0.3	0.0	0.4	1.1
DB-2	2.9	0.2	0.4	0.3	0.1	2.0	0.1
DB-20	3.6	0.3	0.4	0.3	0.0	0.2	0.1
DB-21	0.5	0.2	0.4	0.4	0.0	0.2	0.1
DB-22	1.1	0.2	0.4	0.3	0.1	0.2	0.1
DB-23	0.4	0.9	1.3	6.3	0.0	0.2	0.1
DB-24	0.4	0.8	0.5	0.7	0.0	0.2	0.1
DB-24 DUP	0.4	0.8	0.5	0.9	0.0	0.2	0.1
DB-25	0.4	0.7	0.5	0.6	0.0	0.2	0.1
DB-26	0.9	0.8	0.6	1.1	0.0	0.2	0.1
DB-27	2.2	0.7	1.4	5.3	0.0	0.2	0.1
DB-27 DUP	2.3	0.7	1.4	5.4	0.0	0.2	0.1
DB-28	1.1	2.1	1.7	9.6	0.0	0.2	0.5
DB-29	2.1	0.7	1.2	5.4	0.0	0.2	0.1
DB-3	2.1	0.2	0.4	0.3	0.0	0.9	0.1
DB-3 DUP	2.1	0.2	0.4	0.2	0.0	0.9	0.1

Appendix F: continued

Sample Name	Sodium (mg/L)	Potassium (mg/L)	Magnesium (mg/L)	Calcium (mg/L)	Fluoride (mg/L)	Chloride (mg/L)	Sulfate (mg/L)
DB-30	2.9	0.7	1.0	4.2	0.0	0.2	0.1
DB-31	1.7	1.1	0.4	1.0	0.0	0.2	0.1
DB-32	3.1	0.3	0.3	0.3	0.0	0.2	0.1
DB-33	2.8	0.8	0.7	4.1	0.0	0.2	0.2
DB-34	1.6	0.6	0.3	0.4	0.0	0.2	0.1
DB-34 DUP	1.6	0.5	0.3	0.4	0.0	0.2	0.1
DB-35	3.1	1.6	0.4	1.2	0.0	0.2	0.4
DB-36	3.5	1.8	0.4	1.1	0.0	0.2	0.1
DB-37	2.2	0.5	n.a.	0.3	0.0	0.2	0.2
DB-38	3.3	0.5	0.3	0.3	0.0	0.2	0.2
DB-38 DUP	3.4	0.6	0.3	0.3	0.0	0.2	0.2
DB-39	3.1	1.0	0.3	0.5	0.0	0.2	0.6
DB-4	2.3	0.2	0.4	0.3	0.0	0.9	0.1
DB-40	4.1	0.4	0.3	0.3	0.0	0.2	0.1
DB-41	4.0	0.3	n.a.	0.2	0.0	0.2	0.2
DB-42	3.2	0.4	n.a.	0.2	0.0	0.2	0.0
DB-43	3.5	0.4	n.a.	0.2	0.1	0.2	0.2
DB-44	3.9	0.4	n.a.	0.2	0.1	0.2	0.1
DB-45	11.4	0.6	0.4	2.5	0.0	0.2	0.1
DB-46	1.3	0.2	0.3	0.3	1.5	0.2	0.1
DB-47	1.5	0.5	0.6	0.7	0.1	0.3	0.1
DB-48	0.8	1.0	0.6	0.8	1.1	0.3	0.2
DB-49	0.9	0.8	0.6	0.9	0.0	0.2	0.2
DB-49 DUP	0.9	0.8	0.6	0.9	0.0	0.2	0.1
DB-5	3.8	0.4	0.4	0.3	0.1	1.4	0.1
DB-50	1.7	1.5	0.5	1.1	0.0	0.3	0.2
DB-51	1.7	1.1	1.2	5.3	0.0	0.2	0.1
DB-52	2.4	2.2	1.2	7.6	0.1	0.2	0.2
DB-53	2.6	0.9	0.5	1.0	0.1	0.2	0.0
DB-53 DUP	2.7	0.9	0.5	0.9	0.1	0.2	0.1
DB-54	2.4	0.3	0.3	0.3	0.0	0.2	0.2
DB-55	1.5	0.8	0.4	1.0	0.0	0.3	0.1
DB-56	3.1	0.4	0.3	0.3	0.0	0.2	0.1
DB-57	2.0	1.0	0.5	2.4	0.0	0.3	0.2
DB-58	5.0	1.0	0.3	0.3	0.0	0.2	0.1
DB-59	2.9	0.2	n.a.	0.2	0.0	0.2	0.1
DB-6	3.8	0.2	0.4	0.3	0.1	0.6	0.1
DB-60	3.3	0.2	n.a.	0.2	0.0	0.2	0.2
DB-61	5.8	0.7	0.3	0.3	0.1	0.3	0.1
DB-61 DUP	5.6	0.7	0.3	0.3	0.1	0.3	0.1

Appendix F: continued

Sample Name	Sodium (mg/L)	Potassium (mg/L)	Magnesium (mg/L)	Calcium (mg/L)	Fluoride (mg/L)	Chloride (mg/L)	Sulfate (mg/L)
DB-62	3.3	0.2	n.a.	0.2	0.0	0.3	0.1
DB-63	7.8	0.9	0.3	0.4	0.1	0.3	0.2
DB-64	5.7	2.1	0.4	2.3	0.0	0.2	4.9
DB-64 DUP	5.5	2.2	0.4	2.4	0.0	0.2	4.8
DB-65	2.1	0.5	n.a.	0.3	0.0	0.6	0.2
DB-66	2.3	0.3	0.7	2.6	0.0	1.9	0.1
DB-67	3.0	0.3	0.3	0.4	0.1	0.6	0.1
DB-68	2.1	0.3	0.3	0.3	0.1	0.4	0.1
DB-69	1.6	0.2	0.3	0.2	0.0	0.2	0.1
DB-7	5.4	1.2	0.4	0.3	0.0	0.8	0.8
DB-70	2.1	0.7	0.4	0.4	0.0	0.2	0.0
DB-71	2.6	0.2	0.3	0.2	0.0	0.2	0.1
DB-72	4.0	0.4	0.3	0.3	0.0	0.2	0.2
DB-73	3.8	0.4	0.3	0.3	0.1	0.2	0.2
DB-73 DUP	3.8	0.4	0.3	0.3	0.1	0.2	0.3
DB-74	2.8	0.2	0.3	0.2	0.0	0.2	0.1
DB-75	2.9	0.2	0.3	0.2	0.0	0.2	0.1
DB-76	1.8	0.9	0.5	5.8	0.0	0.3	0.1
DB-77	3.8	0.2	0.3	0.2	0.0	0.3	0.1
DB-78	3.1	0.2	0.3	0.2	0.0	0.2	0.1
DB-79	3.6	0.3	0.1	0.1	0.0	0.2	0.1
DB-8	3.3	0.8	0.4	0.3	0.1	0.3	1.6
DB-80	5.4	1.3	0.4	6.4	0.1	0.2	0.1
DB-80 DUP	5.5	1.3	0.4	6.8	0.1	0.2	0.1
DB-81	5.0	1.3	0.3	5.5	0.1	0.2	0.1
DB-82	1.8	0.9	0.3	5.9	0.0	0.2	0.1
DB-83	3.5	0.2	0.2	0.1	0.1	0.2	0.1
DB-84	3.0	0.8	0.3	3.8	0.0	0.3	0.1
DB-85	3.0	0.2	0.1	0.0	0.0	0.2	0.1
DB-86	3.7	0.2	0.1	0.1	0.0	0.2	0.1
DB-87	3.8	0.2	n.a.	0.0	0.0	0.2	0.1
DB-88	2.5	0.2	n.a.	0.0	0.0	0.4	0.1
DB-89	4.9	0.3	0.1	0.1	0.1	0.2	0.1
DB-9	4.4	0.8	0.4	0.5	0.1	0.2	0.3
DB-90	2.0	0.3	n.a.	0.1	0.0	0.4	0.1
DB-91	2.8	0.7	0.2	4.7	0.0	0.2	0.0
DB-92	4.2	0.3	0.1	0.1	0.0	0.2	0.0
DB-92 DUP	4.3	0.3	0.1	0.1	0.0	0.2	0.1

Appendix F: continued

Sample Name	Sodium (mg/L)	Potassium (mg/L)	Magnesium (mg/L)	Calcium (mg/L)	Fluoride (mg/L)	Chloride (mg/L)	Sulfate (mg/L)
SB-1	0.1	0.4	n.a.	n.a.	0.0	0.2	0.1
SB-1 DUP	0.1	0.4	n.a.	n.a.	0.0	0.1	0.1
SB-10	0.1	0.4	0.4	0.3	0.1	0.0	0.7
SB-11	0.1	1.5	0.6	5.0	0.1	0.0	0.6
SB-12	0.3	0.7	0.4	0.7	0.1	0.8	1.5
SB-13	0.1	2.4	1.0	8.4	0.2	0.1	2.5
SB-13 DUP	0.1	2.4	1.0	8.2	0.2	0.7	2.6
SB-14	0.3	0.8	0.9	1.4	0.0	0.2	2.2
SB-15	1.9	3.3	0.9	0.9	0.2	2.0	3.7
SB-16	0.2	0.7	0.4	0.3	0.1	1.2	1.4
SB-17	0.0	0.4	0.4	0.3	0.0	0.1	0.1
SB-18	0.0	0.5	0.4	0.3	0.1	0.6	0.6
SB-19	5.1	0.3	1.8	0.7	0.1	12.1	0.7
SB-2	0.1	0.3	n.a.	n.a.	0.1	0.0	0.0
SB-20	0.8	0.5	0.6	0.4	0.0	1.9	0.7
SB-21	0.1	0.2	0.5	0.3	0.1	2.0	1.7
SB-22	0.6	2.6	0.9	5.9	0.1	0.0	1.1
SB-23	0.1	0.5	3.8	9.0	0.1	0.2	0.3
SB-24	0.5	0.8	0.5	0.7	0.4	0.2	1.6
SB-24 DUP	-0.1	0.7	0.4	0.3	0.4	0.6	2.0
SB-25	0.4	1.2	0.4	0.4	0.1	0.2	50.3
SB-26	0.8	0.6	n.a.	0.3	0.1	0.0	1.8
SB-27	0.0	0.7	0.8	1.3	0.1	0.7	7.6
SB-28	0.9	3.0	1.0	0.5	0.1	0.2	0.4
SB-28 DUP	-0.1	0.4	0.4	0.2	0.1	0.2	0.5
SB-29	1.4	1.8	1.0	1.4	0.1	0.6	0.9
SB-3	0.0	0.3	n.a.	n.a.	0.0	0.6	0.6
SB-30	0.4	0.5	0.5	0.4	0.1	0.3	0.8
SB-31	6.3	1.1	2.2	2.8	0.2	16.4	2.8
SB-32	8.6	0.1	0.4	0.3	0.1	9.5	1.3
SB-33	2.1	0.1	0.3	0.3	0.1	1.1	1.0
SB-33 DUP	2.2	0.1	0.3	0.3	0.1	1.9	1.6

Appendix F: continued

Sample Name	Sodium (mg/L)	Potassium (mg/L)	Magnesium (mg/L)	Calcium (mg/L)	Fluoride (mg/L)	Chloride (mg/L)	Sulfate (mg/L)
SB-34	0.3	0.6	n.a.	0.2	0.0	0.3	0.7
SB-35	0.3	1.1	0.6	6.5	0.1	0.9	3.0
SB-36	1.1	0.2	n.a.	0.2	0.1	0.6	1.3
SB-37	1.2	0.7	0.6	0.6	0.2	2.3	1.1
SB-38	1.4	0.9	0.4	0.3	0.0	1.5	1.8
SB-39	0.0	0.9	0.4	0.4	0.1	0.9	1.0
SB-39 DUP	0.0	0.9	0.4	0.4	0.0	0.6	0.6
SB-4	0.4	0.2	0.4	-0.1	0.1	0.0	0.0
SB-40	-0.1	0.4	n.a.	0.3	0.0	0.0	1.1
SB-5	1.4	0.1	0.3	0.0	0.2	0.4	0.2
SB-6	0.4	1.2	0.9	3.6	0.1	0.7	0.6
SB-7	0.4	0.7	0.5	0.5	0.0	0.2	4.2
SB-7 DUP	0.3	0.8	0.5	0.8	0.1	0.7	3.8
SB-8	0.6	0.6	0.5	0.5	0.0	0.2	1.0
SB-9	0.4	0.3	0.5	1.7	0.0	0.1	0.2
WB-1	3.4	0.2	0.3	0.2	0.1	0.2	0.3
WB-10	2.9	0.7	0.3	0.7	0.2	3.0	4.7
WB-11	0.1	0.5	-0.1	4.6	0.0	0.2	0.3
WB-12	0.2	0.8	0.4	4.3	0.0	0.1	0.1
WB-12 DUP	n.a.	1.0	n.a.	0.1	n.a.	n.a.	n.a.
WB-13	0.3	0.1	0.4	0.5	0.0	0.1	0.1
WB-14	1.7	0.1	-0.1	-0.2	0.0	0.2	0.1
WB-15	0.5	0.3	0.5	0.2	0.1	0.2	0.1
WB-16	0.5	2.0	0.4	5.5	0.1	0.2	0.1
WB-17	0.5	2.4	0.4	5.7	0.1	0.4	0.1
WB-17 DUP	0.4	2.2	0.9	6.1	0.1	0.3	0.0
WB-18	0.5	1.9	0.1	5.9	0.1	0.2	0.1
WB-19	0.3	1.3	0.2	5.8	0.1	0.1	0.2
WB-2	5.5	0.1	n.a.	0.2	0.0	2.2	1.8
WB-20	0.4	1.5	0.9	5.6	0.0	0.3	0.2
WB-21	0.3	0.9	0.7	6.3	0.0	0.5	0.1
WB-22	0.4	1.2	0.9	5.4	0.0	0.4	0.4
WB-23	0.3	1.4	1.0	5.8	0.1	0.2	0.4
WB-24	2.8	0.5	0.9	6.1	0.0	0.3	0.7
WB-24 DUP	0.3	1.0	0.9	6.3	0.1	0.5	0.9
WB-25	0.3	1.1	0.7	5.5	0.0	0.2	0.1

Appendix F: continued

Sample Name	Sodium (mg/L)	Potassium (mg/L)	Magnesium (mg/L)	Calcium (mg/L)	Fluoride (mg/L)	Chloride (mg/L)	Sulfate (mg/L)
WB-26	0.3	0.9	0.6	5.8	0.0	0.3	0.1
WB-27	0.6	1.1	0.3	5.3	0.0	0.3	0.3
WB-28	0.4	1.8	0.5	6.1	0.1	0.7	0.1
WB-29	0.2	0.7	0.5	4.6	0.0	0.1	0.0
WB-3	1.4	0.4	n.a.	n.a.	0.1	0.2	0.2
WB-3 DUP	1.1	0.1	n.a.	n.a.	0.1	0.2	0.2
WB-30	0.7	1.5	1.1	5.4	0.1	0.1	0.0
WB-30 DUP	0.7	1.5	1.2	5.5	0.1	0.1	0.1
WB-31	0.2	1.3	1.0	5.3	0.0	0.1	0.0
WB-32	0.5	2.2	0.9	5.4	0.1	0.2	0.1
WB-33	0.9	1.1	0.7	4.0	0.1	0.1	0.1
WB-34	4.0	0.8	0.4	5.5	0.0	3.1	1.4
WB-35	0.2	0.7	1.1	5.5	0.0	0.1	0.1
WB-36	0.5	1.6	1.1	4.6	0.1	0.1	0.1
WB-36 DUP	0.6	1.6	1.1	4.7	0.0	0.4	0.3
WB-37	0.8	0.7	1.2	5.3	0.0	0.2	0.2
WB-38	0.7	0.5	1.1	5.3	0.0	0.2	0.1
WB-39	1.2	0.2	0.4	0.1	0.1	0.1	0.1
WB-40	0.8	1.2	1.1	4.9	0.0	0.2	0.1
WB-41	0.7	1.0	0.9	5.7	0.0	0.2	0.2
WB-42	1.1	1.4	1.6	5.9	0.1	0.1	0.1
WB-43	0.4	0.9	1.0	5.7	0.0	0.1	0.1
WB-44	0.4	1.4	1.2	6.1	0.0	0.1	0.1
WB-44 DUP	0.4	1.4	1.2	6.1	0.0	0.1	0.1
WB-45	0.4	1.7	1.0	4.9	0.0	0.1	0.1
WB-46	0.7	1.8	1.3	5.3	0.1	0.1	0.1
WB-47	0.5	1.0	0.8	6.3	0.1	0.4	0.3
WB-48	0.4	0.9	0.9	7.1	0.0	0.2	2.8
WB-49	0.7	1.7	1.2	7.1	0.1	0.5	0.2
WB-49 DUP	0.7	1.7	1.1	7.0	0.1	0.5	0.2
WB-5	0.4	0.4	0.4	0.1	0.0	0.1	0.1
WB-50	0.5	0.7	0.6	5.7	0.0	0.3	0.2
WB-51	0.4	0.8	0.6	6.5	0.0	0.5	1.3
WB-51 DUP	0.4	0.8	0.5	6.4	0.0	0.4	0.2
WB-52	0.6	1.6	1.1	6.4	0.1	0.1	0.1
WB-53	0.8	1.2	0.9	6.3	0.1	0.4	0.2
WB-54	0.5	1.2	0.7	4.2	0.0	0.4	11.5
WB-55	0.6	1.7	1.5	5.8	0.1	0.2	0.1
WB-56	0.3	1.4	0.7	6.4	0.0	0.1	0.2
WB-6	0.1	1.1	-0.2	3.6	0.0	0.2	0.5
WB-7	0.1	0.6	n.a.	n.a.	0.0	0.2	0.1
WB-8	0.1	0.8	0.2	4.3	0.0	0.1	0.1
WB-9	0.0	1.1	0.2	4.5	0.0	0.2	0.1
<b>Average</b>	<b>1.9</b>	<b>0.8</b>	<b>0.6</b>	<b>2.4</b>	<b>0.1</b>	<b>0.6</b>	<b>0.8</b>